Osaka University

Research Center for Nuclear Physics

DOCTORAL DISSERTATION

Study of heavy baryons from three-body decays

Author:
Ahmad Jafar Arifi

Supervisor:
Prof. Atsushi Hosaka

July, 2020

This dissertation is dedicated to:
my wife and my little daughter.

Acknowledgement

First, I would like to express my gratitude to my supervisor, Prof. Atsushi Hosaka for giving me valuable experience and knowledge, not only about physics but also about life in Japan. I always get insights about enjoying the discovery and keeping excited about what we are doing right now. I would like to thank him for supporting my research work for about five years and also guiding me to attend some conferences, schools, and workshops. I also send my best regards to Prof. Hideko Nagahiro and Dr. Kiyoshi Tanida for nice discussions and helping me to advance my research works. Also, I want to say thank to Dr. Changwoo Joo for providing me some preliminary experimental data for discussions.

For lab member of Research Center for Nuclear Physics (RCNP), I would say thank for helping me out in my daily life at the laboratory. Especially for Prof. Ishii for helping me to get a Mathematica license and Ms. Karasuyama for helping me to complete various documents. Without all of you, then perhaps I can not do my research quite well.

This work is supported by the MEXT scholarship for my doctoral study. I also acknowledge the support from REIMEI research promotion project (Japan Atomic Energy Agency) for allowing me to stay in Advanced Science Research Center (ASRC).

Finally, I would like to send my gratitude to my wife Citra and my little daughter Aisyah for being a source of my motivation to do hard works. Thank you for always supporting me unconditionally.

Best regards,
Ahmad Jafar Arifi

Abstract

In recent years the interest of heavy hadrons containing heavy quarks has been greatly increased by the current experimental facilities such as LHCb and Belle which are actively reporting discoveries. Many heavy hadrons are newly observed and some of them may be considered as exotics hadrons. Their nature is not yet well-established and under many discussions due to the creation of a light quark-antiquark pair. Among them, the heavy baryon which contain one heavy quark and light quarks could be a suitable place to study the behavior of light quarks inside the heavy quark environment, which is possibly the key to understand the heavy hadrons including new findings.

In this dissertation, we focus on the study of heavy baryons by investigating their three-body decays. Specifically, we investigate the two-pion emission decays of the low-lying Λ_c resonances; $\Lambda_c^* \to \Lambda_c \pi\pi$. The relevant decay processes such as sequential processes going through $\Sigma_c^{(*)}$ in intermediate states and a direct process have been considered in the calculation. The Λ_b bottom baryons are also studied similarly. We employ effective Lagrangians in a non-relativistic framework where the coupling strengths are computed from the quark model.

In heavy baryons, it is known that the orbital excitations between λ and ρ mode are well separated. By studying the three-body decay of $\Lambda_c^*(2595)$ and $\Lambda_c^*(2625)$, we show that the decay properties are sensitive to their internal structures. In comparison to the experimental data, both resonances are consistent with the λ-mode excitation. We also show that the direct process is particularly important for $\Lambda_c^*(2625)$, and its presence can be tested by measuring the Dalitz plots.

Furthermore, the three-body decay is also helpful to determine the unknown spin and parity of $\Lambda_c^*(2765)$, which still have a one-star rating in PDG. By performing a similar analysis, we show that the newly observed $\Lambda_b^*(6072)$ by LHCb can be an analogous state of $\Lambda_c^*(2765)$. Because of that, we arrive at the conclusion that both states may be related to Roper resonances, $N(1440)$, namely the radial excitation of baryons. This discovery tells us that they have common properties which are independent of their flavor contents. The flavor independent nature of Roper-like resonances may provide an interesting hint to the dynamics of hadron resonances.

Keywords:
Quark model, effective Lagrangian, heavy baryon, Dalitz plot, three-body decay, spin-parity, Roper-like resonance.

List of my publications

1. A. J. Arifi, H. Nagahiro, and A. Hosaka.
   Three-body decay of $\Lambda_c^*(2595)$ and $\Lambda_c^*(2625)$ with consideration of $\Sigma_c(2455)\pi$ and $\Sigma_c^*(2520)\pi$ in intermediate states.
   Phys. Rev. D **95** 114018 (2017).

2. A. J. Arifi, H. Nagahiro, and A. Hosaka.
   Three-body decay of $\Lambda_c^*(2595)$ and $\Lambda_c^*(2625)$ with the inclusion of a direct two-pion coupling.
   Phys. Rev. D **98** 114007 (2018).

3. A. J. Arifi, H. Nagahiro, and A. Hosaka.
   A systematic study of charmed baryon decays.
   JPS Conf. Proc. **26** 022031 (2019).

4. A. J. Arifi, H. Nagahiro, A. Hosaka, and K. Tanida.
   Three-body decay of $\Lambda_c^*(2765)$ and determination of its spin-parity
   Phys. Rev. D **101** 094023 (2020).

5. A. J. Arifi, H. Nagahiro, A. Hosaka, and K. Tanida.
   Roper-like resonances with various flavor contents and their two-pion emission decays.
   Phys Rev D **101** 111502 (R) (2020).

PS: For the reader, if you find any mistakes, please leave me a message. I will update it accordingly and give you the most updated one. e-mail: aj.arifi@yahoo.com

Contents

List of Figures

List of Tables

Part I

Introduction and review

Chapter 1
Introduction

1.1 QCD and quark model

As we may know, atomic nuclei are composed of protons and neutrons. The proton itself is a composite particle made of three quarks which is classified as a hadronic particle. The quarks and gluons inside the hadrons interact strongly to each other governed by a fundamental theory so-called quantum chromodynamics (QCD). The strong interaction is one of the fundamental interactions in nature along with gravitation, electromagnetic, and weak interactions. Even though we have a theory of hadrons, there are many unsolved problems and puzzles in the low-energy regime due to its non-perturbative nature. It can be understood that the strong interaction is described by the strong coupling α_s, which is energy-dependent. Opposite to the electromagnetic interaction, the strong coupling is quite large in the low-energy region. Consequently, we cannot make use of the perturbation theory and therefore we need to construct an alternative model respecting the symmetries of QCD to understand various properties of hadrons in this region.

As mentioned above, one of the most important problems in studying hadrons is how to construct effective models which is suitable at the low-energy regime. The effective models have an important role to give us an intuitive description of hadrons at this regime. In reality, it is quite challenging that one model can explain all properties of hadrons. But, by comparing several models with various experimental observables, we may obtain the relevant description of hadrons or even model-independent relation. Up to now, various effective models such as the quark model, the skryme model, the bag model and so forth have been developed in attempts to explain various hadronic phenomena from different perspectives. In addition, Lattice QCD simulation which is based on the first principle of QCD is also being developed recently following the rise of high-performance computers.

The quark model is one of the successful effective models in explaining various properties of the ground state and the low-lying excited hadrons [1, 2]. In this description, baryons and mesons are composed of three quarks and quark-antiquark pairs, respectively. Despite its success, it is quite problematic to explain the properties of the higher excited hadrons. For example, the quark model predicts a lot of states compared to the observed hadrons in nature, leading to the term called "missing resonances". In the nucleon sector, there is also a well-known state called Roper resonance, $N(1440)$, which is now believed to be a radial excitation state of the nucleon. The mass ordering of this state cannot be explained by the simple quark model. Moreover, there are also some excited states which are not compatible with the quark model expectation. These states are known as the "exotic states". Therefore, it is fair to say that there reside many problems that cannot be answered by the conventional quark model. Now, the questions are to what extent we can use the quark model in studying hadrons and what the next step is to go beyond the quark model.

1.2 Exotic states and heavy baryons

In recent years, there are significant developments in experimental facilities constructed by various collaborations around the world. These experimental facilities are equipped by high-energy accelerators and high precision detectors. Owing to these experimental developments, many new hadrons are discovered recently [3]. With the high-energy beam, new kinds of hadrons containing a heavy quark are also observed in the experiment. These hadrons are usually called heavy hadrons. The charm and bottom quarks are considered as heavy quarks because their masses are considerably larger than the standard QCD scale Λ_{QCD} of around 300 MeV. Because of that, there is an emergence of a new symmetry so-called heavy-quark symmetry that governs the interaction of heavy hadrons [4]. In this symmetry, the heavy quark acts as the static object which is decoupled from the other two light quarks, making the dynamics of heavy hadrons simpler as compared to conventional hadrons such as nucleon. Therefore, heavy hadrons will provide a good place to test effective models in explaining the properties of hadrons with various flavor contents. Understanding the dynamics of heavy hadrons may shed light on the structure of hadrons in general.

In the past decades, heavy hadron spectroscopy is enriched by the discoveries of X, Y, and Z exotic states and also P_c pentaquarks [5–8]. These states are beyond the standard understanding of hadrons which may be in the form of either baryons or mesons. However, the observations of these states tell us that the tetraquarks and pentaquarks, or even multiquark states can exist. Although such states are allowed in QCD, the nature of these states should be clarified in the future. Furthermore, these states are not compatible with the quark model expectations which is mainly due to the opening thresholds. The effect of the opening thresholds is not yet well understood which may be a source of the debate about how we interpret the observed states. In fact, the observed exotics states are generally located near the thresholds. The suitable parameterizations of the experimental data and the more comprehensive models are certainly of importance to advance our knowledge about these states. Of course, the more precise experimental data and measurements of various observables will also help to clarify their nature.

One common thing about the above-mentioned exotic states is that they contain at least one heavy quark. One of the simplest systems containing a heavy quark is a singly heavy baryon. It contains a heavy quark along with two light quarks. As explained before, the opening threshold may influence the properties of the exotic states. This opening threshold is actually due to the creation of a pair of light quark-antiquark which makes the system more complicated. The (singly) heavy baryons will provide an ideal platform to study the dynamics of the light quarks in the heavy quark environments. Hence, studying the heavy baryons may give a hint on the structure of exotic states.

In this dissertation, we study the heavy baryons in particular their excited states within the quark model descriptions. In this manner, the low-lying heavy baryons are investigated to see how the quark model works. By studying this way, we may get to know when the quark model expectation will deviate from the experimental data, and we can think of when we should go beyond the quark model and see the possibility of the exotic states.

1.3 Three-body decays

There are a lot of ways how we can study the heavy baryons, *e.g.* studying their mass spectra, productions, decays, and so on. Among them, three-body decay provides a good place to study heavy baryons because of the additional kinematical variables as compared to two-body decay. Moreover, many heavy baryons mainly decays into three particles such as $\Lambda_c^* \to Lambda_\pi \pi$. Indeed, the experimental groups such as Belle and LHCb have a large amount of experimental data that has not yet released. Moreover, it is rather difficult to conduct the scattering experiments of heavy baryons because their lifetimes are very small. In fact, the exotic states including pentaquarks are recently found by analyzing the three-body decays. This situation stimulates us to study the three-body decay more comprehensively.

In the standard way, the three-body decay is described by a two-dimensional plot so-called Dalitz plot. This Dalitz plot is made by a combination of two invariant masses. Generally, the structure inside the plot contains all information about the underlying decay mechanism from which we can study the structure of heavy baryons. Dalitz plot can be directly compared with the experimental data by which we can testify our theoretical models. We may also deform the shape of the Dalitz plots to which it gives a more clearer picture. Also, studying other related quantities such as invariant mass distribution, projection of Dalitz plot into one of the axis, will be useful to extract the relevant information about the structure.

1.4 Purpose

In this dissertation, we aim to study the structures of heavy baryons through their two-pion emission decays. The heavy baryons are described in the quark model picture and the pion is regarded as a Nambu-Goldstone boson. We will make the use of effective Lagrangians in non-relativistic approximation for actual computations of three-body decay amplitude. The Dalitz plots and other related quantities are investigated to extract the information on their structures from the experimental data.

1.5 Outline

The dissertation is organized as the following:

Part 1: we review the heavy baryons from both the experimental and theoretical sides.

Chapter 2: we review the experimental progress on charmed and bottom baryons separately for each flavor. The heavy baryons are limited to the singly heavy baryons. The baryons with two or more heavy quarks are not discussed in the present work. We also limit our discussions to the strong and radiative decays. We notice that there are many experimental data on weak interactions related to heavy baryons, but they are beyond our scopes.

Chapter 3: the theoretical perspectives in attempts to elucidate the observed heavy baryons are reviewed. First, we explain the general properties of heavy baryons. Then, we discuss the various theoretical models which have been proposed and the interpretations of each heavy baryons according to those models.

Part 2: we introduce our formulations used in the present study.

Chapter 4: the basic formulation of the quark model is explained. We explain the heavy baryon wave function in the quark model description and their interaction between pion and quark. The concrete calculation of the amplitude of heavy baryons decays is discussed in detail.

Chapter 5: the effective Lagrangian is formulated to calculate the three-body decay amplitudes. The non-relativistic reduction is performed and the spin transfer matrices are introduced. We also show how to extract the coupling strength from the quark model.

Chapter 6: Dalitz plots and three-body decay kinematics are introduced. The various relations related to Dalitz plots are also explained.

Part 3: The results of our studies are presented and discussed.

Chapter 7: we start the investigation by considering the sequential processes going through $\Sigma_c^{(*)}$ in intermediate states for the low-lying charmed baryon resonances, $\Lambda_c^*(2595)$ and $\Lambda_c^*(2625)$. Here, we will discuss how the invariant mass distributions are useful to distinguish the internal structures of heavy baryons.

Chapter 8: We take into account the direct process for $\Lambda_c^*(2595)$ and $\Lambda_c^*(2625)$ decays. We propose to study the angular correlations to further clarify the role of the direct process especially for $\Lambda_c^*(2625)$ decay. This direct process is closely related to the chiral partner structures of light diquarks inside the heavy baryons.

Chapter 9: The comprehensive analysis is performed in order to determine the spin and parity of the $\Lambda_c^*(2765)$ baryon. The Dalitz plots have been made for various spin and parity assignments, and the convolution of the Dalitz plots have been also made. It turns out that the ratio and the angular correlations are the keys to spin and parity determination.

Chapter 10: We discuss the newly observed $\Lambda_b^*(6072)$ as a Roper-like resonance. We show that the Dalitz plots and other related quantities are consistent with the experimental data. The result implis that there is a flavor-independent nature of the Roper-like resonance, which is the first radial excitation of baryons with spin and parity $J^P = 1/2^+$.

Part 4: We summarize the results and discuss the future prospects of our studies.

Chapter 11: We summarize and discuss the possible interpretations of our results. Then, we will give some remarks and messages on the structure of heavy baryons studied from the two-pion emission decays. Also, we will discuss some parts of our investigations which are not yet done in this study and some possible natural extensions.

"The begining is the most important part of the work", Pluto

Chapter 2
Experimental progresses

In this chapter, we shall review the experimental status of observed heavy baryons so far. We focus on the review of the charmed and bottom baryons which contain only one heavy quark. This is one of the simplest systems containing a heavy quark. As we may wonder, there are also heavy baryons with more than one heavy quark as shown in Fig. 2.1, however, they are beyond our scope. There also exists the heaviest quark, namely top quark, but we will not discuss here. It is because the top quark decay through weak interaction before it forms hadronic particles. Moreover, we mainly cover the strong decay of heavy baryons, the weak decay of ground state heavy baryons are not covered here. Before going further, the interested reader may visit Refs [1, 3, 9–16] for the detail review on heavy baryons.

As we may realize later, the observed heavy baryon resonances have relatively narrow decay widths compared to light baryons such as nucleon or hyperon resonances. For example, the $1/2^-$ and $3/2^-$ states in the Λ baryons, $\Lambda(1405)$ and $\Lambda(1520)$ have widths of about 50 MeV and 15 MeV, respectively, while the analogue states in the charm sector, $\Lambda_c(2593)$ and $\Lambda_c(2625)$ have widths of around 2.5 MeV and < 1.0 MeV, respectively. This sort of situation gives the advantage to study them experimentally. Thanks to the narrow width, it is experimentally easy to discover heavy baryons and measure various properties.

Many of the excited states of heavy baryons are discovered e^+e^- collider experiments such as CLEO, Belle, and BaBar. Historically, CLEO discovered the low-lying excited states while the next generation B-factory experiments discovered higher excited states. Very recently, LHCb also joins the spectroscopy of charmed and bottom baryons. Because of the continuous developments of experimental facilities, the interest of the heavy baryon physics has been increased recently. Furthermore, we expect a lot of new states will be discovered by the current facilities in the near future.

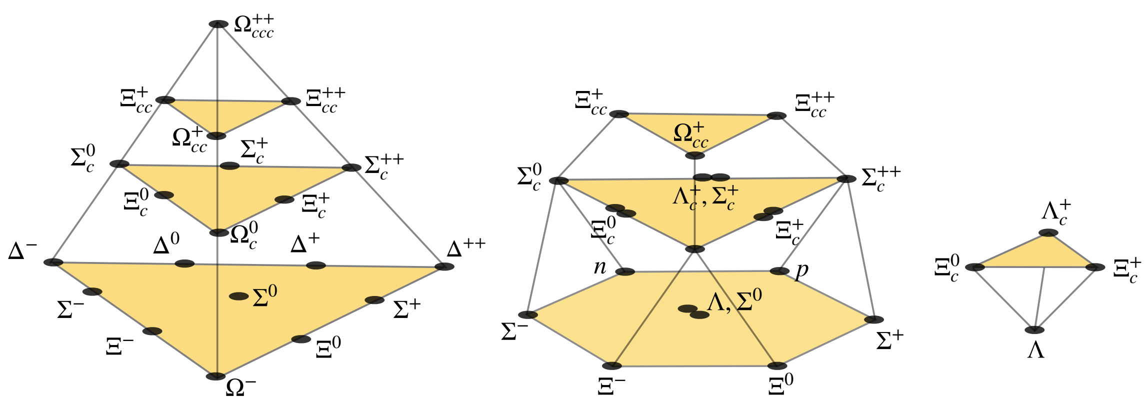

Figure 2.1. SU(4) multiplet of baryons made of u, d, s, and c quarks. The figure is adopted from PDG. In this work, we focus on heavy baryon containing one heavy quark.

2.1 Experimental facilities

When we are talking about the experiment for the heavy-baryon production, we will find that heavy baryons are usually studied in B-factory. The B-factory experiment is an electron-positron collider experiment that is originally designed to test the CP violation by studying B-meson decays, not for studying heavy baryons. However, it is later found that the huge amount of B meson decay and e^+e^- collision data can be used to study heavy baryons. In such experiments, the electron-positron collide at *c.m.* energy of around 11 GeV and an excited bottomonium state $\Upsilon(4S)$ is produced which subsequently decays mainly into a B and anti B meson pair as described in Fig. 2.2. This is the origin of the name B-factory.

There are two B-factory experimental facilities built around the 1990s. One is the Belle experiment at the KEKB in Tsukuba, Japan and the other one is the BaBar experiment which is built at SLAC laboratory, California, US. Both experiments have completed the data collection around 2010. However, it does not mean that the experiments have been stopped. Now, there are still many ongoing analyses of the existing data and the results will be reported in the near future. The next-generation of B-factories have been proposed and to be built after 2010. However, some of them have been canceled or they are not approved yet. In Japan, on the other hand, an upgrade of the Belle experiment, so-called Belle II experiment, has been approved and then constructed around 2018. It is worth noting that these experiments are mostly used for the charmed baryon.

In addition to B factories, there is the LHCb experiment at the LHC, Europe, which started the operation in 2010 and is currently active in collecting the experimental data. Although this LHCb experiment is studying hadrons containing the bottom quark, it is not considered as a B factory. It is because they are using a proton-proton collider experiment and it is not solely for studying the physics of hadrons with bottom quark. Thanks to high-energy beam, the bottom baryon can be studied and many excited stated of bottom baryons are discovered recently in this LHCb experiment.

We note that heavy baryons are mainly produced from the decay of B meson and the fragmentation of $c\bar{c}$ (or $b\bar{b}$ for bottom baryon) from pp or e^-e^+ collision. For B meson decay, the analysis of the spin determination is relatively easy due to the spin 0 of Bmeson. For the latter one, the production rate is much higher but they suffer a high level of background.

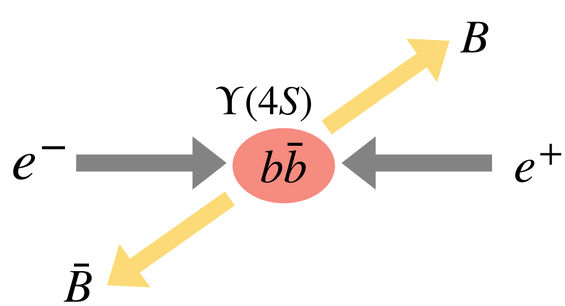

Figure 2.2. The illustration of B-meson production in B factory experiment. The B-meson is produced by the collision of asymmetric energy e^+e^-.

2.2 Charmed baryon

In this section, we review the charmed baryons. Up to now about 20 states have been discovered. Among them, all ground states of charmed baryons have been established experimentally. However, the higher excited state are not well established despite the several experiments have been done. Here, we shall review them for each baryon separately in the following.

2.2.1 Λ_c family

Λ_c baryon is an isospin-0 charmed baryon consisted of udc quarks. The ground state of Λ_c is firstly discovered by Fermilab in 1976 [17]. The most precise measurement of its mass was performed by BaBar in 2005 [18]: $m_{\Lambda_c} = (2286.46 \pm 0.14)$ MeV, which is later adopted by PDG. Most of the Λ_c excited states are discovered before the B-factory experiments. In recent years, the higher excited states are observed by B-factories and LHCb.

The observed Λ_c^+ baryons are listed in Table 2.1. They are observed in $\Lambda_c^+\pi^+\pi^-$ and pD^0 invariant masses. The first two excited states $\Lambda_c(2595)^+$ and $\Lambda_c(2625)^+$ are the first orbital excitations. However, the spin and parity are determined by the quark model, not yet measured experimentally. These states has been observed in numerous experiments [19–25].

Table 2.1. Mass spectra and widths of Λ_c^+ with their decay modes.

State	J^P	Mass (MeV)	Width (MeV)	Decay modes	Refs
Λ_c^+	$\frac{1}{2}^+$	2286.46 ± 0.14	-	Weak	Fermilab [17]
$\Lambda_c(2595)^+$	$\frac{1}{2}^-$	2592.25 ± 0.28	2.6 ± 0.6	$\Lambda_c\pi\pi,\ \Sigma_c\pi$	CLEO [23]
$\Lambda_c(2625)^+$	$\frac{3}{2}^-$	2628.11 ± 0.19	< 0.97	$\Lambda_c\pi\pi,\ \Sigma_c\pi$	ARGUS [19]
$\Lambda_c(2765)^+$	$?^?$	2766.6 ± 2.4	50	$\Lambda_c\pi\pi,\ \Sigma_c^{(*)}\pi$	CLEO [26]
$\Lambda_c(2860)^+$	$\frac{3}{2}^+$	$2856.1^{+2.3}_{-6.0}$	68^{+12}_{-22}	pD^0	LHCb [27]
$\Lambda_c(2880)^+$	$\frac{5}{2}^+$	2881.63 ± 0.24	$5.6^{+0.8}_{-0.6}$	$\Lambda_c\pi\pi,\ \Sigma_c^{(*)}\pi,$	CLEO [26]
				pD^0	BaBar [28]
$\Lambda_c(2940)^+$	$\frac{3}{2}^-$	$2939.6^{+1.3}_{-1.5}$	20^{+6}_{-5}	$\Lambda_c\pi\pi,\ \Sigma_c^{(*)}\pi,$	Belle [29]
				pD^0	BaBar [28]

The spin and parity of the higher excited states of Λ_c^+ are still not well determined. Moreover, there are many quark model states predicted in this mass regions and there are several opening thresholds nearby. More analysis needs to be done to resolve the problems. The $\Lambda_c(2765)^+$ state is firstly found by CLEO [26]. Recently, Belle determine the isospin of $\Lambda_c(2765)^+$ to be zero [30]. Before that, it is not resolved whether it is a Σ_c or Λ_c state. However, the spin-parity determination is still underway [31]. Despite the clear existence of $\Lambda_c(2765)^+$, PDG still regards it as a one-star resonance [1].

The new $\Lambda_c(2860)^+$ is observed by LHCb in pD^0 invariant mass [27]. However, its existence needs to be confirmed by other experiments in pD^0 and also $\Lambda_c^+\pi^+\pi^-$ invariant masses. If it does exist, this resonance can be naturally assigned as $3/2^+$ which is a D-wave partner of $\Lambda_c(2880)^+$ with $5/2^+$. Note that the spin 5/2 of $\Lambda_c(2880)^+$ is determined by analyzing its decay angular distributions of $\Sigma_c(2455)\pi$ by Belle [29]. The last $\Lambda_c(2940)^+$ is reported by Belle, BaBar, and LHCb [27–29]. LHCb claims that its spin-parity of $3/2^-$ is favored. However, the higher spin-parity such as 7/2 can not be ruled out.

2.2.2 Σ_c family

Σ_c baryons are composed of the c quark and two ud quarks with an isospin one resulting in isotriplet of Σ_c. There are two ground state of Σ_c, namely $\Sigma_c(2455)$ and $\Sigma_c(2520)$. They are a heavy quark spin doublet with spin-parity $1/2^+$ and $3/2^+$ with brown muck spin $j = 1$. Both ground states are found before B-factory experiments. The higher excited state $\Sigma_c(2800)$ is discovered by Belle and BaBar. The observed Σ_c states are summarized in Table 2.2.

The ground state $\Sigma_c(2455)$ is unique compared to Σ in the strange sector, that $\Sigma_c(2455)$ can decay strongly to $\Lambda_c\pi$. $\Sigma_c(2455)^{++}$ and $\Sigma_c(2455)^+$ are firstly observed by BNL in 1975 [32]. The neutral $\Sigma_c(2455)^0$ is later found by BEBC in 1980 [33]. Later it is confirmed by CLEO [34]. This states has been observed in many experiments [35–43]. In the last decade, new measurements have been conducted by CDF [24] with more precise experimental instruments. The $\Sigma_c(2455)$ state is confirmed by B-factory experiments: Belle[44] and BaBar[45]. The spin of $\Sigma_c(2455)$ state is measured by analyzing the angular correlations in $B \to \Lambda_c\bar{p}\pi$ decay performed by BaBar[45]. The result fit favors spin 1/2 hypothesis. The helicity of $\Sigma_c(2455)$ is fixed to be 1/2 due to the helicity conservation and the fact that the B-meson has spin 0 and proton has spin 1/2.

The ground state $\Sigma_c(2520)^{++}$ is firstly discovered by SKAT in 1993 [46]. Later, isotriplet $\Sigma_c(2520)$ states are discoved by CLEO [40, 47, 49]. The more precise measurement is done by CDF [24] and Belle [44]. However, it is not seen in BaBar analysis [45]. The spin-parity of $\Sigma_c(2520)$ is not measured yet in the experiment. Both $\Sigma_c(2455)$ and $\Sigma_c(2520)$ states are found in $\Lambda_c\pi$ invariant mass implying that they are indeed isotriplet states.

The highest state of isotriplet $\Sigma_c(2800)$ which is rather a broad state is discovered by Belle in 2005 [48]. The $\Sigma_c(2800)$ state is seen in $\Lambda_c\pi$ confirming that it is isotriplet state. It is also found that there is no peak corresponding to $\Lambda_c/\Sigma_c(2765)$ in $\Lambda_c\pi$ indicating that it is Λ_c state [48]. The $\Sigma_c(2800)$ state is later confirmed in $B \to \Lambda_c\bar{p}\pi$ by BaBar [45]. The observed mass has a discrepancy compared to the one measured by Belle. The measured mass by BaBar is $(2846 \pm 8 \pm 10)$ MeV and it is 3σ away from Belle. It could be a distinct state, but, for now, it is considered to be the same state. Furthermore, it is not enough statistics to perform angular analysis for this state. Belle II experiment is expected to have enough statistics to analyze this decay channel to measure the spin of $\Sigma_c(2800)$. So far $\Sigma_c(2800)$ is not seen in $\Lambda_c\pi\pi$ invariant mass, it is only seen in $\Lambda_c\pi$ invariant mass. In fact, the quark model calculation predicts several states in this mass region. With upgraded experimental

Table 2.2. Mass spectra and widths of Σ_c with their decay modes.

State	J^P	Mass (MeV)	Width (MeV)	Decay modes	Refs
$\Sigma_c(2455)^{++}$		2453.97 ± 0.14	$1.89^{+0.09}_{-0.18}$	$\Lambda_c^+\pi^+$	BNL [32]
$\Sigma_c(2455)^{+}$	$\frac{1}{2}^+$	2452.9 ± 0.4	< 4.6	$\Lambda_c^+\pi^0$	TST [33]
$\Sigma_c(2455)^{0}$		2453.75 ± 0.14	$1.83^{+0.11}_{-0.19}$	$\Lambda_c^+\pi^-$	BNL [32]
$\Sigma_c(2520)^{++}$		$2518.41^{+0.21}_{-0.19}$	$14.78^{+0.30}_{-0.40}$	$\Lambda_c^+\pi^+$	SKAT [46]
$\Sigma_c(2520)^{+}$	$\frac{3}{2}^+$	2517.4 ± 2.3	< 17	$\Lambda_c^+\pi^0$	CLEO [47]
$\Sigma_c(2520)^{0}$		2518.48 ± 0.20	$15.3^{+0.4}_{-0.5}$	$\Lambda_c^+\pi^-$	CLEO [40]
$\Sigma_c(2800)^{++}$		2801^{+4}_{-6}	75^{+22}_{-17}	$\Lambda_c^+\pi^+$	Belle [48]
$\Sigma_c(2800)^{+}$	$?^?$	2792^{+14}_{-5}	62^{+60}_{-40}	$\Lambda_c^+\pi^0$	Belle [48]
$\Sigma_c(2800)^{0}$		2806^{+5}_{-7}	72^{+22}_{-15}	$\Lambda_c^+\pi^-$	Belle [48]

facilities, we expect the nature of $\Sigma_c(2800)$ state would be revealed in the near future.

2.2.3 Ξ_c family

Ξ_c baryons are composed of cs quarks and one u or d quark. Five Ξ_c states were observed prior to the B-factory experiments: ground state Ξ_c, and the doublets: $\Xi_c', \Xi_c(2645)$, and another P-wave doublet: $\Xi_c(2790)$, and $\Xi_c(2815)$. The B-factory experiments have established three new excited Ξ_c states. Recently, LHCb discovered several new Ξ_c states in $\Lambda_c K$ invariant mass. The observed Ξ_c states are summarized in Table. 2.3.

The Ξ_c^+ ground state was first observed by CERN in 1983 [50]. Its isospin partner Ξ_c^0 was discovered later in the $\Xi^-\pi^+$ final states by the CLEO in 1988 [51]. Meanwhile, the Ξ_c' isospin doublet is discovered by CLEO in 1998 by analyzing their electromagnetic decay $\Xi_c\gamma$ [52]. These two resonances are the flavor symmetric partner of Ξ_c. The mass difference between Ξ_c and Ξ_c' us too small to allow the strong decay $\Xi_c' \to \Xi_c\pi$. The only allowed decay modes between them are the radiative decays, which were the observed channels. Around 1995, the $\Xi_c(2645)$ state was reported by the CLEO [53, 54] and later reported by E687 [62]. Belle confirmed these resonances with more precise mass measurements in [59, 63] and recently in 2016 [64]. Although its spin-parity has not been measured, $\Xi_c(2645)$ was identified to be $J^P = 3/2^+$ state.

The two excited Ξ_c states $\Xi_c(2790)$ and $\Xi_c(2815)$ were first observed by the CLEO. The $\Xi_c(2790)$ was observed in the decay $\Xi_c'\pi$ by CLEO [55] and confirmed by Belle [59, 64]. Then, the $\Xi_c(2815)$ were also observed by CLEO in the decays into $\Xi_c\pi^+\pi^-$ via the intermediate states $\Xi_c(2645)$ respectively [56] and Belle confirmed their existence [59]. In 2016, more precise measurement is done by Belle [64].

Table 2.3. Mass spectra and widths of Ξ_c and Ξ_c' with their decay modes.

States	J^P	Mass (MeV)	Width (MeV)	Decay modes	Refs
Ξ_c^+	$\frac{1}{2}^+$	$2467.94^{+0.17}_{-0.20}$	-	Weak	CERN [50]
Ξ_c^0		$2470.90^{+0.22}_{-0.29}$	-	Weak	CLEO [51]
$\Xi_c'^+$	$\frac{1}{2}^+$	2578.4 ± 0.5	-	$\Xi_c\gamma$	CLEO [52]
$\Xi_c'^0$		2579.2 ± 0.5	-	$\Xi_c\gamma$	CLEO [52]
$\Xi_c(2645)^+$	$\frac{3}{2}^+$	$2645.56^{+0.24}_{-0.30}$	2.14 ± 0.19	$\Xi_c\pi$	CLEO [53]
$\Xi_c(2645)^0$		$2646.38^{+0.20}_{-0.23}$	2.35 ± 0.22	$\Xi_c\pi$	CLEO [54]
$\Xi_c(2790)^+$	$\frac{1}{2}^-$	2792.4 ± 0.5	8.9 ± 1.0	$\Xi_c'\pi$	CLEO [55]
$\Xi_c(2790)^0$		2794.1 ± 0.5	10.0 ± 1.1	$\Xi_c'\pi$	CLEO [55]
$\Xi_c(2815)^+$	$\frac{3}{2}^-$	$2816.74^{+0.20}_{-0.23}$	2.43 ± 0.26	$\Xi_c\pi\pi, \Xi_c^*\pi,$	CLEO [56]
				$\Xi_c'\pi$	CLEO [55]
$\Xi_c(2815)^0$		$2820.25^{+0.25}_{-0.31}$	2.54 ± 0.25	$\Xi_c\pi\pi, \Xi_c^*\pi,$	CLEO [56]
				$\Xi_c'\pi$	CLEO [55]
$\Xi_c(2923)^0$	$?^?$	2923.04 ± 0.25	7.1 ± 0.8	$\Lambda_c\bar{K}$	LHCb [57]
$\Xi_c(2939)^0$	$?^?$	2938.55 ± 0.21	10.2 ± 0.8	$\Lambda_c\bar{K}$	LHCb [57]
$\Xi_c(2965)^0$	$?^?$	2964.88 ± 0.26	14.1 ± 0.9	$\Lambda_c\bar{K}$	LHCb [57]
$\Xi_c(2970)^+$	$?^?$	$2966.34^{+0.17}_{-1.00}$	$20.9^{+2.4}_{-3.5}$	$\Lambda_c\bar{K}\pi, \Sigma_c\bar{K},$	Belle [58]
				$\Xi_c\pi\pi$	Belle [59]
$\Xi_c(2970)^0$		$2970.9^{+0.4}_{-0.6}$	$28.1^{+3.4}_{-4.0}$	$\Lambda_c\bar{K}\pi, \Sigma_c\bar{K},$	Belle [58]
				$\Xi_c\pi\pi$	Belle [59]
$\Xi_c(3055)^+$	$?^?$	3055.9 ± 0.4	7.8 ± 1.9	$\Lambda_c\bar{K}\pi, \Sigma_c\bar{K},$	BaBar [60]
				$D\Lambda$	Belle [61]
$\Xi_c(3080)^+$	$?^?$	3077.0 ± 0.4	3.6 ± 1.1	$\Lambda_c\bar{K}\pi, \Sigma_c^{(*)}\bar{K},$	Belle [58]
				$D\Lambda$	Belle [61]
$\Xi_c(3080)^0$		3079.9 ± 1.4	5.6 ± 2.2	$\Lambda_c\bar{K}\pi, \Sigma_c^{(*)}\bar{K},$	Belle [58]
				$D\Lambda$	Belle [61]
$\Xi_c(3123)^+$	$?^?$	3122.9 ± 1.3	4.4 ± 3.8	$\Lambda_c\bar{K}\pi, \Sigma_c^*\bar{K}$	BaBar [60]

Both $\Xi_c(2790)$ and $\Xi_c(2815)$ states were interpreted as the charmed strange partner of the $\Lambda_c(2595)^+$ and $\Lambda_c(2625)^+$.

The $\Xi_c(2930)^0$ state was seen in the $\Lambda_c^+ K^-$ invariant mass in $B \to \bar{\Lambda}_c^- \Lambda_c^+ K^-$ decay by BaBar[65]. This Dalitz plot and its projection to $\Lambda_c^+ K^-$ support this resonance as shown. It is also confirmed recently by Belle [66]. Recently LHCb made a measurement on $\Lambda_c K$ invariant mass with better statistics [57]. As a result, several Ξ_c states are found and two of them, $\Xi_c(2923)$ and $\Xi_c(2935)$, could be related to previously observed $\Xi_c(2930)$ state.

In 2006, the Belle Collaboration reported a new charmed strange baryons, $\Xi_c(2970)$, decaying into $\Lambda_c^+ K^- \pi^+$ and $\Lambda_c^+ K_c^0 \pi^-$ [58]. The $\Xi_c(2970)$ was confirmed later by Belle in its decay into $\Xi_c(2645)\pi$[59]. In 2016, more precise measurement is done by Belle [64]. However, it is not seen in $\Lambda_c^+ K^-$ invariant mass by BaBar[65]. Later, this state is confirmed in $\Lambda_c^+ K^- \pi^+$ invariant mass by BaBar in 2008 [60]. Also, the $\Xi_c(2965)$ state is discovered recently whose mass is very close to the $\Xi_c(2970)$ [57]. But, their decay widths are significantly different implying that they could be distinct particles.

In 2008, the $\Xi_c(3055)$ is reported by BaBar in $\Lambda_c^+ K^- \pi^+$ invariant mass [60]. Later in 2014, the $\Xi_c(3055)$ state is confirmed by Belle in $\Lambda_c^+ K^- \pi^+$ invariant mass with higher statistics [63]. Recently, the $\Xi_c(3055)$ is studied in ΛD channel by Belle [61] and measure the branching ratio

$$\frac{\mathcal{B}(\Xi_c(3055)^+ \to \Lambda D^+)}{\mathcal{B}(\Xi_c(3055)^+ \to \Sigma_c^{++} K^-)} = 5.09 \pm 1.01 \pm 0.76. \tag{2.1}$$

In 2006, the $\Xi_c(3080)$ is reported along with $\Xi_c(2970)$, decaying into $\Lambda_c^+ K^- \pi^+$ and $\Lambda_c^+ K_c^0 \pi^-$[58]. In 2008, the $\Xi_c(3080)$ is also reported by BaBar in $\Lambda_c^+ K^- \pi^+$ invariant mass [60]. Later in 2014, the $\Xi_c(3080)$ state is confirmed by Belle in $\Lambda_c^+ K^- \pi^+$ invariant mass [63]. Recently, the $\Xi_c(3055)$ is studied in ΛD channel by Belle [61] and measure the branching ratio

$$\frac{\mathcal{B}(\Xi_c(3080)^+ \to \Lambda D^+)}{\mathcal{B}(\Xi_c(3080)^+ \to \Sigma_c^{++} K^-)} = 1.29 \pm 0.30 \pm 0.15, \tag{2.2}$$

$$\frac{\mathcal{B}(\Xi_c(3080)^+ \to \Sigma_c^{*++} K^-)}{\mathcal{B}(\Xi_c(3080)^+ \to \Sigma_c^{++} K^-)} = 1.07 \pm 0.27 \pm 0.01. \tag{2.3}$$

The $\Xi_c(3123)$ is also reported by BaBar [60]. However, it is not seen in the latest Belle report [63]. This resonance still has a one-star rating in PDG. The quantum numbers for all these excited Ξ_c states have not been determined yet. More experimental information is required to constrain the allowed possibilities.

2.2.4 Ω_c family

Ω_c baryons are composed of a c quark and two s quarks with isospin 0. The ground states have been established and there are several excited states observed which are possibly related to the p-wave excitations. The observed Ω_c baryons are summarized in Table. 2.4.

The Ω_c^0 ground state was first reported in 1985 by the experiment WA62 [67] prior to the B-factories. BaBar observed the spin partner $\Omega_c(2770)^0$ in the $\Omega_c\gamma$ final state [68]. In 2009, the Belle Collaboration provided a more precise mass measurement of the Ω_c[69].

In the same experiment of Belle, the excited state $\Omega_c(2770)^0$ was also reconstructed in the $\Omega_c^0\gamma$ mode[69]. This resonance $\Omega_c(2770)^0$ was originally discovered by BaBar in the same channel [68]. Such a mass difference is too small for any hadronic strong decay to occur. Although its J^P has not been measured, the $\Omega_c(2770)^0$ was predicted to be the $J^P = 3/2^+$ partner of the $\Sigma_c(2520)$.

LHCb observed 5 excited Ω_c states $\Omega_c(3000)^0, \Omega_c(3050)^0, \Omega_c(3065)^0, \Omega_c(3090)^0$, and $\Omega_c(3120)^0$, in the $\Xi_c^+K^-$ final state (The evidence of $\Omega_c(3188)^0$ was also reported, but it is not significant)[70]. Belle confirmed the existence of these states except for $\Omega_c(3120)^0$[71]. Naively, five excited Ω_c states are expected (one $1/2^-$, two $3/2^-$, and $5/2^-$) in the P-wave state as the spin of the two strange quarks is one. Some of these newly discovered states should correspond to these P-wave states.

Table 2.4. Mass spectra and widths of Ω_c with their decay modes.

States	J^P	Mass (MeV)	Width (MeV)	Decay modes	Refs
Ω_c^0	$\frac{1}{2}^+$	2695.2 ± 1.7	-	Weak	WA62 [67]
$\Omega_c^0(2770)$	$\frac{3}{2}^+$	2765.9 ± 2.0	-	$\Omega\gamma$	BaBar [68]
$\Omega_c^0(3000)$	$?^?$	3000.41 ± 0.22	4.5 ± 0.7	$\Xi_c K$	LHCb [70]
$\Omega_c^0(3050)$	$?^?$	3050.20 ± 0.13	< 1.2	$\Xi_c K$	LHCb [70]
$\Omega_c^0(3066)$	$?^?$	3065.46 ± 0.28	3.5 ± 0.4	$\Xi_c K$	LHCb [70]
$\Omega_c^0(3090)$	$?^?$	3090.0 ± 0.5	8.7 ± 1.3	$\Xi_c K$	LHCb [70]
$\Omega_c^0(3120)$	$?^?$	3119.1 ± 1.0	< 2.6	$\Xi_c K$	LHCb [70]

2.3 Bottom baryon

In this section, we review the bottom baryons. All the ground state bottom baryons have been observed, except the Ω_b^* of $J^P = 3/2^+$. Hence, we only list their averaged masses and widths from PDG together with the experiments first observing them, but we note that not all of them are well known. Recently, the bottom baryons are mainly discovered by LHCb experiments. Here, we shall review the baryon for each flavor separately in the following.

2.3.1 Λ_b family

Λ_b baryon consists of u, d, and b quark. Even though the ground states have been reported in 1981 by CERN R415 Collaboration [72], not many observations of the excited states until the LHCb began their operations. Now, it seems that the number of excited states is similar to its charm counterpart Λ_c baryon. The observed Λ_b baryons are summarized in Table. 2.5.

In 2012, the negative parity doublet, the $\Lambda_b(5912)^0$ of $1/2^-$ and the $\Lambda_b(5920)^0$ of $3/2^-$, were first reported by LHCb [73] in the $\Lambda_b^0\pi^+\pi^-$ invariant mass. Later, the $\Lambda_b(5920)^0$ was confirmed by the CDF Collaboration [74]. We may notice that the mass difference is about 8 MeV which is much smaller than of Λ_c negative parity doublet. This is understood by the spin-dependent interaction is suppressed as the heavy quark mass increases under the heavy-quark symmetry. Furthermore, both states have a very narrow width, less than 1 MeV. This is mainly because the $\Sigma_b^{(*)}$ channel is kinematically closed. Therefore, the main contribution is from the non-resonant process and hence the width is small.

Very recently, the $\Lambda_b(6072)$ is observed by CMS [75] and it is confirmed and reanalized by LHCb [76]. It is expected to be a radial excited state with spin-parity $1/2^+$ from the excitation energy. It also bears a resemblance with $\Lambda_c(2765)$ whose width is quite broad around 70 MeV. In this dissertation, we discuss that it is most likely $1/2^+$ by studying its three-body decay. In contrast to the negative parity states, the decay of this state is dominated by the $\Sigma_b^{(*)}$ resonant processes.

The $\Lambda_b(6146)$ and $\Lambda_b(6152)$ baryons are observed by LHCb in 2019 [77] which are expected to a D-wave doublet if we analyze their mass. However, further investigation is still needed from their decay properties to clarify their nature. It is also important to note that, the decay width of Λ_b is relatively smaller than Λ_c, except for $\Lambda_b(6072)$. It could show a hint for a flavor-independent nature of the radial excited state.

Table 2.5. Mass spectra and widths of Λ_b^0 with their decay modes.

State	J^P	Mass (MeV)	Width (MeV)	Decay modes	Refs
Λ_b^0	$\frac{1}{2}^+$	5619.51 ± 0.23	-	Weak	CERN [72]
$\Lambda_b(5912)^0$	$\frac{1}{2}^-$	5912.21 ± 0.03	< 0.25	$\Lambda_b\pi\pi$	LHCb [73]
$\Lambda_b(5920)^0$	$\frac{3}{2}^-$	5920.11 ± 0.02	< 0.19	$\Lambda_b\pi\pi$	LHCb [73]
$\Lambda_b(6072)^0$	$?^?$	6072.3 ± 2.9	72 ± 11	$\Lambda_b\pi\pi,\ \Sigma_b^{(*)}\pi$	CMS [75]
$\Lambda_b(6146)^0$	$?^?$	6146.17 ± 0.33	2.9 ± 1.3	$\Lambda_b\pi\pi,\ \Sigma_b^{(*)}\pi$	LHCb [77]
$\Lambda_b(6152)^0$	$?^?$	6152.51 ± 0.26	2.1 ± 0.8	$\Lambda_b\pi\pi,\ \Sigma_b^{(*)}\pi$	LHCb [77]

2.3.2 Σ_b family

The Σ_b baryons are made of u, d, and b quark with isospin 1. Similar to Σ_c, the ground state doublet of Σ_b are observed and one state of a possibly p-wave state is also observed. However, only charged Σ_b are observed while the neutral state remains unobserved. Also, the mass difference between the different charge states seems quite large around 5 MeV compared to the Σ_c baryons which are around 1 MeV. The Σ_b baryon observed in experiments are tabulated in Table 2.6.

The two ground state Σ_b baryons, were discovered in the $\Lambda_b^0\pi$ invariant mass by CDF [78] in 2007. Later they confirmed them with better statistics [79]. In 2018, the more precise measurement is done by LHCb [80]. Still, no measurement has been done so far for the neutral state of $\Sigma_b^{(*)}$.

Along with the precise measurement of ground state Σ_b, LHCb also reported the excited state of $\Sigma_b(6097)$ [80]. This resonance is relatively broad around 30 MeV. Since the quark model predict many several states in this energy region which also happen to Ξ_b and Ω_b states, two adjacent state scenario can not be ruled out.

Table 2.6. Mass spectra and widths of Σ_b with their decay modes.

State	J^P	Mass (MeV)	Width (MeV)	Decay modes	Refs
$\Sigma_b(5810)^+$	$\frac{1}{2}^+$	5810.55 ± 0.11	4.83 ± 0.31	$\Lambda_b^0\pi^+$	CDF [78]
$\Sigma_b(5810)^-$		5815.64 ± 0.14	5.33 ± 0.42	$\Lambda_b^0\pi^-$	CDF [78]
$\Sigma_b(5830)^+$	$\frac{3}{2}^+$	5830.28 ± 0.14	9.34 ± 0.47	$\Lambda_b^0\pi^+$	CDF [78]
$\Sigma_b(5830)^-$		5834.73 ± 0.17	10.68 ± 0.60	$\Lambda_b^0\pi^-$	CDF [78]
$\Sigma_b(6097)^+$	$?^?$	6095.8 ± 1.7	31.0 ± 5.5	$\Lambda_b^0\pi^+$	LHCb [80]
$\Sigma_b(6097)^-$		6098.0 ± 1.7	28.9 ± 4.2	$\Lambda_b^0\pi^-$	LHCb [80]

2.3.3 Ξ_b family

The Ξ_b baryon consists of three different quarks: up or down, strange, and bottom quarks. This baryon has not yet explored enough as only one excited state $\Xi_b(6227)$ observed, along with the ground state Ξ_b and Ξ_b'. The number of excited states is too few compared to the Ξ_c case in the charm sector as shown in Table 2.7.

The Ξ_b ground state was reported by the DELPHI in 1995 [81]. Almost twenty years later, the Ξ_b' state of $1/2^+$ was firstly observed in the $\Xi_b^0\pi^-$ invariant mass by LHCb [82] and the Ξ_b' partner with $3/2^+$ $\Xi_b(5945)^0$ was observed two years before, in 2012, by CMS [83]. Another state, $\Xi_b^*(5955)^-$, was later observed by the LHCb [82] and it is believed as the charged partner of $\Xi_b(5945)^0$ despite some discrepancies in their masses.

In 2018 the $\Xi_b(6277)^-$ was observed by the LHCb in $\Xi_b\pi$ and $\Lambda_b K$ invariant mass [84]. This state could be the p-wave excited state of Ξ_b' baryon, and again there should be several states appear in this energy region. In the charm sector, three states are discovered in $\Lambda_c K$. Therefore, further investigation with higher statistics is certainly needed.

It is worth noting that the excited states of Ξ_b are not found at all. By simply changing the flavor from charm to bottom for Ξ baryons, we expect there will be some reports for the negative parity doublet, radial excited states, and so forth by LHCb in the near future. These states are possibly found in $\Xi_b\pi\pi$ invariant mass.

Table 2.7. Mass spectra and widths of Ξ_b and Ξ_b' with their decay modes.

States	J^P	Mass (MeV)	Width (MeV)	Decay modes	Refs
Ξ_b^0	$\frac{1}{2}^+$	5791.9 ± 0.5	-	Weak	DELPHI [81]
Ξ_b^-		5797.0 ± 0.9	-	Weak	DELPHI [81]
$\Xi_b^{\prime -}$	$\frac{1}{2}^+$	5935.02 ± 0.05	< 0.08	$\Xi_b\pi$	LHCb [82]
$\Xi_b(5945)^0$	$\frac{3}{2}^+$	5952.3 ± 0.9	0.90 ± 0.18	$\Xi_b\pi$	CMS [83]
$\Xi_b(5955)^-$		5955.33 ± 0.13	1.65 ± 0.33	$\Xi_b\pi$	LHCb [82]
$\Xi_b(6227)^-$	$?^?$	6226.9 ± 2.0	18.1 ± 5.4	$\Xi_b\pi$,	LHCb [84]
				$\Lambda_b K$	LHCb [84]

2.3.4 Ω_b family

The Ω_b^- baryon consists of two strange and bottom quarks belong to symmetric multiplet. The observed Ω_b^- baryons are summarized in Table. 2.8. Up to now, only Ω_b^- ground state of $1/2^+$ is observed so far by the $D\emptyset$ Collaboration [85]. But, the Ω_b^- partner with $J^P = 3/2^+$ is not reported by any experiments. Similar to the charm sector, the Ω_b^- with $J^P = 3/2^+$ can be discovered by analyzing the radiative decay. In 2020, LHCb surprisingly reported several adjacent excited states of Ω_b^- [86]. This situation is very similar to the Ω_c^0 baryon, and show the hyperfine splitting phenomena in heavy baryons. Although the observation of several Ω_b^- states are following the quark model prediction, we still need to clarify their spin and parity.

Table 2.8. Mass spectra and widths of Ω_b^- with their decay modes.

States	J^P	Mass (MeV)	Width (MeV)	Decay modes	Refs
Ω_b^-	$\frac{1}{2}^+$	6046.1 ± 1.7	-	Weak	$D\emptyset$ [85]
$\Omega_b(6316)^-$	$?^?$	6315.64 ± 0.31	< 2.8	$\Xi_b K$	LHCb [86]
$\Omega_b(6330)^-$	$?^?$	6330.30 ± 0.28	< 3.1	$\Xi_b K$	LHCb [86]
$\Omega_b(6340)^-$	$?^?$	6339.71 ± 0.26	< 1.5	$\Xi_b K$	LHCb [86]
$\Omega_b(6350)^-$	$?^?$	6349.88 ± 0.35	1.4 ± 0.1	$\Xi_b K$	LHCb [86]

2.4 Summary

In this chapter, we have reviewed the experimental progress on charmed and bottom baryon spectroscopy. Heavy baryons observed in various experiments are summarized in Fig. 2.3. There are several remarks related to the progress on heavy baryons spectroscopy given as the following:

It is observed that the ground states of heavy baryons are well established except the Ω_b^- with spin-parity $3/2^+$. The missing Ω_b^- will be a future search that can be performed by LHCb collaboration. Since the missing Ω_b^- cannot decay strongly, the experimental search on its gamma decay will be helpful.

The negative parity doublet of anti-triplet heavy baryons is mostly established, except for the case of Ξ_b baryons. These states should be observed in $\Xi_b\pi\pi$ invariant mass. Again, this can be confirmed by LHCb collaboration.

The negative parity states of sextet heavy baryons are predicted to have five adjacent states in the quark model. Since their mass splitting is quite narrow, there could be the observed states are overlapping states. Therefore, the nature of these states should be clarified with higher statistics by the Belle II or LHCb experiment.

The positive parity (the first radial excitation) of anti-triplet heavy baryons have been observed except for Ξ_b. This state has unusual features compared to other heavy baryons that their decay width is quite broad. The higher excited states of anti-triplet heavy baryons are observed. They could be related to D-wave excitation. However, the D-wave partner need to be studied further in the future.

As explained above, there are still some puzzles and missing resonances in the heavy baryon sectors. With the existing experiments, it is expected to be able to observe more the missing resonances and solve some of the puzzles. Following that, the theoretical developments are certainly of importance to give essential input to experimentalists and more importantly to understand the underlying structure of heavy baryons.

"Gentlemen, we have run out of money. It's time to start thinking.", Ernest Rutherford

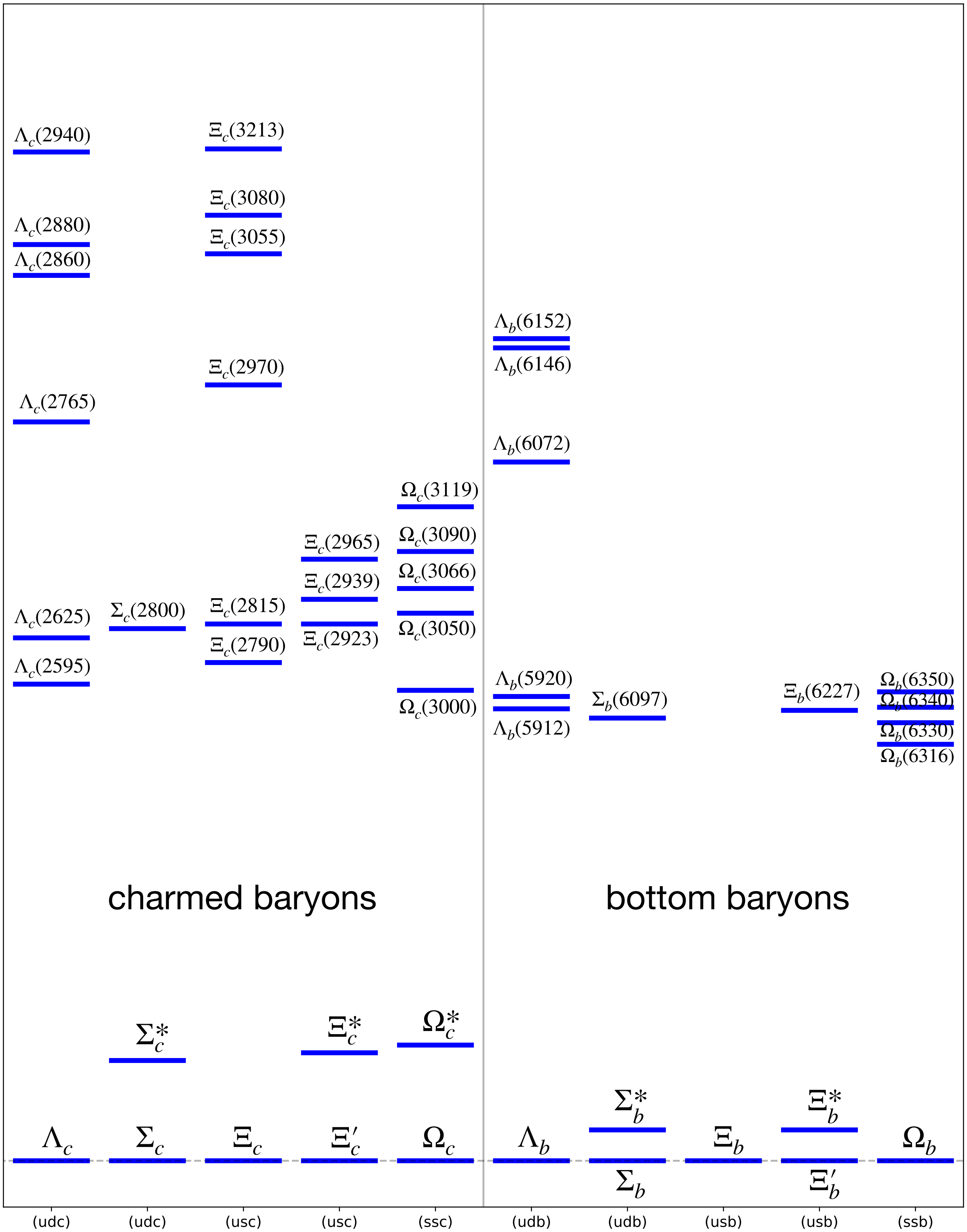

Figure 2.3. Spectra of charmed and bottom baryons observed in various experiments. The heavy baryon spectra are plotted with the excitation energy normalized to their respective ground states.

Chapter 3
Theoretical perspectives

In this chapter, we will review heavy baryons in theoretical perspectives. As mentioned before, to study baryon resonances we would like to make the use of effective models due to the non-perturbative nature of QCD. Up until now, there are lots of phenomenological models developed by various groups around the globe to understand the properties of heavy baryons. In addition to that, there is a Lattice QCD calculation based on the first principle of QCD which is progressively performed recently in the rise of the high-performance computer.

Historically, the hadron containing charm quark was discovered a long time ago in 1974. Two groups from SLAC and Brookhaven national lab reported the same particle simultaneously. They called the particle differently as J and ψ particles, which are later known as a J/ψ particle. This discovery is called as November Revolution since it opened a new area of research in hadron physics and changed our view about the elementary particle.

In 1990, the heavy-quark symmetry is introduced [87]. This symmetry is widely used in constructing effective models to study heavy baryons. In this work, we will discuss charmed and bottom baryons separately and are limited to the singly heavy baryons. Also, we will discuss each resonance in view of various models. However, the details of the models are not discussed here. The reader may consults to Refs. [3, 13] for details. The models we are using in this thesis are discussed in Part II. Formulation.

3.1 General properties

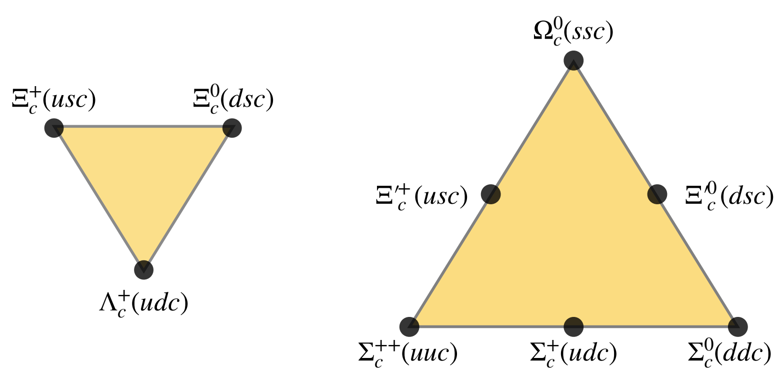

Figure 3.1. SU(3) multiplets of singly-charmed baryons. For the bottom baryon, the charm quark is replaced by bottom quark.

Generally, singly heavy baryons are composed of one heavy quark and two light quarks. The light quarks include up, down, and strange quarks. The charm and bottom quarks are considered to be

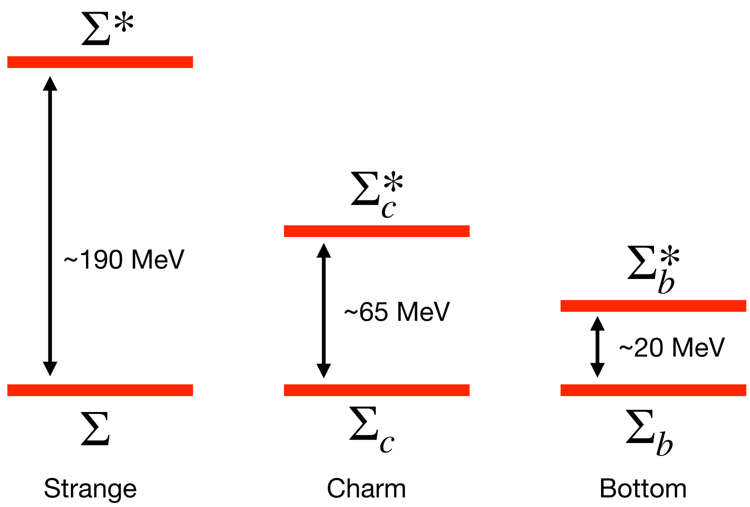

Figure 3.2. Comparison of the mass difference between an HQS doublet with various flavors. The mass difference is getting smaller as one of the quark mass is increasing.

heavy quarks because their masses about 1500 MeV and 5000 MeV, respectively, are significantly larger than Λ_{QCD} around 300 MeV. Consequently, heavy baryons posses a new symmetry a so-called heavy-quark symmetry. In this symmetry, the heavy quark is decoupled to that two light quarks. For example, the multiplet of heavy baryons are constructed by two light quarks with SU(3) symmetry as the following

$$\mathbf{3} \otimes \mathbf{3} = \bar{\mathbf{3}} \oplus \mathbf{6} \tag{3.1}$$

where the multiplet is described in Fig. 3.1.

In heavy-quark symmetry, we may introduce a new quantum number so-called brown-muck spin j, which represents a total angular momentum of light quarks. Along with the heavy quark spin, the total spin J of heavy baryon is constructed. In this way, there will be a so-called HQS (Heavy-Quark Symmetry) doublet where the spin is made of $J = j \pm 1/2$. However, for brown muck spin $j = 0$, there will be an HQS singlet instead. Moreover, in heavy quark spin symmetry, it is known that the spin-dependent interaction is suppressed by a factor of $1/m_Q$. This factor is leading to a suppression of mass difference between an HQS doublet as portrayed in Fig. 3.2. In heavy quark limit, namely when $m_Q = \infty$, the heavy quark spin will be decoupled completely to the spin of the light quark.

As shown in Eq. (3.1), two light quarks inside heavy baryons, we use the term “diquark” to represent them, can have either symmetric or anti-symmetric flavor wave functions. For the ground states heavy baryons, we will obtain the diquark having either spin 0 (good diquark) or spin 1 (bad diquark). Keep in mind that we need to anti-symmetrize the total wave function including color,

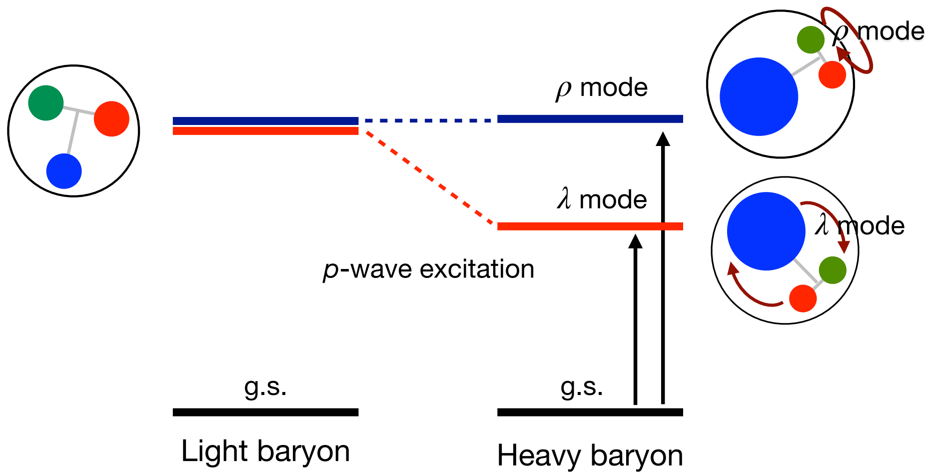

Figure 3.3. A schematic picture of separation between λ and ρ mode excitation in heavy baryons. The orbital excitations are mixed when the three quarks have similar masses as in light baryons.

flavor, spin, and orbital wave function as

$$\text{Good diquark } (j=0) \quad \rightarrow \quad \bar{3}_{flavor}(A), \quad l_{\text{orbital}}(S), \quad S_{\text{spin}}(A) \tag{3.2}$$

$$\text{Bad diquark } (j=1) \quad \rightarrow \quad 6_{flavor}(S), \quad l_{\text{orbital}}(S), \quad S_{\text{spin}}(S) \tag{3.3}$$

where we put a label inside a parenthesis either S (symmetric) or A (anti-symmetric) for each wave function. Noted that the color wave function is anti-symmetric. We will discuss more detail in the chapter of the quark model. Consequently, the sextet heavy baryons will have an HQS doublet with $J^P = 1/2^+$ and $3/2^+$. Meanwhile, the anti-triplet heavy baryons will be an HQS singlet with $J^P = 1/2^+$. Historically, the good diquarks are named so because they are easily observed than of the bad diquarks.

Another feature of heavy baryon is that there is a separation of the orbital motions due to the mass difference between light and heavy quark. One is so-called λ mode which is the relative motion between heavy quark and the center of mass of light quarks. The other one is the relative motion between two light quark called ρ mode. The orbital motion is related to Jacobi coordinates which are widely used for the analysis of a three-body system such as heavy baryon. In more concrete manner, the coordinates are defined as

$$\vec{\rho} \quad = \quad \vec{r}_2 - \vec{r}_2, \tag{3.4}$$

$$\vec{\lambda} \quad = \quad \frac{1}{2}(\vec{r}_1 + \vec{r}_2) - \vec{r}_3. \tag{3.5}$$

As discussed above, these λ and ρ mode orbital excitations are well separated. For singly heavy baryons, the λ mode excitation appears lower than of the ρ mode. This ordering can be understood that the moment inertia of the λ mode excitation is larger such that it can be excited more easily. Because of

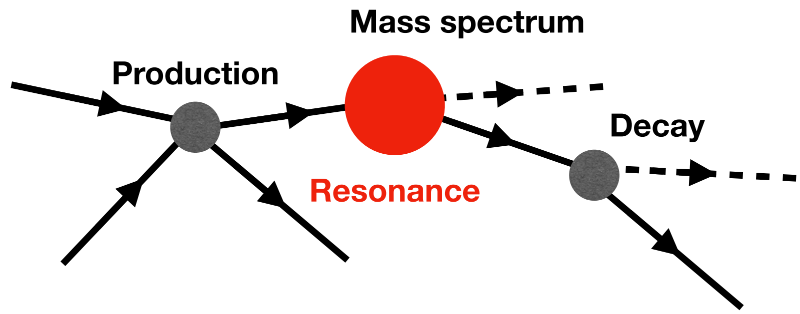

Figure 3.4. Some ways to study heavy baryons: production, mass spectrum, and decay.

the separation of the orbital excitation, the heavy baryon could be exclusively dominated by λ mode rather than ρ mode. In fact, the observed heavy baryons seem to correspond to λ mode although further investigation should be done. For the time being, there is no decisive way to distinguish whether a heavy baryon is related to λ or ρ mode excitation. On the other hand, if the mass of the three quarks is similar, the orbital excitations are mixed and become indistinguishable. A schematic picture of the separation of orbital excitation is given in Fig. 3.3.

The internal structure of heavy baryons is in general reflected in their spectrum, production, and decay as depicted in Fig 3.4. There are many investigations devoted to explaining those properties by constructing effective models. Even though the study of heavy baryon properties seems to be simpler than of light baryons because of the heavy-quark symmetry, there are still many puzzles that remain to be solved in the heavy baryon sector. Furthermore, the connection between the properties of light and heavy baryons are not well understood easily. In this following, we will review the theoretical developments in this direction to get a complete picture of baryon resonances.

3.2 Modeling decay process

Here, we focus on reviewing various models in attempts to study heavy baryons from their decay process. Up to date, there are several models commonly used to study heavy baryons. As we can see later, the decay process is helpful to extract the internal structure of heavy baryons. It is interesting to note that the heavy baryon decays are saturated with the three-body decay (or two-pion emission decay) unless it is forbidden. However, it is adequate to study the one-pion emission for the first step.

First, the heavy baryon decay is studied in the **chiral quark model**. In this model, the heavy baryon wave functions are described in the quark model where the pion is regarded as Nambu-Goldstone boson (a point-like particle). The axial-vector type coupling is used to model the interaction between quark and pion in accordance with the low-energy theorem. The schematic picture of this model is described in Fig. 3.5. This model has been applied to the one-pion emission decay of Λ_c [88], and later the model is calculated by the j-j scheme which is suitable with heavy-quark symmetry [89].

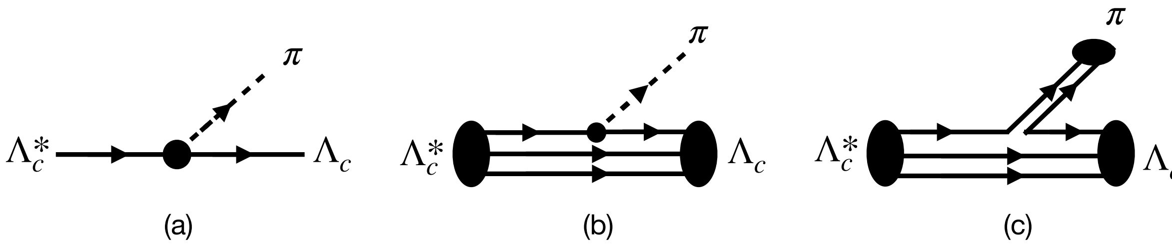

Figure 3.5. Degree of freedom in different model (a) heavy-hadron chiral perturbation theory (b) chiral model, and (c) quark-pair creation model.

In the past years, this model has been applied to the various flavors of heavy baryons, not only charmed baryons [90–94], but also bottom baryons [95–99]. The radiative decay can also be calculated in studying heavy baryons [94]. There is also an attempt to calculate the D-meson emission decay by assuming $SU(4)$ symmetry. However, it is rather difficult to explain the experimental data [90].

The $^3\boldsymbol{P_0}$ **model** or quark-pair creation model is another kind of model in studying heavy-baryon decay. In this description, a pair of quark is created during the decay process in a vacuum and along with the initial three quarks, the pair of quark regroup into meson and baryon in final states. The baryons wave functions are described by the quark model. This model has been applied to the various flavor of heavy baryons [100–106]. Another attempt of studying heavy baryon decay is by using **Eichten-Hill-Quigg** decay formula. In this formula, the geometric factor is factored out which described by the six-j symbol in addition to the transition factor which is computed from $^3P_0$ model. This model has been used to study various heavy baryons [107–112].

The other model, which is called **heavy-hadron chiral perturbation theory**, is constructed by incorporating heavy-quark and chiral symmetry to model the interaction between the heavy baryons and Nambu-Goldstone bosons. In this case, the effective degrees of freedom are in the hadron level. This model is applied to study one-pion emission decay of various heavy baryons [113–117]. The ratio of the decay rate into $\Sigma_c^*\pi$ and $\Sigma_c\pi$ channels, respecting the heavy-quark symmetry, is also discussed in addition to the comparison of decay width. Another method using the hadron degree of freedom is using **light-cone sum rule**, which based on heavy-quark effective theory (HQET). The method is applied to many heavy baryons [118–121].

Recently, the two-pion emission decay is analyzed by the **effective Lagrangian** with the input of the chiral quark model [122]. The three-body decay is also studied in the effective Lagrangian respecting the chiral and heavy-quark symmetry [123, 124]. This model also employs the **chiral partner structure** to estimate the coupling of direct process, where the experimental prediction on the Dalitz plot is provided in Ref. [125]. It is also found that three-body decay can be used to determine the spin-parity [126, 127]. The extraction of the ND scattering length can also be done to study the heavy baryon [128]. Moreover, many hyperons, nucleons, or meson resonances can be studied in the three-body weak decay of ground state heavy baryons [129–131].

3.3 Charmed baryon

In this section, we summarize the theoretical discussions about the charmed baryons which have been observed so far in the experiments. As mentioned previously, we limit the discussion to the charmed baryon containing only one charm quark. We may notice that all of the ground states of charmed baryons have already been observed and their masses are consistent with the expectation from various theoretical calculations. However, the nature of the excited states of charmed baryons is not well known.

3.3.1 $\Lambda_c(2595)$, $\Lambda_c(2625)$, $\Xi_c(2790)$ and $\Xi_c(2815)$

Since Λ_c and Ξ_c belong to anti-triplet charmed baryons, there is a doublet of $1/2^-$ and $3/2^-$ respectively for P-wave excitations with λ-mode in quark model description. These observed $\Lambda_c(2595)$, $\Lambda_c(2625)$ and $\Xi_c(2790), \Xi_c(2815)$ can be naturally assigned to the P-wave excited states. Furthermore, their excitation energy and mass difference are consistent with various theoretical analysis [132–134].

The one-pion emission decay are analyzed by various models, *e.g.* Refs [88, 89, 100, 107, 113]. From such analysis, it is shown that $\Lambda_c(2595)$ and $\Lambda_c(2625)$ could belong to λ-mode excitation of $1/2^-$ and $3/2^-$, respectively. The detailed analysis of their two-pion emission decay processes is also helpful to discuss their internal structures [122]. Note that $\Lambda_c(2595)$ shows an isospin breaking effect where the decay width is dominated by the $\Lambda_c\pi^0\pi^0$ neutral channel due to the slightly larger phase space which is mainly originated from the mass difference from pion. It is also known from the PDG that $\Lambda_c(2625)$ has a large contribution from the non-resonant process which may originate from direct or $\Sigma_c^*(2520)$ process. The large contribution of the direct process is predicted in the chiral partner structure of heavy baryons [123], which later extended to the case of Ξ_c [124]. This direct process will modify the structure on Dalitz plots which provided in Ref [125] and therefore it is interesting to test the chiral partner structure in heavy baryons.

Since $\Lambda_c(2595)$ is located near $\pi\Sigma_c$ threshold, it is subject to the discussion of its compositeness. $\Lambda_c(2595)$ is discussed to be dominated by three-quark state by analyzing their scattering length and effective range which found to be unnatural and in terms of the compositeness [135]. The more delicate analysis is done and asserts the result that $\Lambda_c(2595)$ is dominated by three-quark state [136]. However, the compositeness condition could be model-dependent and it is shown that $\Lambda_c(2595)$ have a meson-baryon dominant unless for large N_c [137]. There is an attempt to model the DN interaction and regard $\Lambda_c(2595)$ as a dynamically generated state, similar to $\Lambda(1405)$ [138]. It is also shown in lattice QCD simulation is that the $\Lambda_c(2595)$ is dominated by the three-quark state unlike its counterpart in the strange sector $\Lambda(1405)$ [139]. Recently, the interplay between the bare three-quark state and $\pi\Sigma_c$ threshold is analyzed where the $\Lambda_c(2595)$ has a predominant molecular state [140]. From the above discussions, the $\Lambda_c(2595)$ is most likely a quark model state.

3.3.2 $\Sigma_c(2800)$, several Ξ'_c and Ω_c

The Σ_c, Ξ'_c, and Ω_c baryons belong to the symmetric sextet in which there are five P-wave λ-mode excitations. According to the mass spectrum analysis, $\Sigma_c(2800)$ is consistent with the P-wave excitation [141, 142]. The decay properties of $\Sigma_c(2800)$ have also been examined where it could be P-wave excitation [94, 107]. However, more resonances are expected in this energy region. The molecular state is also discussed for $\Sigma_c(2800)$ since it is located near DN threshold [143–146]. Furthermore, the extraction of DN threshold parameter may be important to understand $\Sigma_c(2800)$ [129].

The recently observed $\Xi_c(2923), \Xi_c(2935)$, and $\Xi_c(2965)$ states in $\Lambda_c K$ could correspond to the P-wave excitations from their excitation energies [91, 102, 119]. Moreover, the $\Xi_c(2930)$ could be overlapping states of $\Xi_c(2923)$ and $\Xi_c(2935)$. The molecular description of these states is also discussed [147]. It is worth noting that $\Xi_c(2965)$ mass is very close to that of $\Xi_c(2970)$. But, their decay rate differs significantly, indicating that they may be distinct states.

Lastly, the $\Omega_c(3000), \Omega_c(3050), \Omega_c(3066)$, and $\Omega_c(3090)$, which was found in $\Xi_c K$ invariant mass, may also correspond to P-wave excitations from the mass spectrum analysis [148–150]. The decay process has also been analyzed within the quark model with various possible decaying channels [94, 117, 151]. Moreover, Lattice QCD simulation is performed and the result supports the P-wave excitation [152]. Beside the quark model description, there exists other interpretation such as pentaquark states [153–155] or molecular description [156–159].

3.3.3 $\Lambda_c(2765)$ and $\Xi_c(2970)$

The $\Lambda_c(2765)$ was discovered in $\Lambda_c\pi\pi$ invariant mass by CLEO around the 2000s. This state has unusual behavior with a large decay width compared to other charmed baryons. It is also quite difficult to say whether $\Lambda_c(2765)$ is Λ_c with $1/2^+$ or the Σ_c resonance with $1/2^-$ or $3/2^-$ [88]. To determine the isospin of this state, Belle measures the $\Lambda_c\pi\pi$ invariant mass with the wrong sign, and the enhancement is not found, indicating that this state is Λ_c baryon.

From the mass spectrum analysis, these two states can be interpreted as $2S$ excitation [160–167]. If that is the case, these states have similarities with other resonances with excitation energy around 500 MeV, which is called Roper-like resonances. For this assignment, the quark model predicts a narrow decay width, which contradicts the experimental data [88, 89, 107, 114, 168]. The possible interpretation is that this Roper-like resonance has strong coupling to the meson clouds [169] which is also supported by the Lattice simulation [170, 171]. There are alternative ideas such collective monopole vibrations [172], deformed oscillator states [173], pion exchange interaction [174] and so on.

Recently, the study of their three-body decay turns out to be helpful to determine the spin-parity unambiguously by measuring the ratio R between $\Sigma_c^*\pi$ and $\Sigma_c\pi$ channel; and angular correlations [126]. However, there is an interference region between Σ_c^{*++} and Σ_c^{*0} which makes the analysis a bit complicated. Moreover, it is implied from the experimental observation that the $f_0(500)$ or σ meson contribution is insignificant, which may provide a hint to its dynamical content.

Similarly, $\Xi_c(2970)$ state is observed in $\Xi_c\pi\pi$ and $\Lambda_c K\pi$ invariant masses. This state has a rather large decay width, implying that it is a potential analog state of $\Lambda_c(2765)$ in the strange-charm sector.

From the mass spectrum analysis, it might be $\Xi_c(2S)$ state although it is always difficult to say whether it belongs to sextet or anti-triplet Ξ_c baryon [133, 161]. In fact, there is another $\Xi_c(2965)$ observed with almost the same mass.

From decay analysis, the $\Xi_c(2970)$ baryon is predicted to be a narrow resonance in the quark model if the $\Xi_c(2S)$ is assigned [90, 100, 113, 175]. Compared with the absolute value of the decay width, it is discussed as P-wave excitation of Ξ_c' baryon. A similar angular correlation analysis can be done for the two-pion emission decay of $\Xi_c(2970)$. In this case, the analysis will be easier because there is no kinematical reflection, resulting in no complicated intereferences [126]. Therefore, measuring the angular correlation is quite interesting to disentangle its internal structure.

3.3.4 $\Lambda_c(2860), \Lambda_c(2880)$ and $\Lambda_c(2940)$

The $\Lambda_c(2860)$ resonance is first observed in $\Lambda_b \to Dp\pi$ decay, which is located slightly above Dp threshold. This state has a broad width of around 60 MeV and its spin-parity is determined as $3/2^+$ by LHCb. However, it is not yet seen in $\Lambda_c\pi\pi$ invariant mass and not yet confirmed by other experiments in Dp invariant mass, which makes the existence of this state questionable. From its mass spectrum, $\Lambda_c(2860)$ can be naturally assigned as $3/2^+$[107, 176, 177] where it forms a D-wave doublet along with $\Lambda_c(2880)$. Moreover, by assigning $\Lambda_c(2860)$ as $3/2^+$, it is predicted that its decay width has a considerable contribution from $\Lambda_c\pi\pi$ [93, 113]. More experimental evidence is required to establish this state.

In contrast to $\Lambda_c(2860)$, the $\Lambda_c(2880)$ resonance is already found in $\Lambda_c\pi\pi$ and Dp invariant masses; and has a narrow decay width. Its existence is also rather established and its spin-parity has been determined to be $5/2^+$ by measuring its angular distribution of $\pi\Sigma_c$ and ratio R. It is also supported by the mass spectrum analysis that this state is compatible with the $5/2^+$ assignment [161, 178, 179]. However, it seems that $\Lambda_c(2880)$ has brown-muck spin $j = 3$, not $j = 2$, which is implied from the measured ratio R [88, 100, 108]. It is also discussed that the ratio R is largely contaminated by the broad $\Lambda_c(2860)$ [93]. Beside, if $\Lambda_c(2880)$ state has $j = 3$, it implies that the higher state $\Lambda_c(2940)$ could be its D-wave partner [89]. A more comprehensive discussion should be done to understand the internal structure of $\Lambda_c(2880)$.

So far, the highest excited state observed is $\Lambda_c(2940)$. It is observed in both $\Lambda_c\pi\pi$ and Dp invariant masses in various experiments and therefore the existence is undoubted. Also, the spin-parity is determined to be $3/2^-$ by LHCb although other possibilities such as $7/2^+$ can not be ruled out. In fact, it is difficult to assign this state as $3/2^-$ in the quark model description because the calculated mass is significantly higher than the observed one [177, 178]. In addition to that, from the analysis of its decay, this state is compatible with $3/2^-$ or $7/2^+$ assignment within the quark model [89, 101]. Because of this fact, there also exist molecular interpretations [143, 180–182]. Moreover, it is also supported by the fact that it is located slightly below the D^*p threshold. Furthermore, the two-pion emission decay of $\Lambda_c(2940)$ could provide important constraints, ratio, and angular correlation, to determine its spin-parity [126], which is crucial for understanding its nature.

3.3.5 $\Xi_c(3055), \Xi_c(3080)$ and $\Xi_c(3123)$

The $\Xi_c(3055)$ resonance is observed in $\Lambda_c K\pi$ and ΛD. Opposite to $\Lambda_c(2860)$, the width of this state is rather narrow. From its excitation energy, it is compatible with a D-wave excitation of Ξ_c with $J^P = 3/2^+$ [133, 177]. The strong decay has been analyzed in various models [90, 93, 107, 183]. However, the quark model with $SU(4)$ symmetry assumption failed to predict the experimental data of branching ratio between ΛD and $\Sigma_c K$ where one of the sources of the problem is the significant breaking of $SU(4)$ symmetry [93]. By assigning this state as $3/2^+$, it is also predicted that the $\Xi_c\pi\pi$ is rather suppressed [107].

Similarly, the $\Xi_c(3080)$ resonance is found in $\Lambda_c K\pi$ and ΛD. By analyzing its excitation energy, this state could be $5/2^+$ or D-wave excitation of Ξ_c [133, 161, 177]. From its strong decay, the ratio between $\Sigma_c K$ and $\Sigma_c^* K$ is almost unity. However, the prediction from the various model for $5/2^+$ with λ mode excitation, the decay is dominated by $\Sigma_c^* K$. Therefore, it is not easy to assign this state as a $5/2^+$ with λ mode [93, 107, 114, 145]. The situation is similar to $\Lambda_c(2880)$ where the ratio can not be easily explained by the λ-mode D-wave excitation.

The $\Xi_c(3123)$ resonance is found only in $\Lambda_c K\pi$ with $\Sigma_c^* K$ as a dominant mode. There is no more evidence or confirmation from other experiments and it has a one-star rating in PDG. In the theoretical perspectives, several predictions have been made, but there are a lot of uncertainties [90, 183]. Given the present data, it is fair that it is quite difficult to clarify its nature.

3.4 Bottom baryon

In this section, we will discuss the bottom baryons observed by the experiment. Up until now, the ground state bottom baryons have been already observed, except Ω_b with $J^P = 3/2^+$ which could be potentially observed in the radiative decay. Here, we will discuss the theoretical perspectives of the excited states of bottom baryons.

3.4.1 $\Lambda_b(5912)$ and $\Lambda_b(5920)$

$\Lambda_b(5912)$ and $\Lambda_b(5920)$ are observed in $\Lambda_b\pi\pi$ by LHCb. These states can be naturally assigned to be P-wave doublet of $1/2^-$ and $3/2^-$ from their mass spectra in the various quark model [134, 164, 178]. The three-body decay of $\Lambda_b(5912)$ and $\Lambda_b(5920)$ are studied in several models such as chiral partner structures [123, 184]. Since the $\Sigma_b^{(*)}\pi$ channel is closed, the decay is dominated by the direct process. Therefore, the decay rate is very small, less than 1 MeV. In this situation, the branching fraction of the radiative decay could be large [94]. Similar with the P-wave doublet of Λ_c, these states are compatible with the quark model expectation. In addition to that, the dynamical contents of these states are also investigated [185–189].

3.4.2 $\Sigma_b(6097), \Xi_b(6227)$, and several Ω_b.

$\Sigma_b(6097)$ is a candidate of P-wave excited state of Σ_b baryon observed by LHCb. In PDG, the spin-parity is not assigned yet because there are many states predicted in this energy region from the mass spectrum analysis [177, 190–192]. Moreover, the observed decay width is relatively large. Therefore, the possibility of a superposition of two states can not be ignored. As we have already seen, there are several Ω_c and Ω_b states observed in recent years. One may expect such structures also occur for the case of Σ_b. Tentatively, the $\Sigma_b(6072)$ may be either $3/2^-$ or $5/2^-$ by analyzing their decay properties [97, 111, 121, 193, 194]. In addition to that, there is a claim that the newly observed $\Lambda_b(6072)$ could be a Σ_b states with negative parity [96]. Beside, a molecular interpretation is also possible [188].

$\Xi_b(6227)$ is found in $\Lambda_b K$ and $\Xi_b\pi$ invariant mass by LHCb. This state is expected to be a P-wave excited state of Ξ_b' analyzed by its mass spectrum [133, 161, 164, 177, 179, 195]. Again, as there are several states predicted, there are possibilities to be a superposition of several states and therefore the spin-parity of $\Xi_b(6227)$ is not yet assigned in PDG. Another perspective from their decay properties, $\Xi_b(6227)$ can be tentatively assigned as $3/2^-$ or $5/2^-$ [94, 97, 111, 121, 196]. Furthermore, the ratio between decay rate into $\Lambda_b K$ and $\Xi_b\pi$ is measured and would be an important constraint to determine their spin and parity. This state may also be a molecular state as discussed in various models [186, 197–199]. But, more precise data is needed before proceeding further. In fact, $\Xi_b\pi\pi$ invariant mass is not yet explored by LHCb and will perhaps provide interesting constraints or even find new states of Ξ_b [124, 127].

Recently LHCb discovered four Ω_b resonances in $\Xi_b K$ invariant masses, namely $\Omega_b(6136), \Omega_b(6330)$, $\Omega_b(6340)$ and $\Omega_b(6350)$. From their mass excitation, these states can be interpreted as $1P$-wave or possibly $2S$ excitations of Ω_b baryon in the various models [111, 134, 148, 161, 177, 200–203]. These observations are similar to that of several Ω_c baryon in $\Xi_c K$ where the quark contents of Ω_c are changed from bss to be css. However, it is predicted that one state is missing in the Ω_b spectrum. Their decay properties have been investigated and it is suggested that these states are compatible with the P-wave excitations [99, 106, 204]. The narrow widths of these states can be understood that Ω_b has no non-strange quark which does not couple to pion directly. Furthermore, other interpretation such as molecular state is also discussed [205, 206].

3.4.3 $\Lambda_b(6072)$

The $\Lambda_b(6072)$ is first observed by CMS and subsequently confirmed by LHCb in 2020. This state is predicted to be $\Lambda_b(2S)$ state by looking at its excitation energy which has been calculated in the various quark model [133, 164, 177, 178] and recently in QCD sum rule [207]. In addition to that, other observables such as decay properties should also be examined to determine its spin-parity more decisively.

Different from other heavy baryons, this state has a broad width around 70 MeV which is very similar to $\Lambda_c(2765)$. This resemblance indicates that both states may have similar dynamics. Moreover, its decay channel is saturated with the $\Lambda_b\pi\pi$. The excitation energy around 500 MeV and similar decay properties with $\Lambda_c(2765)$ has led us to the discussion of the flavor independent nature of Roper-like resonance. Moreover, the study of its three-body decay of $\Lambda_b(6072) \to \Lambda_b\pi\pi$ suggests that its spin and parity is $1/2^+$. It is found that the angular correlation can be a strong constraint that can be measured by the LHCb experiment. Although $f_0(500)$ or σ meson is expected to contribute to the three-body decay of $\Lambda_b(6072)$, the experimental data shows that such contribution is not important [127]. This empirical fact might also provide a constraint to its dynamics. Here, we also notice that there are a considerable isospin breaking of Σ_b mass, which is studied in Refs [208, 209]

Since it is not yet well established, there are several other interpretations of this state. It is discussed in the quark model that $\Lambda_b(6072)$ could be a ρ-mode excitation by looking at its decay rates [104]. Note that the quark model predicts a narrow $\Lambda_b(2S)$ state which can not explain the observed broad $\Lambda_b(6072)$. This finding has brought us an alternative idea about the exotic description of this state such as dynamically generated resonances. As $\Lambda_b(6072)$ solely decay into $\Lambda_b\pi\pi$, not into $\Lambda_b\pi$, the possibility being Σ_b state is disfavored. Even so, it is also discussed that there are negative parity Σ_b state around this energy [96]. So, it is fair to say that more experimental information is crucial to pin down the internal structure of $\Lambda_b(6072)$.

3.4.4 $\Lambda_b(6146)$ and $\Lambda_b(6152)$

This Λ_b doublet is observed by LHCb experiment and one of them is later confirmed by CMS. From their excitation energy, $\Lambda_b(6146)$ and $\Lambda_b(6152)$ are predicted to be D-wave excitations with spin-parity $3/2^+$ and $5/2^+$, respectively, by various models [133, 164, 178, 210]. Recently $\Lambda_b(6146)$ is studied to be $3/2^+$ within QCD sum rule along with its charm partner $\Lambda_c(2860)$. Moreover, Regge trajectory analysis also supports these assignments [211]. Unlike their analog states in charm sectors, $\Lambda_c(2860)$ and $\Lambda_c(2880)$, the BN threshold is closed resulting in the narrow decay width.

It is rather difficult to say which D-wave doublet they belong to because the study of their decay properties suggests that there is a mass inversion [95, 103]. More concretely, $\Lambda_b(6146)$ and $\Lambda_b(6152)$ is best suited to $5/2^+$ and $3/2^+$, respectively, by inspecting the ratio R between the decay rate into $\Sigma_b^*\pi$ and $\Sigma_b\pi$. Since the mass difference between Σ_b and Σ_b^* states are quite small, the ratio R may be contaminated by the interference terms resulting in the problem of the mass inversion. Furthermore, $f_0(500)$ state may also contribute and change the observables since the model calculated so far only analyze their one-pion emission decay. Therefore, the analysis of their three-body decay is quite important.

Another scenario is also made. The recent analysis of these states within the QCD sum rule suggests that these states could correspond to $5/2^+$ and $7/2^+$ [212]. This is similar to the analysis for charmed baryons in Ref [89]. It is also worth noting that the angular analysis may also help to determine their spin as done for $\Lambda_c(2880)$.

3.5 Summary

In the past year, theoretical models have been developed significantly, induced by continuous reports from various experimental groups. It turns out that the study of baryons with various flavor may give a hint to underlying structures. Especially, investigating differences and similarities among baryons with different flavors would unravel the dynamics of baryon resonances.

Up until now, most of the observed heavy baryons could be naturally assigned to the λ-mode excitations in the quark model description. In addition to that of λ mode, the quark model also predicts other states containing ρ mode excitations which have not been observed in the experiments. According to the theoretical calculations, these ρ mode states have larger masses compared to that of λ mode. As we have noticed, the problem of missing resonances seems to also occur in the case of heavy baryons.

Furthermore, we have already seen that the quark model does not work well for the higher excited states, even with λ mode assignments. This fact would result in other interpretations, *i.e.* exotic state which is beyond the quark model. One of the reason is due to the opening thresholds that may affect the resonance dynamics. Therefore, careful treatment of the interplay between the quark model and the opening threshold would be one of the keys to understanding the higher excited states of heavy baryons. In addition to that, a more precise machine is certainly needed, but the developments of the existing theory are also important to unveil the nature of baryon resonances.

"If I could remember the names of these particles, I would have been a botanist.", Enrico Fermi

Part II

Formulation

Chapter 4
Quark model

4.1 Introduction

In the quark model description, hadrons are classified according to their valence quarks which are confined inside of hadrons. Generally, there are two types of hadrons: baryons, and mesons as described in Fig. 4.1 (a). Baryons are composed of three quarks and mesons are composed of a pair of quark and anti-quark.

$$|Baryon\rangle = |qqq\rangle \tag{4.1}$$

$$|Meson\rangle = |q\bar{q}\rangle \tag{4.2}$$

where q and $\bar{q}$ represent quark and anti-quark respectively. However, there could be other states such as tetraquarks, pentaquarks, and so forth as depicted in Fig. 4.1 (b). These types of states are usually called exotic states which are beyond the simple picture of baryons and mesons [6].

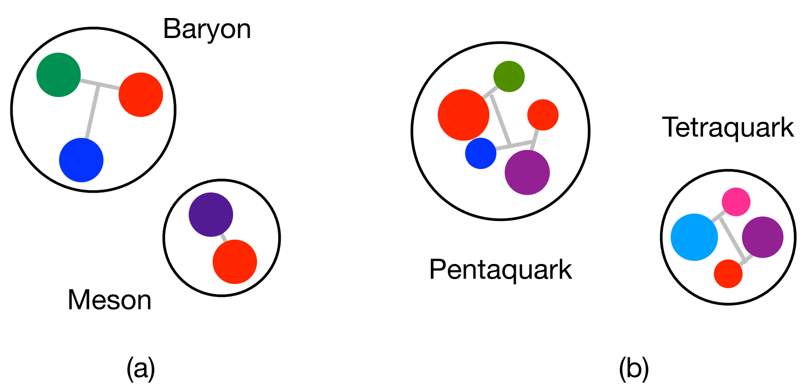

Figure 4.1. Hadrons are classified in terms of their valence quarks. (a) conventional hadron, and (b) exotic states.

In the quark model, the quantum numbers of hadrons, *e.g.* spin and flavor, are determined by the combination of the quantum numbers of their valence quarks. The quark is classified as fermion, which has spin-1/2 and therefore baryons have ahalf-integer spin (fermion), while mesons have an integer spin (boson). Moreover, the quark has six different flavors: up, down, strange, charm, bottom and top, in which they have different mass, charge, *etc.* With a proper combination of quark's quantum numbers, the hadron quantum numbers are made. Later, the classification of hadrons is proposed by Gell-Mann so-called eightfold way for hadrons containing u, d, and s quarks [2].

Another important quantum number of quarks is called color. Historically, color is introduced to describe Δ^{++} state. In the quark model, Δ^{++} has totally symmetric wavefunction, including its flavor and spin, which is not allowed if quarks are fermions. One solution is to introduce an additional anti-symmetric quantum number, so-called color. The quark has color either red, green, or blue, and only colorless objects such as baryons and mesons are observables. In other words, the quark itself can not be observed directly because the quark is a colored object. This situation is usually called color confinement.

It is also worth noting that the quark considered here is the so-called constituent quark. Its mass is made of the current (bare) quark mass dressed by the interactions through virtual quarks and gluons. The consituent quark mass is rather large about $M_u \approx 350$ MeV compared to its bare mass, $m_u \approx 3$ MeV.

Despite its simple picture, the quark model is successful to explain the hadron spectroscopy. But, there are still some problems and limitations which should be addressed in the future. In this chapter, we will introduce the quark model that we are using for the analysis of heavy baryon decays. As we will find later, the quark model works well for the description of the low-lying heavy baryon.

4.2 Baryon in the quark model

As we have discussed previously, baryons are composed of three constituent quarks. In the quark model, baryon wavefunctions consist of a combination of orbital, spin, flavor, and color wavefunction of each quark. Since a baryon is a fermion, we need to construct the wavefunction totally anti-symmetric under the interchange of two quarks as given by

$$|Baryon\rangle = |qqq\rangle_A = \Psi_{orbital} \otimes \psi_{spin} \otimes \phi_{flavor} \otimes \phi_{color}, \tag{4.3}$$

Since the color wavefunction is always anti-symmetric,

$$\phi_{color} = \frac{1}{\sqrt{6}}(rgb - rbg + gbr - grb + brg - bgr) \tag{4.4}$$

The combination between orbital, spin, and flavor wavefunctions should be symmetric. Let us first discuss in detail each wavefunction before constructing the total wavefunction. Note that we consider the singly heavy baryon containing one heavy quark in this work.

4.2.1 Orbital part

In this calculation, we assume that quarks inside a heavy baryon are confined in the harmonic oscillator potential as illustrated in Fig. 4.2 (a). Beside its simplicity, one of the advantages of using the harmonic oscillator is that the analytical or exact solution is known. The spring constant or potential parameter k is also assumed to be independent of the quark flavor. The Hamiltonian of harmonic oscillator model in the non-relativistic form can be written as

$$H = -\sum_{i=1}^{3} \frac{\vec{\nabla}_i^2}{2m_i} + \sum_{i<j} \frac{k}{2}(\vec{r}_i - \vec{r}_j)^2 \tag{4.5}$$

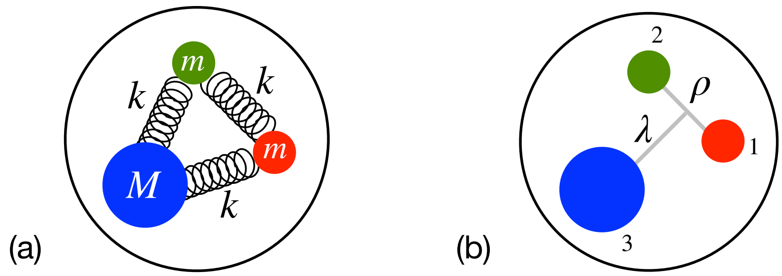

Figure 4.2. Definitions and notations used in the calculation. (a) Harmonic oscillator model and (b) Jacoobi cordinate.

where $\vec{r}_i$ and m_i are the coordinate and mass of the i-th quark.

To seperate between the internal motion ($\vec{\lambda}$ and $\vec{\rho}$) and *c.m.* motion of quark ($\vec{X}$), the Hamiltonian can be re-expressed by

$$H = \frac{1}{2(2m+M)}\vec{\nabla}^2_X + \frac{1}{2m_\rho}\vec{\nabla}^2_\rho + \frac{1}{2}m_\rho\omega_\rho\vec{\rho}^2 + \frac{1}{2m_\lambda}\vec{\nabla}^2_\lambda + \frac{1}{2}m_\lambda\omega_\lambda\vec{\lambda}^2 \tag{4.6}$$

where the light and heavy quark masses are denoted as $m_1 = m_2 = m$ and $m_3 = M$. Also, the reduced masses are defined by

$$m_\rho = \frac{m}{2}, \qquad m_\lambda = \frac{2mM}{2m+M}. \tag{4.7}$$

Then, the oscillator energies are denoted as

$$\omega_\rho = \sqrt{\frac{3k}{m}} = \sqrt{\frac{3k}{2m_\rho}}, \tag{4.8}$$

$$\omega_\lambda = \sqrt{\frac{k(2m+M)}{mM}} = \sqrt{\frac{2k}{m_\lambda}}, \tag{4.9}$$

and potential strengths are given by

$$a_\lambda = \sqrt{m_\lambda\omega_\lambda}, \tag{4.10}$$

$$a_\rho = \sqrt{m_\rho\omega_\rho}, \tag{4.11}$$

which is not independent to each other, they are related by

$$a^2_\lambda = \sqrt{\frac{8M}{3(2m+M)}}a^2_\rho \tag{4.12}$$

The relation between the Jacobi and spatial coordinates can be found in Appendix A.

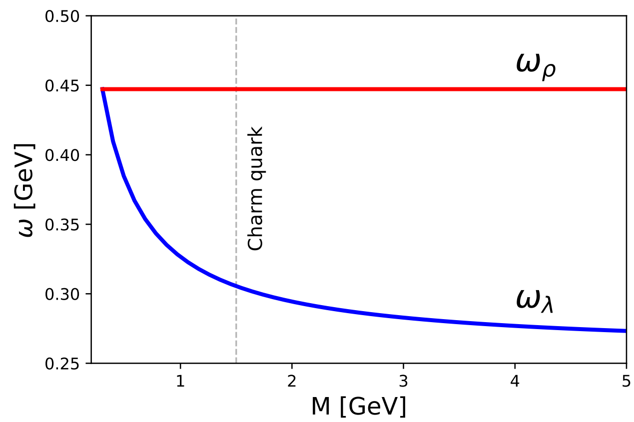

Figure 4.3. The behavior of the λ and ρ mode excitation energy with the increase of heavy-quark mass.

It is also interesting to see that the ω_ρ and ω_λ are well separated for heavy baryons as described in Fig. 4.3. For the singly heavy baryons, ω_λ turns out to be smaller than ω_ρ, implying that the low-lying heavy baryons are dominated by the λ mode excitation. We also notice that the ω_ρ does not change with the increase of heavy quark mass. The ratio between the ω_λ and ω_ρ is given by

$$\frac{\omega_\lambda}{\omega_\rho} = \sqrt{\frac{1}{3}\left(1 - \frac{2m}{M}\right)} \leq 1. \tag{4.13}$$

As we can see, that the gap between ω_λ and ω_ρ is getting larger for heavier mass M. This is the unique feature of heavy baryons, which we have discussed in the earlier chapter. In the actual situation, heavy baryon could be mixed between λ and ρ mode excitations. However, for simplicity, we will treat them exclusively.

The orbital wavefunction is made of the product between the wavefunction related to the internal and $c.m.$ motions as given by

$$\Psi(\vec{r}_1, \vec{r}_2, \vec{r}_3) = \psi(\vec{\lambda})\ \psi(\vec{\rho})\ e^{i\vec{P}\cdot\vec{X}} \tag{4.14}$$

where $\psi(\vec{\lambda})$ and $\psi(\vec{\rho})$ are the wave function of harmonic oscillator in Jacobi coordinates, and $e^{i\vec{P}\cdot\vec{X}}$ corresponds to the $c.m.$ motion. The wavefunction of the harmonic oscillator is identified as

$$\psi_{nlm}(\vec{r}) = R_{nl}(r)\ Y_{lm}(\hat{r}) \tag{4.15}$$

where the radial functions $R_{nl}(r)$ and the spherical harmonic function $Y_{lm}(\hat{r})$ are given in detail in Appendix A.

The total principal quantum number is denoted as

$$N = N_\lambda + N_\rho, \tag{4.16}$$

where $N_\lambda = 2n_\lambda + l_\lambda$ and $N_\rho = 2n_\rho + l_\rho$ are those related to λ and ρ mode excitation, respectively. We define n and l as the nodal and orbital angular momentum quantum numbers. The total orbital angular momentum is given by

$$\vec{l} = \vec{l}_\lambda + \vec{l}_\rho. \tag{4.17}$$

In the present work, we limit the discussion up to the principal quantum number $N = 2$ or the excitation energy $2\hbar\omega$.

It is also worth noting that the orbital wavefunction has symmetry under the interchange of the light quarks. Except $\psi_{01}(\vec{\rho})$, the other orbital wavefunction is symmetric as described in Table 4.1. For mixed $\lambda\rho$ mode, the orbital wavefunction $\psi_{01}(\vec{\lambda})\psi_{01}(\vec{\rho})$ is anti-symmetric since it contains $\psi_{01}(\vec{\rho})$.

Table 4.1. Symmetry properties of orbital wavefunction under the interchange of two light quarks.

Symmetry	Orbital wavefunction
Symmetric (S)	$\psi_{00}(\vec{\lambda}), \psi_{00}(\vec{\rho})$
	$\psi_{01}(\vec{\lambda})$
	$\psi_{10}(\vec{\lambda}), \psi_{10}(\vec{\rho})$
	$\psi_{02}(\vec{\lambda}), \psi_{02}(\vec{\rho})$
Anti-symmetric (A)	$\psi_{01}(\vec{\rho})$

4.2.2 Spin part

There are two types of coupling for combining the spin and angular momentum of three particles, namely, LS and jj couplings. For the light baryon, it is customary to use the LS coupling as

$$[[l_\lambda, l_\rho]^l, [[s_1, s_2], s_3]^s]^J. \tag{4.18}$$

However, for heavy baryons, the later one is compatible with the heavy-quark spin symmetry [89] which can be written as

$$[[[l_\lambda, l_\rho]^l, [s_1, s_2]^s]^j, s_3]^J. \tag{4.19}$$

Because of that, we will separate between the spin of the two light quarks and the heavy quark.

The heavy quark spin itself can be either $\uparrow$ $(+1/2)$ or $\downarrow$ $(-1/2)$, where we denote it as χ_c. Meanwhile, the two light quark spin can be combined as

$$\frac{\mathbf{1}}{\mathbf{2}} \otimes \frac{\mathbf{1}}{\mathbf{2}} = \mathbf{1} + \bar{\mathbf{0}}. \tag{4.20}$$

The wavefunction of the two light quarks can be found in Table 4.2. We may notice that the spin-1 (spin-0) wavefunction is symmetric (anti-symmetric) under the interchange of quarks. Here, we have defined the spin of the light quarks as d^1 and d^0 for that of spin 1 and spin 0, respectively.

Table 4.2. Spin wavefunction of two light quarks inside heavy baryons.

Spin	Notation	Wavefunction
	d^1_1	$\uparrow\uparrow$
$\mathbf{1}$	d^1_0	$\frac{1}{\sqrt{2}}\left(\uparrow\downarrow + \downarrow\uparrow\right)$
	d^1_{-1}	$\downarrow\downarrow$
$\bar{\mathbf{0}}$	d^0_0	$\frac{1}{\sqrt{2}}\left(\uparrow\downarrow - \downarrow\uparrow\right)$

4.2.3 Flavor part

For the case of heavy baryons, they contain at least a heavy quark, charm or bottom quarks, in addition to the light quarks: up, down, and strange quarks. As already discussed, the heavy quark is decoupled from the light quarks due to its heavy mass. The flavor wavefunction of the two light quarks which belong to $SU(3)$ symmetry can be combined as follows

$$\mathbf{3} \otimes \mathbf{3} = \bar{\mathbf{3}} + \mathbf{6}, \tag{4.21}$$

which is tabulated in Table 4.3. For references, the quark mass for each flavor is given by

$$m_{u(d)} = 350 \text{ MeV}, \tag{4.22}$$
$$m_s = 450 \text{ MeV}, \tag{4.23}$$
$$m_c = 1500 \text{ MeV}, \tag{4.24}$$
$$m_b = 5000 \text{ MeV}. \tag{4.25}$$

In this sense, it is interesting to say that $\Xi_{c(b)}$ baryon have three different quarks. However, we will regard the strange quark in the same footing as the up and down quarks for the first approximation. To this date, the treatment of three different quarks is not quite well established because we, strictly speaking, cannot introduce λ or ρ coordinate. In contrast, the Λ_c, Σ_c, and Ω_c can be treated more easily. In this distertation, we will focus on Λ_c and Σ_c baryons along with their bottom partners. The other heavy baryons can be studied in similar manners, in which we will do it for future studies.

Table 4.3. Flavor wavefunction of singly charmed baryons. For bottom baryons, we can replace charm quark by bottom quark.

Multiplet	Heavy baryon	Flavor wavefunction
	Σ_c^{++}	uuc
	Σ_c^{+}	$\frac{1}{\sqrt{2}}(ud+du)c$
	Σ_c^{0}	ddc
6	Ξ_c^{+}	$\frac{1}{\sqrt{2}}(us+su)c$
	Ξ_c^{0}	$\frac{1}{\sqrt{2}}(ds+sd)c$
	Ω_c^{0}	ssc
	$\Xi_c'^{+}$	$\frac{1}{\sqrt{2}}(us+su)c$
$\bar{\mathbf{3}}$	$\Xi_c'^{0}$	$\frac{1}{\sqrt{2}}(ds+sd)c$
	Λ_c^{+}	$\frac{1}{\sqrt{2}}(ud-du)c$

4.2.4 Configuration

In this subsection, we will construct the total wavefunction of Λ_c and Σ_c. Based on the observed excited states, we limit the discussion up to $N=2$ for Λ_c and $N=1$ for Σ_c, respectively. Here, we will omit the color wavefunction which is known to be anti-symmetric. The total wavefunction including orbital, spin and flavor

$$\Lambda_c(J(j)^P) = \left[\left[\psi_{nlm}(\vec{\lambda})\ \psi_{nlm}(\vec{\rho}),\ d\right]^j,\ \chi_c\right]^J_m \phi_{\Lambda_c}, \tag{4.26}$$

$$\Sigma_c(J(j)^P) = \left[\left[\psi_{nlm}(\vec{\lambda})\ \psi_{nlm}(\vec{\rho}),\ d\right]^j,\ \chi_c\right]^J_m \phi_{\Sigma_c}, \tag{4.27}$$

should be symmetric. We also note that the jj coupling scheme is used for the spin and orbital part which is compatible with heavy-quark symmetry. For bottom baryons, the total wavefunction is similar to the charmed baryon. The only difference is that the charm quark is replaced by the bottom quark in flavor wavefunction. Here, we also introduce a so-called brown muck spin j, which is the total angular momentum of light quarks.

Ground state

The ground states of charm baryons are constructed as

$$\Lambda_c(1S,1/2(0)^+) = \left[\left[\psi_{00}(\vec{\lambda})\psi_{00}(\vec{\rho}),d^0\right]^0,\chi_c\right]^{1/2}_m \phi_{\Lambda_c}, \tag{4.28}$$

and

$$\Sigma_c(1S, 1/2(1)^+) = \left[\left[\psi_{00}(\vec{\lambda})\psi_{00}(\vec{\rho}), d^1\right]^1, \chi_c\right]^{1/2}_m \phi_{\Sigma_c}, \tag{4.29}$$

$$\Sigma_c(1S, 3/2(1)^+) = \left[\left[\psi_{00}(\vec{\lambda})\psi_{00}(\vec{\rho}), d^1\right]^1, \chi_c\right]^{3/2}_m \phi_{\Sigma_c}. \tag{4.30}$$

As we know, the ϕ_{Λ_c} is anti-symmetric such that the light quark spin should zero (anti-symmetric), resulting in a HQS singlet. On the other hand, for Σ_c, the light quark spin is one which forms a so-called HQS doublet. In heavy baryons, the HQS doublet is formed when j is not equal to zero. Otherwise, the HQS singlet is formed instead.

Negative parity state

For negative parity excitation states ($N = 1$), there are two possibilities: λ-mode ($l_\lambda = 1$) or ρ-mode ($l_\rho = 1$) excitations. For Λ_c baryon, the wavefunctions are given by

$$\Lambda_c^*(1P_\lambda, J(1)^-) = \left[\left[\psi_{01}(\vec{\lambda})\psi_{00}(\vec{\rho}), d^0\right]^1, \chi_c\right]^{1\pm1/2}_m \phi_{\Lambda_c}, \tag{4.31}$$

$$\Lambda_c^*(1P_\rho, J(j)^-) = \left[\left[\psi_{00}(\vec{\lambda})\psi_{01}(\vec{\rho}), d^1\right]^j, \chi_c\right]^{J}_m \phi_{\Lambda_c}. \tag{4.32}$$

In order to anti-symmetrize the wavefunction, the Λ_c with λ-mode excitation is formed with the light quark spin $d = 0$, and make a HQS doublet $J^P = 1/2^-, 3/2^-$ with brown-muck spin $j = 1$. For ρ-mode excitation, the light quark spin $d = 1$ is needed, resulting in five possible states with $j = 0, 1,$ and 2. In total, there are seven possible configurations for negative parity states as

$$\Lambda_c^*(1/2^-) = \Lambda_c^*(1P_\lambda, 1/2(1)^-), \Lambda_c^*(1P_\rho, 1/2(0)^-), \Lambda_c^*(1P_\rho, 1/2(1)^-), \tag{4.33}$$

$$\Lambda_c^*(3/2^-) = \Lambda_c^*(1P_\lambda, 3/2(1)^-), \Lambda_c^*(1P_\rho, 3/2(1)^-), \Lambda_c^*(1P_\rho, 3/2(2)^-), \tag{4.34}$$

$$\Lambda_c^*(5/2^-) = \Lambda_c^*(1P_\rho, 5/2(2)^-). \tag{4.35}$$

The list of possible configurations of negative parity states are summarized in Table 4.4. Although a physical state could be a mixing of several configurations with the same spin-parity, we will treat them exclusively as a first step because λ and ρ mode excitation energies are well separated. We also expect that the low-lying excited states might correspond to the λ-mode excitations.

For Σ_c baryons, there are also seven negative parity states. However, there are now five states related to the λ-mode excitations. It can be understood because Σ_c has opposite symmetry of flavor wavefunction. The wavefunctions read

$$\Sigma_c^*(1P_\lambda, J(j)^-) = \left[\left[\psi_{01}(\vec{\lambda})\psi_{00}(\vec{\rho}), d^1\right]^j, \chi_c\right]^J_m \phi_{\Sigma_c}, \tag{4.36}$$

$$\Sigma_c^*(1P_\rho, J(1)^-) = \left[\left[\psi_{00}(\vec{\lambda})\psi_{01}(\vec{\rho}), d^0\right]^1, \chi_c\right]^{1\pm1/2}_m \phi_{\Sigma_c}. \tag{4.37}$$

Table 4.4. Negative parity states of Λ_c baryon: 2 λ-mode and 5 ρ-mode states. For Σ_c baryons, they appear inversely. See the text for the details.

l_λ	l_ρ	l_{total}	d	j	χ_c	J^P	
1	0	1	0	1	1/2	$1/2^-$	$3/2^-$
0	1	1	1	0	1/2	$1/2^-$	
				1	1/2	$1/2^-$	$3/2^-$
				2	1/2	$3/2^-$	$5/2^-$

Positive parity state

Up until now, there are several excited states of Λ_c observed which may correspond to the positive parity states. Because of that, it is also certainly of interest to examine those states in the quark model description. Here, we will provide the wavefunctions of positive parity states for Λ_c baryons.

In the quark model, the positive parity states are related to the $N = 2$ or $2\hbar\omega$ excitations. In this energy region, the quark model predicts a lot of states which are classified into radial (nodal) excitation ($n = 1$) and D-wave excitation ($l = 2$). For radial (nodal) excitations, we have

$$\Lambda_c^*(2S_{\lambda\lambda}, 1/2(0)^+) = \left[\left[\psi_{10}(\vec{\lambda})\psi_{00}(\vec{\rho}), d^0\right]^0, \chi_c\right]^{1/2}_m \phi_{\Lambda_c}, \tag{4.38}$$

$$\Lambda_c^*(2S_{\rho\rho}, 1/2(0)^+) = \left[\left[\psi_{00}(\vec{\lambda})\psi_{10}(\vec{\rho}), d^0\right]^0, \chi_c\right]^{1/2}_m \phi_{\Lambda_c}. \tag{4.39}$$

In this case the nodal excited states $n = 1$ is excited, the form of the wavefunction is similar to the ground state. Since the brown muck spin $j = 0$, the radial excitation forms an HQS singlet.

For D-wave excitations, there are several possible combinations, *i.e.* λ mode ($l_\lambda = 2$), ρ mode ($l_\rho = 2$), and mixed $\lambda\rho$ mode ($l_\lambda = 1, l_\rho = 1$). For λ and ρ mode, the wavefunctions are written as

$$\Lambda_c^*(1D_{\lambda\lambda}, J(2)^+) = \left[\left[\psi_{02}(\vec{\lambda})\psi_{00}(\vec{\rho}), d^0\right]^2, \chi_c\right]^{2\pm1/2}_m \phi_{\Lambda_c}, \tag{4.40}$$

$$\Lambda_c^*(1D_{\rho\rho}, J(2)^+) = \left[\left[\psi_{00}(\vec{\lambda})\psi_{02}(\vec{\rho}), d^0\right]^2, \chi_c\right]^{2\pm1/2}_m \phi_{\Lambda_c}, \tag{4.41}$$

Table 4.5. Positive parity states of Λ_c baryon: 2 radial ($n = 1$) and 17 D-wave ($l = 2$) excitations.

n_λ	n_ρ	l_λ	l_ρ	l_{total}	d	j	χ_c	J^P	
1	0			0	0		1/2	$1/2^+$	
0	1			0	0		1/2	$1/2^+$	
		2	0	2	0	2	1/2	$3/2^+$	$5/2^+$
		0	2	2	0	2	1/2	$3/2^+$	$5/2^+$
		1	1	0	1	1	1/2	$1/2^+$	$3/2^+$
				1	1	0	1/2	$1/2^+$	
						1	1/2	$1/2^+$	$3/2^+$
						2	1/2	$3/2^+$	$5/2^+$
				2	1	1	1/2	$1/2^+$	$3/2^+$
						2	1/2	$3/2^+$	$5/2^+$
						3	1/2	$5/2^+$	$7/2^+$

where the light quarks have spin zero. As we can see, D-wave excitations form an HQS doublet of $J^P = (3/2^+, 5/2^+)$ with $j = 2$.

For the mixed $\lambda\rho$ excitations, the wavefunction is given by

$$\Lambda_c^*(1D_{\lambda\rho}, J(j)^+) \quad = \quad \left[\left[\psi_{01}(\vec{\lambda})\psi_{01}(\vec{\rho}), d^1\right]^j, \chi_c\right]^J_m \phi_{\Lambda_c}. \tag{4.42}$$

where the light quark spin is one. In this case the total angular momentum have several possibilites $l = (l_\lambda + l_\rho) = 0, 1$, and 2, resulting in 13 $\lambda\rho$ mode excitation states. If we collect all the the positive parity states from $N = 2$, we obtain

$$\begin{aligned}
\Lambda_c^*(1/2^+) \quad &= \quad \Lambda_c^*(2S_{\lambda\lambda}, 1/2(0)^+), \Lambda_c^*(2S_{\rho\rho}, 1/2(0)^+), \Lambda_c^*(1D_{\lambda\rho}, 1/2(1)_0^+), \\
&\quad\ \Lambda_c^*(1D_{\lambda\rho}, 1/2(0)_1^+), \Lambda_c^*(1D_{\lambda\rho}, 1/2(1)_1^+), \Lambda_c^*(1D_{\lambda\rho}, 1/2(1)_2^+), \qquad (4.43) \\
\Lambda_c^*(3/2^+) \quad &= \quad \Lambda_c^*(1D_{\lambda\lambda}, 3/2(2)^+), \Lambda_c^*(1D_{\rho\rho}, 3/2(2)^+), \Lambda_c^*(1D_{\lambda\rho}, 3/2(1)_0^+), \\
&\quad\ \Lambda_c^*(1D_{\lambda\rho}, 3/2(1)_1^+), \Lambda_c^*(1D_{\lambda\rho}, 3/2(2)_1^+), \Lambda_c^*(1D_{\lambda\rho}, 3/2(1)_2^+), \\
&\quad\ \Lambda_c^*(1D_{\lambda\rho}, 3/2(2)_2^+), \qquad (4.44) \\
\Lambda_c^*(5/2^+) \quad &= \quad \Lambda_c^*(1D_{\lambda\lambda}, 5/2(2)^+), \Lambda_c^*(1D_{\rho\rho}, 5/2(2)^+), \Lambda_c^*(1D_{\lambda\rho}, 5/2(2)_1^+), \\
&\quad\ \Lambda_c^*(1D_{\lambda\rho}, 5/2(2)_2^+), \Lambda_c^*(1D_{\lambda\rho}, 5/2(3)_2^+) \qquad (4.45) \\
\Lambda_c^*(7/2^+) \quad &= \quad \Lambda_c^*(1D_{\lambda\rho}, 7/2(3)_2^+). \qquad (4.46)
\end{aligned}$$

where there are 19 configurations in total. The positive parity states are summarized in Table. 4.5.

As we may notice, there are a lot of states predicted by the quark model in this energy region. However, there are only a few states observed in experiments so far, leading to a well-known problem called missing resonances. Note that the potential we are using in this quark model is the harmonic oscillator. The different choices of potential may give distinct excitation states. The thorough experimental exploration in this energy region with various flavor contents may give a hint to the underlying dynamics.

4.3 Interaction between quarks and pion

In the quark model description, we assume that a pion couples to a single light quark inside a heavy baryon as a dominant process. Here, the pion is effectively regarded as a Nambu-Goldstone boson (point-like particle) based on the low-energy chiral dynamics. One of the reasons we treat the pion as a point-like particle is because its mass is quite small.

In relativistic framework, there are two type of coupling between quarks and the pion, namely, axial-vector and psudo-scalar types as

$$\mathcal{L}^{pv}_{\pi qq} = \frac{g^q_A}{2f_\pi}\bar{q}\gamma_\mu\gamma_5\vec{\tau}q\cdot\partial^\mu\vec{\pi}, \tag{4.47}$$

$$\mathcal{L}^{ps}_{\pi qq} = \frac{g^q_A}{2f_\pi}\bar{q}\gamma_5\vec{\tau}q\cdot\vec{\pi}. \tag{4.48}$$

where g^q_A is denoted as the quark axial coupling and f_π is the pion decay constant [1]. The pion and quark field are defined as π and q respectively. These two couplings are equivalent to the case of on-shell particles. However, it does not apply to the quarks confined in heavy baryons, which are off-shell. In this case, these couplings are no longer equivalent. In principle, we can use one of them or their linear combinations by imposing some constraints.

In non-relativistic framework, the interaction translates as

$$\text{nonderivative} \rightarrow \vec{\sigma}\cdot\vec{q}, \tag{4.49}$$

$$\text{derivative} \rightarrow \vec{\nabla}\cdot\vec{\sigma}. \tag{4.50}$$

where $\vec{q}$ is the pion momentum and $\vec{\sigma}$ is the Pauli matrix. The axial-vector coupling contains both of them, but the pseudo-scalar one consist of only the nonderivative piece. For heavy baryons, we may show that the pion momentum $\vec{q}$ is almost zero for $\Lambda^*_c(2595)$ decay. However, the finite decay rate is observed, indicating that the derivative piece $\vec{\nabla}\cdot\vec{\sigma}$ is quite important since the $\vec{\sigma}\cdot\vec{q}$ piece would result in a negligible contribution. By this observation, we will employ the axial-vector coupling for our present calculation, which is consistent with the low-energy theorem in chiral dynamics.

[1] We use the convention $f_\pi = 93$ MeV in our calculation.

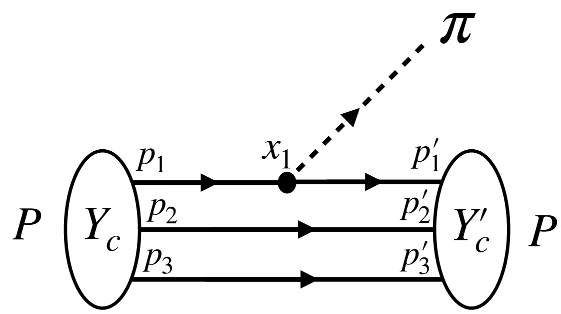

Figure 4.4. Illustration of one-pion emission decay of heavy baryon (Y_c) in the quark model.

4.4 Matrix elements of heavy baryon decay

In this section, we will calculate the matrix elements of heavy baryon decay in the quark model as described in Fig. 4.4. The matrix elements are obtained by sandwiching the interaction Lagrangian between the pion and quarks with the heavy baryon wavefunction in the quark model. Remind that the pion can couple to a single light quark.

The momentum representation of the heavy baryon state, for instance Λ_c or Σ_c, is given by

$$|Y_c(P,J)\rangle = \sqrt{2M_{Y_c}}\sum_{s,l}\int \frac{d^3\vec{p}_\rho}{(2\pi)^3}\frac{d^3\vec{p}_\lambda}{(2\pi)^3}\frac{\psi_{l_\rho}(\vec{p}_\rho)\psi_{l_\lambda}(\vec{p}_\lambda)}{\sqrt{2m}\sqrt{2m}\sqrt{2M}}\,|q_1(p_1,s_1)\rangle\,|q_2(p_2,s_2)\rangle\,|q_3(p_3,s_3)\rangle \quad (4.51)$$

where the heavy baryon state consists of the three quark states $|q_1\rangle\,|q_2\rangle\,|q_3\rangle$ and the sum is taken to make the spin J heavy baryon out of the spin and angular momentum of the three quarks. The heavy baryon state is calculated in its rest frame with mass M_{Y_c}, spin J, the relative momenta

$$\vec{p}_\lambda = \frac{1}{2m+M}(M\vec{p}_1 + M\vec{p}_2 - 2m\vec{p}_3) \qquad \text{and} \qquad \vec{p}_\rho = \frac{1}{2}(\vec{p}_1 - \vec{p}_2), \quad (4.52)$$

and the total momentum

$$\vec{P} = \vec{p}_1 + \vec{p}_2 + \vec{p}_3. \quad (4.53)$$

The quark states are normalized by the factor $1/\sqrt{2m}$ such that

$$\int \frac{d^3p_j}{(2\pi)^3}|\psi(\vec{p}_j)|^2 = 1. \quad (4.54)$$

Now, we have obtained the wavefunction of the initial and final heavy baryons.

The decay amplitude for $Y_c \to Y'_c\pi$ process can be written as

$$i\mathcal{T}_{Y_c\to Y'_c\pi} = \int d^4x_1\,\langle Y'_c(P',J')\pi(q)|i\mathcal{L}(x_1)|Y_c(P,J)\rangle \quad (4.55)$$

where we first assume the pion couples the first light quark q_1. Meanwhile, the other quarks act as spectators. For the first quark transition, we perform the non-relativistic reduction as

$$\left\langle q_1'(p_1', s_1')\pi(q)|i\mathcal{L}_{\pi qq}(x_1)|q_1(p_1, s_1)\right\rangle \approx -\frac{g_A^q}{2\pi} e^{i(p_1'-p_1+q)\cdot x_1} \left\langle \chi_{s_1'} \middle| \left(\omega_\pi(\vec{p}_1 + \vec{p}_1') \cdot \vec{\sigma} - 2m\vec{q}\cdot\vec{\sigma}\right) \middle| \chi_{s_1} \right\rangle \quad (4.56)$$

where we denote the energy and momentum of pion as ω_π and $\vec{q}$, respectively. The matrix elements of the other quarks are just a delta function given by

$$\left\langle q_j'(p_j', s_j')|q_j(p_j, s_j)\right\rangle = 2E_j(2\pi)^3\delta^{(3)}(\vec{p}_j' - \vec{p}_j)\delta_{s_j s_j'} = 2E_j \int d^3x_j e^{-i(\vec{p}_j'-\vec{p}_j)\cdot\vec{x}_j} \left\langle \chi_{s_j'} \middle| \chi_{s_j} \right\rangle \quad (4.57)$$

where $j = 2, 3$.

If we collect all of the x-integral, we will obtain

$$\int dx_1^0 d^3x_1 d^3x_2 d^3x_3 e^{-i(E_1-E_1'-\omega_\pi)\cdot x_0} e^{-i(\vec{p}_1'-\vec{p}_1+\vec{q})\cdot\vec{x}_1} e^{-i(\vec{p}_2'-\vec{p}_2)\cdot\vec{x}_2} e^{-i(\vec{p}_3'-\vec{p}_3)\cdot\vec{x}_3}. \quad (4.58)$$

Here we can observe that there are the integrals of the space and time. The time integral will give the energy conservation $(2\pi)\delta(E_1 - E_1' - \omega_\pi)$ in $q \to q'\pi$ in the quark level or $(2\pi)\delta(E - E' - \omega_\pi)$ in the baryon level where the total energy of three quark is given by $E = E_1 + E_2 + E_3$. To evaluate the space integral, we make a coordinate change into Jacobi coordinates

$$\int d^3X d^3\rho d^3\lambda e^{-i(\vec{P}'-\vec{P})\cdot\vec{X}} e^{-i(\vec{p}_\rho'-\vec{p}_\rho)\cdot\vec{\rho}} e^{-i(\vec{p}_\lambda'-\vec{p}_\lambda)\cdot\vec{\lambda}} e^{-i\vec{q}\cdot(\vec{X}+\frac{M}{2m+M}\vec{\lambda}+\frac{1}{2})}, \quad (4.59)$$

where it gives a momentum conservation $(2\pi)^3\delta(\vec{P} - \vec{P}' - \vec{q})$ by integrating $\vec{X}$.

Now, we can write the decay amplitude as

$$\begin{aligned} -i\mathcal{T} \;\; = \;\; & -\frac{g_A^q}{2f_\pi}\frac{\sqrt{2M_{Y_c}}\sqrt{2M_{Y_c'}}}{2m} \sum_{\Lambda_c,\Sigma_c} \int d^3\vec{\lambda} d^3\vec{\rho}\; e^{-i\vec{q}_\lambda\cdot\vec{\lambda}} e^{-i\vec{q}_\rho\cdot\vec{\rho}}\; \frac{d^3\vec{p}_\rho}{(2\pi)^3}\left(\psi_{l_\rho}(\vec{p}_\rho)e^{i\vec{p}_\rho\cdot\vec{\rho}}\right) \times \\ & \frac{d^3\vec{p}_\lambda}{(2\pi)^3}\left(\psi_{l_\lambda}(\vec{p}_\lambda)e^{i\vec{p}_\lambda\cdot\vec{\lambda}}\right) \frac{d^3\vec{p}_\rho'}{(2\pi)^3}\left(\psi^*_{l_\rho'}(\vec{p}_\rho')e^{-i\vec{p}_\rho'\cdot\vec{\rho}}\right) \frac{d^3\vec{p}_\lambda'}{(2\pi)^3}\left(\psi^*_{l_\lambda'}(\vec{p}_\lambda')e^{-i\vec{p}_\lambda'\cdot\vec{\lambda}}\right) \times \\ & \left\langle \chi_{s_2'} \middle| \chi_{s_2} \right\rangle \left\langle \chi_{s_c'} \middle| \chi_{s_c} \right\rangle \left\{ \omega_\pi \left\langle \chi_{s_1'} \middle| (\vec{p}_\lambda' + 2\vec{p}_\rho')\cdot\vec{\sigma} \middle| \chi_{s_1} \right\rangle + \left(\frac{\omega_\pi M}{2m+M} - 2m\right) \left\langle \chi_{s_1'} \middle| \vec{\sigma}\cdot\vec{q} \middle| \chi_{s_1} \right\rangle \right\} \end{aligned} \quad (4.60)$$

where the transfer momentums are defined by

$$\vec{q}_\lambda = \frac{M}{2m+M}\vec{q} \qquad \text{and} \qquad \vec{q}_\rho = \frac{1}{2}\vec{q}. \quad (4.61)$$

The term in Eq. (4.60) containing the momenta $(\vec{p}_\lambda' + 2\vec{p}_\rho')$ can be replaced by the derivative of the wave functions as

$$\int \frac{d^3\vec{p}'_\rho}{(2\pi)^3}\vec{p}'_\rho \psi^*_{l'_\rho}(\vec{p}'_\rho)e^{-i\vec{p}'_\rho\cdot\vec{\rho}} = i\vec{\nabla}_\rho \int \frac{d^3\vec{p}'_\rho}{(2\pi)^3}\psi^*_{l'_\rho}(\vec{p}'_\rho)e^{-i\vec{p}'_\rho\cdot\vec{\rho}} = i\vec{\nabla}_\rho\psi^*_{l'_\rho}(\vec{\rho}), \tag{4.62}$$

where the one corresponding to λ-mode can be calculated similarly. Finally, the decay amplitude now reads

$$\begin{aligned} -i\mathcal{T}_{\Lambda_c^+\to\Sigma_c^{++}\pi^-} &= -\frac{g_A^q}{2f_\pi}\frac{\sqrt{2M_{\Lambda_c}}\sqrt{2M_{\Sigma_c}}}{2m}\int d^3\vec{\lambda}e^{-i\vec{q}_\lambda\cdot\vec{\lambda}}e^{-i\vec{q}_\rho\cdot\vec{\rho}}\left\langle\Sigma_c\middle|\tau^+_{(1)}\middle|\Lambda_c\right\rangle \times \\ &\left\langle\Sigma_c\middle|\left\{\omega_\pi(i\overleftarrow{\nabla}_\lambda+2i\overleftarrow{\nabla}_\rho)\cdot\vec{\sigma}_{(1)}+\left(\omega_\pi\frac{M}{2m+M}-2m\right)\vec{\sigma}_{(1)}\cdot\vec{q}\right\}\middle|\Lambda_c\right\rangle \end{aligned} \tag{4.63}$$

where we have shown explicitly the isospin factor in the amplitude and the heavy baryon state is redefined as

$$|\Lambda_c\rangle = \left|[[\psi_{l_\lambda}(\lambda)\psi_{l_\rho}(\rho),d]^j,\chi_c]^J_M\right\rangle \equiv \sum_{l,s}\psi_{l_\lambda}(\lambda)\psi_{l_\rho}(\rho)\left|\chi_{s_1}\right\rangle\left|\chi_{s_2}\right\rangle\left|\chi_{s_c}\right\rangle. \tag{4.64}$$

Note that the operator σ and τ act on the first quark. To this end, we also need to consider when the pion couples to the other light quark $q_2(x_2)$. However, after following the similar procedures, the resulting amplitude has the same form and therefore we can simply insert factor two into the amplitude in Eq. (4.63).

4.5 Helicity amplitude

When calculating the decay amplitude, there are two different choices of basis, the partial wave basis and helicity basis as depicted in Fig. 4.5. In the partial wave basis, the spin of the final state is quantized along the same z' axis with the initial state. Here, we will use the later one, which makes the computation easier. In helicity basis, the spin of final state is now quantized along its momentum direction as

$$\left|Y'_c(\vec{p}',h)\right\rangle = \left|Y'_c(\vec{p}',J',h)\right\rangle_z. \tag{4.65}$$

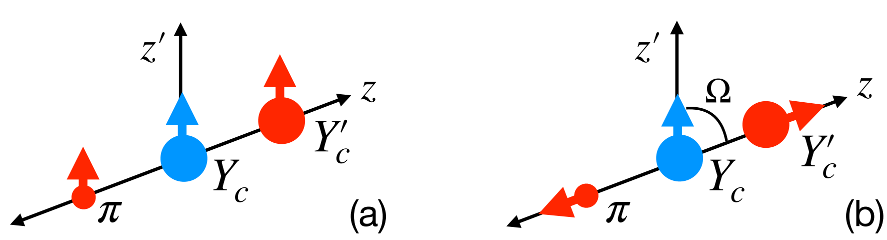

Figure 4.5. The choice of the quantization axis: (a) partial wave basis and (b) helicity basis.

For the spin of the inital state, we can rotate it into z axis by

$$|Y_i(J,J)\rangle_{z'} = \sum_m D^J_{mJ}(-\phi,\theta,\phi)\,|Y_i(J,m)\rangle_z\,, \tag{4.66}$$

where $D^J_{mJ}(-\phi,\theta,\phi)$ is the Wigner D-function. Then, the matrix element can be written as

$$_z\big\langle Y_f(\vec{p}',J',h)\pi(-\vec{p}')\,|\mathcal{T}|\,Y_i(J,J)\big\rangle_{z'} \;=\; D^J_{mJ}(-\phi,\theta,\phi)_z\,\big\langle Y_f(\vec{p}',J',h)\pi(-\vec{p}')\,|\mathcal{T}|\,Y_i(J,J)\big\rangle_z\,, \tag{4.67}$$

where the angular dependences are factored out. For convenience, we define the helicity amplitude as

$$(2\pi)^4\delta^{(4)}(P_f-P_i)A_h =_z \big\langle Y_f(\vec{p}',J',h)\pi(-\vec{p}')\,|\mathcal{T}|\,Y_i(J,J)\big\rangle_z\,. \tag{4.68}$$

Note that the helicity is conserved in the decay process, implying that only diagonal components survive.

To estimate the decay width for the one-pion emission decay, we need to take into account not only the decay amplitude but also the phase space factor. We will discuss the decay kinematics in detail in Chapter 6. For the reference, the decay width calculated in different basis is given as follows,

$$\text{Partial wave basis} \rightarrow \qquad \Gamma = \frac{1}{16\pi^2}\frac{q}{2M_i^2}\int d\Omega \sum_f |\mathcal{T}|^2, \tag{4.69}$$

$$\text{Helicity basis} \rightarrow \qquad \Gamma = \frac{1}{4\pi}\frac{q}{2M_i^2}\frac{1}{2J+1}\sum_h |\mathcal{A}_h|^2. \tag{4.70}$$

where the pion momentum q and the initial particle mass M_i. The concrete form of decay amplitudes can be found in Appendix A.

4.6 Model parameter

In the quark model, there are three parameters in the harmonic oscillator model, the light and heavy quark masses, and the spring constant k. Here, we fix the quark mass for each flavor as in Eqs. (4.22)-(4.25). Meanwhile, the sprint constant k is adjusted such that ω_λ reproduces excitation energy of the low-lying excited state, *e.g.* $\Lambda_c(2595)$ and the radius of heavy baryon as $\sqrt{\langle R^2\rangle} = 0.45 - 0.55$ fm. Note that we have assumed that $\Lambda_c(2595)$ is λ-mode excitation state. From the input parameters, we obtain other output parameters as

$$m, M, k \;\;\rightarrow\;\; \omega_\lambda, \omega_\rho, a_\lambda, a_\rho, \sqrt{\langle R^2\rangle}. \tag{4.71}$$

The value of the parameters including the model ambiguities for charmed baryons with various flavors are tabulated in Table 4.6. For bottom baryons, we can just replace the charm quark mass by the bottom quark mass and keep the spring constants the same. It is worth mentioning that there are model uncertainties, originating from the quark axial coupling g_A^q and the pion decay constant f_π.

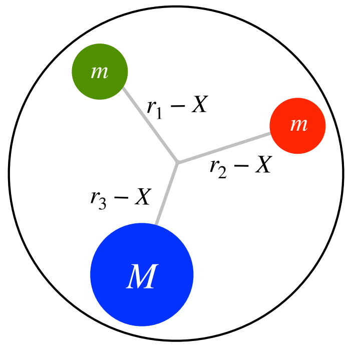

Figure 4.6. Estimation of the heavy baryon radius in the quark model.

Here, the baryon radius is defined as the average distance of each quark from the center-of-mass as described in Fig. 4.6. Then, the radius can be written as

$$\langle R^2 \rangle = \frac{1}{3}\sum_{i=1}^{3}(\vec{r}_i - \vec{X})^2 = \frac{1}{3}\left[\frac{2(2m^2+M^2)}{(2m+M)^2}\langle \lambda^2 \rangle + \frac{1}{2}\langle \rho^2 \rangle\right], \tag{4.72}$$

$$\langle \lambda^2 \rangle = \int \mathrm{d}^3\lambda \; \lambda^2 \psi^*_{00}(\vec{\lambda})\psi_{00}(\vec{\lambda}) = \frac{3}{2}\frac{1}{a_\lambda^2}, \tag{4.73}$$

$$\langle \rho^2 \rangle = \int \mathrm{d}^3\rho \; \rho^2 \psi^*_{00}(\vec{\rho})\psi_{00}(\vec{\rho}) = \frac{3}{2}\frac{1}{a_\rho^2}. \tag{4.74}$$

where $\langle \lambda^2 \rangle$ and $\langle \rho^2 \rangle$ are computed by using the ground states in the harmonic oscillator.

Table 4.6. Parameters used in quark model for charmed baryon with various flavors.

	Parameter	$\Lambda_c(udc)$	$\Xi_c(usc)$	$\Omega_c(ssc)$
Input	m	0.3-0.4 GeV	0.35-0.45 GeV	0.4-0.5 GeV
	M	1.4-1.6 GeV	1.4-1.6 GeV	1.4-1.6 GeV
	k	0.02-0.04 GeV^3	0.02-0.04 GeV^3	0.02-0.04 GeV^3
Output	ω_λ	0.27-0.44 GeV	0.26-0.41 GeV	0.25-0.40 GeV
	ω_ρ	0.39-0.63 GeV	0.37-0.59 GeV	0.35-0.55 GeV
	a_λ	0.36-0.45 GeV	0.37-0.46 GeV	0.38-0.47 GeV
	a_ρ	0.26-0.33 GeV	0.27-0.34 GeV	0.28-0.35 GeV
	$\sqrt{\langle R^2 \rangle}$	0.42-0.56 fm	0.41-0.53 fm	0.39-0.51 fm

"The world of quark has everything to do with a jaguar circling in the night", Murray Gell-Mann

Chapter 5
Effective Lagrangian approach

5.1 Introduction

In this chapter, we will introduce our strategies in investigating the three-body decay of heavy baryons. In the previous chapters, we have discussed the quark model to describe two-body decay. However, to study their three-body decay, we need to employ another phenomenological model to simplify the calculation.

In the present work, we employ a so-called effective Lagrangian approach to describe the decay process. In this approach, we first need to determine relevant tree-level Feynman diagrams that contribute to the decay process as described in Fig. 5.1(a). Also, the parameters in the effective Lagrangian are usually unknown and should be fixed either by the experimental data or other microscopic models. Here, we will fix the parameter by the input from the quark model. This method is also called the isobar model where we put some resonances in intermediate states by hand. This model may suffer more uncertainties when we consider more resonances in the decay process. In this study, however, only several resonances may contribute to the process which makes the analysis has fewer uncertainties.

Generally, the isobar model suffers an inherent problem such as it violates the unitarity. However, in the heavy baryon decay, in particular, $\Lambda_c^* \to \Lambda_c \pi\pi$ decay, the opening threshold is sufficiently far, which justify the application of this method where the unitarity is not badly violated. If the opening thresholds play dominant roles, the dynamical model is certainly needed to maintain the unitarity. In fact, the dynamical model, as described in Fig. 5.1(b), is a more complete model and has been studied extensively in various studies, *e.g.* Ref [213]. But, depending on the situation, the isobar model can work sufficiently well and in some works, the momentum dependence in the propagator is introduced to restore the unitarity.

Effective Lagrangians are usually constructed in the relativistic framework as done in many works *e.g.* Ref [214]. In this framework, the Lagrangian consists of the relevant meson and baryon fields with Cillford algebra. The calculation will be complicated as we consider the higher spin-parity resonances. However, in this study, the pion momentum in $\Lambda_c^* \to \Lambda_c \pi\pi$ decay is quite small where the non-relativistic approximation is quite good. Therefore, we perform the non-relativistic reduction of the amplitudes for practical calculation [122]. In this way, it not only simplifies the calculation but also

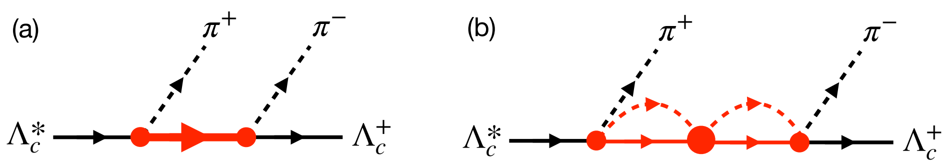

Figure 5.1. How to model the three-body decay: (a) isobar model and (b) dynamical model.

gives more intuitive pictures of the underlying problem. In particular, the angular dependence can be derived more intuitively in this method as we will see later.

5.2 Non-relativistic reduction

In calculating the heavy-baryon decay, we practically employ effective Lagrangians in the non-relativistic framework. This approximation is sufficiently good because the energy of the emitting pion is relatively small in heavy-baryon decay. Here, we will give some examples of how the relativistic effective Lagrangian can be reduced into the non-relativistic one, by picking up the leading order term. The concrete formulations that we use in the present work will be discussed in the next section.

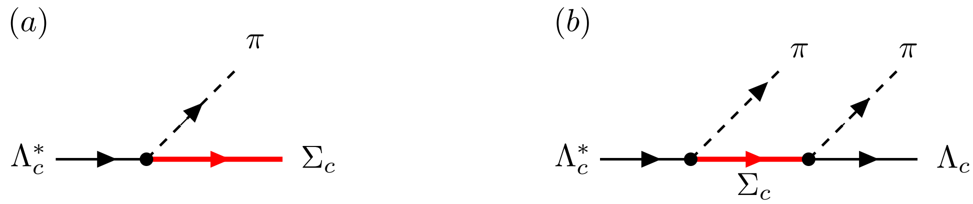

Figure 5.2. (a) two-body decay of $\Lambda_c^* \to \Sigma_c \pi$ and (b) three-body decay of $\Lambda_c^* \to \Lambda_c \pi\pi$ going through Σ_c in intermediate state.

5.2.1 Two-body decay

First, let us consider the two-body decay of $\Lambda_c^*(p) \to \Sigma_c(p')\pi(q)$ which is depicted in Fig. 5.2(a). Note that the corresponding momentum is written in the parenthesis. The effective Lagrangian is given by

$$\mathcal{L}_{\Lambda_c^* \Sigma_c \pi} = g\ \bar{\psi}_{\Sigma_c} \Gamma_5 \psi_{\Lambda_c^*} \pi + h.c., \tag{5.1}$$

where $h.c.$ stands for hermitian conjugate. Also, we omit the isospin for simplicity and we define

$$\Gamma_5 = \begin{cases} 1 & \text{for } \Lambda_c^*(1/2^-), \\ \gamma_5 & \text{for } \Lambda_c^*(1/2^+). \end{cases} \tag{5.2}$$

Remember that Σ_c has spin-parity $1/2^+$.

For the case of $\Lambda_c(1/2^-)$, we obtain the amplitude as

$$-i\mathcal{T} = g\ \bar{u}(p')u(p). \tag{5.3}$$

The amplitude can be expanded as

$$
\begin{aligned}
-i\mathcal{T} &= g\,\sqrt{E'+m'}\sqrt{E+m}\left(\chi^\dagger_{\Sigma_c}, -\chi^\dagger_{\Sigma_c}\frac{\boldsymbol{\sigma}\cdot\mathbf{p}'}{E'+m'}\right)\left(\begin{array}{c}\chi_{\Lambda_c^*}\\ \dfrac{\boldsymbol{\sigma}\cdot\mathbf{p}}{E+m}\chi_{\Lambda_c^*}\end{array}\right)\\
&= g\,\sqrt{2m'}\sqrt{2m}\;\chi^\dagger_{\Sigma_c}\left(1-\frac{\boldsymbol{\sigma}\cdot\mathbf{p}'}{2m'}\frac{\boldsymbol{\sigma}\cdot\mathbf{p}}{2m}\right)\chi_{\Lambda_c^*}
\end{aligned}
\tag{5.4}
$$

where the energy and mass of the baryons are denoted as E and m, respectively. We denote the spin state of Λ_c^* and Σ_c as $\chi_{\Lambda_c^*}$ and χ_{Σ_c}, respectively. The leading oder term of this amplitude is given by

$$
-i\mathcal{T}_{nr} \propto g\;\chi^\dagger_{\Sigma_c}1\chi_{\Lambda_c^*},
\tag{5.5}
$$

where the amplitude does not have pion momentum dependent, which is consistent with the s-wave decay of $\Lambda_c(1/2^-)\to\Sigma_c\pi$.

For the case of $\Lambda_c(1/2^+)$, we obtain the amplitude as

$$
-i\mathcal{T} = g\;\bar{u}(p')\gamma_5 u(p).
\tag{5.6}
$$

We expand the amplitude as

$$
\begin{aligned}
-i\mathcal{T} &= g\,\sqrt{E'+m'}\sqrt{E+m}\left(\chi^\dagger_{\Sigma_c}, -\frac{\boldsymbol{\sigma}\cdot\mathbf{p}'}{E'+m'}\chi^\dagger_{\Sigma_c}\right)\left(\begin{array}{cc}0 & 1\\ 1 & 0\end{array}\right)\left(\begin{array}{c}\chi_{\Lambda_c^*}\\ \dfrac{\boldsymbol{\sigma}\cdot\mathbf{p}}{E+m}\chi_{\Lambda_c^*}\end{array}\right)\\
&= g\,\sqrt{2m'}\sqrt{2m}\chi^\dagger_{\Sigma_c}\left(\frac{\boldsymbol{\sigma}\cdot\mathbf{p}}{2m}-\frac{\boldsymbol{\sigma}\cdot\mathbf{p}'}{2m'}\right)\chi_{\Lambda_c^*}\\
&= g\,\sqrt{2m'}\sqrt{2m}\chi^\dagger_{\Sigma_c}\left(\frac{\boldsymbol{\sigma}\cdot\mathbf{q}}{m+m'}\right)\chi_{\Lambda_c^*}
\end{aligned}
\tag{5.7}
$$

By taking the pion momentum $p-p'=q$, we obtain the amplitude as

$$
-i\mathcal{T}_{nr} \propto g\;\chi^\dagger_{\Sigma_c}\left(\boldsymbol{\sigma}\cdot\mathbf{q}\right)\chi_{\Lambda_c^*},
\tag{5.8}
$$

where it is now propotional to the pion momentum $\mathbf{q}$. We will obtain the similar result by using different type of coupling, namely the psudovector coupling. The interaction Lagrangian is given by

$$
\mathcal{L}_{\Lambda_c^*\Sigma_c\pi} = g'\;\bar{\psi}_{\Sigma_c}\gamma_\mu\gamma_5\psi_{\Lambda_c^*}\partial^\mu\pi + h.c.,
\tag{5.9}
$$

Then, we obtain the amplitude

$$
-i\mathcal{T} = g'\;\bar{u}(p')\not{k}\gamma_5 u(p).
\tag{5.10}
$$

The non-relativistic expansion is obtained as

$$
\begin{aligned}
-i\mathcal{T} &= g'\,\sqrt{E'+m'}\sqrt{E+m}\left(\chi^\dagger_{\Sigma_c}, -\frac{\boldsymbol{\sigma}\cdot\mathbf{p}'}{E'+m'}\chi^\dagger_{\Sigma_c}\right)\begin{pmatrix}\omega & -\boldsymbol{\sigma}\cdot\mathbf{q}\\ \boldsymbol{\sigma}\cdot\mathbf{q} & -\omega\end{pmatrix}\begin{pmatrix}0 & 1\\ 1 & 0\end{pmatrix}\begin{pmatrix}\chi_{\Lambda_c^*}\\ \dfrac{\boldsymbol{\sigma}\cdot\mathbf{p}}{E+m}\chi_{\Lambda_c^*}\end{pmatrix}\\
&= g'\,\sqrt{2m'}\sqrt{2m}\chi^\dagger_{\Sigma_c}\left[-\boldsymbol{\sigma}\cdot\mathbf{q}+\omega\left(\frac{\boldsymbol{\sigma}\cdot\mathbf{p}}{2m}+\frac{\boldsymbol{\sigma}\cdot\mathbf{p}'}{2m'}\right)\right]\chi_{\Lambda_c^*}+\ldots \qquad (5.11)
\end{aligned}
$$

where "..." corresponds to the higher momentum term. As we can see, the leading order term is proportional to the pion momentum $\mathbf{q}$, which is similar to that of Eq. (5.8). The difference is the dimension of the coupling strength

$$
g = g'(m+m'). \qquad (5.12)
$$

For the Λ_c with spin-parity $3/2^\pm$, we need to introduce the Rarita-Schwinger field, and the non-relativistic reduction can be performed similarly. In the non-relativistic approximation, the resulting amplitude is proportional to the momentum q^L with the suitable spin operator. Note that L is the relative angular momentum of the outgoing particles.

5.2.2 Three-body decay

Now let us consider the three-body decay of $\Lambda_c^* \to \Sigma_c\pi \to \Lambda_c\pi\pi$ as illustrated in Fig. 5.2(b). Suppose the the initial state Λ_c^* has the spin and parity $1/2^-$, then we have the Lagrangian for the first and the second vertices as

$$
\begin{aligned}
\mathcal{L}_{\Lambda_c^*\Sigma_c\pi} &= g_1\,\bar\psi_{\Sigma_c}\psi_{\Lambda_c^*}\pi + h.c., &(5.13)\\
\mathcal{L}_{\Sigma_c\Lambda_c\pi} &= g_2\,\bar\psi_{\Lambda_c}\gamma_5\psi_{\Sigma_c}\pi + h.c. &(5.14)
\end{aligned}
$$

Then, the decay amplitude can be written as

$$
\begin{aligned}
-i\mathcal{T} &= g_1g_2\,\bar u(p_3)\gamma_5\frac{i}{\not p_2+\not p_3-m_{\Sigma_c}}u(p)\\
&= g_1g_2\,\bar u(p_3)\gamma_5\frac{\not p_2+\not p_3+m_{\Sigma_c}}{(p_2+p_3)^2-m^2_{\Sigma_c}}u(p) = g_1g_2\,\bar u(p_3)\frac{(-\not p_2-m_{\Lambda_c}+m_{\Sigma_c})\gamma_5}{(p_2+p_3)^2-m^2_{\Sigma_c}}u(p)\\
&= -g_1g_2\,\bar u(p_3)\frac{\not p_2\gamma_5}{(p_2+p_3)^2-m^2_{\Sigma_c}}u(p), \qquad (5.15)
\end{aligned}
$$

where here the p_1, p_2, and p_3 correspond to the momentum of π_1, π_2 and Λ_c in final states. By performing the non-relativistic reduction, we will obtain the amplitude as

$$
-i\mathcal{T}_{nr} \propto g_1g_2\,\frac{\chi^\dagger_{\Lambda_c}\,(\boldsymbol{\sigma}\cdot\mathbf{p}_2)\,\chi_{\Lambda_c^*}}{(p_2+p_3)^2-m^2_{\Sigma_c}}. \qquad (5.16)
$$

Now, we can see that the amplitudes are propotional to $\mathbf{p}_2$ where the Σ_c decay into $\Lambda_c\pi$ in p wave, whereas no $\mathbf{p}_1$ dependence in the amplitude which is telling us that the Λ_c^* decay in s wave. If we use the pseudovector coupling for the second vertex, we will obtain a similar result.

5.3 Non-relativistic Feynman rule

Now let us try to construct Feynman's rule for the three-body decay in the non-relativistic framework based on our observations. We first consider the Lagrangian for each vertex as

$$\begin{aligned}
\mathcal{L}_{\Lambda_c^*\Sigma_c\pi} &= g_1\,\bar{\psi}_{\Sigma_c}\Gamma_1\psi_{\Lambda_c^*}\pi + h.c., && (5.17)\\
\mathcal{L}_{\Sigma_c\Lambda_c\pi} &= g_2\,\bar{\psi}_{\Lambda_c}\Gamma_2\psi_{\Sigma_c}\pi + h.c. && (5.18)
\end{aligned}$$

Then, we can write amplitudes as

$$\begin{aligned}
-i\mathcal{T}_1 &= g_1\,\chi^\dagger_{\Sigma_c}\,(v_1)\,\chi_{\Lambda_c^*}, && (5.19)\\
-i\mathcal{T}_2 &= g_2\,\chi^\dagger_{\Lambda_c}\,(v_2)\,\chi_{\Sigma_c}, && (5.20)
\end{aligned}$$

where v_1 and v_2 are the leading order terms in the non-relativistic expansion. The propagator is given by

$$\frac{i}{p^2_{\Sigma_c}-m^2_{\Sigma_c}} \to \frac{i}{p^2_{\Sigma_c}-(m_{\Sigma_c}-i\Gamma_{\Sigma_c}/2)^2}, \tag{5.21}$$

where the Σ_c has a finite width Γ_{Σ_c}.

The three-body decay amplitude can be expressed as

$$\begin{aligned}
-i\mathcal{T} &= \langle -i\mathcal{T}_2\rangle \frac{i}{p^2_{\Sigma_c}-(m_{\Sigma_c}-i\Gamma_{\Sigma_c}/2)^2}\langle -i\mathcal{T}_1\rangle\\
&= ig_1g_2\sqrt{E_{\Lambda_c}+m_{\Lambda_c}}\sqrt{E_{\Lambda_c^*}+m_{\Lambda_c^*}}(E_{\Sigma_c}+m_{\Sigma_c})\,\frac{\chi^\dagger_{\Lambda_c}(v_2)\chi_{\Sigma_c}\;\chi^\dagger_{\Sigma_c}(v_1)\,\chi_{\Lambda_c^*}}{m^2_{23}-(m_{\Sigma_c}-i\Gamma_{\Sigma_c}/2)^2}. && (5.22)
\end{aligned}$$

where we have replace $p^2_{\Sigma_c}=(p_2+p_3)^2=m^2_{23}$ in the second line. This m^2_{23} is usually known as the invariant mass of particle 2 (π_2) and 3 (Λ_c). We can further approximate the propagator

$$\begin{aligned}
m^2_{23}-\tilde{m}^2_{\Sigma_c} &= (m_{23}+\tilde{m}_{\Sigma_c})(m_{23}-\tilde{m}_{\Sigma_c})\\
&\approx (E_{\Sigma_c}+m_{\Sigma_c})(m_{23}-\tilde{m}_{\Sigma_c}). && (5.23)
\end{aligned}$$

such that the amplitude can be written as

$$-i\mathcal{T} = ig_1g_2\sqrt{E_{\Lambda_c}+m_{\Lambda_c}}\sqrt{E_{\Lambda_c^*}+m_{\Lambda_c^*}}\,\frac{\chi^\dagger_{\Lambda_c}(v_2)\,(v_1)\,\chi_{\Lambda_c^*}}{m_{23}-m_{\Sigma_c}+i\Gamma_{\Sigma_c}/2}. \tag{5.24}$$

This approximation is valid for the slowly moving Σ_c resonance and near $m_{23} \approx m_{\Sigma_c}$, which is the case for our practical calculation.

5.4 Decay amplitude

In the present work, we are interested in studying the two-pion emission decays of heavy baryons, such as $\Lambda_c, \Xi_c, \Lambda_b$, and Ξ_b. To model such a three-body decay process, we employ the Lagrangian in the non-relativistic framework, which is sufficiently well for these baryons. If we revisit the quark model configuration up to $N = 2$, there are many possible states with spin and parity $J^P = 1/2^{\pm}, 3/2^{\pm}, 5/2^{\pm}$ and $7/2^+$. In this calculation, we will consider such spin-parity assignments for the initial particle.

In this section, let us consider $\Lambda_c^* \to \Lambda_c\pi\pi$ decay going through $\Sigma_c(1/2^+)$ and $\Sigma_c^*(3/2^+)$ in intermediate states. What we need to calculate first is the decay amplitude for each vertex. For that purpose, we denote the spin transition operators as given in Table 5.1, which are represented in the cartesian coordinates. We can construct them by using Wigner-Eckart theorem as

$$\left\langle J_f \; m_f \left| S^L_\mu \right| J_i \; m_i \right\rangle \;\; = \;\; \left(J_i \; m_i \; L \; \mu \middle| J_f \; m_f \right), \tag{5.25}$$

where the operator is expressed in the spherical basis. From the equation above, the matrix element of the spin transition operators is related to the Clebsh-Gordan coefficients. The rank of the operator L is following the partial wave of the outgoing pion. We have defined the reduced matrix element equal to unity for the spin transition operators. Note that the arbitrariness is taken into account in the coupling strength of the amplitude. The concrete forms of the spin transition operator can be found in Appendix C.

Table 5.1. Definitions of the spin transition operators used in this calculation.

Spin operator		Spin transition operator	
$\boldsymbol{\sigma}$	spin 1/2	$\mathbf{S}^\dagger$	spin 1/2 to 3/2
$\boldsymbol{\Sigma}$	spin 3/2	$\mathbf{T}^\dagger$	spin 3/2 to 5/2
		$\mathbf{U}^\dagger$	spin 5/2 to 7/2
		$\mathbf{V}^\dagger_{ij}$	spin 3/2 to 3/2 (d-wave)
		$\mathbf{W}^\dagger_{ijk}$	spin 3/2 to 3/2 (f-wave)
		$\mathbf{X}^\dagger_{ijk}$	spin 3/2 to 5/2 (f-wave)

Next let us consider the first vertex, $\Lambda_c^* \to \Sigma_c^{(*)}\pi$ decay. The amplitude with the various spin-parity assignment of Λ_c^* is given in Table 5.2. Remind that $\mathbf{p}_1$ and $\mathbf{p}_2$ correspond to the pion momentum emitted from the first and second vertex, respectively. The coupling strength g_{1a} and g_{1b} are related to that of Σ_c and Σ_c^*, respectively, where the partial wave of pion is written as a superscript.

We observe that there is only one partial wave of pion is possible for $\Sigma_c\pi$ channel. On the other

Table 5.2. Amplitudes of $\Lambda_c^* \to \Sigma_c^{(*)}\pi$ decay with various spin-parity assignments of Λ_c^*. The definitions can be found in the text.

Initial state	$-i\mathcal{T}_{\Lambda_c^*\to\Sigma_c\pi}$	$-i\mathcal{T}_{\Lambda_c^*\to\Sigma_c^*\pi}$
$\Lambda_c^*(1/2^-)$	$g_{1a}^s\ \chi_{\Sigma_c}^\dagger \chi_{\Lambda_c^*}$	$g_{1b}^d\ \chi_{\Sigma_c^*}^\dagger (\mathbf{S}^\dagger\cdot\mathbf{p}_1)(\boldsymbol{\sigma}\cdot\mathbf{p}_1)\chi_{\Lambda_c^*}$
$\Lambda_c^*(3/2^-)$	$g_{1a}^d\ \chi_{\Sigma_c}^\dagger (\boldsymbol{\sigma}\cdot\mathbf{p}_1)(\mathbf{S}\cdot\mathbf{p}_1)\chi_{\Lambda_c^*}$	$g_{1b}^s\ \chi_{\Sigma_c^*}^\dagger \chi_{\Lambda_c^*} +$ $g_{1b}^d\ \chi_{\Sigma_c^*}^\dagger (\mathbf{p}_1\cdot\mathbf{V}\cdot\mathbf{p}_1)\,\chi_{\Lambda_c^*}$
$\Lambda_c^*(5/2^-)$	$g_{1a}^d\ \chi_{\Sigma_c}^\dagger (\mathbf{S}\cdot\mathbf{p}_1)(\mathbf{T}\cdot\mathbf{p}_1)\chi_{\Lambda_c^*}$	$g_{1b}^d\ \chi_{\Sigma_c^*}^\dagger (\boldsymbol{\Sigma}\cdot\mathbf{p}_1)(\mathbf{T}\cdot\mathbf{p}_1)\chi_{\Lambda_c^*}$
$\Lambda_c^*(1/2^+)$	$g_{1a}^p\ \chi_{\Sigma_c}^\dagger (\boldsymbol{\sigma}\cdot\mathbf{p}_1)\chi_{\Lambda_c^*}$	$g_{1b}^p\ \chi_{\Sigma_c^*}^\dagger (\mathbf{S}^\dagger\cdot\mathbf{p}_1)\chi_{\Lambda_c^*}$
$\Lambda_c^*(3/2^+)$	$g_{1a}^p\ \chi_{\Sigma_c}^\dagger (\mathbf{S}\cdot\mathbf{p}_1)\chi_{\Lambda_c^*}$	$g_{1b}^p\ \chi_{\Sigma_c^*}^\dagger (\boldsymbol{\Sigma}\cdot\mathbf{p}_1)\chi_{\Lambda_c^*} +$ $g_{1b}^f\ \chi_{\Sigma_c^*}^\dagger (W_{ijk}\ p_{1i}\ p_{1j}\ p_{1k})\,\chi_{\Lambda_c^*}$
$\Lambda_c^*(5/2^+)$	$g_{1a}^f\ \chi_{\Sigma_c}^\dagger (\boldsymbol{\sigma}\cdot\mathbf{p}_1)(\mathbf{S}\cdot\mathbf{p}_1)(\mathbf{T}\cdot\mathbf{p}_1)\chi_{\Lambda_c^*}$	$g_{1b}^p\ \chi_{\Sigma_c^*}^\dagger (\mathbf{T}\cdot\mathbf{p}_1)\chi_{\Lambda_c^*} +$ $g_{1b}^f\ \chi_{\Sigma_c^*}^\dagger (X_{ijk}\ p_{1i}\ p_{1j}\ p_{1k})\,\chi_{\Lambda_c^*}$
$\Lambda_c^*(7/2^+)$	$g_{1a}^f\chi_{\Sigma_c}^\dagger (\mathbf{S}\cdot\mathbf{p}_1)(\mathbf{T}\cdot\mathbf{p}_1)(\mathbf{U}\cdot\mathbf{p}_1)\chi_{\Lambda_c^*}$	$g_{1b}^f\chi_{\Sigma_c^*}^\dagger (\boldsymbol{\Sigma}\cdot\mathbf{p}_1)(\mathbf{T}\cdot\mathbf{p}_1)(\mathbf{U}\cdot\mathbf{p}_1)\chi_{\Lambda_c^*}$

hand, there are two possible partial waves for the case of $\Sigma_c^*\pi$ channel, except for $\Lambda_c(1/2^\pm)$. For the case of $\Lambda_c(5/2^-)$ and $\Lambda_c(7/2^+)$, although the higher partial waves (g and h wave, respectively) are possible in baryon level, there is a brown-muck selection rule in the quark model which forbids such transition. Therefore, we will not consider them in the calculation.

Similarly, we can compute the amplitude for the second vertex $\Sigma_c \to \Lambda_c\pi$ and $\Sigma_c^* \to \Lambda_c\pi$ as

$$
\begin{aligned}
-i\mathcal{T}_{\Sigma_c\to\Lambda_c\pi} &= g_{2a}^p\ \chi_{\Lambda_c}^\dagger\,(\boldsymbol{\sigma}\cdot\mathbf{p}_2)\,\chi_{\Sigma_c}, &(5.26)\\
-i\mathcal{T}_{\Sigma_c^*\to\Lambda_c\pi} &= g_{2b}^p\ \chi_{\Lambda_c}^\dagger\,(\mathbf{S}\cdot\mathbf{p}_2)\,\chi_{\Sigma_c^*}, &(5.27)
\end{aligned}
$$

where both $\Sigma_c^{(*)}$ decay into $\Lambda_c\pi$ in p wave.

5.4.1 Helicity amplitude

The amplitude can also be expressed in the helicity amplitudes. This procedure can simplify the calculation because we do not have to calculate whole the matrix element of the spin transition operators. Moreover, we will compare this helicity amplitude to that of the quark model.

Here, we will provide some example of calculating the helicity amplitudes. Let us start from

Table 5.3. Helicity amplitudes calculated in effective Lagrangians with various spin and parity assignments of Λ_c^* for $\Lambda_c^* \to \Sigma_c^{(*)}\pi$ and $\Sigma_c^{(*)} \to \Lambda_c\pi$ decays.

Initial state	h	$A_h(\Lambda_c^* \to \Sigma_c\pi)$	$A_h(\Lambda_c^* \to \Sigma_c^*\pi)$	
$\Lambda_c^*(1/2^-)$	1/2	g_{1a}^s	$\sqrt{\frac{2}{3}}g_{1b}^d\ p^2$	
$\Lambda_c^*(3/2^-)$	1/2	$-\sqrt{\frac{2}{3}}g_{1a}^d\ p^2$	g_{1b}^s	$-\frac{1}{\sqrt{5}}g_{1b}^d\ p^2$
	3/2		g_{1b}^s	$+\frac{1}{\sqrt{5}}g_{1b}^d\ p^2$
$\Lambda_c^*(5/2^-)$	1/2	$\sqrt{\frac{2}{5}}g_{1a}^d\ p^2$	$-\sqrt{\frac{3}{5}}g_{1b}^d\ p^2$	
	3/2		$-\sqrt{\frac{18}{5}}g_{1b}^d\ p^2$	
$\Lambda_c^*(1/2^+)$	1/2	$g_{1a}^p\ p$	$\sqrt{\frac{2}{3}}g_{1b}^p\ p$	
$\Lambda_c^*(3/2^+)$	1/2	$-\sqrt{\frac{2}{3}}g_{1a}^p\ p$	$g_{1b}^p\ p$	$-\frac{3}{\sqrt{35}}g_{1b}^f\ p^3$
	3/2		$3g_2^p\ p$	$+\frac{1}{\sqrt{35}}g_2^f\ p^3$
$\Lambda_c^*(5/2^+)$	1/2	$\sqrt{\frac{2}{5}}g_{1a}^f\ p^3$	$-\sqrt{\frac{3}{5}}g_{1b}^p\ p$	$+\sqrt{\frac{6}{35}}g_{1b}^f\ p^3$
	3/2		$-\sqrt{\frac{2}{5}}g_2^p\ p$	$-\frac{3}{\sqrt{35}}g_{1b}^f\ p^3$
$\Lambda_c^*(7/2^+)$	1/2	$-\sqrt{\frac{8}{35}}g_{1a}^f\ p^3$	$\sqrt{\frac{12}{35}}g_{1b}^f\ p^3$	
	3/2		$\sqrt{\frac{12}{7}}g_{1b}^f\ p^3$	
		$A_h(\Sigma_c^{(*)} \to \Lambda_c\pi)$		
$\Sigma_c(1/2^+)$	1/2	$g_{2a}^p\ p$		
$\Sigma_c^*(3/2^+)$	1/2	$-\sqrt{\frac{2}{3}}g_{2b}^p\ p$		

$\Lambda_c^*(1/2^-)$ decays, the helicity amplitudes are calculated as

$$-iA_{1/2}(\Lambda_c^* \to \Sigma_c\pi) \;=\; g_{1a}^s \left\langle \tfrac{1}{2}, \tfrac{1}{2}\right| \left. \tfrac{1}{2}, \tfrac{1}{2}\right\rangle = g_{1a}^s, \tag{5.28}$$

$$-iA_{1/2}(\Lambda_c^* \to \Sigma_c^*\pi) \;=\; g_{1b}^d \left\langle \tfrac{3}{2}, \tfrac{1}{2}\right| (\mathbf{S}^\dagger \cdot \mathbf{p})(\boldsymbol{\sigma} \cdot \mathbf{p}) \left| \tfrac{1}{2}, \tfrac{1}{2}\right\rangle = \sqrt{\frac{2}{3}} g_{1b}^d\ p^2. \tag{5.29}$$

As we may notice, the amplitudes now consist of the momentum and coupling strength along with the suitable constants which originiated form the Clebsh-Gordon coefficients.

Similarly, for $\Lambda_c^*(3/2^-) \to \Sigma_c\pi$ decay, we obtain

$$-iA_{1/2}(\Lambda_c^* \to \Sigma_c\pi) \;=\; g_{1a}^d \left\langle \tfrac{1}{2}, \tfrac{1}{2}\right| (\boldsymbol{\sigma} \cdot \mathbf{p})(\mathbf{S} \cdot \mathbf{p}) \left| \tfrac{3}{2}, \tfrac{1}{2}\right\rangle = -\sqrt{\frac{2}{3}} g_{1a}^d\ p^2. \tag{5.30}$$

Note that for $\Sigma_c^*\pi$ channel, we have two helicity amplitudes $A_{1/2}$ and $A_{3/2}$ because now Σ_c^* has spin 3/2. Also, there are two partial waves available, namely s and d waves. For the case of s-wave, the amplitudes are given by

$$
\begin{aligned}
-iA_{1/2}(\Lambda_c^* \to \Sigma_c^*\pi) &= g_{1b}^s \left\langle \tfrac{3}{2}, \tfrac{1}{2} \middle| \tfrac{3}{2}, \tfrac{1}{2} \right\rangle = g_{1b}^s, && (5.31)\\
-iA_{3/2}(\Lambda_c^* \to \Sigma_c^*\pi) &= g_{1b}^s \left\langle \tfrac{3}{2}, \tfrac{3}{2} \middle| \tfrac{3}{2}, \tfrac{3}{2} \right\rangle = g_{1b}^s, && (5.32)
\end{aligned}
$$

and for the case of d-wave, they are written as

$$
\begin{aligned}
-iA_{1/2}(\Lambda_c^* \to \Sigma_c^*\pi) &= g_{1b}^d \left\langle \tfrac{3}{2}, \tfrac{1}{2} \right| (\mathbf{p}\cdot\mathbf{V}\cdot\mathbf{p}) \left| \tfrac{3}{2}, \tfrac{1}{2} \right\rangle = g_2^d\, p^2 \left\langle \tfrac{3}{2}, \tfrac{1}{2} \right| V_{zz} \left| \tfrac{3}{2}, \tfrac{1}{2} \right\rangle = -\frac{1}{\sqrt{5}} g_{1b}^d\, p^2, && (5.33)\\
-iA_{3/2}(\Lambda_c^* \to \Sigma_c^*\pi) &= g_{1b}^d \left\langle \tfrac{3}{2}, \tfrac{3}{2} \right| (\mathbf{p}\cdot\mathbf{V}\cdot\mathbf{p}) \left| \tfrac{3}{2}, \tfrac{3}{2} \right\rangle = \frac{1}{\sqrt{5}} g_{1b}^d\, p^2. && (5.34)
\end{aligned}
$$

Thus, the helicity amplitudes for $h = 1/2$ and $3/2$ are given by

$$
\begin{aligned}
-iA_{1/2}(\Lambda_c^* \to \Sigma_c^*\pi) &= g_{1b}^s - \frac{1}{\sqrt{5}} g_{1b}^d\, p^2, && (5.35)\\
-iA_{3/2}(\Lambda_c^* \to \Sigma_c^*\pi) &= g_{1b}^s + \frac{1}{\sqrt{5}} g_{1b}^d\, p^2. && (5.36)
\end{aligned}
$$

We can also calculate the helicity amplitude of second vertex $\Sigma_c^{(*)} \to \Lambda_c\pi$ in similar manner as

$$
\begin{aligned}
-iA_{1/2}(\Sigma_c \to \Lambda_c\pi) &= g_{2a}^p \left\langle \tfrac{1}{2}, \tfrac{1}{2} \right| (\boldsymbol{\sigma}\cdot\mathbf{p}) \left| \tfrac{1}{2}, \tfrac{1}{2} \right\rangle = g_{2a}^p\, p \left\langle \tfrac{1}{2}, \tfrac{1}{2} \right| \sigma_z \left| \tfrac{1}{2}, \tfrac{1}{2} \right\rangle = g_{2a}^p\, p, && (5.37)\\
-iA_{1/2}(\Sigma_c^* \to \Lambda_c\pi) &= g_{2b}^p \left\langle \tfrac{1}{2}, \tfrac{1}{2} \right| (\mathbf{S}\cdot\mathbf{p}) \left| \tfrac{3}{2}, \tfrac{1}{2} \right\rangle = g_{2b}^p\, p \left\langle \tfrac{1}{2}, \tfrac{1}{2} \right| S_z \left| \tfrac{3}{2}, \tfrac{1}{2} \right\rangle = -\sqrt{\frac{2}{3}} g_{2b}^p\, p. && (5.38)
\end{aligned}
$$

Other amplitudes are computed similarly. Then, we summarize the helicity amplitude of the effective Lagrangian in Table 5.3.

5.5 Coupling strength

The coupling strengths in the effective Lagrangian are unknown and need to be fixed by either experimental data or microscopic model. In this present work, these coupling strengths are computed from the quark model [89]. We can extract the coupling by equating

$$
A_h^{el} = A_h^{qm}, \qquad (5.39)
$$

where A_h^{el} and A_h^{qm} are the helicity amplitudes computed from the effective Lagrangian and quark model, respectively.

Table 5.4. The obtained coupling strengths computed from the quark model. The definition of the quark model states $\Lambda_c^*(nl_\xi, J(j)^P)$ can be found in the text.

Excitation	Channel	Coupling constant
$\Lambda_c^*(1P_\lambda, 1/2(1)^-)$	$\Sigma_c\pi(s)$	$g_{1a}^s = -\frac{1}{\sqrt{2}}C_0^\lambda + \frac{1}{3\sqrt{2}}p^2C_2^\lambda$
	$\Sigma_c^*\pi(d)$	$g_{1b}^d = -\frac{1}{\sqrt{6}}C_2^\lambda$
$\Lambda_c^*(1P_\lambda, 3/2(1)^-)$	$\Sigma_c\pi(d)$	$g_{1a}^d = \frac{1}{\sqrt{6}}C_2^\lambda$
	$\Sigma_c^*\pi(s)$	$g_{1b}^s = -\frac{1}{\sqrt{2}}C_0^\lambda + \frac{1}{3\sqrt{2}}p^2C_2^\lambda$
	$\Sigma_c^*\pi(d)$	$g_{1b}^d = -\frac{\sqrt{5}}{3\sqrt{2}}C_2^\lambda$
$\Lambda_c^*(1P_\rho, 5/2(2)^-)$	$\Sigma_c\pi(d)$	$g_{1a}^d = \frac{1}{\sqrt{6}}C_2^\rho$
	$\Sigma_c^*\pi(d)$	$g_{1b}^d = -\frac{1}{3\sqrt{2}}C_2^\rho$
$\Lambda_c^*(2S_{\lambda\lambda}, 1/2(0)^+)$	$\Sigma_c\pi(p)$	$g_{1a}^p = \frac{1}{3\sqrt{2}}C_1^{\lambda\lambda} - \frac{1}{6\sqrt{2}}p^2C_3^{\lambda\lambda}$
	$\Sigma_c^*\pi(p)$	$g_{1b}^p = -\frac{1}{3}\sqrt{\frac{3}{2}}C_1^{\lambda\lambda} + \frac{1}{6}\sqrt{\frac{3}{2}}p^2C_3^{\lambda\lambda}$
$\Lambda_c^*(1D_{\lambda\lambda}, 3/2(2)^+)$	$\Sigma_c\pi(p)$	$g_{1a}^p = -\sqrt{\frac{5}{12}}C_1^{\lambda\lambda} + \sqrt{\frac{1}{60}}p^2C_3^{\lambda\lambda}$
	$\Sigma_c^*\pi(p)$	$g_{1b}^p = -\frac{1}{6\sqrt{5}}C_1^{\lambda\lambda} + \frac{1}{30\sqrt{5}}p^2C_3^{\lambda\lambda}$
	$\Sigma_c^*\pi(f)$	$g_{1b}^f = -\frac{\sqrt{7}}{10}C_3^{\lambda\lambda}$
$\Lambda_c^*(1D_{\lambda\lambda}, 5/2(2)^+)$	$\Sigma_c\pi(f)$	$g_{1a}^f = \frac{1}{2\sqrt{6}}C_3^{\lambda\lambda}$
	$\Sigma_c^*\pi(p)$	$g_{1b}^p = -\frac{1}{\sqrt{2}}C_1^{\lambda\lambda} + \frac{1}{5\sqrt{2}}p^2C_3^{\lambda\lambda}$
	$\Sigma_c^*\pi(f)$	$g_{1b}^f = -\frac{\sqrt{7}}{15}C_3^{\lambda\lambda}$
$\Lambda_c^*(1D_{\lambda\rho}, 7/2(3)^+)$	$\Sigma_c\pi(f)$	$g_{1a}^f = \frac{1}{2\sqrt{3}}C_3^{\lambda\rho}$
	$\Sigma_c^*\pi(f)$	$g_{1b}^f = -\frac{1}{6}C_3^{\lambda\rho}$
$\Sigma_c(1S, 1/2(1)^+)$	$\Lambda_c\pi(p)$	$g_{2a}^p = -\frac{1}{\sqrt{3}}C_1$
$\Sigma_c^*(1S, 3/2(1)^+)$	$\Lambda_c\pi(p)$	$g_{2b}^p = -C_1$

For example, the coupling strength for $\Lambda_c^*(1P_\lambda, 3/2(1)^-) \to \Sigma_c\pi$ decay can be obtained by

$$
\begin{aligned}
-iA_{1/2}^{el} &= -iA_{1/2}^{qm}, \\
\sqrt{\frac{2}{3}} g_{1a}^d \, p^2 &= \left(-\frac{1}{3}\right) p^2 C_2^\lambda, \\
g_{1a}^d &= -\frac{1}{\sqrt{6}} C_2^\lambda
\end{aligned}
\tag{5.40}
$$

where only $h = 1/2$ is allowed. For the case of $\Lambda_c^*(1P_\lambda, 3/2(1)^-) \to \Sigma_c^*\pi$, we have , however, two helicity amplitudes, $A_{1/2}$ and $A_{3/2}$ where their coupling strengths are computed as

$$A_{1/2}^{el} = A_{1/2}^{qm}, \tag{5.41}$$

$$A_{3/2}^{el} = A_{3/2}^{qm}. \tag{5.42}$$

For convenience, we denote D_l^{2h} where $l = s$ or d and $h = 1/2$ or $3/2$ for the coefficient in the helicity amplitudes calculated in the quark model. Hence, we can equate the helicity amplitudes as

$$g_{1b}^s - \frac{1}{\sqrt{5}} g_{1b}^d \, p^2 = D_s^1 + D_d^1 \, p^2, \tag{5.43}$$

$$g_{1b}^s + \frac{1}{\sqrt{5}} g_{1b}^d \, p^2 = D_s^3 + D_d^3 \, p^2, \tag{5.44}$$

where two partial wave s and d waves are allowed. Now, the coupling strengths g_{1b}^s and g_{1b}^d can be extracted as

$$g_{1b}^s = \tfrac{1}{2}(D_s^1 + D_s^3) + \tfrac{1}{2}(D_d^1 + D_d^3) \, p^2 = -\frac{1}{\sqrt{2}} C_0^\lambda + \frac{1}{3\sqrt{2}} C_2^\lambda \, p^2, \tag{5.45}$$

$$g_{1b}^d = -\tfrac{\sqrt{5}}{2}(D_d^1 - D_d^3) = -\frac{\sqrt{5}}{3\sqrt{2}} C_2^\lambda. \tag{5.46}$$

So, we have demonstrated to compute the coupling strengths when one or two partial waves are allowed. The other coupling strengths can be extracted similarly without complications. The resulting coupling strengths of various Λ_c^* and $\Sigma_c^{(*)}$ decays are given in Table 5.4.

5.6 Three-body decay amplitude

Now, we have all of the ingredients for calculating the three-body decay amplitudes. Let us first consider $\Lambda_c^* \to \Lambda_c\pi^+\pi^-$ going through Σ_c as depicted in Fig 5.3. There are two charged states of Σ_c^0 and Σ_c^{++} originated from the direct and cross diagrams, respectively. These decay amplitudes are

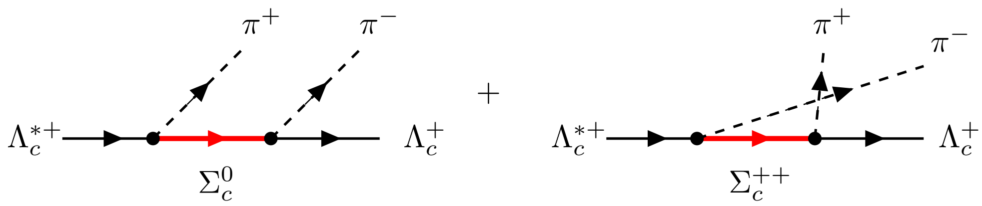

Figure 5.3. Three-body decay of $\Lambda_c^+ \to \Lambda_c^+\pi^+\pi^-$ going through Σ_c^0 and Σ_c^{++} in intermediate states.

given by

$$-i\mathcal{T}\left[\Sigma_c^0\right] = \left\langle -i\mathcal{T}_{\Sigma_c^0\to\Lambda_c^+\pi^-}\right\rangle \frac{i}{m_{23} - m_{\Sigma_c^0} + \frac{i}{2}\Gamma_{\Sigma_c^0}} \left\langle -i\mathcal{T}_{\Lambda_c^{*+}\to\Sigma_c^0\pi^+}\right\rangle, \tag{5.47}$$

$$-i\mathcal{T}\left[\Sigma_c^{++}\right] = \left\langle -i\mathcal{T}_{\Sigma_c^{++}\to\Lambda_c^+\pi^+}\right\rangle \frac{i}{m_{13} - m_{\Sigma_c^{++}} + \frac{i}{2}\Gamma_{\Sigma_c^{++}}} \left\langle -i\mathcal{T}_{\Lambda_c^{*+}\to\Sigma_c^{++}\pi^-}\right\rangle, \tag{5.48}$$

where the two-body decay amplitudes can be found in the previous sections. Note that in the propagator part, the m_{23} invariant mass is replaced by m_{13} for the Σ_c^{++}, the cross diagram. The other resonance contribution such as $\Sigma_c^*(3/2^+)$ can be calculated similarly. Then, we sum the amplitudes coherently. It is worth noting that there is no phase ambiguity when we use the quark model for the coupling strengths. The actual forms and the squared amplitudes with various spin-parity assignments of Λ_c^* are discussed in detail in Appendix C.

"It is not unscientific to make a guess, although many people who are not in science think it is.",
Richard Feynman

Chapter 6
Dalitz plot analysis

6.1 Introduction

The standard way to describe the three-body decay is by using the so-called Dalitz plot. This name is originated from Richard Dalitz who developed this technique [215]. The modern Dalitz plot is a bit different from its original version where now the plot is represented by the invariant masses as shown in Fig. 6.1. Although three-body decay is more complicated than two-body decay, it contains rich information due to the additional kinematical variables. In this chapter, we will introduce the general aspects of the Dalitz plot, which is useful for practical analysis.

This method is very powerful for finding a new resonance these days because the scattering experiment is difficult to perform directly especially for heavy hadron whose lifetime is very short. One of the examples, the pentaquarks P_c are recently observed in $\Lambda_b \to J/\psi K p$ decay [7]. Furthermore, there are many other exotic hadrons found in the three-body decay process. Therefore, developing the Dalitz plot analysis will be crucial for the hadron spectroscopy in the future, in particular, constructing a suitable parameterization for the three-body decay.

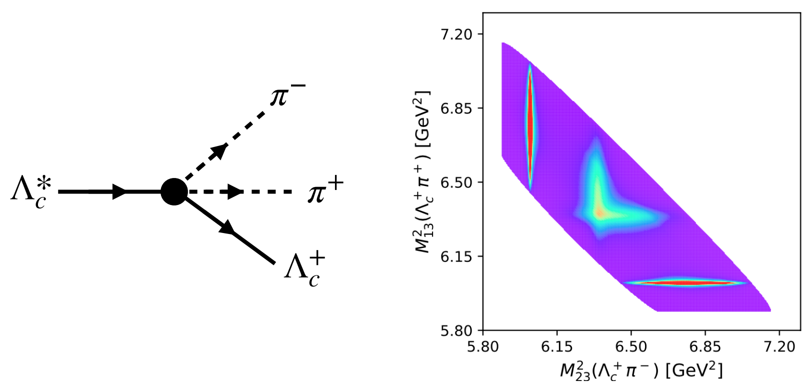

Figure 6.1. (left) Two-pion emission decay of $\Lambda_c^* \to \Lambda_c^+\pi^+\pi^-$ and (right) the typical Dalitz plot.

The Dalitz plot is also useful for the determination of the spin and parity of the resonances. As we can observe in Fig. 6.1, the resonance is represented as a band and the angular distribution along the band may reflect its spin and parity. In this present study, we will show how to determine the spin and parity of heavy baryons by using the Dalitz plot. Moreover, we can measure the Dalitz plot directly from the experiment by which we can study the decay mechanism. This is one of the advantages of this work, we can not only discuss the spin and parity of the resonance but also other possible structures. This sort of analysis should be pursued in the future to clarifying the nature of hadron resonances.

6.2 Kinematics

Before going into detail, let us review the kinematics of two-body and three-body decay. Then, we may have some intuitions in discussing the Dalitz plots.

6.2.1 Two-body decay

Let us first consider the Λ_c with mass M decays into two particles: (1) Σ_c and (2) π as shown in Fig. 6.2. In the final states, there are two particles defined by four components (energy and three momenta). In total, there are eight degrees of freedom. But, we have some constraints such as:

1. Well-defined final state mass, namely $p_1^2 = m_1^2$ and $p_2^2 = m_2^2$ (two constraints).

2. Energy and momentum conservation, $P = p_1 + p_2$ (four constraints).

As a result, we have two degrees of freedom left. Since the decay occurs on one axis, one can choose two angular parameters (θ, ϕ) and then determine other kinematical variables.

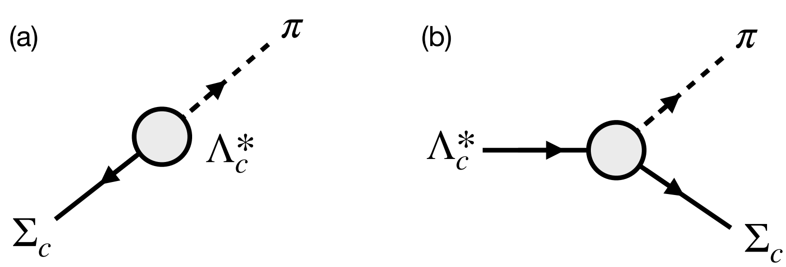

Figure 6.2. Two-body decay of $\Lambda_c^* \to \Sigma_c \pi$ (a) in the rest frame and (b) in the moving frame of the initial particle

Now let us calculate the energy and momentum of the final states in the rest frame of the initial particle where $P = (M, \mathbf{0})$. For particle 1, we can write the relation

$$p_2 = P - p_1, \tag{6.1}$$

and then we take the square

$$\begin{aligned} p_2^2 &= (P - p_1)^2, \\ m_2^2 &= P^2 + p_1^2 - P \cdot p_1 = M^2 + m_1^2 - (ME_1 - \mathbf{0} \cdot \mathbf{p_1}), \\ m_2^2 &= M -^2 + m_1^2 - ME_1. \end{aligned} \tag{6.2}$$

Thus, the energy of particle 1 is given by

$$E_1 = \frac{M^2 + m_1^2 - m_2^2}{2M}. \tag{6.3}$$

In the same way, we can also obtain

$$E_2 = \frac{M^2 + m_2^2 - m_1^2}{2M}. \tag{6.4}$$

Their momentum can be calculated by using the relation $|\mathbf{p}_1| = \sqrt{E_1^2 - m_1^2}$, resulting in

$$|\mathbf{p}_1| \;=\; \frac{\sqrt{\lambda(M^2, m_1^2, m_2^2)}}{2M}, \tag{6.5}$$

where $\lambda(x, y, z)$ is defined by

$$\lambda(x, y, z) = x^2 + y^2 + z^2 - 2(xy + xz + yz). \tag{6.6}$$

In two-body decay, the energy and momentum of daughter particles can be well determined when we know the mass of each participating particles. It is also worth noting that the daughter particles are always going back to back, $\mathbf{p}_2 = -\mathbf{p}_1$, in the rest frame of the initial particle.

The situation is a bit different when we boost the initial particle with a momentum P, such that

$$E \;=\; \sqrt{P^2 + M^2}, \tag{6.7}$$

$$\gamma \;=\; \frac{E}{M}, \tag{6.8}$$

$$v \;=\; \frac{P}{M}, \tag{6.9}$$

and it moves with a certain velocity toward one direction as shown in Fig. 6.2(b). This is a moving frame of the initial particle or usually called a lab frame. In this case, the daughter particles will not go back to back, but they create a decay angle. The momentum and energy in this frame can be obtained by performing a Lorentz transformation

$$p'_{1x} \;=\; p_{1x}, \tag{6.10}$$

$$p'_{1z} \;=\; \gamma(p_{1z} + vE_1), \tag{6.11}$$

$$\tan\theta_1 \;=\; \frac{p'_{1x}}{p'_{1z}} \tag{6.12}$$

by assuming the initial particle move toward z-axis.

The decay width of a parent particle decaying into two daughter particles is given by

$$\begin{aligned} \Gamma &= \int \frac{(2\pi)^4}{2M}\overline{|\mathcal{T}|^2} d\Phi_2(P, p_1, p_2), \\ &= \int \frac{(2\pi)^4}{2M}\overline{|\mathcal{T}|^2}\delta^4(P - p_1 - p_2)\frac{d^3p_1}{2E_1(2\pi)^3}\frac{d^3p_2}{2E_2(2\pi)^3}. \end{aligned} \tag{6.13}$$

Integrating p_2 will give the momentum conservation and transforming the p_1 integral in spherical coordinate will result in

$$\Gamma = \frac{1}{8M(2\pi)^2}\int \overline{|\mathcal{T}|^2}\delta(M-E_1-E_2)\frac{p_1^2\ dp_1\ d\Omega}{E_1E_2}. \tag{6.14}$$

where we denote $p_1 = |\mathbf{p_1}|$. The Dirac δ function can be evaluated as

$$\begin{aligned}
\delta(f(p_1))dp_1 &= |f'(p^*)|^{-1}\delta(p_1-p^*)\ dp_1, \\
\delta(M-E_1-E_2)\ dp_1 &= \delta\left(M-\sqrt{m_1^2+p_1^2}-\sqrt{m_2^2+p_1^2}\right)\ dp_1 \\
&= \left|p_1\frac{E_1+E_2}{E_1E_2}\right|^{-1}\delta(p_1-p^*)\ dp_1,
\end{aligned} \tag{6.15}$$

where p^* is the value of p_1 that satisfies the original δ-function. Then, the decay width becomes

$$\begin{aligned}
\Gamma &= \frac{1}{8M(2\pi)^2}\int \overline{|\mathcal{T}|^2}\left|p_1\frac{E_1+E_2}{E_1E_2}\right|^{-1}\delta(p_1-p^*)\ \frac{p_1^2\ dp_1\ d\Omega}{E_1E_2} \\
&= \frac{1}{16\pi^2}\frac{p_1}{2M^2}\int \overline{|\mathcal{T}|^2}d\Omega.
\end{aligned} \tag{6.16}$$

6.2.2 Three-body decay

Next let us consider the decay of Λ_c^* with mass M into three particles: (1) π^+, (2) π^- and (3) Λ_c which are depicted in Fig. 6.3. In this case, there are twelve degrees of freedom in the final states coming from the energy and momenta of the three particles. Such degrees of freedom are constraints by

1. The well-defined mass, $p_i^2 = m_i^2$ (three constraints),
2. Energy and momentum conservation, $P = p_1 + p_2$ (four constraints),
3. Orientation of the decay plane (three constraints).

Now, we have two remaining degrees of freedom which can be described by introducing invariant masses such as

$$\begin{aligned}
s &= P^2 = M^2, && (6.17)\\
m_{23}^2 &= (P-p_1)^2 = (p_2+p_3)^2, && (6.18)\\
m_{13}^2 &= (P-p_2)^2 = (p_1+p_3)^2, && (6.19)\\
m_{12}^2 &= (P-p_3)^2 = (p_1+p_3)^2, && (6.20)
\end{aligned}$$

where m_{23} shows the invariant mass of particle 2 and 3. In similar manner, m_{13} and m_{12} can be defined as the invariant mass of particle (1,3) and (1,2), respectively. Those invariant masses are not

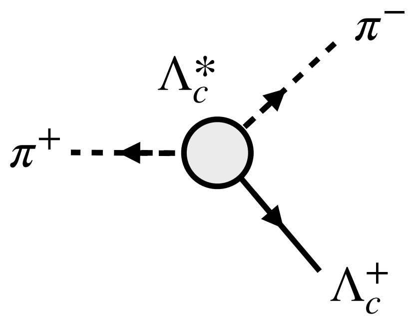

Figure 6.3. Three-body decay of $\Lambda_c^* \to \Lambda_c^+\pi^+\pi^-$ in the rest frame of Λ_c^*.

independent but related to each other by the following equation

$$m_{23}^2 + m_{12}^2 + m_{13}^2 = M^2 + m_1^2 + m_2^2 + m_3^2. \tag{6.21}$$

In the three-body decay, the energy and momentum will depend on a combination of two invariant masses out of the m_{23}^2, m_{13}^2 and m_{12}^2, from which we can make a two-dimensional plot a so-called Dalitz plot. This plot represents a kinematical region of a certain decay whose boundary is determined by the mass of the participating particles. One point inside the Dalitz plot corresponds to a certain configuration of the three-body decay. We will introduce them in detail shortly.

The rest frame of initial particle

Let us first consider the rest frame of Λ_c^* with $P = (M, 0)$ as shown in Fig. 6.3. We can imagine that the final states can go to any directions as long as they satisfy the total energy and momentum conservation. For instance, let us compute the energy and momentum of particle 1. The energy of particle 1 is given by

$$\begin{aligned} m_{23}^2 &= (P - p_1)^2 = M^2 + m_1^2 - 2ME_1, \\ E_1 &= \frac{1}{2M}(M^2 + m_1^2 - m_{23}^2), \end{aligned} \tag{6.22}$$

Table 6.1. Energy and momentum of final states in the rest frame of initial particle.

Variables	Particle 1	Particle 2	Particle 3
E_i	$\frac{1}{2M}\left(M^2 + m_1^2 - m_{23}^2\right)$	$\frac{1}{2M}\left(M^2 + m_2^2 - m_{13}^2\right)$	$\frac{1}{2M}\left(M^2 + m_3^2 - m_{12}^2\right)$
p_i^2	$\frac{1}{4M^2}\,\lambda\left(M^2,\ m_1^2,\ m_{23}^2\right)$	$\frac{1}{4M^2}\,\lambda\left(M^2,\ m_2^2,\ m_{13}^2\right)$	$\frac{1}{4M^2}\,\lambda\left(M^2,\ m_3^2,\ m_{12}^2\right)$

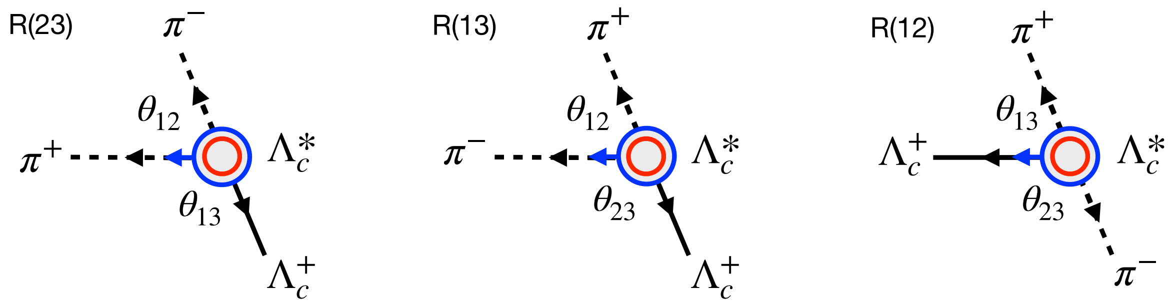

Figure 6.4. Three-body decay of $\Lambda_c^* \to \Lambda_c^+\pi^+\pi^-$ in the moving frame of Λ_c^* such that the resonance is at rest.

and momentum is computed by

$$\begin{aligned} E_1^2 &= m_1^2 + p_1^2, \\ p_1^2 &= E_1^2 - m_1^2 = \frac{1}{4M^2}\lambda(M^2, m_1^2, m_{23}^2). \end{aligned} \tag{6.23}$$

The other variables can be calculated similarly. The energy and momentum of the final states are summarized in Table 6.1. We notice that the energy and momentum depend on not only the particle masses but also the invariant masses. This condition is different from the case of two-body decay.

The rest frame of intermediate state

We can boost the system with appropriate velocity to achieve the rest frame of the intermediate state as shown in Fig. 6.4. Basically, there are three options of the way we boost the system which are denoted as

$$R(12) \rightarrow \text{Rest frame of particle 1 and 2,} \tag{6.24}$$

$$R(13) \rightarrow \text{Rest frame of particle 1 and 3,} \tag{6.25}$$

$$R(23) \rightarrow \text{Rest frame of particle 2 and 3.} \tag{6.26}$$

For example, let us boost the system in order to get the $R(23)$ rest frame. First, we need to boost the system opposite to the particle 3 with velocity

$$v = -\frac{|\mathbf{p}_2 + \mathbf{p}_3|}{E_2 + E_3} = -\frac{|\mathbf{p}_1|}{(M - E_1)}, \tag{6.27}$$

$$\gamma = \frac{1}{\sqrt{1 - v^2}} = \frac{M - E_1}{m_{23}}, \tag{6.28}$$

such that the particle 1 and 2 will be going back to back. Note that the minus sign means opposite to particle 3. Then, the energy and momentum are transformed via Lorentz transformation

$$P'_\mu = \Lambda_\mu^\nu \; P_\nu \qquad \text{and} \qquad p'_\mu = \Lambda_\mu^\nu \; p_\nu, \tag{6.29}$$

where the P and p are the momentum of the initial and final states, respectively. For example, the energy of the moving initial particle can be obtained as

$$E' = \gamma M = \frac{M^2 + m_1^2 - m_{23}^2}{2m_{23}}, \tag{6.30}$$

and its momentum is given by

$$P'^2 = -v\gamma M = \frac{\lambda(M^2, m_1^2, m_{23}^2)}{4m_{23}^2}. \tag{6.31}$$

The energy of the particle 1 is computed as

$$\begin{aligned} E' &= m_{23} + E'_1, \\ E'_1 &= E' - m_{23} = \frac{M^2 - m_1^2 - m_{23}^2}{2m_{23}} \end{aligned} \tag{6.32}$$

while its momentum is obtained as

$$\begin{aligned} E' &= m_{23} + E'_1, \\ \sqrt{M^2 + P'^2} &= m_{23} + \sqrt{m_1^2 + {p'_1}^2}, \\ {p'_1}^2 &= \frac{\lambda(M^2, m_1^2, m_{23}^2)}{4m_{23}^2}, \end{aligned} \tag{6.33}$$

where the momentum of initial particle and particle 1 is the same, $p'_1 = P'$, in the $R(23)$ rest frame. Similarly, we can calculate other varibales of final states. The other kinematical variables are summarized in Table 6.2.

Besides the energy and momentum, another useful kinematical variable is usually called helicity angle. For example, this angle is formed between particles 1 and 2 in the $R(23)$ rest frame as shown in Fig. 6.4. Note that there is a convention of this angle whether the reference axis is along the direction of particle 1, or the opposite direction. In the present study, we will use the former one, which is shown in Fig. 6.4.

Now let us calculate this helicity angle θ_{12} in the $R(23)$ rest frame. For the fix value of m_{23}^2, we can find the range of the m_{12} as

$$m_{12}^2 = (p_1 + p_2)^2 = m_1^2 + m_2^2 + 2\left(E'_1 \; E'_2 - p'_1 \; p'_2 \cos\theta_{12}\right), \tag{6.34}$$

$$(m_{12}^2)_\pm = m_1^2 + m_2^2 + 2\left(E'_1 \; E'_2 \pm p'_1 \; p'_2\right). \tag{6.35}$$

Table 6.2. Energy and momentum of final states in the rest frame of various intermediate states.

Variables	$R(23)$	$R(13)$	$R(12)$
E_1'	$\frac{1}{2m_{23}}\left(M^2-m_1^2-m_{23}^2\right)$	$\frac{1}{2m_{13}}\left(m_{13}^2+m_1^2-m_3^2\right)$	$\frac{1}{2m_{12}}\left(m_{12}^2+m_1^2-m_2^2\right)$
E_2'	$\frac{1}{2m_{23}}\left(m_{23}^2+m_2^2-m_3^2\right)$	$\frac{1}{2m_{13}}\left(M^2-m_2^2-m_{13}^2\right)$	$\frac{1}{2m_{12}}\left(m_{12}^2+m_2^2-m_1^2\right)$
E_3'	$\frac{1}{2m_{23}}\left(m_{23}^2+m_3^2-m_2^2\right)$	$\frac{1}{2m_{13}}\left(m_{13}^2+m_3^2-m_1^2\right)$	$\frac{1}{2m_{12}}\left(M^2-m_2^2-m_{12}^2\right)$
p_1'	$\frac{1}{2m_{23}}\sqrt{\lambda\left(m_{23}^2,\ M^2,\ m_1^2\right)}$	p_3'	$\frac{1}{2m_{12}}\sqrt{\lambda\left(m_{12}^2,\ m_1^2,\ m_2^2\right)}$
p_2'	$\frac{1}{2m_{23}}\sqrt{\lambda\left(m_{23}^2,\ m_2^2,\ m_3^2\right)}$	$\frac{1}{2m_{13}}\sqrt{\lambda\left(m_{13}^2,\ M^2,\ m_2^2\right)}$	p_1'
p_3'	p_2'	$\frac{1}{2m_{13}}\sqrt{\lambda\left(m_{13}^2,\ m_1^2,\ m_3^2\right)}$	$\frac{1}{2m_{12}}\sqrt{\lambda\left(m_{12}^2,\ M^2,\ m_3^2\right)}$

where $\cos\theta_{12} = \pm 1$ at max and min value. Then, we can compute the $\cos\theta_{12}$ as

$$\cos\theta_{12} = \frac{(m_{12}^2)_+ + (m_{12}^2)_- - 2m_{12}^2}{(m_{12}^2)_+ - (m_{12}^2)_-} \tag{6.36}$$

This angle is not independent quantity but it depends on the invariant masses. In this $R(23)$ rest frame, we can observe that

$$\theta_{13} = \pi - \theta_{12}, \tag{6.37}$$

$$\theta_{23} = \pi. \tag{6.38}$$

The relations of other angles can be found in Table 6.3. The straight line at the fixed value of m_{23}^2 represents the angular distribution ranging from $\cos\theta_{12} = -1$ to $\cos\theta_{12} = +1$ as shown in Fig. 6.5.

6.2.3 Dalitz boundary

Next, we will compute the boundary of the Dalitz plots or the kinematical regions of the three-body decay. In the rest frame of initial particle, we have

$$m_{23}^2 = (P - p_1)^2 = M^2 + m_1^2 - 2ME_1. \tag{6.39}$$

Because the decay should occur when $E_1 \geq m_1$, then we can obtain

$$(m_{23}^2)_{max} = (M - m_1)^2, \tag{6.40}$$

Table 6.3. Helicity angles in the rest frame of intermediate states.

Rest frame	Helicity angle	Relation
$R(13)$	$\cos\theta_{23}$	$\dfrac{(m_{23}^2)_+ + (m_{23}^2)_- - 2m_{23}^2}{(m_{23}^2)_+ - (m_{23}^2)_-}$
$R(23)$	$\cos\theta_{12}$	$\dfrac{(m_{12}^2)_+ + (m_{12}^2)_- - 2m_{12}^2}{(m_{12}^2)_+ - (m_{12}^2)_-}$
$R(12)$	$\cos\theta_{13}$	$\dfrac{(m_{13}^2)_+ + (m_{13}^2)_- - 2m_{13}^2}{(m_{13}^2)_+ - (m_{13}^2)_-}$

that is when the particle 1 is at rest and the particle 2 and 3 going back to back. The minimum value can be achieved when the particle 2 and 3 going out in the same direction with no relative velocity

$$(m_{23}^2)_{min} = (p_2 + p_3)^2 = (m_2 + m_3)^2, \tag{6.41}$$

and the particle one is going in the opposite direction. These limits are portrayed in Fig. 6.5.

We can summarize the limits of the invariants as

$$\begin{aligned}
(m_2 + m_3)^2 &\leq m_{23}^2 \leq & (M - m_1)^2, && (6.42)\\
(m_1 + m_3)^2 &\leq m_{13}^2 \leq & (M - m_2)^2, && (6.43)\\
(m_1 + m_2)^2 &\leq m_{12}^2 \leq & (M - m_3)^2. && (6.44)
\end{aligned}$$

However, not the entire cube is accesible for the decay process. For example, we calculate the boundary of the Dalitz plot in m_{23}^2, m_{12}^2 plane. Then, max and limit of m_{23}^2 are given above. Meanwhile, for the fixed value of m_{23}^2, the limit of m_{12}^2 is given by

$$(m_{12}^2)_\pm \quad = \quad m_1^2 + m_2^2 + 2\left(E_1' \; E_2' \pm p_1' \; p_2'\right). \tag{6.45}$$

From the equation above, we can obtain the boundary of the Dalitz plot as given in Fig. 6.5. The other Dalitz plots with different combinations of invariant masses can be calculated similarly.

In principle, there are three combinations of the invariant masses to form a Dalitz plot with different shapes. However, in this case, there are two particles, pions, having the same mass in the final states resulting in only two different shapes of the Dalitz plot as shown in Fig. 6.6. Generally, these Dalitz plots contain the same information about the decay mechanism. The difference is that from which point of view we see that information. We may notice that the Dalitz plot in the middle and right panel in Fig. 6.6 have a larger area which makes us easier to observe the structure inside.

Furthermore, the size of the Dalitz plot depends on the initial mass. The heavier the initial mass, the larger the size of the Dalitz plot. Note that the Dalitz plot is made with a fixed value of the initial

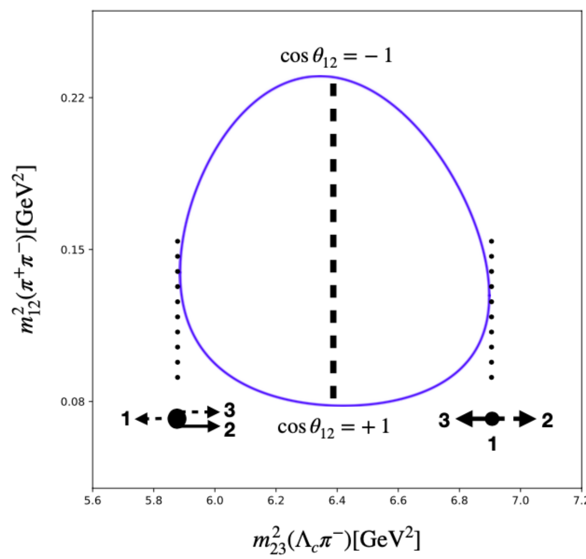

Figure 6.5. The boundary of the Dalitz plot in m_{23}^2, m_{12}^2 plane for $\Lambda_c^* \to \Lambda_c\pi\pi$ decay with initial mass $M = 2765$ MeV.

mass. Here, we show for example the Dalitz plot with the variation of the initial mass as described in Fig. 6.7. This knowledge is very useful when we are trying to study the broad resonance such as $\Lambda_c(2765)$, where the Dalitz plot is convoluted by the plots with various initial masses. A detailed explanation will be given in the part of the result and discussion.

6.3 Resonance in intermediate state

One of the usages of the Dalitz plot is to search for resonance in three-body decay. This search can be done by analyzing the Dalitz plot whether there is an expected structure as theory predicts. Generally, the resonance will appear as a band inside the Dalitz plot. If such a band is found inside the plot, it means that we have found a resonance. Interestingly, the resonance can have non-trivial distribution along the band, in our language, we call it an angular correlation. Such distribution along the resonance band reflects the spin and parity of the participating particles. Therefore, the Dalitz plot is useful to not only search a resonance but also determine the spin and parity.

6.3.1 Resonance band

Now suppose we "artificially" have three resonances which couple to particle (2,3), (1,3), and (1,2), respectively. If we plot the resonance separately, the Dalitz plot will appear as described in Fig. 6.8. The resonance bands appear in different directions, namely perpendicular to the axis of invariant masses where the resonance couples to. Note that we make the Dalitz plot in m_{23}^2, m_{12}^2 plane, the similar behavior also happens when we plot it in different shapes of Dalitz plot.

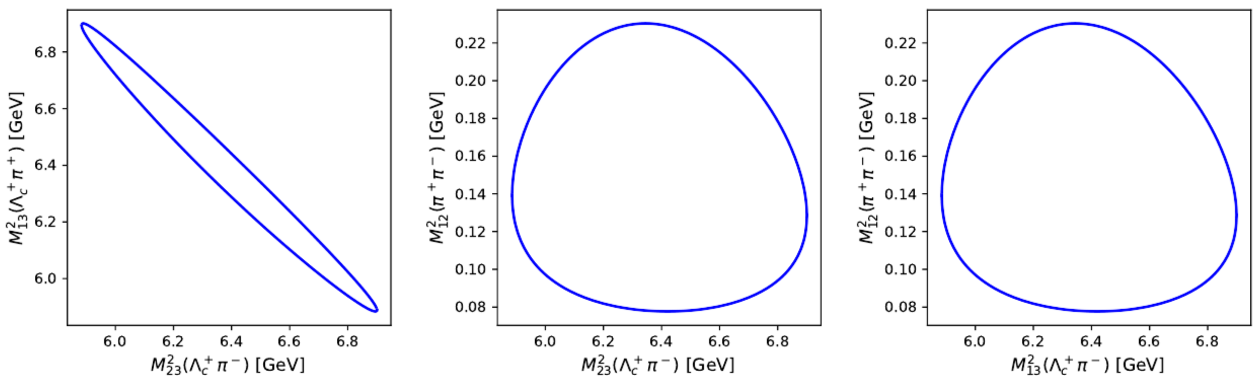

Figure 6.6. The boundary of the Dalitz plot with three different combination of invariant masses. Since there are two identical particles in $\Lambda_c^* \to \Lambda_c\pi\pi$ decay, two Dalitz plots will appear to be the same. Here, we fix the initial mass $M = 2765$ MeV.

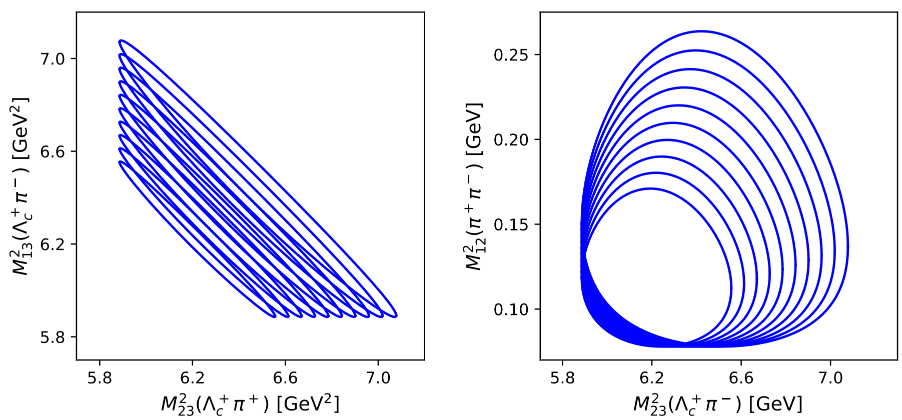

Figure 6.7. The boundary of Dalitz plot with various initial masses. The biggest plot corresponds to the largest initial mass. We vary the initial mass from 2700 to 2800 MeV.

For the plot in the left panel in Fig. 6.8, if we make a projection into m_{23}^2 invariant mass, there will be a peak located at $m_{23}^2 = M_{res}^2$ with the width of the peak correspond to Γ_{res}. However, for the plot in the middle panel where the resonance band has a horizontal direction, there will be no significant peak in m_{23}^2 invariant mass. This happens because the resonance couple to different final states, m_{12}^2, which we call it as kinematical reflection. In some cases, the kinematical reflection can mimic a resonance peak due to its angular correlation along its band. Therefore, we should be careful when we find a peak in the invariant mass distribution in the experiment because the peak could not necessarily correspond to the resonance peak we are interested in.

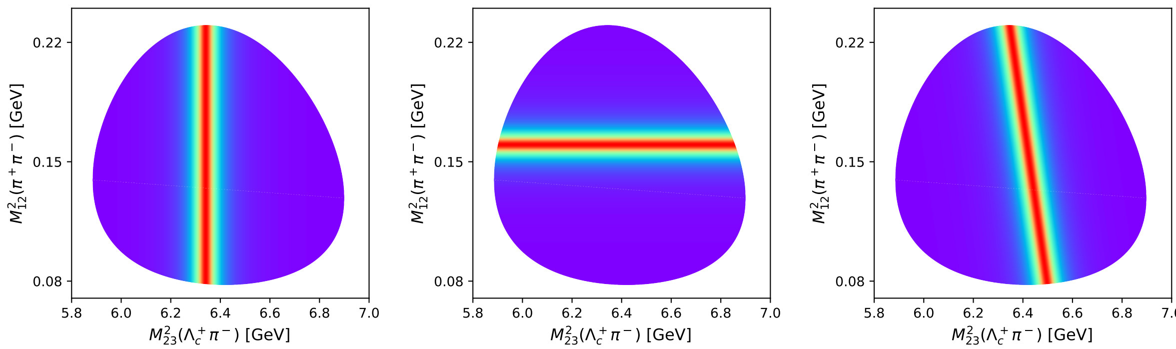

Figure 6.8. The Dalitz plot in m_{23}^2, m_{12}^2 plane with one resonance couples to (left) particle 2 and 3, (middle) particle 1 and 3, (right) particle 1 and 2.

Interference

In a more realistic situation, there could be more than one resonance or other processes can involve. In such a case, there will be interference among them which is similar to the double-slit experiments. Like the wave phenomena, the resonances can interfere each other either contructively or destructively, depending on the relative phase between them

$$|\mathcal{T}|^2 = \left|a_1 e^{-i\delta_1} + a_2 e^{-i\delta_2}\right|^2. \tag{6.46}$$

For instance, we instance we show how the resonance interfere to each other as shown in Fig. 6.9. From the interference pattern, we may extract the information on the relative phase of the resonance. Note that there may also exist the non-resonant contribution which interferes with the resonance contribution. In this case, one needs to be careful about choosing a suitable parameterization.

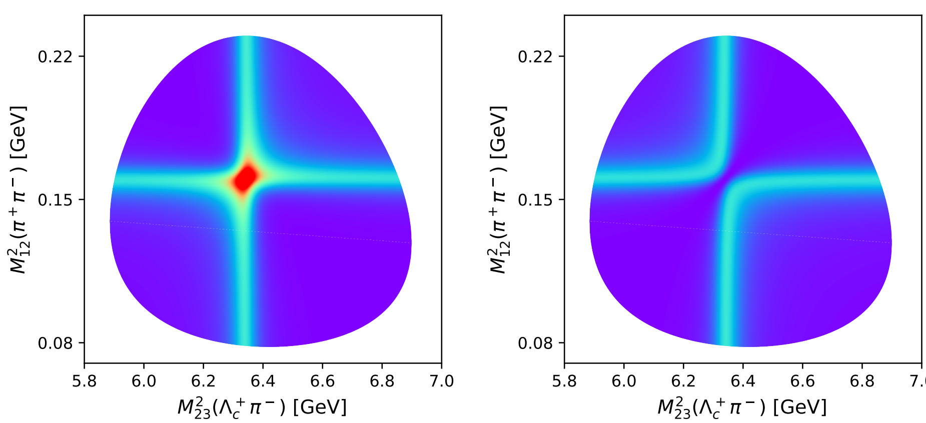

Figure 6.9. The interference between two resonances in Dalitz plot: (left) constructive and (right) destructive patterns.

It is also worth noting that the branching fraction is one of the useful values measured in experiments. Refering to Eq. (6.46), we calculate the branching fraction between a_1 and a_2 as

$$\mathcal{B}_1 = \frac{|a_1|^2}{|\mathcal{T}|^2} \qquad \text{and} \qquad \mathcal{B}_2 = \frac{|a_2|^2}{|\mathcal{T}|^2} \tag{6.47}$$

Then, due to the interference effect, the addition between $\mathcal{B}_1$ and $\mathcal{B}_2$ is not necessarily unity. In a practical situation, this branching fraction is measured by cutting the resonance band where it is not possible to separate the interference terms. Another method is to perform a multi-dimensional fit by assuming a model. Also, the ratio between them $R = \mathcal{B}_1/\mathcal{B}_2$ is strongly affected by the interference if there is an overlapping region.

6.3.2 Angular correlation

Another important aspect of the resonance properties observed in the Dalitz plot is its angular correlation. The angle along the resonance band is depicted in Fig. 6.5 where the definition can be found in Fig. 6.4. Up until now, there are some formalisms can be used to determine the angular correlations such as helicity formalism, relativistic formalism, tensor formalism, and so forth. Here, we show some examples how the resonance band looks like in Fig. 6.10 with a given angular correlation

$$\text{left} \quad \rightarrow \quad 1, \tag{6.48}$$

$$\text{middle} \quad \rightarrow \quad 1 + 3\cos^2\theta, \tag{6.49}$$

$$\text{right} \quad \rightarrow \quad 1 + 3\sin^2\theta. \tag{6.50}$$

Practically, we need to take into account all the spin and parity of the paritcipating particles to determine the angular correlation. Even though it seems to be simple to observe the angular correlation, in the real situation, there are many other processes that may contribute which contaminate it such that the analysis becomes more complicated. Of course, more statistics are needed to see such distribution along the resonance band in the experiment.

6.4 Three-body decay phase space

So far we have already had the boundary of Dalitz plot and defined all independent variables which determine the shape of the Dalitz plot. Let us now examine the three-body decay phase space which is expressed by

$$\mathrm{d}\Gamma = \frac{(2\pi)^4}{2M}|\mathcal{T}|^2\ \delta^4(P - p_1 - p_2 - p_3)\frac{\mathrm{d}^3p_1}{(2\pi)^3 2E_1}\frac{\mathrm{d}^3p_2}{(2\pi)^3 2E_2}\frac{\mathrm{d}^3p_3}{(2\pi)^3 2E_3}, \tag{6.51}$$

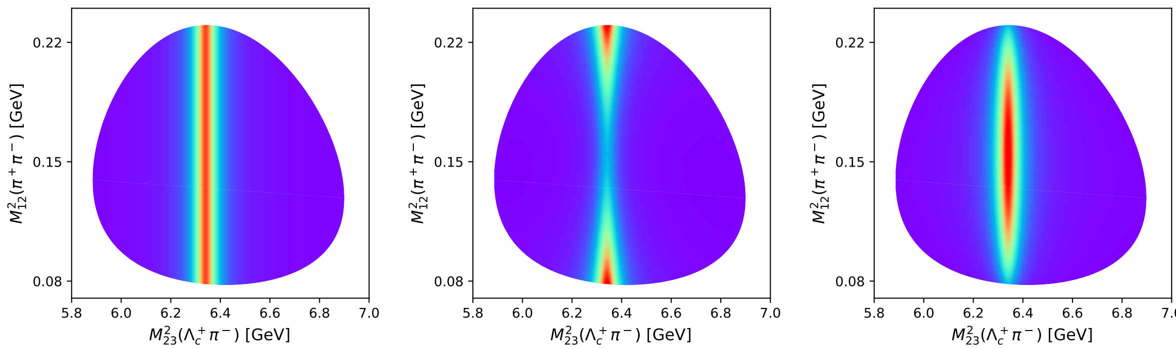

Figure 6.10. The angular correlation along the resonance band: (left) flat, (middle) valley, and (right) hill.

By integrating over d^3p_2, then we have

$$\mathrm{d}\Gamma = \frac{1}{2M}\frac{1}{(2\pi)^5}|\mathcal{T}|^2\ \delta(M - E_1 - E_2 - E_3)\ \frac{p_1^2\ \mathrm{d}p_1\ d\Omega_1\ p_3^2\ \mathrm{d}p_3\ \mathrm{d}\Omega_{13}}{8E_1E_2E_3}, \tag{6.52}$$

where we have changed the integration of momentum vector in spherical coordinate. Important to note that, if we choose to integrate d^3p_1 or d^3p_3 instead, we will get other angular variables.

The next step is to make the transformation as following to express momentum variable in terms of energy

$$\mathrm{d}p_1 \quad = \quad \frac{E_1}{p_1}\ \mathrm{d}E_1, \tag{6.53}$$

which is obtained by taking derivative on the equation of $E_1^2 = m_1^2 + p_1^2$. Then, the decay width becomes

$$\mathrm{d}\Gamma = \frac{1}{2M}\frac{1}{(2\pi)^5}|\mathcal{T}|^2\delta(M - E_1 - E_2 - E_3)\frac{p_1\mathrm{d}E_1\mathrm{d}\cos\theta_1\mathrm{d}\phi_1\ p_3\mathrm{d}E_3\mathrm{d}\cos\theta_{13}\mathrm{d}\phi_{13}}{8E_2}, \tag{6.54}$$

Here, we can express the delta function as

$$\delta(M - E_1 - E_2 - E_3)\ \mathrm{d}\cos\theta_{13} = \left|\frac{p_1p_3}{E_2}\right|^{-1}\delta(\cos\theta_{13} - \cos\tilde{\theta}_{13})\ \mathrm{d}\cos\theta_{13}, \tag{6.55}$$

where $\cos\tilde{\theta}_{13}$ is the value when the energy conservation hold and we have used

$$\frac{\partial(M - E_1 - E_2 - E_3)}{\partial\cos\theta_{13}} = \frac{p_1p_3}{E_2}. \tag{6.56}$$

Now we have

$$\mathrm{d}\Gamma = \frac{1}{16M}\frac{1}{(2\pi)^5}|\mathcal{T}|^2\ \mathrm{d}E_1\ \mathrm{d}E_3\ \mathrm{d}\cos\theta_1\ \mathrm{d}\phi_1\ \mathrm{d}\phi_{13}. \tag{6.57}$$

Next we can also transform E_1 and E_3 in term of invariant mass m_{23}^2 and m_{13}^2 as follow

$$\mathrm{d}E_1 \quad = \quad \frac{\mathrm{d}m_{23}^2}{2M}, \tag{6.58}$$

The decay width is written as

$$\mathrm{d}\Gamma = \frac{1}{64M^3}\frac{1}{(2\pi)^5}|\mathcal{T}|^2\ \mathrm{d}m_{12}^2\ \mathrm{d}m_{23}^2\ \mathrm{d}\cos\theta_1\ \mathrm{d}\phi_1\ \mathrm{d}\phi_{13}. \tag{6.59}$$

If we integrate over the angles, we will obtain

$$\mathrm{d}\Gamma = \frac{1}{32M^3}\frac{1}{(2\pi)^3}|\mathcal{T}|^2\ \mathrm{d}m_{12}^2\ \mathrm{d}m_{23}^2. \tag{6.60}$$

Alternatively, we can calculate the decay width by considering the three-body decay as two quasi two-body decay. This is done by inserting

$$\int \mathrm{d}^4p_{23}\ \delta^4(p_{23} - p_2 - p_3) = 1 \tag{6.61}$$

As a result, the decay width is now written as

$$\mathrm{d}\Gamma = \frac{(2\pi)^4}{2M}|\mathcal{T}|^2\left[\delta^4(p_{23} - p_2 - p_3)\frac{\mathrm{d}^3p_2}{(2\pi)^3 2E_2}\frac{\mathrm{d}^3p_3}{(2\pi)^3 2E_3}\right]\left[\delta^4(P - p_1 - p_{23})\mathrm{d}^4p_{23}\frac{\mathrm{d}^3p_1}{(2\pi)^3 2E_1}\right] \tag{6.62}$$

Because the terms inside each brace is Lorentz invariant quantity, we can evaluate both terms in different frame. We evaluate the first brace in the resonance rest frame m_{23} while the second brace is evaluated in the rest frame of the initial particle. Here, we put apostrophe to indicate the quantities evaluated in the resonance rest frame. Firstly, we calculate the first brace as

$$[1] = \delta^4(p_{23} - p_2' - p_3')\frac{\mathrm{d}^3p_2'}{(2\pi)^3 2E_2'}\frac{\mathrm{d}^3p_3'}{(2\pi)^3 2E_3'} = \frac{p_2'}{4m_{23}}\frac{\mathrm{d}\phi_{12}'\ \mathrm{d}\cos\theta_{12}'}{(2\pi)^6}. \tag{6.63}$$

We have integrated over d^3p_3' at first but it is also possible to integrate over d^3p_2' and in the end we will have Ω_{13} instead. The second brace is calculated as

$$[2] = \delta^4(P - p_1 - p_{23})\ \mathrm{d}^4p_{23}\ \frac{\mathrm{d}^3p_1}{(2\pi)^3 2E_1} = \frac{p_1\ m_{23}\ \mathrm{d}m_{23}}{2M}\frac{\mathrm{d}\Omega_1}{(2\pi)^3}. \tag{6.64}$$

Thus, the decay width is now given by

$$\mathrm{d}\Gamma = \frac{1}{16M^2(2\pi)^5}|\mathcal{T}|^2 \; p_2' \; p_1 \; \mathrm{d}\Omega_1 \; \mathrm{d}\Omega_{12}' \; \mathrm{d}m_{23}. \tag{6.65}$$

If we integrate the angular variables except the helicity angle, we have

$$\mathrm{d}\Gamma = \frac{1}{8M^2(2\pi)^3}|\mathcal{T}|^2 \; p_2' \; p_1 \; \mathrm{d}\cos\theta_{12}' \; \mathrm{d}m_{23}. \tag{6.66}$$

Note that now the Dlaitz plot is potrayed in the combination of helicity angle and invariant mass.

"Dalitz plots led to the discovery of some 100 ephemeral particles, many living no longer than the time taken by the light beam to cross an atomic nucleus", Richard Dalitz

Part III

Results and discussions

Chapter 7
$\Lambda_c^*(2595)$ and $\Lambda_c^*(2625)$ in the quark model

7.1 Motivation

Our study starts with the investigation of the low-lying excited states of Λ_c baryons. This Λ_c baryon is one the lightest baryon containing the heavy quark and two light quarks. As we have already known, the orbital excitation of charmed baryons split into λ and ρ modes. From the Fig. 4.3, the λ-mode excitation appears lower than that of ρ mode. Because of the significant energy difference, the mixing between λ and ρ mode might be small. In that sense, one may expect that the low-lying Λ_c baryons correspond to λ-mode excitation. However, such statements should be proved by a thorough analysis of many observables.

To begin with, we focus on studying $\Lambda_c^*(2595)$ and $\Lambda_c^*(2625)$ states. The excitation energy around 300 MeV suggests that these states may correspond to the negative parity states $l = 1$ in the quark model description. Furthermore, in the mass spectrum analysis, these states can be easily explained by $1/2^-$ and $3/2^-$ with λ-mode as expected [132–134]. The corresponding negative parity states with ρ mode excitations appear significantly higher, implying that these states are dominated by the λ mode excitations. But, more evidences should be confirmed by other methods.

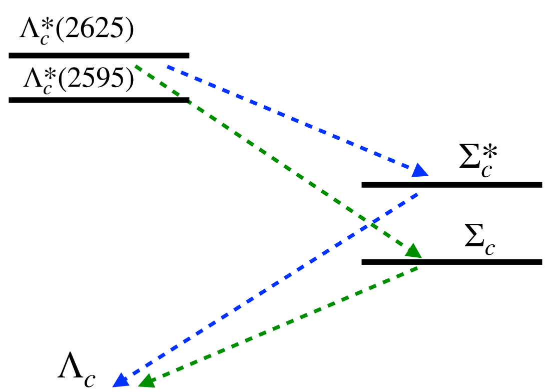

Figure 7.1. Illustration of the sequential processes going through Σ_c and Σ_c^* in intermediate states.

Here, we aim to examine the decay of $\Lambda_c^*(2595)$ and $\Lambda_c^*(2625)$ states to study their internal structures. As shown in PDG, their decay modes are saturated with the two-pion emission decay, namely $\Lambda_c^* \to \Lambda_c\pi\pi$. Up until now, there are several analyses have been performed [88, 89, 100, 107, 113]. But, they are mostly limited to the two-body decay analysis, *i.e.* $\Lambda_c^* \to \Sigma_c\pi$. In such a calculation, the Σ_c baryon is assumed to be a stable particle. In the standard way, the decay rates are estimated and by the comparison with the experimental data, we may exclude some configurations and find a suitable assignment for the observed charmed baryons. However, the absolute value of decay rates predicted in the various models may suffer uncertainties originated from the model parameters. In order to solve the problem, the ratio of the decay rate is often introduced in which such uncertainties are canceled out.

In the present study, we will perform the three-body decay analysis of $\Lambda_c^* \to \Lambda_c\pi\pi$. This sort of analysis has advantages due to the additional kinematical variables and gives a complete picture of their decay processes. Furthermore, this three-body decay analysis is not yet explored rigorously [184, 216]. For the first step, we will consider the sequential processes going through $\Sigma_c(2455)$ and $\Sigma_c^*(2520)$ in intermediate states as shown in Fig. 7.1 and discuss the role of each process. Interestingly, the $\Sigma_c^*(2520)\pi$ channel is kinematically closed and cannot be considered in the two-body decay calculation. However, the $\Sigma_c^*(2520)\pi$ channel can be accessible in the three-body decay analysis. Because it is closed, $\Sigma_c^*(2520)$ will not appear as a peak but a background shape which is originated from its tail. This is particularly interesting because $\Lambda_c^*(2625)$ has a sizable contribution from the non-resonant process where one may expect $\Sigma_c^*(2520)$ closed channel may play a significant role. The detailed study of the three-body decay may unveil the internal structures of the charmed baryons.

7.2 Our strategy

Now let us construct the model to study the two-pion emission decay of $\Lambda_c^*(2595)$ and $\Lambda_c^*(2625)$. First, we consider the relevant Feynman diagrams for these decay processes as shown in Fig. 7.2. For $\Lambda_c^* \to \Lambda_c^+\pi^+\pi^-$, they include the $\Sigma_c^{(*)0}$ and $\Sigma_c^{(*)++}$ in intermediate states which correspond to the first and second diagrams, respectively. Here, we define the $\Sigma_c^{(*)}$ notation for Σ_c and Σ_c^* resonances. Hence, in this total, we have four Feynman diagrams. For the neutral channel $\Lambda_c^* \to \Lambda_c^+\pi^0\pi^0$, there is only Σ_c^+ resonance which appears from both first and second diagrams.

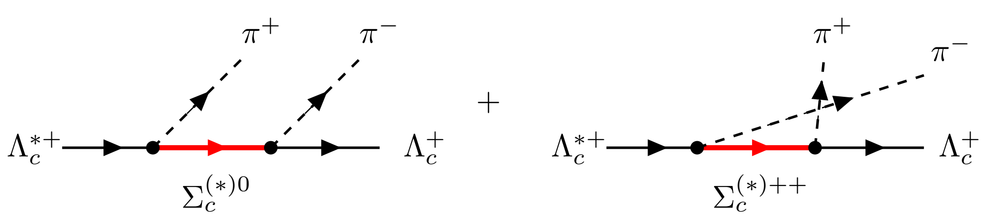

Figure 7.2. The Feynman diagrams considered in this calculation for $\Lambda_c^* \to \Lambda_c^+\pi^+\pi^-$ decay.

Each vertex in the Feynman diagram is then described by the effective Lagrangian in the non-relativistic approximation. The spin-parity of $\Lambda_c^*(2595)$ and $\Lambda_c^*(2625)$ has been determined in PDG[1] as $1/2^-$ and $3/2^-$, respectively. The two-body amplitudes can be found in the first and second rows in Table 5.2. When $\Lambda_c^*(2595)$ is assigned as $\Lambda_c^*(1/2^-)$, it decay into $\Sigma_c\pi$ in s-wave and $\Sigma_c^*\pi$ in d-wave. Because the energy pion is relatively small, we may expect that $\Lambda_c^*(2595)$ will decay dominantly into $\Sigma_c\pi$. On the other hand, $\Lambda_c^*(2625)$ as $\Lambda_c^*(3/2^-)$ will decay into $\Sigma_c^*\pi$ in s-wave and $\Sigma_c\pi$ in d-wave. The

[1] The spin and parity is not measured yet in the experiment, but it is determined in the quark model.

dominant decay mode should be $\Sigma_c^*\pi$, but it is kinematically closed. So, we need to see how large the contribution of $\Sigma_c^*\pi$ in $\Lambda_c^*(2625)$ decay is.

Furthermore, the decay property not only depends on their spin-parity but also their internal structure. In fact, there are several quark model configurations of $1/2^-$ and $3/2^-$ which correspond to λ and ρ mode excitations as given in Table 4.4. Hence, we will consider the quark model configuration as

$$\Lambda_c^*(2595) \rightarrow \Lambda_c^*(1P_\lambda, 1/2(1)^-), \Lambda_c^*(1P_\rho, 1/2(0)^-), \Lambda_c^*(1P_\rho, 1/2(1)^-), \tag{7.1}$$

$$\Lambda_c^*(2595) \rightarrow \Lambda_c^*(1P_\lambda, 3/2(1)^-), \Lambda_c^*(1P_\rho, 3/2(1)^-), \Lambda_c^*(1P_\rho, 3/2(2)^-). \tag{7.2}$$

Then, the coupling strengths in the effective Lagrangians are extracted from the quark model by equating the helicity amplitudes

$$A_h^{EL} = A_h^{QM}. \tag{7.3}$$

We first calculate the three-body decay amplitude of $\Lambda_c^* \rightarrow \Lambda_c\pi^+\pi^-$ as described in Fig. 7.2. The amplitude for the first diagram is given by

$$-i\mathcal{T}\left[\Sigma_c^{(*)0}\right] = \left\langle -i\mathcal{T}_{\Sigma_c^{(*)0}\rightarrow\Lambda_c^+\pi^-}\right\rangle \frac{i}{m_{23} - m_{\Sigma_c^{(*)0}} + \frac{i}{2}\Gamma_{\Sigma_c^{(*)0}}} \left\langle -i\mathcal{T}_{\Lambda_c^{*+}\rightarrow\Sigma_c^{(*)0}\pi^+}\right\rangle, \tag{7.4}$$

and for the second diagram

$$-i\mathcal{T}\left[\Sigma_c^{(*)++}\right] = \left\langle -i\mathcal{T}_{\Sigma_c^{(*)++}\rightarrow\Lambda_c^+\pi^+}\right\rangle \frac{i}{m_{13} - m_{\Sigma_c^{(*)++}} + \frac{i}{2}\Gamma_{\Sigma_c^{(*)++}}} \left\langle -i\mathcal{T}_{\Lambda_c^{*+}\rightarrow\Sigma_c^{(*)++}\pi^-}\right\rangle, \tag{7.5}$$

Then, we sum them up coherently as

$$\mathcal{T} = \mathcal{T}\left[\Sigma_c^0\right] + \mathcal{T}\left[\Sigma_c^{++}\right] + \mathcal{T}\left[\Sigma_c^{*0}\right] + \mathcal{T}\left[\Sigma_c^{*++}\right]. \tag{7.6}$$

The squared amplitudes of the amplitude above can be found in Appendix C.

For the neutral channel $\Lambda_c^* \rightarrow \Lambda_c\pi^0\pi^0$, the neutral pions can not be distinguishable although we assign them as particle 1 and 2. Moreover, the intermediate states that originated from the first and second diagrams have the same charge, namely Σ_c^+. The total amplitude then

$$\mathcal{T} = \mathcal{T}_1\left[\Sigma_c^+\right] + \mathcal{T}_1\left[\Sigma_c^{*+}\right] + \mathcal{T}_2\left[\Sigma_c^+\right] + \mathcal{T}_2\left[\Sigma_c^{*+}\right], \tag{7.7}$$

where we put subscript in the amplitude $\mathcal{T}$ to indicate from which diagram they are originated. Note that we need to divide the squared amplitude by the symmetric factor, $\overline{|T|^2} \rightarrow \frac{1}{2}\,\overline{|T|^2}$.

For the first step, we will use the angle average approximation as

$$(\vec{p}_1 \cdot \vec{p}_2)^2 \rightarrow \frac{1}{3}|\vec{p}_1|^2|\vec{p}_2|^2. \tag{7.8}$$

such that the angular dependence will vanish and the calculation will be less complicated. The equation above is obtained by taking $\langle \cos^2\theta_{12} \rangle = 1/3$. Interestingly, the interference terms vanish as $\langle \cos\theta_{12} \rangle = 0$. The angular dependence will be studied rigorously in the following chapters.

7.3 Numerical results

In this section, we will discuss our numerical results for the $\Lambda_c^*(2595)$ and $\Lambda_c^*(2625)$ decay. We not only discuss their decay rates but also their Dalitz plots and related quantities which can be directly compared with the experimental data. The Dalitz plot for these decays is illustrated in Fig. 7.3. The smaller Dalitz plot is shown for $\Lambda_c^*(2595)$ where we can observe that the Σ_c bands are located at the boundary. For $\Lambda_c^*(2625)$, Σ_c bands are well inside the Dalitz plot. However, in both cases, Σ_c^* bands are completely outside of the plot.

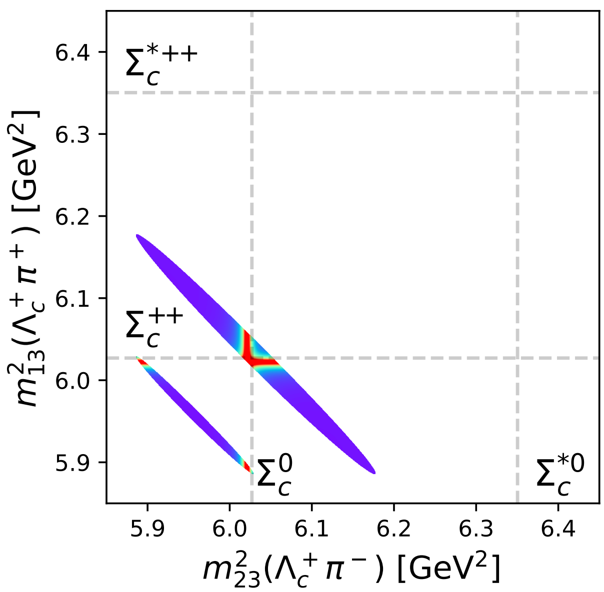

Figure 7.3. The illustration of Dalitz plot for $\Lambda_c^* \to \Lambda_c^+\pi^+\pi^-$: (smaller plot) $\Lambda_c^*(2595)$ decay and (larger plot) $\Lambda_c^*(2625)$ decay.

7.3.1 $\Lambda_c^*(2595)$ decay

The lowest-lying excited state of the charmed baryon is $\Lambda_c^*(2595)$ state. Its mass and width is given by

$$M = 2592.25 \pm 0.28 \text{ MeV}, \tag{7.9}$$

$$\Gamma = 2.6 \pm 0.6 \text{ MeV}, \tag{7.10}$$

Table 7.1. Various components of $\Lambda_c^*(2595) \to \Lambda_c\pi\pi$ decay with various quark model configurations for $J^P = 1/2^-$ (in MeV).

Component	$\Lambda_c^*(1P_\lambda, 1/2(1)^-)$	$\Lambda_c^*(1P_\rho, 1/2(0)^-)$	$\Lambda_c^*(1P_\rho, 1/2(1)^-)$	Exp
$\Sigma_c^{++}\pi^-$	0.237	-	1.001	0.624 (24%)
$\Sigma_c^{0}\pi^+$	0.182	-	0.770	0.624 (24%)
$\Sigma_c^{+}\pi^0$	1.629	-	6.896	-
non-resonant				0.468 (18%)
$\Sigma_c^{*++}\pi^-$	1×10^{-6}	-	6×10^{-7}	-
$\Sigma_c^{*0}\pi^+$	1×10^{-6}	-	7×10^{-7}	-
$\Sigma_c^{*+}\pi^0$	5×10^{-6}	-	3×10^{-6}	-
Γ_{total}	2.048	-	8.667	2.6 ± 0.6

where its excitation energy is about 300 MeV. The spin and parity are identified as $1/2^-$ in PDG which is determined from the quark model, not from the experiment. Its decay is saturated to $\Lambda_c\pi\pi$ mode where $\Sigma_c\pi$ is the dominant channel. From several quark model calculations, they suggested that $\Lambda_c^*(2595)$ might correspond to the λ-mode excitation.

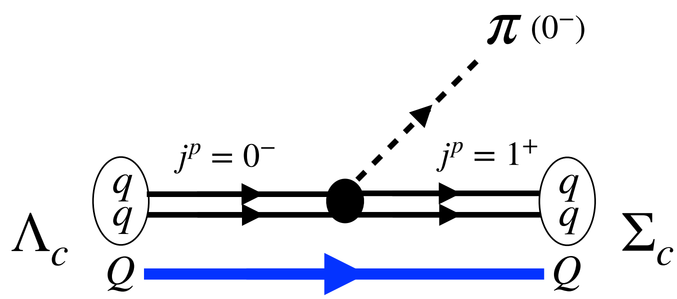

Figure 7.4. The illustration of the brown muck selection rule, *e.g.* the diquark transition $0^- \to 1^+ + 0^-$ is forbidden.

In the present study, we investigate how λ and ρ mode assignments modify its three-body decay properties. The corresponding two-body decay analysis using this model has been done in Ref [89]. As shown in Eq. (7.1), we consider three different quark model configurations. In Table 7.1, we compare our numerical results with the experimental data adopted in PDG. It is shown that $\Lambda_c^*(1P_\lambda, 1/2(1)^-)$ is the most suitable one if we compare the total decay width to the data. For the case of $\Lambda_c^*(1P_\rho, 1/2(0)^-)$, the decays into $\Sigma_c\pi$ and $\Sigma_c^*\pi$ are forbidden due to the brown muck selection rule. This is because the

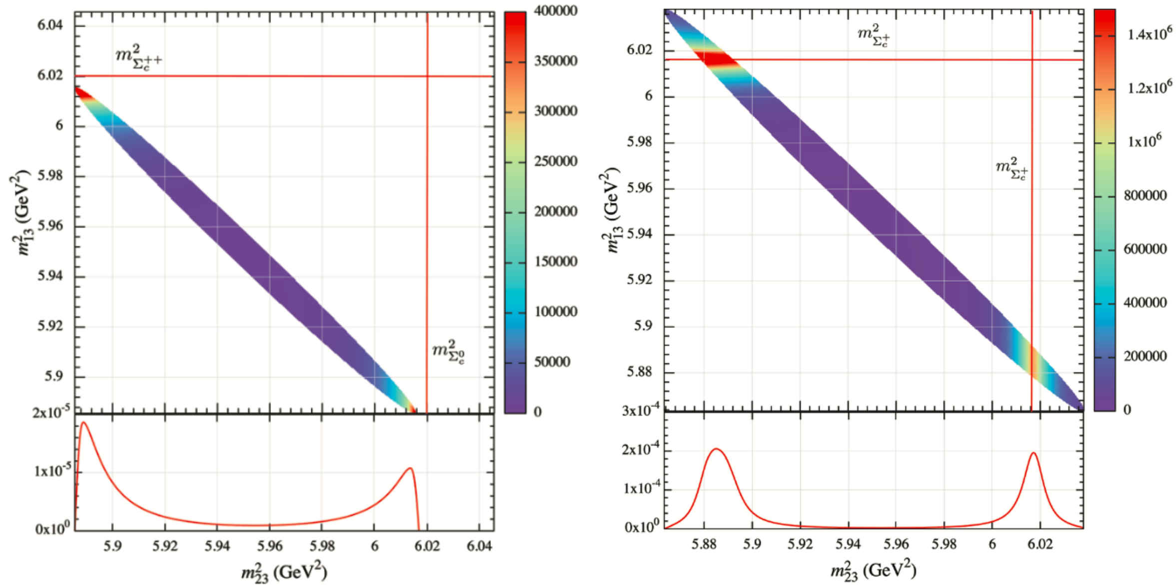

Figure 7.5. The Dalitz plot of $\Lambda_c^*(2595) \to \Lambda_c^+\pi^+\pi^-$ and $\Lambda_c^+\pi^0\pi^0$ with $\Lambda_c^*(1P_\lambda, 1/2(1)^-)$ assignment along with the $\Lambda_c^+\pi^-$ invariant mass distribution.

diquark transition $0^- \to 1^+ + 0^-$ is not allowed as shown in Fig. 7.4. As a result, this configuration can be ruled out. Note that this selection rule may also happen to the decay of other configurations. For $\Lambda_c^*(1P_\rho, 1/2(1)^-)$, the calculated decay witdh over predict the data significantly such that its possibility can be also ruled out.

The components of the decay width are also shown in Table 7.1. The upper and lower three rows are related to Σ_c and Σ_c^* resonances in intermediate states. We observe that the contribution from Σ_c^* resonance is negligible (about 10^{-6}) because it is closed and has the d-wave nature of the first vertex of $\Lambda_c^*(1/2^-) \to \Sigma_c^*\pi$. Also, the $\Sigma_c^+\pi^0$ channel is dominant compared to other charged $\Sigma_c^{++}\pi^-$ and $\Sigma_c^0\pi^+$ channels. This phenomenon is called the isospin breaking effect. The dominance of the neutral channel is due to the mass difference between the neutral and charged pion. In PDG, however, the Σ_c^{++} and Σ_c^0 channel has larger values than our predictions. This is because PDG has assumed the isospin symmetry. Note that the neutral channel has not yet measured in experiments due to the difficulty of detecting neutral pions.

The isospin breaking effect can be seen in the Dalitz plots as described in Fig. 7.5. For the $\Lambda_c\pi^0\pi^0$ channel, the plot size is slightly bigger than that of $\Lambda_c\pi^+\pi^-$. Consequently, the Σ_c^+ band is located completely inside the plot. We also notice that there are two Σ_c^+ bands, vertical and horizontal direction, originated from the first and second diagrams in Fig. 7.2 for the case of $\Lambda_c\pi^0\pi^0$. On the contrary, Σ_c^{++} and Σ_c^0 bands are slightly outside the plot. In the invariant mass distribution, the Σ_c^+ peak is clearly seen while only the tail of Σ_c^0 peak can be seen. It is worth emphasizing that the isospin breaking effect is sizable when the resonance is located very close to the threshold.

In Table 7.1, there is actually another contribution from non-resonant process (denoted as 3-body

$\Lambda_c\pi\pi$ in PDG). However, we can not explain it by introducing the Σ_c^* closed channel. In fact, there is another kind of process such as direct four-point coupling which may contribute to this decay. We will discuss the role of this process in detail in the next chapter.

7.3.2 $\Lambda_c^*(2625)$ decay

Now, let us move to discuss the numerical result of $\Lambda_c^*(2625)$ decay. In PDG, this state has mass and width as

$$M = 2628.11 \pm 0.19 \text{ MeV}, \quad (7.11)$$

$$\Gamma < 0.97 \text{ MeV}. \quad (7.12)$$

In PDG, the spin-parity of the state is determined from the quark model to be $3/2^-$. Its decay is also saturated to $\Lambda_c\pi\pi$ where both Σ_c and non-resonant processes have sizable contributions. The Σ_c contribution has been examined in several analyses. But, the Σ_c^* closed channel is not yet well explored.

In this work, we study the three-body decay properties of $\Lambda_c^*(2625)$ with various quark model configurations as described in Eq. (7.2). The $\Sigma_c\pi$ channel has been investigated, however, the two-body decay analysis can not differentiate their internal structure. In this three-body decay analysis, we primarily examine the role of $\Sigma_c^*\pi$ contribution through the Dalitz plot. We compare our theoretical calculation to the experimental data in Table 7.2. The total decay width calculated in various configurations is consistent with the data. As a result, we can not say which one is a suitable assignment for this state.

Table 7.2. Various components of $\Lambda_c^*(2625) \to \Lambda_c\pi\pi$ decay with various quark model configurations for $J^P = 3/2^-$ (in MeV).

Component	$\Lambda_c^*(1P_\lambda, 3/2(1)^-)$	$\Lambda_c^*(1P_\rho, 3/2(1)^-)$	$\Lambda_c^*(1P_\rho, 3/2(2)^-)$	Exp
$\Sigma_c^{++}\pi^-$	0.037	0.018	0.033	<0.05 (<5%)
$\Sigma_c^0\pi^+$	0.031	0.016	0.030	<0.05 (<5%)
$\Sigma_c^+\pi^0$	0.053	0.027	0.049	-
Non-resonant				(large)
$\Sigma_c^{*++}\pi^-$	0.044	0.190	0	-
$\Sigma_c^{*0}\pi^+$	0.064	0.285	0	-
$\Sigma_c^{*+}\pi^0$	0.071	0.306	0	-
Γ_{total}	0.300	0.842	0.112	< 0.97
R	0.61	0.93	0	

If we look at the components of the decay, the Σ_c contributions are insensitive to the internal structure and consistent with the data. Their values are rather small (0.03 MeV) due to the d-wave nature of the first vertex of $\Lambda_c(3/2^-) \to \Sigma_c\pi$. Moreover, there is no significant isospin breaking effect as compared to that of $\Lambda_c^*(2595)$ since the Σ_c band is completely inside the plot. For the Σ_c^* channel, the contribution is sensitive to their internal structure. $\Lambda_c^*(1P_\lambda, 3/2(1)^-)$ and $\Lambda_c^*(1P_\rho, 3/2(1)^-)$ have rather large contribution because they decay into $\Sigma_c^*\pi$ in s wave. But, $\Lambda_c^*(1P_\rho, 3/2(2)^-)$ has a very small coupling to $\Sigma_c^*\pi$. In this case, there is another brown-muck selection rule where the diquark transition $2^+ \to 1^+ + 0^-$ is forbidden in s-wave. Consequently, $\Lambda_c^*(1P_\rho, 3/2(2)^-)$ decay into $\Sigma_c^*\pi$ in d wave which is the reason why its contribution is suppressed.

In PDG, the non-resonant process has a large contribution. By using this fact, we can rule out the $\Lambda_c^*(1P_\rho, 3/2(2)^-)$ assignment due to its negligible value of Σ_c^* contribution. There is also information about the ratio between the non-resonant contribution and the total decay width as

$$R = \frac{\Gamma(\Lambda_c^* \to \Lambda_c\pi^+\pi^-(\text{non-resonant}))}{\Gamma(\Lambda_c^* \to \Lambda_c\pi^+\pi^-(\text{total}))}, \tag{7.13}$$

The measured ratio is $R = 0.54 \pm 0.14$ [19]. Compared to this value, we may conclude that the λ mode is the most suitable assignment as expected. Therefore, $\Lambda_c^*(2595)$ and $\Lambda_c^*(2625)$ can be explained by a p-wave doublet $(1/2^-, 3/2^-)$ with λ mode. It is important to note that the other process such as direct four-point coupling might contribute to the decay width which might increase the value of ratio R. Even though we include this process, our conclusion on the assignment does not change.

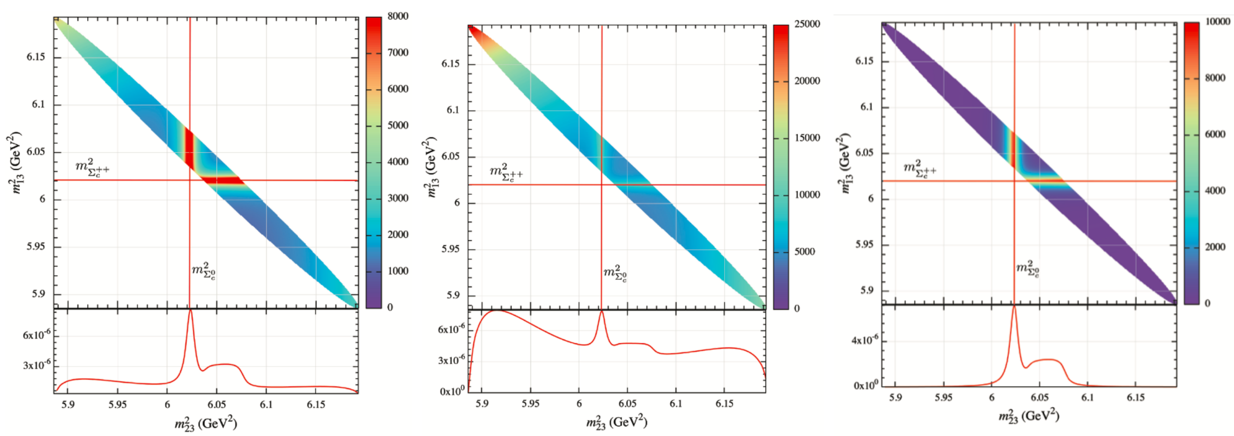

Figure 7.6. The Dalitz plot of $\Lambda_c^*(2625) \to \Lambda_c^+\pi^+\pi^-$ with various assignments and the corresponding $\Lambda_c^+\pi^-$ invariant mass distributions are given in the bottom side of each Dalitz plot.

Now let us discuss the Dalitz plots in Fig. 7.6 made with various quark model configurations for $\Lambda_c^*(2625)$ decay. As we can see, we observe two resonance bands correspond to Σ_c^{++} (horizontal) and Σ_c^0 (vertical) in the middle side of Dalitz plots. Note that we have employed the angle average approximation such that the resonance band looks like flat without any distortions. In the real situation, the resonance band is a little bit distorted due to the interference terms which we will cover in the next chapter. The big difference in the Dalitz plots is the strength of the tail of Σ_c^* closed channel. In the Dalitz plot, it appears as a non-resonant shape, not as a resonance band as seen in Fig 7.6. The difference can be seen more clearly by projecting the Dalitz plot into $\Lambda_c^+\pi^-$ invariant mass. The lineshapes are different depending on the internal structures. We can compare these theoretical results to the experimental data such as from Belle to further study the internal structure of $\Lambda_c^*(2625)$.

7.4 Summary

We have investigated the three-body decay of $\Lambda_c^*(2595)$ and $\Lambda_c^*(2625)$ into $\Lambda_c\pi\pi$. In this analysis, we have considered the sequential processes going through Σ_c and Σ_c^* in intermediate states. We have found that both $\Lambda_c^*(2595)$ and $\Lambda_c^*(2625)$ are best suited to $1/2^-$ and $3/2^-$ assignments, respectively, with λ-mode excitations by examining their decay properties.

For $\Lambda_c^*(2595)$ decay, it is found that $\Sigma_c\pi$ channel plays a significant role due to the s-wave nature, while the $\Sigma_c^*\pi$ contribution is negligible. Also, the decay is dominated by $\Sigma_c^+\pi^0$ due to its larger phase space, leading to the isospin breaking effect. For $\Lambda_c^*(2625)$ decay, the $\Sigma_c^*\pi$ closed channel is important to disentangle the quark model assignments. The comparison of the Dalitz plot and invariant mass distribution may give a hint to its internal structure.

Furthermore, there exist the brown-muck selection rule which forbids the decay of $\Lambda_c^*(1/2^-)$ with $j = 0$ in the view of its light diquark transition. Also, the decay of $\Lambda_c^*(3/2^-)$ with $j = 2$ into $\Sigma_c^*\pi$ is not allowed in s wave due to such selection rule. This selection rule is particularly important which reflects the internal structure of heavy baryons.

Lastly, in this work, we have used the angle average approximation such that the angular correlations and interference terms vanish, and we have not considered the direct four-point coupling which may contribute to the decay in our present calculation. Thus, the comprehensive study of these issues should be pursued in the future. Moreover, the study beyond the quark model is interesting to explore for $\Lambda_c(2595)$. It is because its strange partner $\Lambda(1405)$ can not be explained by the conventional quark model. The study with various flavor is crucial for understanding baryon resonances.

"Reality is complicated. There is no justification for all of the hasty conclusions.", Hideki Yukawa

Chapter 8
Chiral partner structure in heavy baryon decay

8.1 Motivation

In the previous chapter, we have discussed the three-body decay of $\Lambda_c^*(2595)$ and $\Lambda_c^*(2625)$ with the consideration of the Σ_c and Σ_c^* in intermediate states. It is demonstrated that these states are compatible with the λ-mode excitations by analyzing their decay properties. However, it is also shown that the large non-resonant contribution particularly in $\Lambda_c^*(2625)$ decay [1] can not be explained by introducing the Σ_c^* closed channel [122], indicating that there may exist another process in this decay.

As was anticipated, one can come up with the idea of the inclusion of the so-called direct process. In this process, the Λ_c^* is emitting two pions directly as illustrated in Fig. 8.1. But, the problem is that the coupling strength of such a process is not well understood. Therefore, one should estimate it by constructing a model respecting some symmetries or fit it with the experimental data.

Recently Kawakami and Harada proposed a model based on the chiral partner structure to estimate the coupling strength of the direct process [123, 124]. Within this scheme, the $\Lambda_c^*(2625)$ and $\Sigma_c^*(2520)$ are regarded as a chiral partner such that their coupling strengths are equivalent in the chiral limit. Then, they computed the decay width of $\Lambda_c^*(2625)$ and found that the direct process has a substantial contribution. Thus, the further study of this decay in Dalitz plot analysis is certainly of interest to provide more theoretical predictions to be compared with the experimental data.

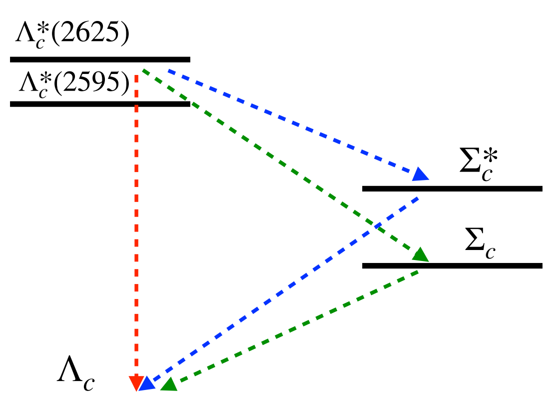

Figure 8.1. Illustration of the direct process (red line) and sequential processes going through Σ_c (green line) and Σ_c^* (blue line).

In this chapter, we will take into account the direct process in addition to the sequential process for $\Lambda_c^*(2595)$ and $\Lambda_c^*(2625)$ decays. We compute the Dalitz plots and related quantities by putting an emphasis on the role of the direct process. In the present work, we also consider the angular correlation in the amplitude concretely which is ignored in our previous calculation. It is found that the angular correlation is crucial to prove the presence of the direct process especially in $\Lambda_c^*(2625)$ decay. The measurements of the corresponding observables may provide a hint on the chiral partner structure in the heavy baryon sector.

8.2 Formalism

8.2.1 Chiral partner structures

As we have introduced in the Introductory part, charm baryons possess a so-called heavy-quark symmetry due to the presence of the charm quark inside. This heavy-quark symmetry is reflected not only in the mass spectrum but also in their transition between the states. In Fig. 8.2, it is shown that there exist the heavy-quark symmetry (HQS) doublet of $[\Lambda_c^*(1/2^-), \Lambda_c^*(3/2^-)]$ with the brown-muck spin $j^P = 1^-$ and $[\Sigma_c(1/2^+), \Sigma_c^*(3/2^+)]$ with $j^P = 1^+$. The mass difference between the HQS partner is originated from the spin-spin dependence interaction which is proportional to the inverse of heavy-quark mass $1/m_Q$. Consequently, the HQS partner will be degenerate in the heavy-quark limit, $m_Q \to \infty$. However, in the real world, the heavy-quark mass has a finite value as $m_Q = 1500$ MeV and 5000 MeV for the charm and bottom quark, respectively. Therefore, they have a finite mass difference for the case of charm baryons that we are considering in the present study. Although it seems to be straightforward to recognize the HQS partner as described in Fig. 8.2, it can be challenging to identify the HQS partner for higher excited states.

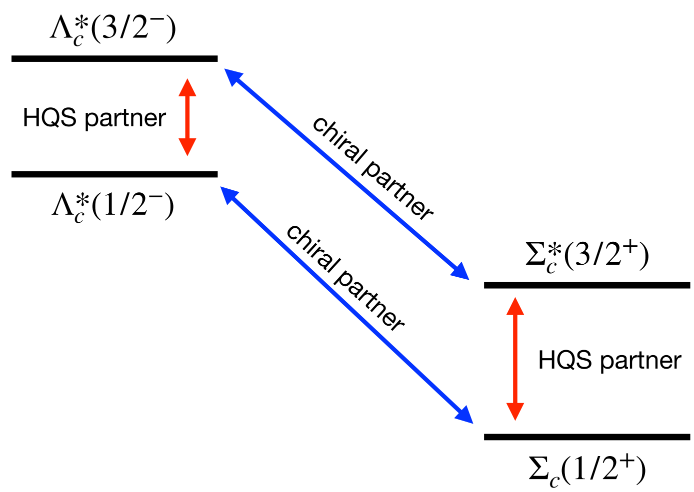

Figure 8.2. Structure of chiral and heavy-quark symmetry partner in the low-lying heavy baryons.

Heavy baryon contains two light quarks together with the heavy quark. The dynamics of these light quarks are governed by the chiral symmetry where the quark can be left-handed q_L or right-handed q_R. These quarks are transformed as

$$q_R \xrightarrow{R} R\, q_R, \qquad \text{and} \qquad q_L \xrightarrow{L} L\, q_L. \tag{8.1}$$

The effective Lagrangian constructred such that it is invariant under this transformation. We have define the R and L as the chiral transformation operators for the case of $SU(2)_L \times SU(2)_R$ symmetry group,

$$R = \exp(-i\boldsymbol{\theta}_R \cdot \boldsymbol{\tau}), \qquad \text{and} \qquad L = \exp(-i\boldsymbol{\theta}_L \cdot \boldsymbol{\tau}), \tag{8.2}$$

where we denote the Pauli matrices $\boldsymbol{\tau}$ in the flavor space and the rotation angles $\boldsymbol{\theta}_R, \boldsymbol{\theta}_L$. We can also construct vector $V = L + R$ and axial-vector $A = R - L$ transformation operators. These transformations relate the so-called chiral partner, for instance $\pi(0^-)$ and $\sigma(0^+)$ meson as

$$\vec{\pi} \xrightarrow{A} \vec{\pi} + \vec{\theta}\sigma, \qquad \text{and} \qquad \sigma \xrightarrow{A} \sigma + \vec{\theta}\vec{\pi}. \tag{8.3}$$

The chiral partner, negative and positve parity states, can be rotated to each other by the chiral transformation as shown above. In the chiral limit, where the quark mass goes to zero $m \to 0$, their masses are degenerate. In reality, the chiral symmetry is spontaneously broken causing the mass difference between the chiral partner.

For the present study, we adopted the chiral partner structures in heavy baryons proposed by Kawakami and Harada as shown in Fig. 8.2, namely,

$$[\Sigma_c(1/2^+), \Lambda_c^*(1/2^-)] \qquad \text{and} \qquad [\Sigma_c^*(3/2^+), \Lambda_c^*(3/2^-)]. \tag{8.4}$$

Note that the chiral partner is actually identified between the light quarks inside of heavy baryons. Generally, the identification of the chiral partner in the hadron level is a new phenomenon that is not well appreciated and should be further studied.

One of the important consequences of this chiral partner structure is that the coupling of $\Lambda_c^* \to \Lambda_c\pi\pi$ direct process is equivalent to the coupling of $\Sigma_c^{(*)} \to \Lambda_c\pi$ (second vertex in the sequential process). In other words, the direct process has a finite contribution in this scheme. If such a direct process is observed in the experiment, it suggests the existence of the chiral partner structure in heavy baryons.

8.2.2 Decay amplitudes

Now, let us compute the three-body decay amplitudes of $\Lambda_c^* \to \Lambda_c\pi\pi$. In the present work, we include the direct four-point coupling as shown in the last diagram in Fig. 8.3. The corresponding sequential processes in the first two diagrams are computed similarly as in the previous chapter. By taking into account the direct process, we have then considered all possible second-order process.

Here, we consider all quark model configurations for $\Lambda_c^*(2595)$ and $\Lambda_c^*(2625)$ with $1/2^-$ and $3/2^-$ assignments, respectively, as done previously for completeness. But, we will focus on the λ-mode excitation for the Dalitz plot analysis as it is the most suitable one. For simplicity, we also neglect the Σ_c^* contribution for the case of $\Lambda_c^*(2595)$ decay since its contribution is found to be insignificant.

In the Dalitz plot, the direct process appears as a background shape which is similar to that of

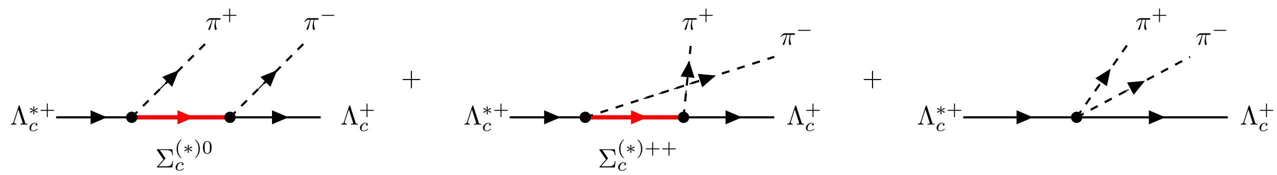

Figure 8.3. The Feynman diagrams of $\Lambda_c^* \to \Lambda_c \pi^+\pi^-$ decay considered in the present work. (left) $\Sigma_c^{(*)0}$ resonance, (middle) $\Sigma_c^{(*)++}$ resonance, and (right) direct process.

Σ_c^* closed channel. However, the event distribution inside the plot originated from the direct process might show a unique structure depending on the participating particles. This analysis is also done to clarify this issue.

For $\Lambda_c^*(2595)$ decay, the amplitude of direct process can be written as

$$
\begin{aligned}
-i\mathcal{T}_{\text{Direct}} &= \frac{g_{1/2}}{f_\pi}\, \bar{u}_{\Lambda_c}(p_1+p_2)_\mu \left(\gamma^\mu + \frac{P^\mu}{M}\right)\gamma_5 u_{\Lambda_c^*}, &(8.5)\\
&\approx \frac{G_{1/2}}{f_\pi}\, \chi^\dagger_{\Lambda_c} \left\{\boldsymbol{\sigma}\cdot(\mathbf{p}_1+\mathbf{p}_2)\right\} \chi_{\Lambda_c^*}, &(8.6)
\end{aligned}
$$

where $g_{1/2}$ is the coupling strength of the direct process and we denote $G_{1/2} = g_{1/2}\sqrt{2m_{\Lambda_c^*}}\sqrt{2m_{\Lambda_c}}$ in the second line after performing the non-relativistic reduction. Here, we follow the same notation used in previous Chapters. By employing the chiral partner structure, we can estimate the direct process coupling as $g_{1/2} = g_{2a}^p$ (coupling of $\Sigma_c \to \Lambda_c\pi$ decay). Similarly, we can write the direct process amplitude for $\Lambda_c^*(2625)$ decay as

$$
\begin{aligned}
-i\mathcal{T}_{\text{Direct}} &= \frac{g_{3/2}}{f_\pi}\, \bar{u}_{\Lambda_c}(p_1+p_2)_\mu u^\mu_{\Lambda_c^*}, &(8.7)\\
&\approx \frac{G_{3/2}}{f_\pi}\, \chi^\dagger_{\Lambda_c} \left\{\mathbf{S}\cdot(\mathbf{p}_1+\mathbf{p}_2)\right\} \chi_{\Lambda_c^*}, &(8.8)
\end{aligned}
$$

where now the coupling of direct process is denoted as $g_{3/2}$ and estimated in the chiral partner structure as $g_{3/2} = g_{2b}^p$ (coupling of $\Sigma_c^* \to \Lambda_c\pi$ decay). We note that the coupling strengths in the sequential processes are extracted from the quark model and all of the decay amplitudes are calculated in the non-relativistic framework. The total amplitudes are obtained by summing up the amplitudes coherently and the relative phases are fixed in the quark model.

We notice that the decay process amplitudes for both decays have similar structures, namely, they are proportional to the pion momentum which means that the outgoing pions have angular momentum $l = 1$. This is because the Λ_c^* with $1/2^-$ and $3/2^-$ directly decay into $\Lambda_c(1/2^+)\pi(0^-)\pi(0^-)$ in p wave. Therefore, the amplitudes obtained by performing the non-relativistic reduction is unique.

8.3 Roles of direct process

In the following, we will discuss the roles of the direct process in Λ_c^* decays. We also stress the usefulness of the Dalitz plots for differentiating the decay mechanisms. The Dalitz plots and other related quantities are presented for the comparison with the experimental data which is currently being analyzed by Belle collaboration.

8.3.1 $\Lambda_c^*(2595)$ decay

First, let us consider the decay of $\Lambda_c^*(2595)$. As was discussed previously, the decay is dominated by the $\Sigma_c\pi$ channel due to the s-wave nature. The results obtained in this work are summarized in Table 8.1. It is shown that the direct process has a small contribution because Λ_c^* directly decays by emitting two pions in p wave. Since we now take into account the angular dependences, the contribution from interference terms become finite. Also, the relative phase between λ and ρ modes are opposite for the direct process, indicated by the different sign of the interference terms. In this case, we can still say that $\Lambda_c^*(2595)$ is dominated by the λ-mode excitation. Note that not only the absolute value of decay width is consistent with the data, but also the calculated branching fraction,

$$\mathcal{B}(\Sigma_c(2455)^0\pi^+) \quad = \quad 0.082, \tag{8.9}$$

has good agreement with the Belle measurement $\mathcal{B}(\Sigma_c(2455)^0\pi^+) = 0.125 \pm 0.035$ [25]. In that sense, it is suggested that $\Lambda_c^*(2595)$ is a quark model states (three-quark state) in the view of their decay properties. Also, we can not neglect the possibility of the chiral partner structure between $\Lambda_c^*(2595)$ and Σ_c resonances.

Table 8.1. Various components of $\Lambda_c^*(2595) \to \Lambda_c\pi\pi$ decay with various quark model configurations for $J^P = 1/2^-$ (in MeV).

Component	$\Lambda_c^*(1P_\lambda, 1/2(1)^-)$	$\Lambda_c^*(1P_\rho, 1/2(0)^-)$	$\Lambda_c^*(1P_\rho, 1/2(1)^-)$	Exp
$\Sigma_c^0\pi^+$	0.182	-	0.770	0.624 (24%)
$\Sigma_c^{++}\pi^-$	0.218	-	0.946	0.624 (24%)
Direct	0.004	-	0.004	-
Interference	0.068	-	-0.122	-
$\Sigma_c^+\pi^0$	0.719	-	7.278	-
Direct	0.005	-	0.005	-
Interference	0.026	-	-0.090	-
Γ_{total}	2.222	-	8.791	2.6 ± 0.6

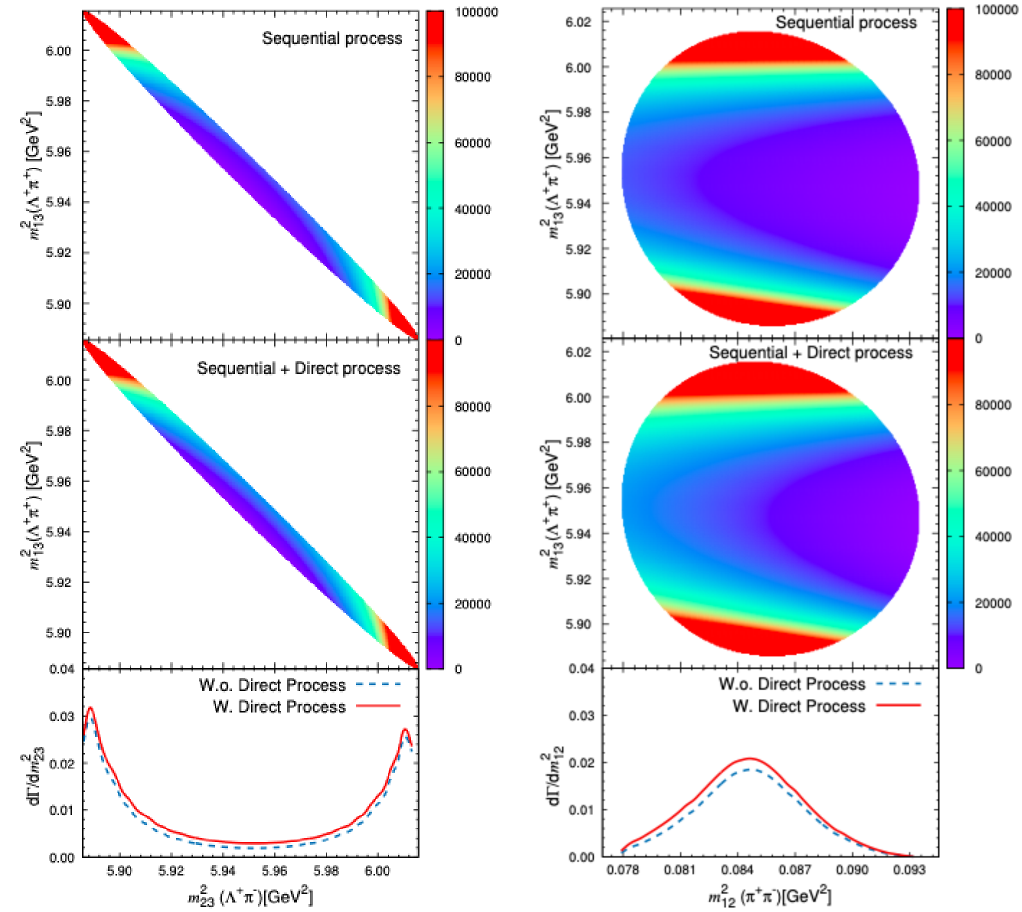

Figure 8.4. The Dalitz plot of $\Lambda_c^*(2595) \to \Lambda_c^+\pi^+\pi^-$ with $\Lambda_c^*(1P_\lambda, 1/2(1)^-)$ assignment along with the $\Lambda_c^+\pi^-$ invariant mass distribution.

Next the Dalitz plots of $\Lambda_c^* \to \Lambda_c^+\pi^+\pi^-$ are shown in Fig. 8.4. Similar to the previous calculation, the plot in (m_{23}^2, m_{13}^2) plane is made on the left side. As we can see, angular dependence is shown in the Dalitz plot where it appears rather inclined along the resonance bands. The angular dependence is mainly from the interference effect and direct process, which contain the terms proportional to $\cos\theta_{12}$. In this case, there is no unique indication of the presence of the direct process. Moreover, there is no significant difference after the inclusion of the direct process in the $\Lambda_c^+\pi^-$ invariant mass distribution. Note that the invariant mass distribution has a similar shape with the one previously calculated in the angle average approximation. This justifies that such an approximation is sufficiently good for this decay.

Here we also show another plot in a different plane, (m_{23}^2, m_{12}^2) plane. This Dalitz plot has an advantage because of its larger area where the structure inside the plot can be seen more clearly. Generally, this plot has exactly the same information as the previous one. The $\pi^+\pi^-$ invariant mass distribution is also presented. If the direct process has a large coupling, the lower region of $\pi^+\pi^-$

invariant mass will be enhanced. This might be an indication of the existence of the direct process.

8.3.2 $\Lambda_c^*(2625)$ decay

Let us now turn the discussion to the $\Lambda_c^*(2625)$ decay. In this case, we observe that the direct process has a significant contribution. This direct process with the p-wave nature can now compete with the d-wave $\Sigma_c\pi$ channel and s-wave $\Sigma_c^*\pi$ closed channel as expected because of the large contribution of the non-resonant process according to PDG. Our numerical result is presented in Table 8.2. Note that the interference terms have different behavior for λ and ρ mode.

Table 8.2. Various components of $\Lambda_c^*(2625) \to \Lambda_c\pi\pi$ decay with various quark model configurations for $J^P = 3/2^-$ (in MeV).

Component	$\Lambda_c^*(1P_\lambda, 3/2(1)^-)$	$\Lambda_c^*(1P_\rho, 3/2(1)^-)$	$\Lambda_c^*(1P_\rho, 3/2(2)^-)$	Exp
$\Sigma_c^0\pi^+$	0.037	0.019	0.034	< 0.050
$\Sigma_c^{++}\pi^-$	0.031	0.016	0.028	< 0.050
$\Sigma_c^{*0}\pi^+$	0.044	0.197	0.000	-
$\Sigma_c^{*++}\pi^-$	0.064	0.314	0.000	-
Direct	0.061	0.061	0.061	-
Interference	0.090	-0.166	-0.011	-
$\Sigma_c^+\pi^0$	0.056	0.029	0.052	-
$\Sigma_c^{*+}\pi^0$	0.072	0.325	0.000	-
Direct	0.045	0.045	0.045	-
Interference	0.070	-0.130	-0.009	-
Γ_{total}	0.570	0.710	0.200	< 0.970

Since the coupling of the direct process is extracted from the $\Sigma_c^* \to \Lambda_c\pi$ decay, its partial decay width is the same for various assignments of the initial $\Lambda_c^*(2625)$. We can see that the direct process contribution is relatively small as compared to the Σ_c^* closed channel for the case of $\Lambda_c^*(1P_\rho, 3/2(1)^-)$ while it is dominant for the case of $\Lambda_c^*(1P_\rho, 3/2(2)^-)$. In the $\Lambda_c^*(1P_\lambda, 3/2(1)^-)$, the direct process has comparable contribution compared to the Σ_c^* closed channel. The component of the non-resonant process could provide the constraint on the internal structure of $\Lambda_c^*(2625)$. Moreover, the calculated branching fraction of the $\Sigma_c(2455)^0\pi^+$ for $\Lambda_c^*(1P_\lambda, 3/2(1)^-)$,

$$\mathcal{B}(\Sigma_c(2455)^0\pi^+) = 0.065, \tag{8.10}$$

has good agreement with the experimental data measured by Belle. This finding might be the evidence that this $\Lambda_c^*(2625)$ corresponds to the λ-mode excitation. Therefore, although we can not say anything from the comparison of the total decay width, the branching fraction of each component could reflect the underlying structure.

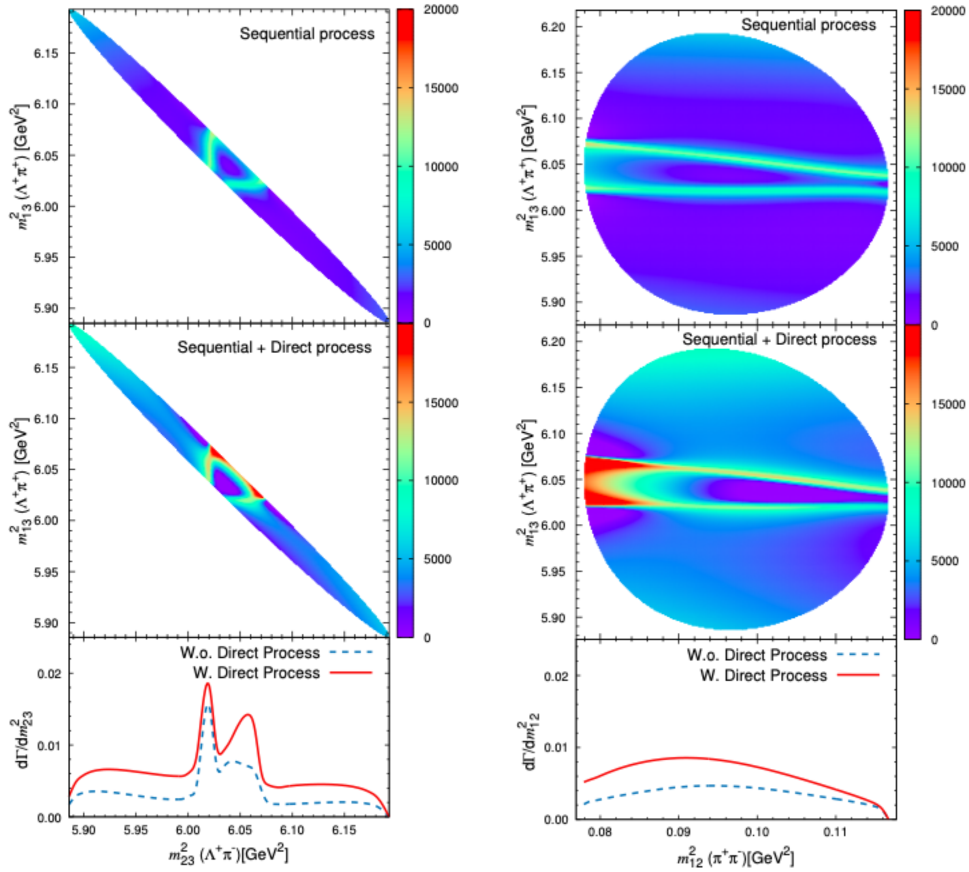

Figure 8.5. The Dalitz plot of $\Lambda_c^*(2625) \to \Lambda_c^+\pi^+\pi^-$ with $\Lambda_c^*(1P_\lambda, 3/2(1)^-)$ assignment along with the $\Lambda_c^+\pi^-$ invariant mass distribution.

The corresponding Dalitz plot is given in Fig. 8.5. We show the plot both in (m_{23}^2, m_{13}^2) and (m_{23}^2, m_{12}^2) planes. For the upper Dalitz plots where only the sequential process is considered, the Σ_c bands in the middle are slightly distorted. This is because of the angular dependence originated from the interference terms between these Σ_c resonances. The bands are far more distorted when the direct process is taken into account as shown in the lower Dalitz plots. Remind that the interference will be enhanced when there is an overlapping region among the amplitudes. This direct process appears as a background shape all over the plot, causing strong interference to the resonance bands. Furthermore, the interference involving the direct process has a characteristic pattern where there is a strong accumulation of signals on the left side of the Dalitz plot in (m_{23}^2, m_{12}^2) plane. We can see further the effect of the direct process in the invariant mass distribution shown on the bottom side of each Dalitz plots. In $\Lambda_c^+\pi^-$ invariant mass distribution, the direct process generally enhances the overall factor. In the middle, there are two peaks projected from the Σ^0 and Σ_c^{++}. When we consider only the sequential process, the Σ_c^{++} peak is lower because it is a known as the kinematical reflection where Σ_c^{++} band appear horizontally in the Dalitz plot in (m_{23}^2, m_{13}^2) plane. However, this peak is much enhanced when we include the direct process. This occurs because of the characteristic interference pattern that is discussed above. Such a pattern also affects the $\pi^+\pi^-$ invariant mass distribution where the lower energy region is more enhanced, leading to asymmetry.

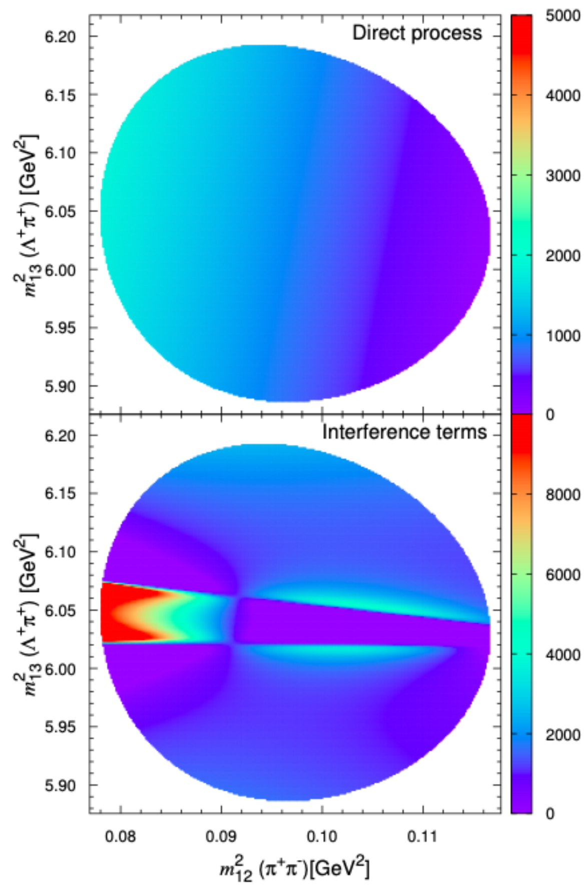

Figure 8.6. The components of the direct process and the interference term are eclusively shown in the Dalitz plot for $\Lambda_c^*(2625)$ decay.

In Fig. 8.6, we show exclusively the contribution from the direct process[1]. In the upper plot, it is shown that the direct process signals spread over the plot. It is also seen that the signals are more enhanced on the left side due to its p-wave nature as discussed in the previous section. Interestingly, the characteristic interference pattern is shown in Fig. 8.5 is originated from the interference involving the direct process. We show such a pattern exclusively in Fig. 8.6.

[1]The lower plot is chosen as a picture in the kaleidoscope of Physical Review D based on the aestetic.

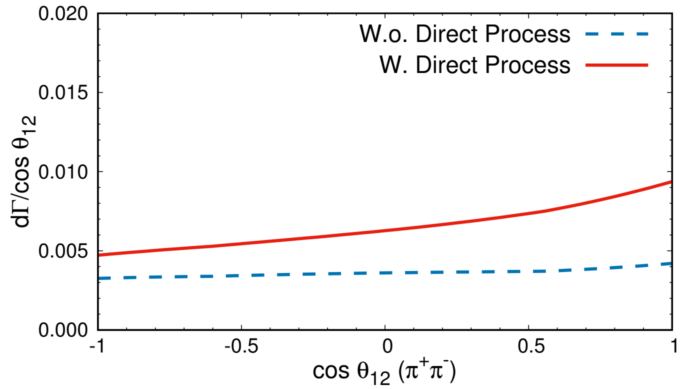

Figure 8.7. The angular correlation along the Σ_c band for $\Lambda_c^*(2625)$ decay.

It is also interesting to plot the angular correlation along the Σ_c resonance band[2]. In this case, we will obtain an asymmetric pattern in the angular correlation as shown in Fig. 8.7 when there exists the direct process. It can be seen that the angular correlation is rather flat when we exclude the direct process. One should also be aware that such asymmetry is mainly originated from the characteristic interference pattern. Here is one of the indications of the presence of the direct process in $\Lambda_c^*(2625)$. If such a pattern is observed in the experiment, it suggests the chiral partner structures between Λ_c^* and Σ_c^* in heavy baryons.

8.4 Summary

In this work, the three-body decay of $\Lambda_c^*(2595)$ and $\Lambda_c^*(2625)$ is revisited with the inclusion of the direct process. We estimate the coupling strengths of the direct process by employing the chiral partner structure. It is found that the direct process has a significant role especially in $\Lambda_c^*(2625)$ decay. We also found several indications of the presence of the direct process in the Dalitz plot and other quantities. The asymmetric patterns are observed along the Σ_c resonance bands. Our prediction can be tested in the current experimental facility such as Belle. If we find good agreement with the data, it suggests the chiral partner structure between Λ_c and Σ_c.

To understand the situation, it is also interesting to futher study the other three-body decays of the negative parity states with various flavors such as the Λ_b, Ξ_c, and Ξ_b resonances. In this direction, we can obtain a more complete picture of the chiral partner structures in heavy baryons. Furthermore, the behavior of such a chiral partner in the medium since the chiral symmetry is partially restored.

"Jibunde wa kataranai, riron ni kataraseru", Yoichiro Nambu

[2] one should be careful of the convention of the angular correlations. In some cases, it is defined as oppositely.

Chapter 9
Spin-parity determination of $\Lambda_c^*(2765)$

9.1 Introduction

Among Λ_c charm baryons, $\Lambda_c^*(2765)$ has poor information about its existence and quantum number although it was discovered around the 2000s. This state still has a one-star rating and its isospin is not yet determined in PDG [1]. One of the reasons is that it is also predicted there may exist the Σ_c state in this energy region. In fact, the $\Lambda_c^*(2765)$ is found in $\Lambda_c^+\pi^+\pi^-$ invariant mass in which the resonances with isospin 0 or 1 are allowed. Recently $\Lambda_c^+\pi^\pm\pi^\pm$ invariant masses are analyzed by Belle and no enhancement is found, indicating that it is not Σ_c state [30]. Therefore, we should call this resonance is associated with the isospin $I = 0$ state, $\Lambda_c^*(2765)$.

Furthermore, the spin and parity of $\Lambda_c^*(2765)$ are not experimentally known. Also, in the quark model, there are a lot of states predicted around this energy region such that the spin and parity are not well determined. Up until now, there are many theoretical analyses in attempts to study this state from various perspectives. The mass spectrum and decay analysis have also been performed thoroughly [89, 107, 114, 160–162]. But, it is not so easy to conclude the spin and parity of this state. In the experimental side, the data on this state has been accumulated over the years, and the analysis for determination of the spin and parity is underway [31].

Unlike other charmed baryons, this particular state $\Lambda_c^*(2765)$ has a broad width of around 50 MeV. This is significantly broader than typical charmed baryon $\Lambda_c^*(2595)$ which has narrow width 2.6 MeV, respectively. The unusual decay property might provide a hint to its internal structure. On top of that, its excitation energy is around 500 MeV which bears resemblance with the so-called Roper resonance, $N(1440)$ with spin and parity $J^P = 1/2^+$. In reality, other Roper-like resonances are also observed in the other flavors, such as $\Lambda(1600)$ and $\Sigma(1660)$ with similar excitation energy. But so far no observed charmed baryons correspond to the analog of the Roper resonance. It is also recognized that such states can not be explained by the quark model. To date, there are a number of alternative pictures to elucidate this state [169, 172–174]. However, before discussing the internal structures more seriously. It is instructive to determine the spin and parity of $\Lambda_c^*(2765)$ in a model-independent way.

Up to now, we have seen the use of the Dalitz plot for determination of spin and parity of resonances. This method has been widely used for the meson spectroscopy where the involving particles have integer spin or even spinless. However, the application of the Dalitz plot is not easy because the participating particles have a half-integer spin. Moreover, particularly $\Lambda_c^*(2625)$, the decay width is rather broad adding more complications in the analysis.

In this work, we aim to study the decay of $\Lambda_c^*(2625)$ by using the Dalitz plot analysis in order to determine its spin and parity. We will consider all of possible spin and parity assignments in the quark model up to $N = 2$ such that we can grasp whole possibilities. In this decay, the $\Sigma_c^*\pi$ channel is open due to the larger phase space as shown in Fig. 9.1 and provide interesting observables, namely

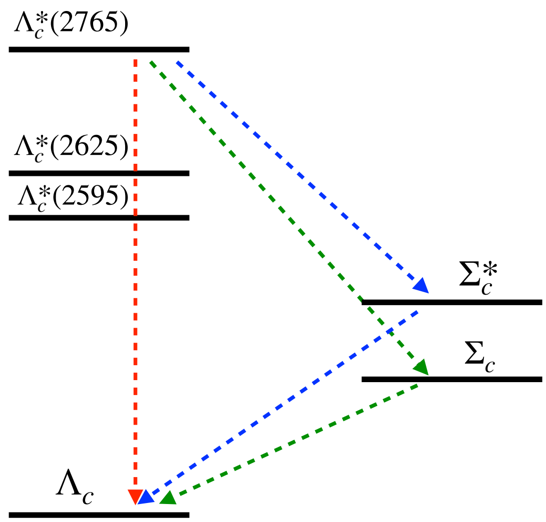

Figure 9.1. Illustration of the sequential and direct processes. In the $\Lambda_c^*(2765)$ decay, $\Sigma_c^*\pi$ channel is now open.

the angular correlations which are helpful to determine the spin and parity. For completeness, the effect of the finite widths is taken into account in the current analysis.

9.2 Our strategy

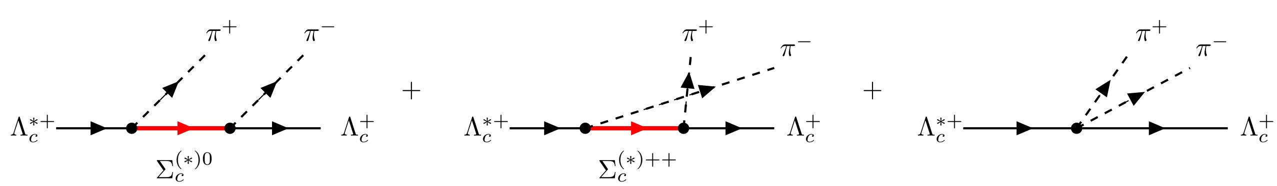

Figure 9.2. The Feynman diagrams of $\Lambda_c^{*+}(2765) \to \Lambda_c^+\pi^+\pi^-$. Note that the direct process is empirically observed to be insignificant.

Before performing the actual analysis, let us first set up our model and limit our interest in this present work. Our main goal is to determine the spin and parity of $\Lambda_c^*(2765)$ from its decay properties. The possible Feynman diagrams for this three-body decay is described in Fig. 9.2. From the experimental observations, the decay is dominated by the Σ_c and Σ_c^* resonances. The contribution from the direct process[1] is not significant, which is implied in Fig. 1 of Ref [29]. Therefore, we will use this empirical fact as our working hypothesis. We then consider only the contribution from $\Sigma_c^{(*)}$ resonances in the present analysis. Keep in mind that if the direct process contribution were

[1]In our language, the direct process includes the contribution from $f_0(500)$ resonance.

Table 9.1. The quark model configuration classified according to the spin-parity J^P and brown muck spin j.

Spin-parity (J^P)	j	Quark model configuration
$\Lambda_c^*(1/2^-)$	0	$\Lambda_c^*(1P_\rho, 1/2(0)^-)$
	1	$\Lambda_c^*(1P_\lambda, 1/2(1)^-), \Lambda_c^*(1P_\rho, 1/2(1)^-)$
$\Lambda_c^*(3/2^-)$	1	$\Lambda_c^*(1P_\lambda, 3/2(1)^-), \Lambda_c^*(1P_\rho, 3/2(1)^-)$
	2	$\Lambda_c^*(1P_\rho, 3/2(2)^-)$
$\Lambda_c^*(5/2^-)$	2	$\Lambda_c^*(1P_\rho, 5/2(2)^-)$
$\Lambda_c^*(1/2^+)$	0	$\Lambda_c^*(2S_{\lambda\lambda}, 1/2(0)^+), \Lambda_c^*(2S_{\rho\rho}, 1/2(0)^+), \Lambda_c^*(1D_{\lambda\rho}, 1/2(0)^+_1)$
	1	$\Lambda_c^*(1D_{\lambda\rho}, 1/2(1)^+_0), \Lambda_c^*(1D_{\lambda\rho}, 1/2(1)^+_1), \Lambda_c^*(1D_{\lambda\rho}, 1/2(1)^+_2)$
$\Lambda_c^*(3/2^+)$	1	$\Lambda_c^*(1D_{\lambda\rho}, 3/2(1)^+_0), \Lambda_c^*(1D_{\lambda\rho}, 3/2(1)^+_1), \Lambda_c^*(1D_{\lambda\rho}, 3/2(1)^+_2)$
	2	$\Lambda_c^*(1D_{\lambda\lambda}, 3/2(2)^+), \Lambda_c^*(1D_{\rho\rho}, 3/2(2)^+), \Lambda_c^*(1D_{\lambda\rho}, 3/2(2)^+_1),$
		$\Lambda_c^*(1D_{\lambda\rho}, 3/2(2)^+_2)$
$\Lambda_c^*(5/2^+)$	2	$\Lambda_c^*(1D_{\lambda\lambda}, 5/2(2)^+), \Lambda_c^*(1D_{\rho\rho}, 5/2(2)^+),$
		$\Lambda_c^*(1D_{\lambda\rho}, 5/2(2)^+_1), \Lambda_c^*(1D_{\lambda\rho}, 5/2(2)^+_2)$
	3	$\Lambda_c^*(1D_{\lambda\rho}, 5/2(3)^+_2)$
$\Lambda_c^*(7/2^+)$	3	$\Lambda_c^*(1D_{\lambda\rho}, 7/2(3)^+_2)$

significant, our results obtained in this work would be greatly modified.

Now, in the quark model, many states are predicted in this energy region. They include the states with the spin and parity $J^P = 1/2^\pm, 3/2^\pm, 5/2^\pm$, and even $7/2^+$ as shown in Table 9.1, in which we collect the configuration with the same spin-parity and brown muck spin j. As we may notice, the $\Lambda_c^*(2595)$ and $\Lambda_c^*(2625)$ states have been assigned by $J^P = 1/2^-$ and $3/2^-$ with λ mode, respectively. But, we still consider such spin and parity assignment because $\Lambda_c^*(2765)$ could correspond to the negative parity with ρ-mode excitation. Our attitude is to consider all configurations that have possibilities to explain this state. For this purpose, we have discuss our methods comprehensively, in Part II. Formulation, which includes the quark model and the effective Lagrangians with the above-mentioned spin and parity assignments.

We first revisit the two-body decays of $\Lambda_c^*(2765) \to \Sigma_c^{(*)}\pi$ with all possible configurations in the quark model as given in Table 9.1. Then, we will inspect the resulting decay width and the ratio

$$R = \frac{\Gamma(\Lambda_c^*(2765) \to \Sigma_c^*(2520)\pi)}{\Gamma(\Lambda_c^*(2765) \to \Sigma_c(2455)\pi)}, \tag{9.1}$$

from which we may be able to extract some information about its spin and parity. In addition to that, we also compare the ratio R obtained from the quark model with the prediction from the heavy-quark spin symmetry [87]. As we have discussed, the heavy quark spin is decoupled from the light quark spin in the heavy-quark limit. As a result, the transition occurs between the brown muck spin $j \to j' + \pi$ where the heavy quark act as the spectator. Thus, we can calculate the decay width of $J(j) \to J'(j') + \pi$ with the six-j symbol as

$$\Gamma = (2j+1)(2J'+1)\left|\begin{Bmatrix} J & J' & L \\ j' & j & s_q \end{Bmatrix}\right|^2 p^{(2L+1)}|M_L|^2. \tag{9.2}$$

where $s_q = 1/2$ is the heavy-quark spin, L is the relative angular momentum of the final states $\Sigma_c^{(*)}\pi$, p the emitted pion momentum, and M_L the reduced matrix element. Note that this prediction of the ratio can only be calculated for the same partial wave where the reduced matrix element $|M_L|^2$ cancels. The ratio R is computed as

$$R = \frac{(2J'_{\Sigma_c^*}+1) \times p(\Sigma_c^*\pi)^{(2L+1)}}{(2J'_{\Sigma_c}+1) \times p(\Sigma_c\pi)^{(2L+1)}} \frac{\left|\begin{Bmatrix} J_{\Lambda_c^*} & J'_{\Sigma_c^*} & L \\ j'_{\Sigma_c^*} & j_{\Lambda_c^*} & s_q \end{Bmatrix}\right|^2}{\left|\begin{Bmatrix} J_{\Lambda_c^*} & J'_{\Sigma_c} & L \\ j'_{\Sigma_c} & j_{\Lambda_c^*} & s_q \end{Bmatrix}\right|^2}. \tag{9.3}$$

The discussion of the ratio R has an advantage with less ambiguity because the uncertaintis coming from the quark model parameters cancel out. It is worth noting that the discussion of ratio R is not applicable for the $\Lambda_c^*(2695)$ and $\Lambda_c^*(2625)$, in the previous chapters, since the Σ_c^* is kinematically closed.

For the three-body decay analysis, one of the prominent problems is that this $\Lambda_c^*(2765)$ is a broad resonance. In actual computation is the Dalitz plot is made with a given (or fixed) value of the initial mass. This method is acceptable for the narrow resonance. Knowing this situation, we first make a narrow cut at the central value of its mass $\Lambda_c^*(2765)$ and discuss the Dalitz plots and related quantities accordingly. Afterward, we try to treat the mass distribution of the $\Lambda_c^*(2765)$ with a simple Breit-Wigner parameterization. In this way, we may have a picture of how the Dalitz plots are transformed for the case of broad resonances. To the end, the Dalitz plots and other related observables computed with various spin and parity assignments given in Table 9.1 are analyzed in an attempt to provide theoretical predictions for the experimentalist what to measure for determination of the spin and parity of $\Lambda_c^*(2765)$.

9.3 Two-body decays

Let us discuss the results obtained from the two-body decay analysis as shown in Table 9.2. So far, the only experimental data, which is available in PDG, is the mass and total decay width $\Gamma_{exp} = 50$ MeV. If we naively compare this value with the results calculated in the quark model, we might have a conclusion that it might correspond to either $1/2^-$ or $3/2^-$ with λ mode excitations, the first two rows in Table 9.2. In fact, only configurations with these spin and parity give rather large decay width which is mainly due to the s-wave decay into either $\Sigma_c\pi$ or $\Sigma_c^*\pi$ channel. But, as we know, these configurations have been assigned to the P-wave doublet of Λ_c^*. One can also argue that the Λ_c^* might correspond to that of the ρ mode where the broad width is produced although it overpredicts the experimental value. This looks promising but it should be supported by the other measurements. Furthermore, if this $\Lambda_c^*(2765)$ has a non-zero brown muck spin j, it suggests that there exists its HQS partner which should be clarified.

The other configurations predict relatively small decay widths where we can simply rule them out in the view of its magnitude of the decay width. As we discussed previously, the direct process has small contributions as implied in the experimental observation. In other words, the decay width is saturated with the $\Sigma_c^{(*)}$ contribution. Therefore, if $\Lambda_c^*(2765)$ is indeed $1/2^+$, which is suggested by many works, it can not be explained by the quark model since we have a contradiction where the predicted width is very small. Needless to say, we can not draw a conclusion at this moment by looking at the total decay width.

In Table 9.2, we also show other components such as the partial decay widths of $\Sigma_c^{(*)}\pi$ channel along with the ratio. In the last column, we show the ratio calculated in the heavy-quark spin symmetry and it is shown that the ratios calculated from the quark model have good agreement with it. This demonstrates that the quark model that we have constructed respect the heavy-quark symmetry.

For the $\Lambda_c^*(1/2^-)$ and $\Lambda_c^*(3/2^-)$ with $j = 1$, the partial waves of $\Sigma_c\pi$ and $\Sigma_c^*\pi$ are different such that the ratio R will be very small and very large, respectively, as

$$R[\Lambda_c^*(1/2(1)^-)] = \frac{\Gamma(\Sigma_c^*\pi)_d}{\Gamma(\Sigma_c\pi)_s} \ll 1, \tag{9.4}$$

$$R[\Lambda_c^*(3/2(1)^-)] = \frac{\Gamma(\Sigma_c^*\pi)_s + \Gamma(\Sigma_c^*\pi)_d}{\Gamma(\Sigma_c\pi)_d} \gg 1, \tag{9.5}$$

where we denote R_{HQ} equal to " - " since it is not applicable. Note that the decay of $\Lambda_c^*(1/2^-)$ with $j = 0$ is forbidden due to the brown-muck selection rule. Interestingly, for the $\Lambda_c^*(3/2^-)$ with $j = 2$, the s wave is also not allowed. In such a case, the ratio R is significantly changed as

$$R_{HQ}[\Lambda_c^*(3/2(2)^-)] = \frac{\Gamma(\Sigma_c^*\pi)_d}{\Gamma(\Sigma_c\pi)_d} = 1 \times \frac{p(\Sigma_c^*\pi)^5}{p(\Sigma_c\pi)^5} = 0.22. \tag{9.6}$$

Table 9.2. Calculated decay widths and the ratios of the decay of $\Lambda_c^*(2765) \to \Sigma_c^{(*)}\pi$ with various quark model configurations.

Excitations	Γ_{total}	$[\Sigma_c\pi]^+$	$[\Sigma_c^*\pi]^+$	R	R_{HQ}
$\Lambda_c^*(1P_\rho, 1/2(0)^-)$	-	-	-	-	-
$\Lambda_c^*(1P_\lambda, 1/2(1)^-)$	65.1-146	61.2-140	3.90-6.10	0.04-0.06	-
$\Lambda_c^*(1P_\rho, 1/2(1)^-)$	326-676	324-673	2.10-3.00	0.004-0.006	-
$\Lambda_c^*(1P_\lambda, 3/2(1)^-)$	52.2-104	7.9-11.9	44.3-92.4	5.60-7.80	-
$\Lambda_c^*(1P_\rho, 3/2(1)^-)$	210-413	4.20-5.80	206-408	49.0-70.0	-
$\Lambda_c^*(1P_\rho, 3/2(2)^-)$	9.40-13.1	7.60-10.5	1.90-2.70	0.25-0.26	0.22
$\Lambda_c^*(1P_\rho, 5/2(2)^-)$	6.30-8.80	3.40-4.70	2.90-4.20	0.87-0.90	0.76
$\Lambda_c^*(2S_{\lambda\lambda}, 1/2(0)^+)$	1.60-4.50	0.86-2.49	0.78-1.98	0.79-0.91	
$\Lambda_c^*(2S_{\rho\rho}, 1/2(0)^+)$	4.69-11.2	2.60-6.55	2.09-4.60	0.70-0.80	0.80
$\Lambda_c^*(1D_{\lambda\rho}, 1/2(0)_1^+)$	0.66-1.79	0.42-1.12	0.25-0.67	0.60-0.60	
$\Lambda_c^*(1D_{\lambda\rho}, 1/2(1)_0^+)$	5.47-13.4	4.53-11.3	0.93-2.10	0.19-0.21	
$\Lambda_c^*(1D_{\lambda\rho}, 1/2(1)_1^+)$	0.24-0.64	0.21-0.56	0.03-0.08	0.15-0.15	0.20
$\Lambda_c^*(1D_{\lambda\rho}, 1/2(1)_2^+)$	11.4-23.8	9.78-20.5	1.61-3.32	0.16-0.16	
$\Lambda_c^*(1D_{\lambda\rho}, 3/2(1)_0^+)$	3.47-8.06	1.13-2.82	2.33-5.24	1.86-2.06	
$\Lambda_c^*(1D_{\lambda\rho}, 3/2(1)_1^+)$	0.13-0.35	0.05-0.14	0.08-0.21	1.49-1.51	1.99
$\Lambda_c^*(1D_{\lambda\rho}, 3/2(1)_2^+)$	6.48-13.4	2.45-5.13	4.03-8.31	1.62-1.65	
$\Lambda_c^*(1D_{\lambda\lambda}, 3/2(2)^+)$	4.70-10.9	4.40-10.1	0.33-0.72	0.07-0.08	
$\Lambda_c^*(1D_{\rho\rho}, 3/2(2)^+)$	11.5-23.3	10.7-21.8	0.77-1.43	0.07-0.06	0.07
$\Lambda_c^*(1D_{\lambda\rho}, 3/2(2)_1^+)$	0.28-0.74	0.26-0.70	0.02-0.04	0.06-0.06	
$\Lambda_c^*(1D_{\lambda\rho}, 3/2(2)_2^+)$	23.5-49.3	22.0-46.2	1.49-3.11	0.07-0.07	
$\Lambda_c^*(1D_{\lambda\lambda}, 5/2(2)^+)$	1.90-4.40	0.13-0.32	1.77-4.04	12.8-13.8	-
$\Lambda_c^*(1D_{\rho\rho}, 5/2(2)^+)$	4.45-8.63	0.13-0.31	4.32-8.32	26.8-33.2	-
$\Lambda_c^*(1D_{\lambda\rho}, 5/2(2)_1^+)$	0.09-0.25	-	0.09-0.25	-	-
$\Lambda_c^*(1D_{\lambda\rho}, 5/2(2)_2^+)$	8.92-18.4	0.19-0.40	8.73-18.0	44.7-44.9	-
$\Lambda_c^*(1D_{\lambda\rho}, 5/2(3)_2^+)$	0.25-0.54	0.22-0.46	0.04-0.08	0.17-0.18	0.15
$\Lambda_c^*(1D_{\lambda\rho}, 7/2(3)_2^+)$	0.17-0.37	0.12-0.26	0.05-0.11	0.41-0.43	0.35

Similarly, $\Lambda_c^*(5/2^-)$ with $j = 2$ decays into both channels in d wave such that the ratio is given by

$$R_{HQ}[\Lambda_c^*(5/2(2)^-)] = \frac{\Gamma(\Sigma_c^*\pi)_d}{\Gamma(\Sigma_c\pi)_d} = \frac{7}{2} \times \frac{p(\Sigma_c^*\pi)^5}{p(\Sigma_c\pi)^5} = 0.76. \tag{9.7}$$

However, we can see that the ratio has different value with that of $\Lambda_c^*(3/2(2)^-)$. The difference is from the factor originated from how angular momentums are coupled, which is represented by the six-j symbol.

For the case of $\Lambda_c^*(1/2^+)$ and $\Lambda_c^*(3/2^+)$, they both decay into $\Sigma_c^{(*)}\pi$ in p wave. Accordingly, the ratio R can be obtained as

$$R_{HQ}[\Lambda_c^*(1/2(0)^+)] = 2 \times \frac{p(\Sigma_c^*\pi)^3}{p(\Sigma_c\pi)^3} = 0.80, \tag{9.8}$$

$$R_{HQ}[\Lambda_c^*(1/2(1)^+)] = \frac{1}{2} \times \frac{p(\Sigma_c^*\pi)^3}{p(\Sigma_c\pi)^3} = 0.20. \tag{9.9}$$

$$R_{HQ}[\Lambda_c^*(3/2(1)^+)] = 5 \times \frac{p(\Sigma_c^*\pi)^3}{p(\Sigma_c\pi)^3} = 1.99, \tag{9.10}$$

$$R_{HQ}[\Lambda_c^*(3/2(2)^+)] = \frac{1}{5} \times \frac{p(\Sigma_c^*\pi)^3}{p(\Sigma_c\pi)^3} = 0.07. \tag{9.11}$$

The above equations explain sufficiently well that the calculated ratio R in the quark model for $\Lambda_c^*(1/2(0)^+)$ is bigger than that of $\Lambda_c^*(1/2(1)^+)$ by factor four. This applies to the case of $\Lambda_c^*(3/2^+)$.

For the case of $\Lambda_c^*(5/2^+)$ with $j = 2$, the ratio is much larger than unity because of the p-wave dominance as

$$R[\Lambda_c^*(5/2(2)^+)] = \frac{\Gamma(\Sigma_c^*\pi)_p + \Gamma(\Sigma_c^*\pi)_f}{\Gamma(\Sigma_c\pi)_f} \gg 1. \tag{9.12}$$

There is an exception for $\Lambda_c^*(1D_{\lambda\rho}, 5/2(2)_1^+)$ where the $\Sigma_c\pi$ channel is forbidden because of the orbital angular momentum conservation. Again, for the higher brown-muck spin, namely $j = 3$, the p-wave decay is not allowed and therefore the ratio can be computed as

$$R_{HQ}[\Lambda_c^*(5/2(3)^+)] = \frac{5}{4} \times \frac{p(\Sigma_c^*\pi)^7}{p(\Sigma_c\pi)^7} = 0.15, \tag{9.13}$$

where the decays occur in f wave. Also for $\Lambda_c^*(7/2(3)^+)$, the ratio is given by

$$R_{HQ}[\Lambda_c^*(7/2(3)^+)] = 3 \times \frac{p(\Sigma_c^*\pi)^7}{p(\Sigma_c\pi)^7} = 0.35. \tag{9.14}$$

In summary, the ratio will give a useful constraint on the spin and parity of the $\Lambda_c^*(2765)$. It is also found that the ratios computed in the quark model follow the heavy-quark symmetry. However, as we may notice, the ratio itself can not be used for the spin and parity determination and therefore we need more constraints. For that reason, we will analyze its three-body decay into $\Lambda_c\pi\pi$ where there are additional kinematical variables, which might give other constraints.

9.4 Three-body decays

To analyze the broad resonance like $\Lambda_c^*(2765)$, we will divide the discussion into two parts. Firstly, we perform a Dalit plot analysis by fixing the mass of $\Lambda_c^*(2765)$ at a certain value. For instance, we choose three different masses as shown in Fig 9.3. The Dalitz plot shows not only different sizes but also different structures. As we go away from the central value, the probability becomes much smaller. In such cases, the comparison to the experimental data could be challenging because of the lack of statistics. To avoid that, we will discuss the Dalitz plot at the central mass. Practically, experimentalists need to make a very narrow cut in order to compare with our calculation.

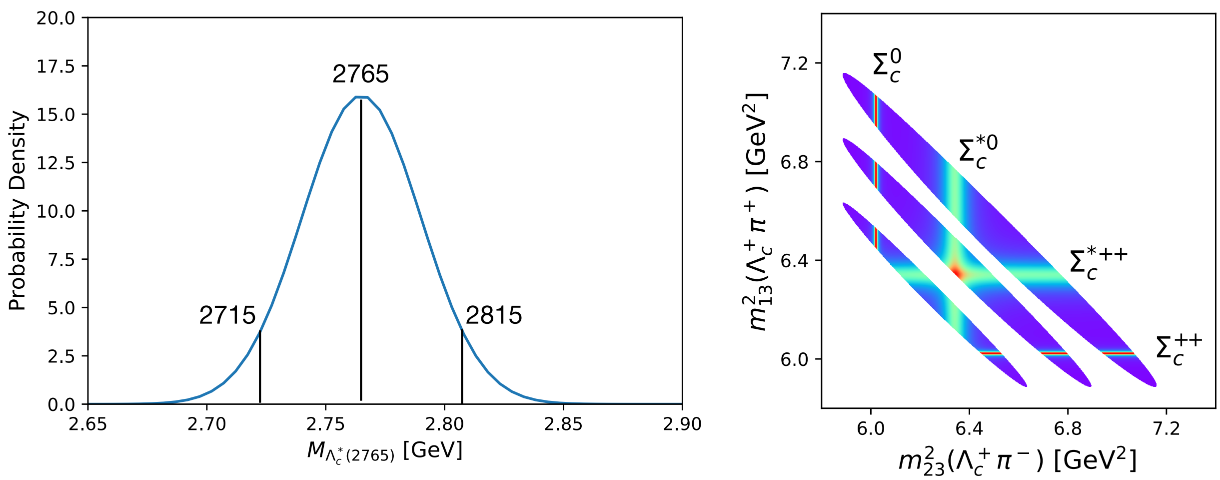

Figure 9.3. The mass distribution of $\Lambda_c^*(2765)$ and The corresponding Dalitz plots with three different initial masses.

Secondly, we will consider the mass distribution of the $\Lambda_c^*(2765)$ and convolute whole Dalitz plots with different initial mass and weighted by the Breit-Wigner distribution. Actually, there is an opening DN channel near 2800 MeV just above the central mass which may distort the Breit-Wigner distribution. This such effect should be taken into account more seriously in the later stage when the experimental data becomes available. Although it is not trivial in the theoretical side, this is what experimentalists usually do because they want to consider all signals. Of course, the statistics will be huge in which the structures inside the Dalitz plot can be seen more clearly. However, one should be careful because after performing the convolution the resulting Dalitz plot may look very different and we could arrive at the wrong conclusion. This is the work to clarify this issue as well.

9.4.1 Dalitz plot with a narrow cut

Let us now look at the Dalitz plots and related quantities for the fixed mass $M = 2765$ MeV. This Dalitz plot corresponds to the middle plot in Fig. 9.3. As we can see, there is actually an accident interference between Σ_c^* with a different charge, bringing a complication in this analysis. In this case, the interference effect should be considered carefully when discussing the structure inside the Dalitz plots.

Here, we consider all different spin and parity as shown in Table 9.1. For a given spin and parity, we can have several configurations. However, it is found that they give similar behavior by looking at the value of the ratio in the two-body analysis. Therefore, we will choose one low-lying configuration for each spin and parity assignment. Furthermore, the other configurations with the same spin and parity are inspected for example.

Relative strengths: ratio

The resulting Dalitz plots in (m_{23}^2, m_{13}^2) plane and $\Lambda_c^+\pi^-$ invariant mass distribution are given in Fig. 9.4 where the spin and parity are written in each plot along with the brown muck spin. It is shown that there are four resonance bands from left to right correspond to $\Sigma_c^0, \Sigma_c^{*0}, \Sigma_c^{*++}$ and Σ_c^{++}, respectively. The $\Sigma_c^{(*)0}$ are the resonances in $\Lambda_c^+\pi^-$ invariant mass and the corresponding $\Sigma_c^{(*)++}$ are the kinematical reflections. In Dalitz plot, the Σ_c^0 and its kinematical reflection have the same strengths of its resonance band. The difference is just the direction of the resonance band in which Σ_c^0 band is vertical while Σ_c^{++} band is diagonal. It is also understood that the peaks originated from the kinematical reflections will look different from the resonance peak in $\Lambda_c^+\pi^-$ invariant mass distribution, but their yields are generally the same because they correspond to the same particle with a different charge.

From the Dalitz plots made with various spin and parity assignments, we can see one notable difference, that is the relative strengths between Σ_c and Σ_c^* bands. For instance, the Σ_c band is stronger than that of Σ_c^* in the Dalitz plot for $\Lambda_c^*(1/2^-)$. On the other hand, the Σ_c^* band is stronger for the case of $\Lambda_c^*(3/2^-)$. This observation is clearly seen in the invariant mass distribution where the relative strengths of the resonance peaks are different from one to other cases. For the case of $\Lambda_c^*(1/2^+)$, the strength of bands is relatively similar. The reason behind this is similar to the discussion of the ratio R that we have discussed previously. We also check the other configuration with the same spin and parity but different brown muck spin j, and the resulting Dalitz plots show the different ratio of relative strengths of resonance bands as expected.

One should be careful because the Σ_c^* band has a strong interference which may contaminate the ratio R to some extents. It is because the R is usually measured by cutting the resonance bands where the interference terms can not be separated. As was mentioned previously, the discussion of the Dalitz plot for the initial mass slightly away from the central value may be helpful because the interference effect will be reduced. In fact, the resonance bands will be well separated as seen in Fig. 9.3. But it may suffer from the small statistics where the structure may not be visible clearly.

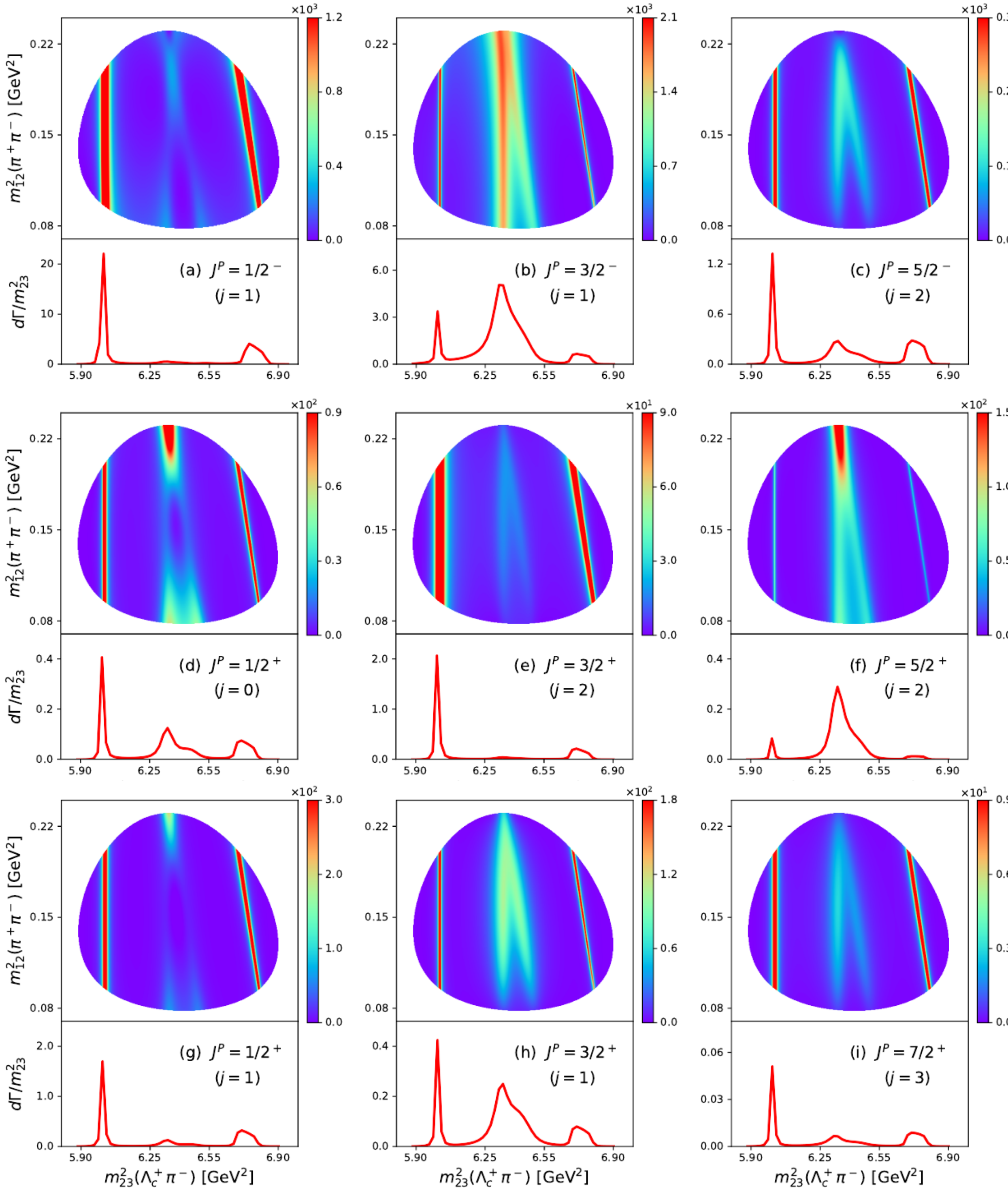

Figure 9.4. The Dalitz plots and $\Lambda_c^+\pi^-$ invariant mass distribution with various spin and parity assignments made by a fixed initial mass at $M = 2765$ MeV.

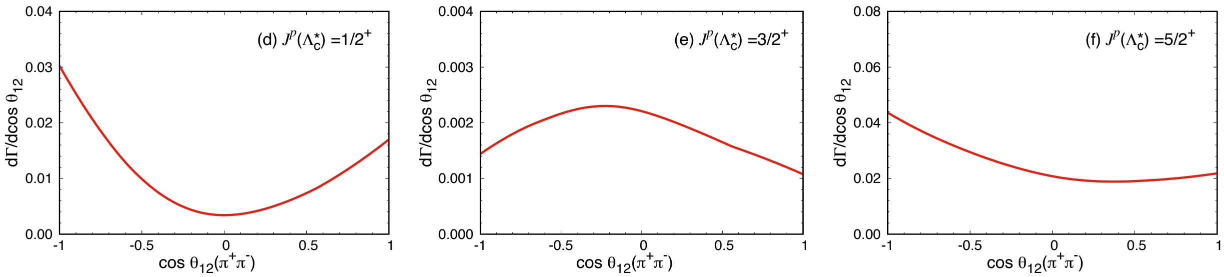

Figure 9.5. The angular correlations obtained by cutting the Σ_c^{*0} resonance band.

Angular correlations

Another notable difference among the Dalitz plots in Fig. 9.4 is the angular correlations along the Σ_c^* resonance band located in the middle. For instance, if we cut the Σ_c^{*0} resonance band, the angular correlations for the positive parity case are given in Fig. 9.5. For $\Lambda_c^*(1/2^+)$, we can observe that the valley structure is exhibited. Meanwhile, for the $\Lambda_c^*(3/2^+)$, the angular correlation shows oppositely like a hill structure and it is rather flat for $\Lambda_c^*(5/2^+)$. Of course, the asymmetric pattern is clearly seen, which is mainly due to the interference at the top side of the Dalitz plot or near the backward angle. In Fig. 9.6, we show the components of angular correlation for the case of $1/2^+$. It can be seen that the large contribution at the backward angle is coming from the interference terms. Apparently, the interference contaminates the angular correlations, but the characteristic shape still remains.

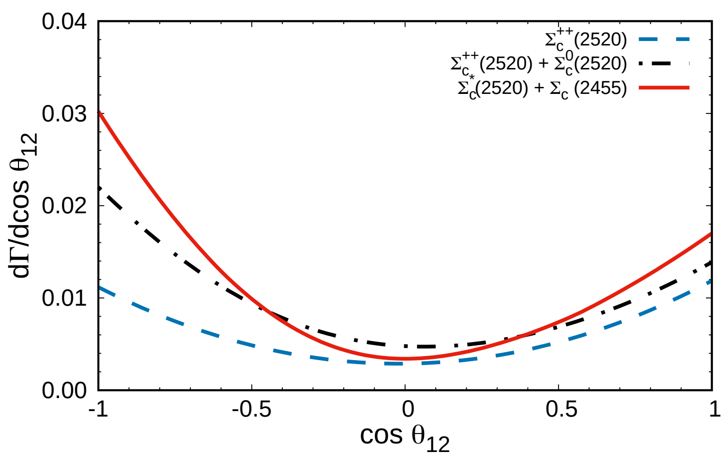

Figure 9.6. The enhancement of the angular correlation at the backward angle due to the interference terms.

The resulting angular correlations are related to the Wigner D function $d^{3/2}_{h_f h_i}(\theta_{12})$ since Σ_c^* has spin 3/2. In such a case, the helicity of Σ_c^* can be either 1/2 and 3/2, which give valley and hill structure in the angular correlation, respectively. The obtained angular correlation is the combination

Table 9.3. The ratio and the angular correlations for various spin and parity assignments. Note that we define two different ratio R and $\tilde{R}$.

$J(j)^P$	$L(\Sigma_c\pi)$	$L(\Sigma_c^*\pi)$	$\tilde{R}$	R	$W(\theta_{12})$
$1/2(0)^-$	$\cancel{s}$	$\cancel{d}$	-	-	-
$1/2(1)^-$	s	d	0	0.05	$1+3\cos^2\theta_{12}$
$1/2(0)^+$	p	p	0	0.80	$1+3\cos^2\theta_{12}$
$1/2(1)^+$	p	p	0	0.20	$1+3\cos^2\theta_{12}$
$3/2(1)^-$	d	s,d	1	6.70	1
$3/2(2)^-$	d	$\cancel{s},d$	1	0.22	1
$3/2(1)^+$	p	$p,\cancel{f}$	9	1.99	$1+6\sin^2\theta_{12}$
$3/2(2)^+$	p	p,f	9	0.07	$1+6\sin^2\theta_{12}$
$5/2(2)^-$	d	$d,\cancel{g}$	6	0.76	$1+(15/4)\sin^2\theta_{12}$
$5/2(2)^+$	f	p,f	2/3	13.3	$1+(1/3)\cos^2\theta_{12}$
$5/2(3)^+$	f	$\cancel{p},f$	3/2	0.15	$1+(3/8)\sin^2\theta_{12}$
$7/2(3)^+$	f	$f,\cancel{h}$	5	0.35	$1+3\sin^2\theta_{12}$

between them, which is given by

$$W(\theta_{12}) \;\propto\; \left|A_{1/2}(\Lambda_c^*\to\Sigma_c^*\pi)\right|^2\times(1+3\cos^2\theta_{12})+\left|A_{3/2}(\Lambda_c^*\to\Sigma_c^*\pi)\right|^2\times 3\sin^2\theta_{12}, \quad (9.15)$$

$$\propto\; 1\times(1+3\cos^2\theta_{12})+\tilde{R}\times 3\sin^2\theta_{12}. \quad (9.16)$$

We observe the ratio $\tilde{R}$ between the helicity amplitudes with $h=1/2$ and $3/2$ control the shape of the angular correlations as

$$\tilde{R}>1 \;\to\; \text{hill}, \quad (9.17)$$

$$\tilde{R}=1 \;\to\; \text{flat}, \quad (9.18)$$

$$0<\tilde{R}<1 \;\to\; \text{valley}. \quad (9.19)$$

In fact, the ratio $\tilde{R}$ can be computed as

$$\tilde{R}=\frac{\left|A_{3/2}(\Lambda_c^*\to\Sigma_c^*\pi)\right|^2}{\left|A_{1/2}(\Lambda_c^*\to\Sigma_c^*\pi)\right|^2}=\frac{|(J\ \tfrac{3}{2}\ L\ 0\ |\tfrac{3}{2}\ \tfrac{3}{2})|^2}{|(J\ \tfrac{1}{2}\ L\ 0\ |\tfrac{3}{2}\ \tfrac{1}{2})|^2}, \quad (9.20)$$

where we have defined J for the spin of $\Lambda_c^*(2765)$ and L the relative angular momentum of $\Sigma_c^*\pi$. It is shown that the ratio $\tilde{R}$ is completely dictated by the Clebsh-Gordan coefficients. The ratio $\tilde{R}$ and

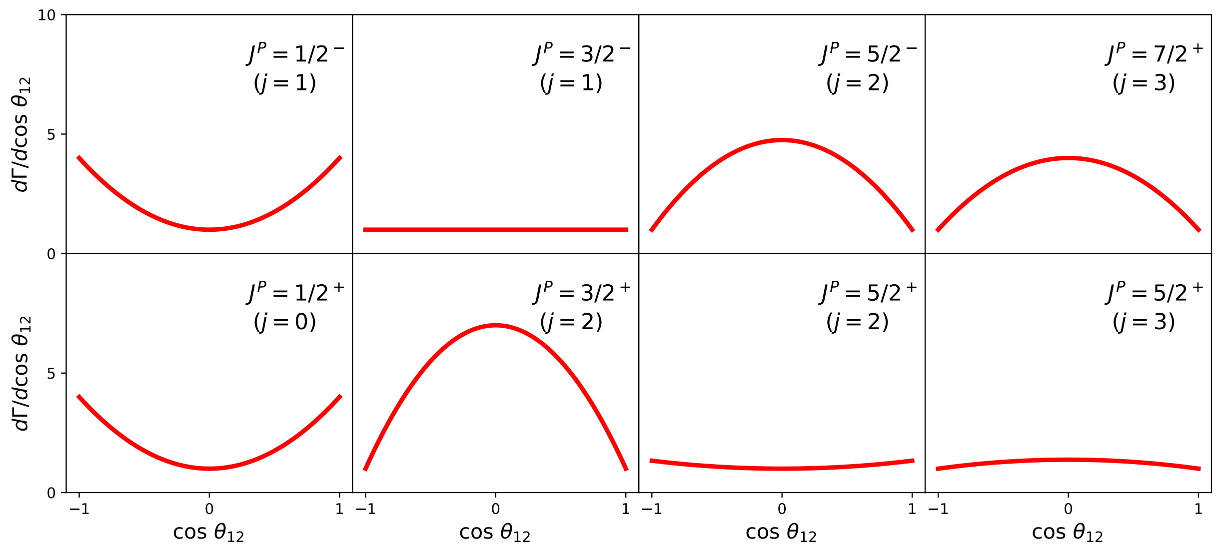

Figure 9.7. The angular correlations along the resonance band of Σ_c^* for various spin and parity assignments in an ideal situation.

the angular correlations $W(\theta_{12})$ are then summarized in Table 9.3 and depicted in Fig. 9.7.

By combining the analysis on its ratio and angular correlations, we can determine the spin and parity of $\Lambda_c^*(2765)$ unambiguously. For the case of $J^P = 1/2^\pm$, the main indication is that the angular correlation is proportional to $1 + 3\cos^2\theta_{12}$, shown as a valley structure. This is because the helicity amplitude with $h = 3/2$ is forbidden, resulting in the $\tilde{R}$ is equal to zero. To differentiate the parity, the ratio R will be useful because the negative parity the ratio becomes very small due to the d wave nature of $\Sigma_c^*\pi$ channel. The determination for other spin and parity can be discussed similarly. Furthermore, the comparison to other observables such as Dalitz plots and invariant mass distribution will give more convincing results.

9.4.2 Convoluted Dalitz plot

Now, we consider the mass distribution of $\Lambda_c^*(2765)$ where the width is around 50 MeV described in Fig. 9.3. Here, we give one example, namely for the case of $1/2^+$ with brown muck spin $j = 0$ to discuss the effect of the convolution of Dalitz plot. The mass distribution is assumed to have a Breit-Wigner form as

$$\tilde{\Gamma} = \frac{1}{N} \int \frac{\Gamma(\tilde{M}_{\Lambda_c^*})\, \mathrm{d}\tilde{M}_{\Lambda_c^*}}{(\tilde{M}_{\Lambda_c^*} - M_{\Lambda_c^*})^2 + \Gamma^2_{\Lambda_c^*}/4}, \tag{9.21}$$

where we define the wdith for a given intial mass as $\Gamma(\tilde{M}_{\Lambda_c^*})$. It can be imagined that we sum up all the Dalitz plot made by initial masses weighted by its mass distribution. The convolution is illustrated in Fig. 9.8 where we can see that the Dalitz plots with different sizes are summed up in one place (at

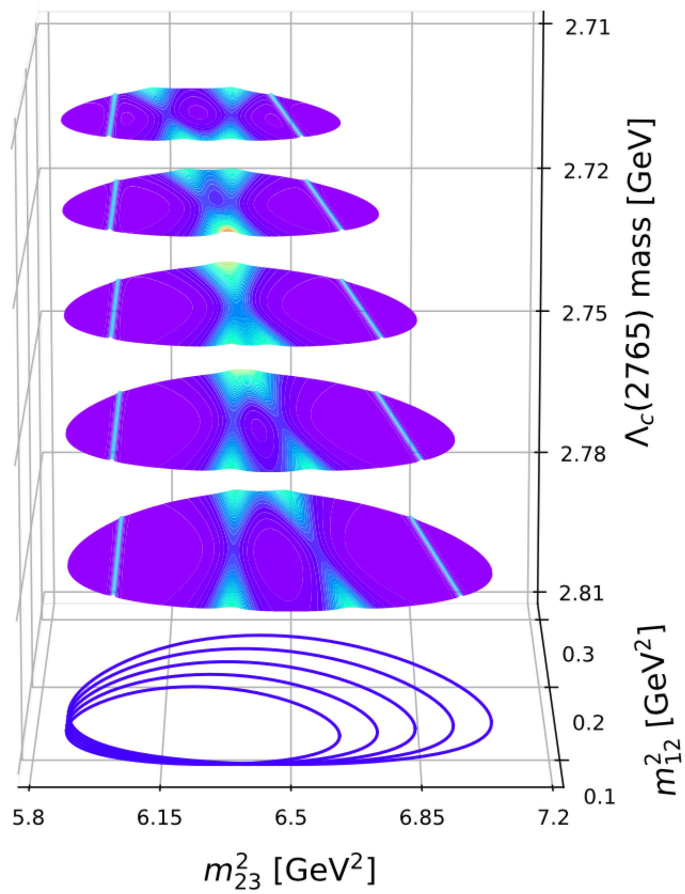

Figure 9.8. The convoluted Dalitz and invariant mass plots for $\Lambda_c^*(2765)$ with $J(j)^P = 1/2(0)^+$.

the bottom).

The resulting plots are given in Fig. 9.9. After the convolution, we first notice that the Dalitz plot has a larger area and the invariant mass distribution has a wider range. In the Dalitz plot in (m^2_{23}, m^2_{13}) plane, we can observe four different bands. However, it is also seen that along the Σ_c bands seem to have a hill structure. But, in reality, we know that the angular correlation along Σ_c is flat. This happens is due to the Dalitz plot is convoluted with the Breit-Wigner as a weight. Therefore, it is not appropriate to look at the angular correlation this way.

Another interesting thing is that the kinematical reflection spread out in the Dalitz plot in (m^2_{23}, m^2_{12}) plane. Moreover, the peak due to kinematical reflection disappears and it becomes a background shape distribution. This is one of the prominent effects of convolution. But, the ratio R between the Σ_c and Σ_c^* stays the same.

Because it is not so easy to see the angular correlation in the Dalitz plot, we also make another version of Dalitz plot which we call the square plot as shown on the right side in Fig. 9.9. In the case of $1/2^+$, we can see the angular correlation in the plot exhibits a valley structure on the Σ_c^* band,

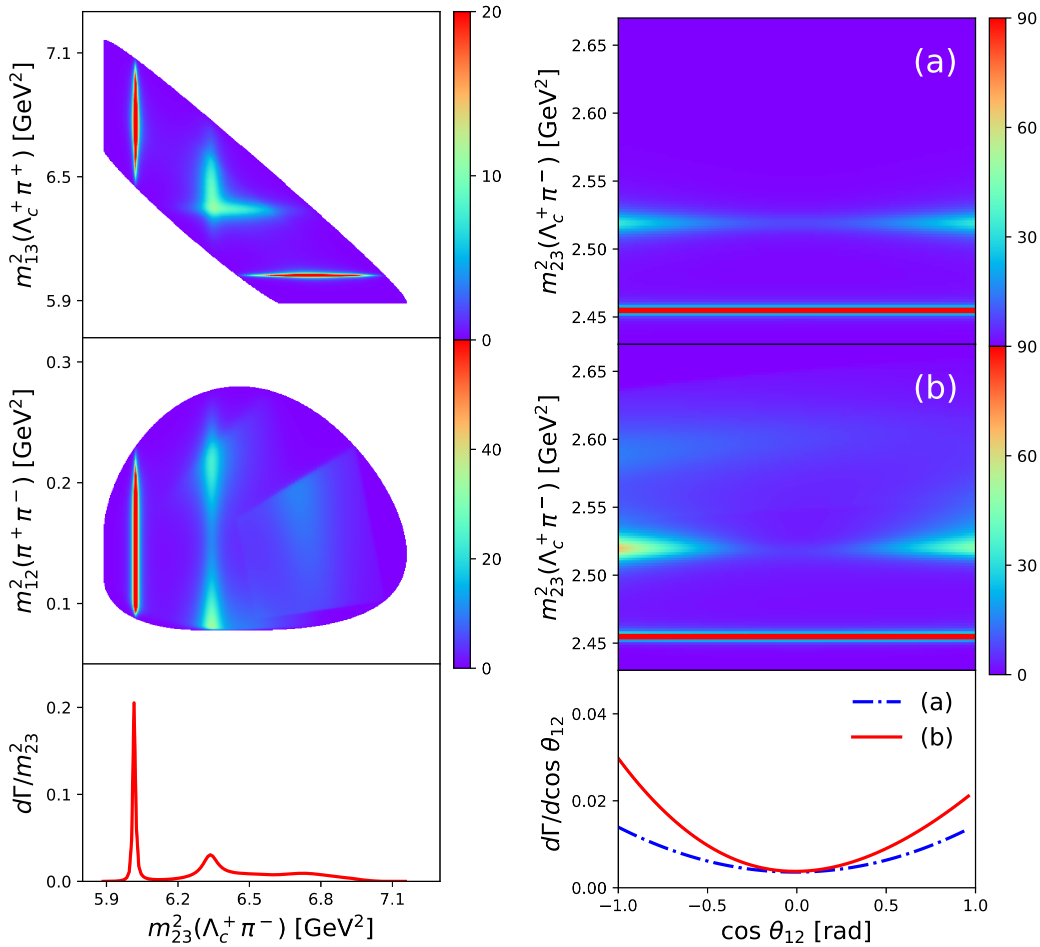

Figure 9.9. The convoluted Dalitz and invariant mass plots for $\Lambda_c^*(2765)$ with $J(j)^P = 1/2(0)^+$.

and it remains flat for Σ_c band. This behavior is similar to what we obtain in the narrow cut analysis. Note that the square plot can be produced by a similar way depicted in Fig. 9.8, but the Dalitz plot is transformed into the square plot at each initial mass such that they convolute in the same area.

Ideally, for the case of $1/2^+$, we should have $W(\theta_{12}) \propto 1 + 3\cos^2\theta_{12}$. However, in the reality, the fitted angular correlation is contaminated by the interference terms so that we obtain

$$W(\theta_{12}) \quad \propto \quad 1 + 6.0\cos^2\theta_{12} - 0.5\cos\theta_{12}. \tag{9.22}$$

where the is additional $\cos\theta_{12}$ term, leading to assymetry pattern. Even though it looks complicated, once we can parameterize the interference, we can still study the angular correlations.

9.5 Summary

In an attempt to determine the spin and parity of the $\Lambda_c^*(2765)$, we have done a comprehensive analysis of their two-body and three-body decay. It is found that the ratio R and angular correlations provide useful constraints for its spin and parity. In addition to that, the comparison of the Dalitz plot and invariant mass distribution will further confirm the result.

In this work, we have considered both negative and positive parity states up to $N = 2$ in the quark model. As for now, we can not conclude which configuration is compatible with the experimental data. On top of that, if $\Lambda_c^*(2765)$ is $1/2^+$ as suggested in many works, then its decay property can not be explained by the quark model. This implies that this state could be beyond the quark model states as discussed for other Roper-like resonances.

In this analysis, we have used the empirical fact that the direct process is suppressed. However, we know that $f_0(500)$ resonance can contribute to this decay. This is also an interesting observation because the suppression of such a process contradicts our expectations. Therefore, it should be clarified in future work.

We note that our results here as tabulated in Table 9.3 are rather universal, which can be applied to other cases with different systems. For instance, this method can also be used to determine the spin-parity of higher excited states of Λ_c. Also, the analysis of the decay of $\Xi_c^* \to \Xi_c \pi\pi$ and their analogs in the bottom sector can be done in principle. Moreover, we also notice that the treatment of the three-body decay of broad resonance is not well established. This issue is certainly important since the excited states usually have a finite width due to the nature of the strong decay. In this case, the development of such a method as done here could play a crucial role in advancing our knowledge in heavy-baryon spectroscopy.

"I never did anything by accident, nor did any of my inventions come by accident; they came by work.", Thomas Edison

Chapter 10
$\Lambda_b^*(6072)$ as a Roper-like resonance

10.1 Introduction

CMS and LHCb recently reported a new broad resonance of $\Lambda_b^*(6072)$ in $\Lambda_b\pi\pi$ invariant mass where its mass and width are measured to be $M = 6072.3 \pm 2.9$ MeV and $\Gamma = 72 \pm 11$ MeV [75, 76]. Because of its excitation energy around 500 MeV, it is tempting to identify them as the analog of Roper resonance $N(1440)$ with spin and parity $1/2^+$. In fact, there exist several Roper-like resonances with various flavor contents as shown in Fig. 10.1.

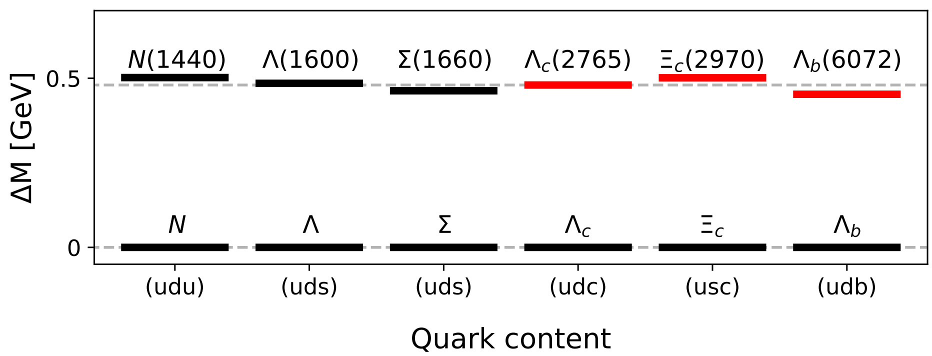

Figure 10.1. The Roper-like resonance candidates with various flavor contents. They have similar excitation energy of around 500 MeV. The red bars are the analog states in heavy baryon sector.

Roper resonance has a long history in hadron physics [217]. It was discovered around the 1970s, but its nature is still mysterious up to now. After tremendous efforts have been done both in the theoretical and experimental side, we are now convinced that it is a first radial excitation with $1/2^+$ [218]. One of the prominent problems is that the Roper resonance has an inverse mass ordering in which it appears lower than that of the negative parity excitation. This inverse mass ordering can not be explained by the simple quark model expectations. Because of that, many alternative ideas were constructed to elucidate such ordering [174].

Recently the analog states are also found in the heavy baryon sector. The most promising candidates are $\Lambda_c(2765), \Xi_c(2970)$, and the newly observed $\Lambda_b(6072)$. There are still other missing states which should be further investigated in future experiments. In fact, they have similarities in their decay properties: large decay width and small coupling to $f_0(500)$. Their width around 70 MeV is observed to be significantly larger than that of heavy baryons in general with only several MeV. Moreover, we also observe that the $f_0(500)$ resonance is surprisingly suppressed as found in our analysis on $\Lambda_c^*(2765)$ and further suggested in the present analysis. This rather peculiar behavior may reflect their internal structures which are independent of the flavor content.

10.2 Dalitz plot analysis

Inspired by our previous study on $\Lambda_c^*(2765)$, we will perform the three-body decay analysis of $\Lambda_b^*(6072)$ and discuss it as the Roper-like resonance with spin and parity $J^P = 1/2^+$. In fact, there are two possible brown muck spins either $j = 0$ and $j = 1$. As we may know, the first radial excitations correspond to $\Lambda_b^*(2S_{\lambda\lambda}, 1/2(0)^+)$ and $\Lambda_b^*(2S_{\rho\rho}, 1/2(0)^+)$ in the quark model. Therefore, we assume this resonance having $j = 0$, implying that $\Lambda_b^*(6072)$ will appear as a singlet without any HQS partner.

10.2.1 Decay amplitude

In this study, we also consider only the sequential processes coming from Σ_b and Σ_b^* in intermediate states. The direct process including the $f_0(500)$ resonance is not considered in this calculation because we will show later that the sequential process is sufficiently good to describe the decay property. Therefore, the direct process contribution is negligible. The Feynman diagrams considered in this work are shown in Fig. 10.2.

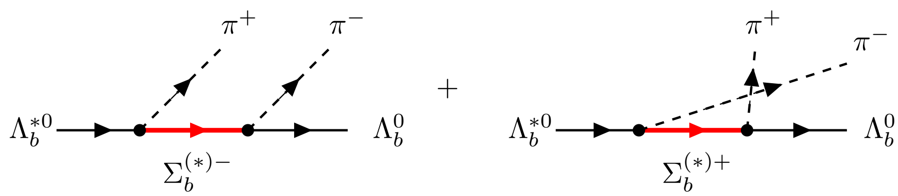

Figure 10.2. Feynman diagrams of $\Lambda_b^{*0} \to \Lambda_b^0\pi^+\pi^-$ with $\Sigma_b^{(*)-}$ and $\Sigma_b^{(*)+}$ in intermediate states.

Here, we also use the non-relativistic reduction as done in the previous chapters. For the case of $\Lambda_b(1/2^+)$, the two-body decay amplitudes for each vertex in the sequential processes going through Σ_b and $\Sigma_b^{;}$ are computed as

$$
\begin{aligned}
-i\mathcal{T}_{\Lambda_b^*\to\Sigma_b\pi} &= g_{1a}^p\ \chi^\dagger_{\Sigma_b}(\boldsymbol{\sigma}\cdot\mathbf{p})\chi_{\Lambda_b^*}, &(10.1)\\
-i\mathcal{T}_{\Lambda_b^*\to\Sigma_b^*\pi} &= g_{1b}^p\ \chi^\dagger_{\Sigma_b^*}(\mathbf{S}^\dagger\cdot\mathbf{p})\chi_{\Lambda_b^*}, &(10.2)\\
-i\mathcal{T}_{\Sigma_b\to\Lambda_b\pi} &= g_{2a}^p\ \chi^\dagger_{\Lambda_b}(\boldsymbol{\sigma}\cdot\mathbf{p})\,\chi_{\Sigma_b}, &(10.3)\\
-i\mathcal{T}_{\Sigma_b^*\to\Lambda_b\pi} &= g_{2b}^p\ \chi^\dagger_{\Lambda_b}(\mathbf{S}\cdot\mathbf{p})\,\chi_{\Sigma_b^*}. &(10.4)
\end{aligned}
$$

where all of the amplitudes is proportional to pion momentum due to the p-wave nature. Then, the three-body decay ampiltudes are then given by

$$
-i\mathcal{T}\left[\Sigma_b^-\right] = \left\langle -i\mathcal{T}_{\Sigma_b^-\to\Lambda_b^0\pi^-}\right\rangle \frac{i}{m_{23} - m_{\Sigma_b^-} + \frac{i}{2}\Gamma_{\Sigma_b^-}} \left\langle -i\mathcal{T}_{\Lambda_b^{*0}\to\Sigma_b^-\pi^+}\right\rangle \tag{10.5}
$$

The obtained amplitudes containing $\Sigma_b^{(*)-}$ and $\Sigma_b^{(*)+}$ are summed up coherently without any polarization.

10.2.2 Coupling strength and ratio

In this work, we do not compute the coupling strengths in the decay amplitudes from the quark model. Because it is demonstrated in the previous chapter that the quark model predicts a small width for the case of $1/2^+$. We have checked it for the case of $\Lambda_b^*(6072)$ that it is indeed the case, indicating that this resonance is not the quark model state.

Instead, we employ the heavy-quark symmetry to constraint the ratio between the coupling strengths in the amplitude as

$$g^p_{1b}/g^p_{1a} = \sqrt{2} \quad \text{for } j=0, \qquad \text{and} \qquad = \frac{1}{\sqrt{2}} \quad \text{for } j=1.) \tag{10.6}$$

Then, the ratio of decay into $\Sigma_c\pi$ and Σ_c^* is computed as

$$R = \frac{\Gamma(\Lambda_b^*(6072) \to \Sigma_b^*\pi)}{\Gamma(\Lambda_b^*(6072) \to \Sigma_b\pi)} = \frac{g^2_{1b}}{g^2_{1a}} \frac{p^{2L+1}(\Sigma_b^*\pi)}{p^{2L+1}(\Sigma_b\pi)}, \tag{10.7}$$

where it contains the phase space factor with $L = 1$ for p-wave decay. We obtain the ratio as

$$R = 1.43 \quad \text{for } j=0, \qquad \text{and} \qquad = 0.36 \quad \text{for } j=1. \tag{10.8}$$

Although the ratio R is not yet measured in the experiment, its value is reflected in the invariant mass distribution. For comparison with the experimental data, we adjust the coupling strengths with the constraints in Eq. (10.6) to reproduce the overall factor. Because the $\Sigma_b(1/2^+)$ and $\Sigma_b^*(3/2^+)$ can decay into $\Lambda_b\pi$, we can dicuss the ratio in the $\Lambda_b\pi$ invariant mass distribution. But, for the case of $\Xi_c^* \to \Xi_c\pi\pi$, the $\Xi_c'(1/2^+)$ can not decay into $\Xi_c\pi$ as shown in Fig. 10.3. In this situation, we cannot discuss the ratio R through the $\Xi_c\pi$ invariant mass distribution because only $\Xi_c^*(3/2^+)$ is observed.

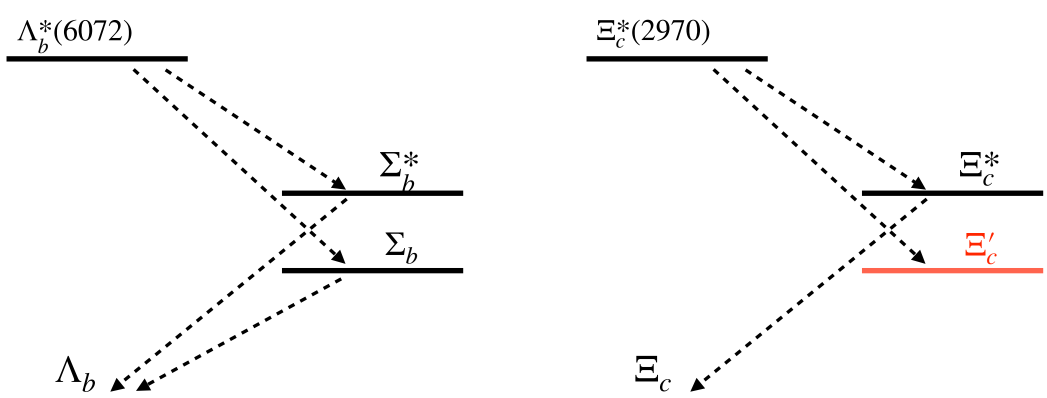

Figure 10.3. The sequential process of Λ_b^* and Ξ_c^*. The Ξ_c' state can not decay into $\Xi_c\pi$ due to insufficient phase space represented by the red bar.

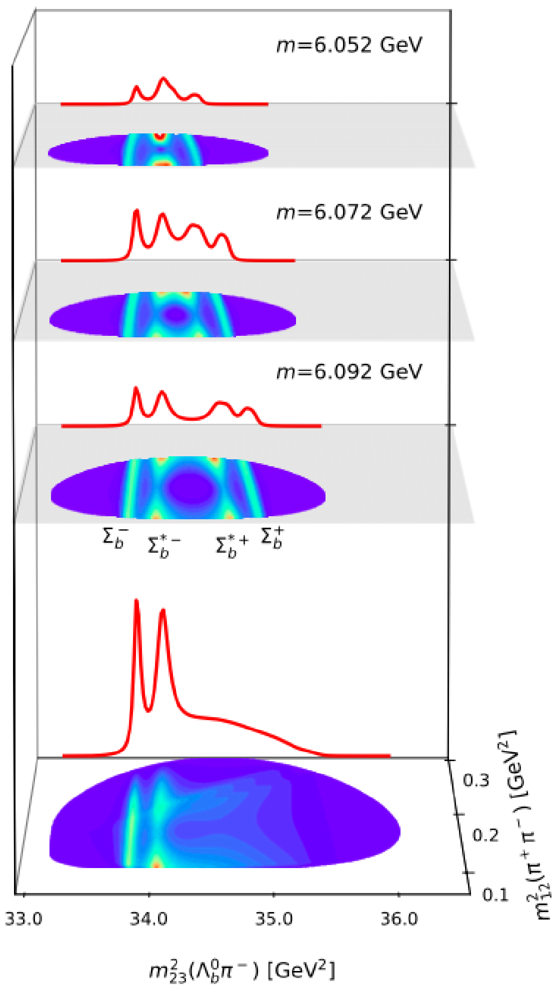

Figure 10.4. The Dalitz plots of $\Lambda_b^*(6072) \to \Lambda_b\pi\pi$ in (m_{12}^2, m_{23}^2) plane. The upper three plots are made by fixed initial masses and the bottom one is the convoluted Dalitz plot.

10.2.3 Dalitz plot and related observables

In order to consider all of the signals of $\Lambda_b^*(6072)$ resonance measured in the experiments, we will perfom a convolution of the Dalitz plots with a Breit-wigner distribution as

$$P(m_{12}^2, m_{23}^2) = \frac{1}{N}\int \frac{P(m; m_{12}^2, m_{23}^2)\ \mathrm{d}m}{(m - M_{\Lambda_b^*})^2 + \Gamma^2_{\Lambda_b^*}/4}, \tag{10.9}$$

with N as a normalization factor. In addition to that, we provide several plots made by a fixed initial mass to show the illustration of how the convoluted Dalitz plot is obtained. In this calculation, we assume its spin and parity $1/2^+$ with $j = 0$, which is the most probable one.

The resulting Dalitz plots are described in Fig. 10.4 where the convoluted one is presented at the bottom level. The Dalitz plots with fixed initial masses at $M = 6.052$, 6072, and 6092 MeV are plotted at the first three layer from the top. We also plot the $\Lambda_b\pi^-$ invariant mass distributions at the back fact for each Dalitz plot. For the Dalitz plots with fixed initial mass, there are four resonance bands as indicated in the figure, but the Σ_c^* resonances with different charges merge at $M = 6052$ MeV. Furthermore, in the convoluted Dalitz plot, only two resonance bands are observed. The kinematical reflections spread out in the Dalitz plot and appear as a background shape.

Now let us compare our result to the experimental data from LHCb collaboration. The only provided data is the invariant mass distribution of $\Lambda_b\pi^\pm$. This is slightly different from the one in Fig. 10.4 at the bottom back face where only $\Lambda_b\pi^-$ invariant mass distribution is shown. To compare with the data, one needs to combine between $\Lambda_b\pi^-$ and $\Lambda_b\pi^+$ invariant mass distribution as demonstrated in Fig. 10.5. We can see that the distribution is well reproduced, indicating that the spin and parity of $1/2(0)^+$ is preferable. It is seen the ratio R between Σ_b and Σ_b^* is roughly equal to unity since where their peaks appear at a similar height. Furthermore, the background shape is mainly originated from the kinematical reflections. This finding suggests that the contribution of the $f_0(500)$ resonance is insignificant. Therefore, the decay is dominated by the $\Sigma_b^{(*)}$ resonant contribution. Note that the $\Sigma_b^{(*)-}$ and $\Sigma_b^{(*)+}$ peaks in $\Lambda_b\pi^-$ and $\Lambda_b\pi^+$ invarant mass distribution, respectively, have different masses

$$m(\Sigma_b^+) - m(\Sigma_b^-) = -5.06 \pm 0.18 \text{ MeV}, \tag{10.10}$$
$$m(\Sigma_b^{*+}) - m(\Sigma_b^{*-}) = -4.37 \pm 0.33 \text{ MeV}, \tag{10.11}$$

as we can see that their peaks are slightly off to each other.

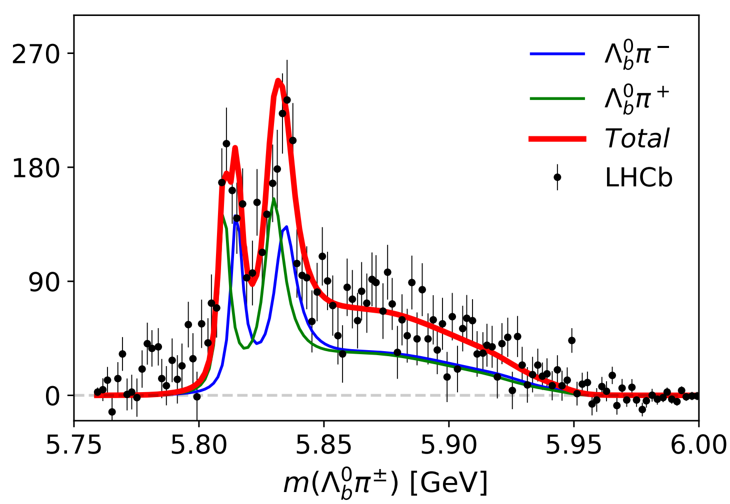

Figure 10.5. The comparison with the experimental data of the $\Lambda_b\pi^\pm$ invariant mass distribution. Our prediction is indicated by the red line. The $\Lambda_b\pi^+$ and $\Lambda_b\pi^-$ components are also shown.

Angular correlation

To measure the spin of the $\Lambda_b^*(6072)$ more seriously, one needs to measure the angular correlation along the Σ_b^* band. Naively, the angular correlation is destroyed or highly contaminated for the case of broad resonance. However, we show that the angular correlation is still reliable for spin determination. The square plot we obtain in this calculation is given in Fig. 10.6 where the angular correlation is shown on the back face.

Let me repeat that the valley structure in the angular correlation is a strong indication that the $\Lambda_b^*(6072)$ has spin 1/2. In general, the angular correlation in this three-body decay is given by

$$W(\theta_{12}) \propto \left|A_{1/2}(\Lambda_b^* \to \Sigma_b^*\pi)\right|^2 \times (1 + 3\cos^2\theta_{12}) + \left|A_{3/2}(\Lambda_b^* \to \Sigma_b^*\pi)\right|^2 \times 3\sin^2\theta_{12}. \tag{10.12}$$

But, for the case of spin 1/2, the amplitude with helicity $h = 3/2$ is forbidden such that the angular correlation will be proportional to $1 + 3\cos^2\theta_{12}$. In actual cases, the interference effect should be considered. We find that the angular correlation is not strongly modified as seen in Fig. 10.6 and is given by

$$W(\theta_{12}) \quad \propto \quad 1 + 3.3\cos^2\theta_{12}. \tag{10.13}$$

If it is indeed the case, $\Lambda_b^*(6072)$ is strongly suggested to have the spin and parity $J^P = 1/2^+$. This measurement of angular correlation can be done with the present experimental data by LHCb. We also note that other spin and parity assignments. But, their possibilities can be ruled out if the angular correlation and $\Lambda_b\pi^\pm$ invariant mass distribution are analyzed simultaneously. Lastly, after the spin and parity of $\Lambda_b^*(6072)$ has been determined, we have still many questions related to their nature and dynamics. The study with an emphasis on its internal structure should be pursued in future works.

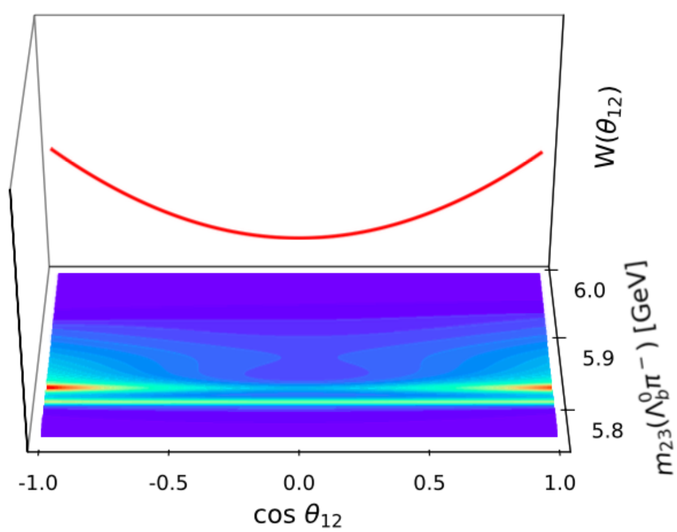

Figure 10.6. The square plot and the angular correlation along the Σ_b^* band for $\Lambda_b^*(6072)$ decay.

10.3 Perspectives

In this chapter, we have discussed the possibility of $\Lambda_b^*(6072)$ as a Roper-like resonance with spin and parity $J^P = 1/2^+$. Other candidates with various flavor contents are shown in Fig. 10.1. However, there are still missing states such as Ξ_b and Ξ resonances, which can be searched in the current experimental facilities such as LHCb, J-Parc, and Belle. Finding and analyzing the candidates of Roper-like resonance are crucial things to do. Then, establishing the similarities among them may be useful for the discussion of their internal structures. So far, the thorough discussions have been done theoretically and experimentally but only limited to the nucleon sector. The extension of such studies for the heavy baryon sector will not only confirm the finding in the nucleon sector, but also show how the observables are transformed with the change of the flavor contents.

For the missing Roper-like resonances in heavy baryon sector, the three-body invariant masses will be helpful since they favor three-body decays. For instance, the $\Xi_c^*(2970)$ is found to decay into $\Xi_c\pi\pi$. Its two-body decay such as $\Lambda_c K$ is forbidden due to the brown-muck selection rule, $0^+ \to 0^+ + 0^-$. In fact, there are several Ξ_c states in $\Lambda_c K$ with the mass similar with $\Xi_c^*(2970)$, but they may not correspond to the Roper-like resonance. Also with the same reason, the missing Ξ_b resonance could be found in $\Xi_b\pi\pi$ invariant mass with similar excitation energy.

Furthermore, it is also meaningful to revisit the light baryon sectors such as $N(1440)$ and $\Lambda(1600)$ to analyze their three-body decays. We also note that their decay widths are also larges among other light baryons and the coupling to $f_0(500)$ resonance is negligible. The other overlooked structures may be unveiled when revisiting their three-body decays more seriously. Actually, we also notice that the $\Xi^*(1820)$ is found in $\Xi\pi\pi$ and ΛK invariant mass at similar energy. It is conjectured that this situation is similar to Ξ_c case where they correspond to different particles. As we know the Xi and Xi' are difficult to distinguish.

Lastly, the unusual behavior of Roper-like resonances can provide an interesting place to understand the hadron resonances in QCD.

"The most beautiful experience we can have is the mysterious.", Albert Einstein

Part IV

Summary and outlook

Chapter 11
Closing remark

11.1 Dalitz plot analysis

In this dissertation, we have investigated three-body decays of heavy baryons for the study of their internal structures. In doing that, we have computed various Dalitz plots along with their related quantities such as the invariant mass distributions and angular correlations. It is shown that we can discuss not only the internal structures as done for $\Lambda_c^*(2595)$ and $\Lambda_c^*(2625)$, but also the spin and parity of the participating particles such as $\Lambda_c^*(2765)$ and $\Lambda_b^*(6072)$.

The Dalitz plot analysis could be one of the powerful tools for heavy hadrons spectroscopy since the scattering process is not practically possible. In this study, we have developed the Dalitz plot based on the effective Lagrangians in a non-relativistic frameworks with isobar models. We found that it is efficient and sufficiently good in describing the three-body decays of the heavy baryons. If we want to do more comprehensively, we should consider the dynamical model to include the coupled channel effects. On top of that, we also discuss the effect of the finite width has been overlooked so far. It is demonstrated that the convolution of the Dalitz plot is necessary for the case of the broad resonances such as $\Lambda_c^*(2765)$ and $\Lambda_b^*(6072)$ because the convoluted Dalitz plot will have slightly different shape and structure. In the future, the parameterization of the three-body decay will be of importance in extracting the resonance information. So far, it has been continuously developed by several groups around the globe. Finding an efficient and effective way is the essential key for future analysis.

Furthermore, this theoretical work is closely related to the experiment. Thus, the communication between theories and experiments in this field is very crucial. In the theoretical side, we should continuously develop our model and propose interesting things to measure for experimentalists. Currently, there are several experimental facilities that are actively reporting discoveries on heavy flavored hadrons. In addition to that, the upgrades of experimental facilities are also being planned. Nowadays, there is a plenty of data available and their potential has not been completely unleashed. Therefore, the study of heavy baryons has a good prospect for the coming decades.

11.2 Baryon with various flavor contents

In this work, we have analyzed the two-pion emission decays of the low-lying Λ_c and Λ_b baryons. This work can be considered as the first step toward the establishment of the heavy baryons studied from the three-body decays. In fact, there are still many states which are not considered in the present calculation as shown in Fig. 2.3. It is instructive to apply our methods to other excited states of heavy baryons to discuss their structures.

For the low-lying Λ_c^* with negative parity, they are found to be compatible with the quark model expectation. In our analysis, the decay properties of $\Lambda_c^*(2595)$ and $\Lambda_c^*(2625)$ can be explained by the quark model with the λ mode excitation as anticipated. However, it is known that the $\Lambda(1405)$ which is the analogous state of $\Lambda_c^*(2595)$ in the strangeness sector could correspond to the exotic state which is beyond the quark model. The different behavior may correspond to the flavor dependent dynamics in which we know that they are related to the orbital excitation. Also, it could be due to the dynamics that originated from the nearby threshold.

On the other hand, $\Lambda_c^*(2765)$ and $\Lambda_b^*(6072)$ have very similar behaviors. In this study, we have shown that they are most probably related to the Roper-like resonances with spin and parity $J^P = 1/2^+$. They share not only similar excitation energy but also decay property, indicating the flavor independent nature. It is also understood that the Roper resonance $N(1440)$ is not compatible with the quark model. We further confirm this fact from the analysis of its analog states in heavy baryons whose decay properties can not be explained by the quark model.

There is also another issue in the higher excited state of $\Lambda_c^*(2860), \Lambda_c^*(2880)$ and $\Lambda_c^*(2940)$. The problem of the identification of D-wave doublet seems to be puzzling. So far, two-body decay and mass spectrum analyses have been done in various models for these states, but it is fair to say that the puzzle is not resolved yet. Therefore, the three-body decay analysis can provide another constraint to solve this puzzle. The analog states in Ξ_c^*, Ξ_b^*, and Λ_b^* states should be also investigated.

In summary, the study of the baryon in various flavor content may also provide interesting pictures of the flavor dependent and independent dynamics. This sort of study may deepen our understanding in the dynamics of hadron resonances.

"Physics is not about how the world is, it is about what we can say about the world.", Neils Bohr

Appendix A
Quark model computations

A.1 Jacoobi coordinate

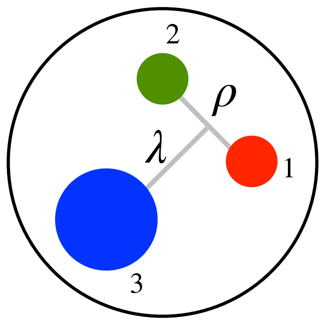

Figure A.1. Definitions of Jacoobi coordinate for three quarks inside baryon.

In the quark model calculation, there are several definitions of Jacoobi coordinates. In this work, we define them as

$$\vec{X} = \frac{1}{2m+M}\left(m\vec{r}_1 + m\vec{r}_2 + M\vec{r}_3\right), \tag{A.1}$$

$$\vec{\lambda} = \frac{1}{2}\left(\vec{r}_1 + \vec{r}_2\right) - \vec{r}_3, \tag{A.2}$$

$$\vec{\rho} = \vec{r}_1 - \vec{r}_2, \tag{A.3}$$

and the position coordinates of each particles are given by

$$\vec{r}_1 = \vec{X} + \frac{M}{2m+M}\vec{\lambda} + \frac{1}{2}\vec{\rho}, \tag{A.4}$$

$$\vec{r}_2 = \vec{X} + \frac{M}{2m+M}\vec{\lambda} - \frac{1}{2}\vec{\rho}, \tag{A.5}$$

$$\vec{r}_3 = \vec{X} - \frac{M}{2m+M}\vec{\lambda}. \tag{A.6}$$

The separation between the center of mass motion $\vec{X}$ and relative coordinates $\vec{\lambda}$ and $\vec{\rho}$ is crucial in the quark model computation. The center of mass motion is related to the translation of the baryon and is not related to the excitation of its internal structure. In heavy baryons, the excitations of the λ and ρ mode are treated exclusively because of the difference on their excitation energy.

A.2 Radial wave function

In the quark model, the harmonic potential is usually used as because the solutions are analitically known. The solution for is given by

$$\psi_{nlm}(\vec{r}) = R_{nl}(r)\ Y_{lm}(\hat{r}), \tag{A.7}$$

where it consists of radial wave function $R_{nl}(r)$ and spherical harmonics $Y_{lm}(\hat{r})$. The radial wave function can be calculated as

$$R_{nl}(r) = N_{nl}\ r^l\ \exp(-a^2r^2/2)\ L_n^{(l+1/2)}(a^2r^2), \tag{A.8}$$

with the normalization

$$N_{nl} = \sqrt{\frac{a^3a^{2l}}{2\sqrt{\pi}}\frac{2^{n+l+3}n!}{(2n+2l+1)!!}}, \tag{A.9}$$

and the generalized Laguerre polynomial

$$L_n^{(z)}(x) = \frac{x^{-z}e^x}{n!}\frac{d^n}{dx^n}\left(e^{-x}x^{n+z}\right). \tag{A.10}$$

We have denoted $a = \sqrt{\mu\omega}$ as a pontential strength. The single and double factorial are different. The double factorial is calculated for example as

$$\begin{aligned} 3!! &= 3\times 1 \qquad \text{(odd)}, && \text{(A.11)}\\ 4!! &= 4\times 2 \qquad \text{(even)}. && \text{(A.12)} \end{aligned}$$

The resulting radial wave function up to $N = 2$ is given by

$$\begin{aligned} R_{00}(r) &= \frac{2\alpha^{3/2}}{\pi^{1/4}}e^{-\alpha^2r^2/2}, && \text{(A.13)}\\ R_{01}(r) &= \left(\frac{8}{3}\right)^{1/2}\frac{\alpha^{5/2}}{\pi^{1/4}}r\ e^{-\alpha^2r^2/2}, && \text{(A.14)}\\ R_{02}(r) &= \left(\frac{16}{15}\right)^{1/2}\frac{\alpha^{7/2}}{\pi^{1/4}}r^2\ e^{-\alpha^2r^2/2}, && \text{(A.15)}\\ R_{10}(r) &= \frac{\sqrt{6}\alpha^{7/2}}{\pi^{1/4}}\left(\frac{2}{3}\alpha^2r^2\right)e^{-\alpha^2r^2/2}. && \text{(A.16)} \end{aligned}$$

The higher excitation can be calculated by using Eq. (A.8). The spherical harmonics are discussed in Appendix B.

A.3 Wave function in the quark model

Here, we only discuss the wave function of Λ_c and Σ_c up to $N = 2$ in the quark model. Other heavy baryons with different flavor can be computed similarly. Moreover, the z component of the heavy baryon spin can have either positive and negative sign. Here, we focus on the positive sign which is sufficient for the actual computation. We use the notation $Y_c(nL_\zeta, J(j)^P, m)$ for the quark model configuration, the definition of which is defined in the main text. Note that the isospin wave function is denoted by ϕ_{Λ_c} and ϕ_{Σ_c}.

The coupling between two angular momenta are given by

$$Y_{lm} = \sum_{m_1} \langle l_1\ l_2\ m_1\ m - m_1 | l_1\ l_2\ l\ m\rangle\, Y_{l_1 m_1} Y_{l_2 (m-m_1)}, \tag{A.17}$$

where $m = m_1 + m_2$ and Clebsh-Gordon coefficient $\langle l_1\ l_2\ m_1\ m - m_1 | l_1\ l_2\ l\ m\rangle$. For instance, we couple the first excited state with $l = 1$ and spin-1/2,

$$\begin{aligned} [\psi_{01}, \chi_c]^{1/2}_{1/2} &= \langle 1\ 1\ 1/2\ -1/2|\ 1/2\ 1/2\rangle\, \psi_{011}\downarrow_c + \langle 1\ 0\ 1/2\ 1/2|\ 1/2\ 1/2\rangle\, \psi_{010}\uparrow_c, \\ &= \sqrt{\frac{2}{3}}\psi_{011}\downarrow_c - \sqrt{\frac{1}{3}}\psi_{010}\uparrow_c, \end{aligned} \tag{A.18}$$

In this section, the wave function is obtained by the above algebra.

A.3.1 Ground states

Λ_c baryon

The ground state is given by

$$\begin{aligned} \Lambda_c(1S, 1/2(0)^+, 1/2) &= \left[\left[\psi_{00}(\vec{\lambda})\psi_{00}(\vec{\rho}), d^0\right]^0, \chi_c\right]^{1/2}_{1/2} \phi_{\Lambda_c}, \\ &= \frac{1}{\sqrt{2}}(\uparrow\downarrow - \downarrow\uparrow)\uparrow_c \psi_{000}(\vec{\lambda})\psi_{000}(\vec{\rho})\ \phi_{\Lambda_c}. \end{aligned} \tag{A.19}$$

Since the brown muck spin is $j = 0$, the ground state appears as an HQS singlet.

Σ_c baryon

For Σ_c, there are two ground states due to $j = 1$. The first one with spin-parity $J^P = 1/2^+$ is expressed by

$$\begin{aligned} \Sigma_c(1S, 1/2(1)^+, 1/2) &= \left[\left[\psi_{00}(\vec{\lambda})\psi_{00}(\vec{\rho}), d^1\right]^1, \chi_c\right]^{1/2}_{m} \phi_{\Sigma_c}, \\ &= \frac{1}{\sqrt{6}}\{2\uparrow\uparrow\downarrow_c - (\uparrow\downarrow + \downarrow\uparrow)\uparrow_c\}\,\psi_{000}(\vec{\lambda})\psi_{000}(\vec{\rho})\ \phi_{\Sigma_c}, \end{aligned} \tag{A.20}$$

while the second one with $J^P = 3/2^+$ is written as

$$\begin{aligned}
\Sigma_c^*(1S, 3/2(1)^+, 3/2) &= \left[\left[\psi_{00}(\vec{\lambda})\psi_{00}(\vec{\rho}), d^1\right]^1, \chi_c\right]^{3/2}_{3/2} \phi_{\Sigma_c}, \\
&= \uparrow\uparrow\uparrow_c \psi_{000}(\vec{\lambda})\psi_{000}(\vec{\rho})\ \phi_{\Sigma_c}, \qquad (A.21) \\
\Sigma_c^*(1S, 3/2(1)^+, 1/2) &= \frac{1}{\sqrt{3}} \{\uparrow\uparrow\downarrow_c + (\uparrow\downarrow + \downarrow\uparrow)\uparrow_c\} \psi_{000}(\vec{\lambda})\psi_{000}(\vec{\rho})\ \phi_{\Sigma_c}. \qquad (A.22)
\end{aligned}$$

A.3.2 Negative parity states

Λ_c^* baryon with λ mode

For Λ_c baryon, there are two states with λ-mode, thye are given by

$$\begin{aligned}
\Lambda_c^*(1P_\lambda, 1/2(1)^-, 1/2) &= \left[\left[\psi_{01}(\vec{\lambda})\psi_{00}(\vec{\rho}), d^0\right]^1, \chi_c\right]^{1/2}_{1/2} \phi_{\Lambda_c}, \\
&= \frac{1}{\sqrt{6}} \left\{\sqrt{2}(\uparrow\downarrow - \downarrow\uparrow)\downarrow_c \psi_{011}(\vec{\lambda}) - (\uparrow\downarrow - \downarrow\uparrow)\uparrow_c \psi_{010}(\vec{\lambda})\right\} \psi_{000}(\vec{\rho})\phi_{\Lambda_c}, \ (A.23)
\end{aligned}$$

and

$$\begin{aligned}
\Lambda_c^*(1P_\lambda, 3/2(1)^-, 3/2) &= \left[\left[\psi_{01}(\vec{\lambda})\psi_{00}(\vec{\rho}), d^0\right]^1, \chi_c\right]^{3/2}_{m} \phi_{\Lambda_c}, \\
&= \frac{1}{\sqrt{2}}(\uparrow\downarrow - \downarrow\uparrow)\uparrow_c \psi_{011}(\vec{\lambda})\psi_{000}(\vec{\rho})\phi_{\Lambda_c} \qquad (A.24) \\
\Lambda_c^*(1P_\lambda, 3/2(1)^-, 1/2) &= \frac{1}{\sqrt{6}} \left\{(\uparrow\downarrow - \downarrow\uparrow)\downarrow_c \psi_{011}(\vec{\lambda}) + \sqrt{2}(\uparrow\downarrow - \downarrow\uparrow)\uparrow_c \psi_{010}(\vec{\lambda})\right\} \psi_{000}(\vec{\rho})\phi_{\Lambda_c}, \ (A.25)
\end{aligned}$$

Λ_c^* baryon with ρ mode

The ρ-mode excitation is written as,

$$\Lambda_c^*(1P_\rho, J(j)^P, m) = \left[\left[\psi_{00}(\vec{\lambda})\psi_{01}(\vec{\rho}), d^1\right]^j, \chi_c\right]^J_m \phi_{\Lambda_c} \qquad (A.26)$$

where the brown muck spin can be $j = 0, 1$, or 2.

For $j = 0$, the wave function is given by

$$\Lambda_c^*(1P_\rho, 1/2(0)^-, 1/2) = \frac{\psi_{000}(\vec{\lambda})}{\sqrt{3}} \left\{\downarrow\downarrow\uparrow_c \psi_{011}(\vec{\rho}) - \frac{1}{\sqrt{2}}(\uparrow\downarrow + \downarrow\uparrow)\uparrow_c \psi_{010}(\vec{\rho}) + \uparrow\uparrow\uparrow_c \psi_{01-1}(\vec{\rho})\right\} \phi_{\Lambda_c}, \qquad (A.27)$$

For $j=1$, we have two states with $J^P = 1/2^-$ and $3/2^-$. The wave functions are given by

$$\Lambda_c^*(1P_\rho, 1/2(1)^-, 1/2) = \frac{1}{\sqrt{6}}\Big\{[(\uparrow\downarrow + \downarrow\uparrow)\downarrow_c - \downarrow\downarrow\uparrow_c]\,\psi_{011}(\vec{\rho}) - \sqrt{2}\uparrow\uparrow\downarrow_c \psi_{10}(\vec{\rho}) + \uparrow\uparrow\uparrow_c \psi_{01-1}(\vec{\rho})\Big\} \times\psi_{000}(\vec{\lambda})\ \phi_{\Lambda_c}, \tag{A.28}$$

and

$$\Lambda_c^*(1P_\rho, 3/2(1)^-, 3/2) = \frac{1}{2}\Big((\uparrow\downarrow + \downarrow\uparrow)\uparrow_c \psi_{011}(\vec{\rho}) - \sqrt{2}\uparrow\uparrow\uparrow_c \psi_{010}(\vec{\rho})\Big)\psi_{000}(\vec{\lambda})\phi_{\Lambda_c}, \tag{A.29}$$

$$\Lambda_c^*(1P_\rho, 3/2(1)^-, 1/2) = \frac{1}{\sqrt{6}}\left\{\frac{1}{\sqrt{2}}[(\uparrow\downarrow + \downarrow\uparrow)\downarrow_c + 2\downarrow\downarrow\uparrow_c]\,\psi_{011}(\vec{\rho}) - \uparrow\uparrow\downarrow_c \psi_{010}(\vec{\rho}) - \sqrt{2}\psi_{01-1}(\vec{\rho})\uparrow\uparrow\uparrow_c\right\} \times\psi_{000}(\vec{\lambda})\ \phi_{\Lambda_c} \tag{A.30}$$

For $j=2$, we have $J^P = 3/2^-$ or $5/2^-$. They are given by

$$\Lambda_c^*(1P_\rho, 3/2(2)^-, 3/2) = \frac{1}{\sqrt{5}}\left\{\frac{1}{2}[4\uparrow\uparrow\downarrow_c - (\uparrow\downarrow + \downarrow\uparrow)\uparrow_c]\,\psi_{011}(\vec{\rho}) - \frac{1}{\sqrt{2}}\uparrow\uparrow\uparrow_c \psi_{010}(\vec{\rho})\right\}\psi_{000}(\vec{\lambda})\ \phi_{\Lambda_c} \tag{A.31}$$

$$\Lambda_c^*(1P_\rho, 3/2(2)^-, 1/2) = \frac{1}{\sqrt{5}}\left\{\frac{\psi_{011}(\vec{\rho})}{2\sqrt{3}}[3(\uparrow\downarrow + \downarrow\uparrow)\downarrow_c - 2\downarrow\downarrow\uparrow_c] - \frac{\psi_{010}(\vec{\rho})}{\sqrt{6}}[2(\uparrow\downarrow + \downarrow\uparrow)\uparrow_c - 3\uparrow\uparrow\downarrow_c] - \frac{1}{\sqrt{3}}\psi_{01-1}(\vec{\rho})\uparrow\uparrow\uparrow_c\right\}\psi_{000}(\vec{\lambda})\ \phi_{\Lambda_c} \tag{A.32}$$

and for spin $5/2^-$,the wave function is expressed by

$$\Lambda_c^*(1P_\rho, 5/2(2)^-, 5/2) = \psi_{000}(\vec{\lambda})\psi_{011}(\vec{\rho})\uparrow\uparrow\uparrow_c\ \ \phi_{\Lambda_c} \tag{A.33}$$

$$\Lambda_c^*(1P_\rho, 5/2(2)^-, 3/2) = \frac{1}{\sqrt{5}}\Big\{[(\uparrow\downarrow + \downarrow\uparrow)\uparrow_c + \uparrow\uparrow\downarrow_c]\psi_{011}(\vec{\rho}) + \sqrt{2}\uparrow\uparrow\uparrow_c \psi_{010}(\vec{\rho})\Big\}\psi_{000}(\vec{\lambda})\ \phi_{\Lambda_c} \tag{A.34}$$

$$\Lambda_c^*(1P_\rho, 5/2(2)^-, 1/2) = \frac{1}{\sqrt{5}}\left\{\frac{1}{\sqrt{2}}[(\uparrow\downarrow + \downarrow\uparrow)\downarrow_c + \downarrow\downarrow\uparrow_c]\,\psi_{011}(\vec{\rho}) + [(\uparrow\downarrow + \downarrow\uparrow)\uparrow_c + \uparrow\uparrow\downarrow_c]\psi_{010}(\vec{\rho}) + \frac{1}{\sqrt{2}}\psi_{01-1}(\vec{\rho})\uparrow\uparrow\uparrow_c\right\}\psi_{000}(\vec{\lambda})\ \phi_{\Lambda_c} \tag{A.35}$$

The other wave functions can be calculated similarly by using Eq. (A.17).

A.4 Amplitude calculation

Here we provide some examples for the calculation of the decay amplitude in the quark model. The amplitude is calculated in the helicity basis which is divided into two parts: non-derivative and derivative part:

$$A_h = A_h^{\nabla\cdot\sigma} + A_h^{q\cdot\sigma}. \tag{A.36}$$

Each part is given by

$$\begin{aligned} A_h^{q\cdot\sigma} &= -G\frac{I_{q\cdot\sigma}}{m}\int d^3\lambda \int d^3\rho \; e^{-i\vec{q}_\lambda\cdot\vec{\lambda}} e^{-i\vec{q}_\rho\cdot\vec{\rho}} \left\langle B_i \left| \vec{\tau}_1 \;\; \{\vec{\sigma}_1\cdot\vec{q}\} \right| B_f \right\rangle, & \text{(A.37)} \\ A_h^{\nabla\cdot\sigma} &= -iG\frac{\omega_\pi}{m}\int d^3\lambda \int d^3\rho \; e^{-i\vec{q}_\lambda\cdot\vec{\lambda}} e^{-i\vec{q}_\rho\cdot\vec{\rho}} \left\langle B_i \left| \vec{\tau}_1 \;\; \left\{(\vec{\nabla}_\lambda + 2\vec{\nabla}_\rho)\cdot\vec{\sigma}\right\} \right| B_f \right\rangle. & \text{(A.38)} \end{aligned}$$

where we define the kinematical quantities as

$$\begin{aligned} G &= \frac{g_A^q}{2f_\pi}\sqrt{2M_{\Lambda_c}}\sqrt{2M_{\Sigma_c}}, & \text{(A.39)} \\ I_{q\cdot\sigma} &= \frac{M}{2m+M}\omega_\pi - 2m, & \text{(A.40)} \\ I_{\nabla\cdot\sigma} &= \frac{1}{2}q_\lambda + q_\rho, & \text{(A.41)} \end{aligned}$$

A.4.1 $\Sigma_c^{(*)} \to \Lambda_c\pi$ decay

We start our calculation from non-derivative part. More explicitly, it reads

$$A_h^{q\cdot\sigma} = -G\frac{I_{q\cdot\sigma}}{m}\int d^3\lambda \int d^3\rho \; e^{-i\vec{q}_\lambda\cdot\vec{\lambda}} e^{-i\vec{q}_\rho\cdot\vec{\rho}} \left\langle D_c^0 \left| \vec{\tau}_1 \right| D_c^1 \right\rangle \left\langle \Lambda_c(1/2^+) \left| \vec{\sigma}_1\cdot\vec{q} \right| \Sigma_c(1/2^+) \right\rangle. \tag{A.42}$$

The index one in τ_1 means it operate to first quark state. Assuming $\vec{q} = q\hat{z}$, then the values of the Isospin factors $\langle \Lambda_c(1/2^+) \left| \vec{\sigma}_{1z} \; q \right| \Sigma_c(1/2^+) \rangle$ are

$$\begin{aligned} \left\langle D_c^0 \left| \vec{\tau}_1 \right| D_c^{11} \right\rangle &= -1, & \text{(A.43)} \\ \left\langle D_c^0 \left| \vec{\tau}_1 \right| D_c^{10} \right\rangle &= 1, & \text{(A.44)} \\ \left\langle D_c^0 \left| \vec{\tau}_1 \right| D_c^{1-1} \right\rangle &= -1. & \text{(A.45)} \end{aligned}$$

If we choose the Σ_c^+ state, the decay amplitude reads

$$A_h^{q\cdot\sigma} = G\frac{q}{m}I_{q\cdot\sigma}\int d^3\lambda \int d^3\rho \; e^{-i\vec{q}_\lambda\cdot\vec{\lambda}} e^{-i\vec{q}_\rho\cdot\vec{\rho}} \left\langle \Lambda_c(1/2^+) \left| \sigma_{1z} \right| \Sigma_c(1/2^+) \right\rangle. \tag{A.46}$$

The spin and orbital factor in the equation above is computed as

$$\begin{aligned} \left\langle \Lambda_c(1/2^+) \left| \sigma_{1+} \right| \Sigma_c(1/2^+) \right\rangle &= 0, &\text{(A.47)}\\ \left\langle \Lambda_c(1/2^+) \left| \sigma_{1-} \right| \Sigma_c(1/2^+) \right\rangle &= 0, &\text{(A.48)}\\ \left\langle \Lambda_c(1/2^+) \left| \sigma_{1z} \right| \Sigma_c(1/2^+) \right\rangle &= -\frac{1}{\sqrt{3}} \psi_0(\lambda)\psi_0(\rho). &\text{(A.49)} \end{aligned}$$

By inserting those factors into the decay width, we get

$$\begin{aligned} A_h^{q\cdot\sigma} &= G\frac{q}{m} I_{q\cdot\sigma} \left(-\frac{1}{\sqrt{3}}\right) \left(\int d^3\lambda e^{-i\vec{q}_\lambda\cdot\vec{\lambda}} \psi_0^*(\lambda)\psi_0(\lambda)\right) \left(\int d^3\rho\ e^{-i\vec{q}_\rho\cdot\vec{\rho}} \psi_0^*(\rho)\psi_0(\rho)\right), \\ &= G\frac{q}{m} I_{q\cdot\sigma} \left(-\frac{1}{\sqrt{3}}\right) e^{-\frac{q_\lambda^2}{4a_\lambda^2}} e^{-\frac{q_\rho^2}{4a_\rho^2}}, \\ &= \left(-\frac{1}{\sqrt{3}}\right) G\frac{q}{m} I_{q\cdot\sigma} F(q). \end{aligned} \tag{A.50}$$

Let us recall that the derivative part of the decay amplitude is written as

$$A_h^{\nabla\cdot\sigma} = iG\frac{\omega_\pi}{m} \int d^3\lambda \int d^3\rho\ e^{-i\vec{q}_\lambda\cdot\vec{\lambda}} e^{-i\vec{q}_\rho\cdot\vec{\rho}} \left\langle \Lambda_c(1/2^+) \left| (\vec{\nabla}_\lambda + 2\vec{\nabla}_\rho)\cdot\vec{\sigma} \right| \Sigma_c(1/2^+) \right\rangle. \tag{A.51}$$

Before stepping further, we need to work out the derivative piece acting on the wave function as follow

$$\begin{aligned} \vec{\nabla}_\lambda \psi_0^*(\lambda) &= \vec{\nabla}_\lambda \left(R_{00}^*(\lambda) Y_{00}^*(\hat{\lambda}) \right) \\ &= \hat{\lambda} \left(\frac{\partial}{\partial\lambda} R_{00}(\lambda) \right) Y_{00}(\hat{\lambda}) \\ &= \hat{\lambda} \left(\frac{a_\lambda^{3/2}}{\pi^{1/4}} 2(-a_\lambda^2) e^{-a_\lambda^2\lambda^2/2} \right) \frac{1}{\sqrt{4\pi}} \\ &= \hat{\lambda} \left(-2a_\lambda \left(\frac{3}{8}\right)^{1/2} R_{01}^*(\lambda) \right) \frac{1}{\sqrt{4\pi}} \end{aligned} \tag{A.52}$$

Then, the product of $\hat{\lambda}$ and spin operator σ is given by

$$\begin{aligned}
\hat{\lambda}\cdot\vec{\sigma} &= \hat{\lambda}_x\cdot\sigma_x+\hat{\lambda}_y\cdot\sigma_y+\hat{\lambda}_z\cdot\sigma_z,\\
&= \frac{1}{\sqrt{2}}(\hat{\lambda}_x+i\hat{\lambda}_y)\sigma_- + \frac{1}{\sqrt{2}}(\hat{\lambda}_x-i\hat{\lambda}_y)\sigma_+ + \hat{\lambda}_z\cdot\sigma_z,\\
&= \frac{1}{\sqrt{2}}(\sin\theta\cos\phi+i\sin\theta\sin\phi)\sigma_- + \frac{1}{\sqrt{2}}(\sin\theta\cos\phi-i\sin\theta\sin\phi)\sigma_+ + \cos\theta\ \sigma_z,\\
&= \frac{1}{\sqrt{2}}\sin\theta\ e^{i\phi}\sigma_- + \frac{1}{\sqrt{2}}\sin\theta\ e^{-i\phi}\sigma_+ + \cos\theta\ \sigma_z,\\
&= \sqrt{\frac{4\pi}{3}}\left(Y^*_{1-1}(\hat{\lambda})\sigma_- - Y^*_{11}(\hat{\lambda})\sigma_+ + Y^*_{10}(\hat{\lambda})\sigma_z\right). \qquad \text{(A.53)}
\end{aligned}$$

The product is now expressed by the spherical harmonics Y_{lm}. Then, in total we can write

$$\vec{\nabla}_\lambda\psi^*_0(\lambda)\cdot\vec{\sigma} = -\frac{a_\lambda}{\sqrt{2}}R^*_{01}(\lambda)\left(Y^*_{1-1}(\hat{\lambda})\sigma_- - Y^*_{11}(\hat{\lambda})\sigma_+ + Y^*_{10}(\hat{\lambda})\sigma_z\right). \qquad \text{(A.54)}$$

Therefore, the matrix elements become

$$\left\langle \Lambda_c(1/2^+)\left|\vec{\nabla}_\lambda\cdot\vec{\sigma}\right|\Sigma_c(1/2^+)\right\rangle = -\frac{a_\lambda}{\sqrt{2}}\left(-\frac{1}{\sqrt{3}}\right)R^*_{01}(\lambda)Y^*_{10}(\hat{\lambda})\psi_0(\lambda)\psi^*_0(\rho)\psi_0(\rho). \qquad \text{(A.55)}$$

In order to simplify the calculation, we divide the derivative part into two λ and ρ piece. The λ piece reads

$$\begin{aligned}
A_h^{\nabla_\lambda\cdot\sigma} &= iG\frac{\omega_\pi}{m}\left(-\frac{1}{\sqrt{3}}\right)\left(\int d^3\rho\ \psi^*_0(\rho)\psi_0(\rho)e^{-i\vec{q}_\rho\cdot\vec{\rho}}\right)\left(\frac{a_\lambda}{\sqrt{2}}\int d^3\lambda R^*_{01}(\lambda)Y^*_{10}(\hat{\lambda})\psi_0(\lambda)e^{-i\vec{q}_\lambda\cdot\vec{\lambda}}\right),\\
&= iG\frac{\omega_\pi}{m}\left(-\frac{1}{\sqrt{3}}\right)\left(e^{-\frac{q_\rho^2}{4a_\rho^2}}\right)\left(i\frac{q_\lambda}{2}e^{-\frac{q_\lambda^2}{4a_\lambda^2}}\right),\\
&= -G\frac{\omega_\pi}{m}\left(-\frac{1}{\sqrt{3}}\right)\frac{q_\lambda}{2}F(q). \qquad \text{(A.56)}
\end{aligned}$$

whereas the ρ piece is given by

$$A_h^{\nabla_\rho\cdot\sigma} = -G\frac{\omega_\pi}{m}\left(-\frac{1}{\sqrt{3}}\right)q_\rho F(q). \qquad \text{(A.57)}$$

Thus, the derivative part of the decay amplitude is now written as

$$A_h^{\nabla\cdot\sigma} = -G\frac{\omega_\pi}{m}\left(-\frac{1}{\sqrt{3}}\right)I_{\nabla\cdot\sigma}F(q). \qquad \text{(A.58)}$$

For the decay of $\Sigma_c^*(3/2^-)$, it differ only by the spin factor. The corresponding amplitude is given by

$$A_h^{q\cdot\sigma} = -G\frac{\omega_\pi}{m}\left(\sqrt{\frac{2}{3}}\right) I_{q\cdot\sigma}F(q), \tag{A.59}$$

$$A_h^{\nabla\cdot\sigma} = -G\frac{q}{m}\left(\sqrt{\frac{2}{3}}\right) I_{\nabla\cdot\sigma}F(q). \tag{A.60}$$

A.4.2 $\Lambda_c^*(1P_\lambda, 1/2(1)^-) \to \Sigma_c\pi$ decay

We begin the calculation by calculating the spin-orbital factor for corresponding assignment. They are given by

$$\left\langle \Sigma_c(1/2^+)\left|\sigma_z\right|\Lambda_c(1/2^-)\right\rangle = \left(\frac{1}{3}\right)\psi_0^*(\lambda)\psi_{10}(\lambda)\psi_0^*(\rho)\psi_0(\rho), \tag{A.61}$$

$$\left\langle \Sigma_c(1/2^+)\left|\sigma_+\right|\Lambda_c(1/2^-)\right\rangle = \left(-\frac{2}{3}\right)\psi_0^*(\lambda)\psi_{11}(\lambda)\psi_0^*(\rho)\psi_0(\rho), \tag{A.62}$$

$$\left\langle \Sigma_c(1/2^+)\left|\sigma_-\right|\Lambda_c(1/2^-)\right\rangle = 0. \tag{A.63}$$

Decay amplitude of non-derivative part is calculated by assuming that momentum of pion is along z direction. Then, it is written as

$$A_h^{q\cdot\sigma} = -G\frac{q}{m}I_{q\cdot\sigma}\int d^3\lambda\int d^3\rho\; e^{-i\vec{q}_\lambda\cdot\vec{\lambda}}e^{-i\vec{q}_\rho\cdot\vec{\rho}}\left\langle \Sigma_c(1/2^+)\left|\sigma_z\right|\Lambda_c(1/2^-)\right\rangle. \tag{A.64}$$

Inserting the spin-orbital factor into the decay amplitude, we find

$$\begin{aligned} A_h^{q\cdot\sigma} &= -G\frac{q}{m}I_{q\cdot\sigma}\left(\frac{1}{3}\right)\left(\int d^3\lambda e^{-i\vec{q}_\lambda\cdot\vec{\lambda}}\psi_0^*(\lambda)\psi_{10}(\lambda)\right)\left(\int d^3\rho\; e^{-i\vec{q}_\rho\cdot\vec{\rho}}\psi_0^*(\rho)\psi_0(\rho)\right), \\ &= -G\frac{q}{m}I_{q\cdot\sigma}\left(\frac{1}{3}\right)\left(e^{-\frac{q_\rho^2}{4a_\rho^2}}\right)\left(-i\frac{q_\lambda}{\sqrt{2}a_\lambda}e^{-\frac{q_\lambda^2}{4a_\lambda^2}}\right), \\ &= iG\frac{q}{m}I_{q\cdot\sigma}\left(\frac{1}{3}\right)\frac{q_\lambda}{\sqrt{2}a_\lambda}F(q). \end{aligned} \tag{A.65}$$

We write the decay amplitude of derivative part as

$$A_h^{\nabla\cdot\sigma} = -iG\frac{\omega_\pi}{m}\int d^3\lambda\int d^3\rho\; e^{-i\vec{q}_\lambda\cdot\vec{\lambda}}e^{-i\vec{q}_\rho\cdot\vec{\rho}}\left\langle \Sigma_c(1/2^+)\left|(\vec{\nabla}_\lambda + 2\vec{\nabla}_\rho)\cdot\vec{\sigma}\right|\Lambda_c(1/2^-)\right\rangle. \tag{A.66}$$

The λ piece is computed as

$$
\begin{aligned}
A_h^{\nabla_\lambda\cdot\sigma} &= -iG\frac{\omega_\pi}{m}\int d^3\lambda\int d^3\rho\; e^{-i\vec{q}_\lambda\cdot\vec{\lambda}}e^{-i\vec{q}_\rho\cdot\vec{\rho}}\left\langle\Sigma_c(1/2^+)\left|\vec{\nabla}_\lambda\cdot\vec{\sigma}\right|\Lambda_c(1/2^-)\right\rangle,\\
&= -iG\frac{\omega_\pi}{m}\int d^3\lambda\int d^3\rho\; e^{-i\vec{q}_\lambda\cdot\vec{\lambda}}e^{-i\vec{q}_\rho\cdot\vec{\rho}}\left(-\frac{a_\lambda}{\sqrt{2}}R^*_{01}(\lambda)\right)\\
&\quad\times\left(Y^*_{1-1}(\lambda)\left\langle\sigma_-\right\rangle - Y^*_{11}(\lambda)\left\langle\sigma_+\right\rangle + Y^*_{10}(\lambda)\left\langle\sigma_z\right\rangle\right)\psi_{1m}(\lambda)\psi^*_0(\rho)\psi_0(\rho),\\
&= iG\frac{\omega_\pi}{m}\left\{\left(\frac{a_\lambda}{\sqrt{2}}\right)\int d^3\lambda e^{-i\vec{q}_\lambda\cdot\vec{\lambda}}\left[\left(\frac{2}{3}\right)\psi^*_{11}(\lambda)+\left(\frac{1}{3}\right)\psi^*_{10}(\lambda)\right]\psi_{1m}(\lambda)\right\}\\
&\quad\times\left\{\int d^3\rho\; e^{-i\vec{q}_\rho\cdot\vec{\rho}}\psi^*_0(\rho)\psi_0(\rho)\right\},\\
&= iG\frac{\omega_\pi}{m}\left(e^{-\frac{q_\rho^2}{4a_\rho^2}}\right)\left(\frac{a_\lambda}{\sqrt{2}}\right)\left\{\int d^3\lambda e^{-i\vec{q}_\lambda\cdot\vec{\lambda}}\left[\left(\frac{2}{3}\right)\psi^*_{11}(\lambda)\psi_{11}(\lambda)+\left(\frac{1}{3}\right)\psi^*_{10}(\lambda)\psi_{10}(\lambda)\right]\right\},\\
&= iG\frac{\omega_\pi}{m}\left(e^{-\frac{q_\rho^2}{4a_\rho^2}}\right)\left(\frac{a_\lambda}{\sqrt{2}}\right)\left(\frac{1}{6a_\lambda^2}(6a_\lambda^2-q_\lambda^2)e^{-\frac{q_\lambda^2}{4a_\lambda^2}}\right),\\
&= iG\frac{\omega_\pi}{m}\frac{1}{6\sqrt{2}a_\lambda}(6a_\lambda^2-q_\lambda^2)F(q). \qquad \text{(A.67)}
\end{aligned}
$$

Meanwhile, ρ piece reads

$$
\begin{aligned}
A_h^{\nabla_\rho\cdot\sigma} &= -iG\frac{\omega_\pi}{m}\int d^3\lambda\int d^3\rho\; e^{-i\vec{q}_\lambda\cdot\vec{\lambda}}e^{-i\vec{q}_\rho\cdot\vec{\rho}}\left\langle\Sigma_c(1/2^+)\left|2\vec{\nabla}_\rho\cdot\vec{\sigma}\right|\Lambda_c(1/2^-)\right\rangle,\\
&= -2iG\frac{\omega_\pi}{m}\int d^3\lambda\int d^3\rho\; e^{-i\vec{q}_\lambda\cdot\vec{\lambda}}e^{-i\vec{q}_\rho\cdot\vec{\rho}}\left(-\frac{a_\rho}{\sqrt{2}}\right)\psi^*_0(\lambda)\psi_1(\lambda)\psi_0(\rho)\\
&\quad\times\left(\psi^*_{1-1}(\rho)\left\langle\sigma_-\right\rangle - \psi^*_{11}(\rho)\left\langle\sigma_+\right\rangle + \psi^*_{10}(\rho)\left\langle\sigma_z\right\rangle\right),\\
&= 2iG\frac{\omega_\pi}{m}\left\{\left(\frac{a_\rho}{\sqrt{2}}\right)\int d^3\lambda e^{-i\vec{q}_\lambda\cdot\vec{\lambda}}\int d^3\rho\; e^{-i\vec{q}_\rho\cdot\vec{\rho}}\psi^*_0(\lambda)\psi_0(\rho)\right.\\
&\quad\left.\times\left[\left(\frac{2}{3}\right)\psi^*_{11}(\rho)\psi_{11}(\lambda)+\left(\frac{1}{3}\right)\psi^*_{10}(\rho)\psi_{10}(\lambda)\right]\right\},\\
&= 2iG\frac{\omega_\pi}{m}\left(\frac{a_\rho}{3\sqrt{2}}\right)\left\{\int d^3\lambda e^{-i\vec{q}_\lambda\cdot\vec{\lambda}}\psi^*_0(\lambda)\psi_{10}(\lambda)\right\}\left\{\int d^3\rho\; e^{-i\vec{q}_\rho\cdot\vec{\rho}}\psi^*_{10}(\rho)\psi_0(\rho)\right\},\\
&= iG\frac{\omega_\pi}{m}\left(\frac{a_\rho}{3\sqrt{2}}\right)\left(-i\frac{q_\lambda}{\sqrt{2}a_\lambda}e^{-\frac{q_\rho^2}{4a_\rho^2}}\right)\left(-i\frac{q_\rho}{\sqrt{2}a_\rho}e^{-\frac{q_\rho^2}{4a_\rho^2}}\right),\\
&= -iG\frac{\omega_\pi}{m}\frac{1}{3\sqrt{2}a_\lambda}(q_\lambda q_\rho)F(q). \qquad \text{(A.68)}
\end{aligned}
$$

Thus, In total the decay amplitude of derivative part is written as

$$\begin{aligned} A_h^{\nabla\cdot\sigma} &= A_h^{\nabla_\lambda\cdot\sigma} + A_h^{\nabla_\rho\cdot\sigma}, \\ &= -iG\frac{\omega_\pi}{m}\left\{\left(-\frac{1}{\sqrt{2}}\right)a_\lambda + \left(\frac{1}{3}\right)I_{\nabla\cdot\sigma}\frac{q_\lambda}{\sqrt{2}a_\lambda}\right\}F(q). \end{aligned} \tag{A.69}$$

A.4.3 $\Lambda_c^*(1P_\rho, 1/2(1)^-) \to \Sigma_c\pi$ decay

For this assignment, the spin-orbital factors associated to the decay amplitude are given by

$$\left\langle \Sigma_c(1/2^+)\left|\sigma_z\right|\Lambda_c(1/2^-)\right\rangle = \left(-\frac{\sqrt{2}}{3}\right)\psi_0^*(\lambda)\psi_{10}(\lambda)\psi_0^*(\rho)\psi_0(\rho), \tag{A.70}$$

$$\left\langle \Sigma_c(1/2^+)\left|\sigma_+\right|\Lambda_c(1/2^-)\right\rangle = \left(\frac{\sqrt{2}}{2}\right)\psi_0^*(\lambda)\psi_{11}(\lambda)\psi_0^*(\rho)\psi_0(\rho), \tag{A.71}$$

$$\left\langle \Sigma_c(1/2^+)\left|\sigma_-\right|\Lambda_c(1/2^-)\right\rangle = \left(-\frac{\sqrt{2}}{6}\right)\psi_0^*(\lambda)\psi_{1-1}(\lambda)\psi_0^*(\rho)\psi_0(\rho). \tag{A.72}$$

The decay amplitude of non-derivative part is written as

$$A_h^{q\cdot\sigma} = -G\frac{q}{m}I_{q\cdot\sigma}\int d^3\lambda\int d^3\rho\ e^{-i\vec{q}_\lambda\cdot\vec{\lambda}}e^{-i\vec{q}_\rho\cdot\vec{\rho}}\left\langle \Sigma_c(1/2^+)\left|\sigma_z\right|\Lambda_c(1/2^-)\right\rangle. \tag{A.73}$$

We insert the spin-orbital factors to the equation above, and we obtain

$$\begin{aligned} A_h^{q\cdot\sigma} &= -G\frac{q}{m}I_{q\cdot\sigma}\left(-\frac{\sqrt{2}}{3}\right)\left(\int d^3\lambda e^{-i\vec{q}_\lambda\cdot\vec{\lambda}}\psi_0^*(\lambda)\psi_0(\lambda)\right)\left(\int d^3\rho\ e^{-i\vec{q}_\rho\cdot\vec{\rho}}\psi_0^*(\rho)\psi_{10}(\rho)\right), \\ &= -G\frac{q}{m}I_{q\cdot\sigma}\left(-\frac{\sqrt{2}}{3}\right)\left(-i\frac{q_\rho}{\sqrt{2}a_\rho}e^{-\frac{q_\rho^2}{4a_\rho^2}}\right)\left(e^{-\frac{q_\lambda^2}{4a_\lambda^2}}\right), \\ &= iG\frac{q}{m}I_{q\cdot\sigma}\left(\frac{-\sqrt{2}}{3}\right)\frac{q_\rho}{\sqrt{2}a_\rho}F(q). \end{aligned} \tag{A.74}$$

The decay amplitude of derivative part is

$$A_h^{\nabla\cdot\sigma} = -iG\frac{\omega_\pi}{m}\int d^3\lambda\int d^3\rho\ e^{-i\vec{q}_\lambda\cdot\vec{\lambda}}e^{-i\vec{q}_\rho\cdot\vec{\rho}}\left\langle \Sigma_c(1/2^+)\left|(\vec{\nabla}_\lambda + 2\vec{\nabla}_\rho)\cdot\vec{\sigma}\right|\Lambda_c(1/2^-)\right\rangle \tag{A.75}$$

where the λ piece is computed by

$$
\begin{aligned}
A_h^{\nabla_\lambda\cdot\sigma} &= -iG\frac{\omega_\pi}{m}\int d^3\lambda\int d^3\rho\; e^{-i\vec{q}_\lambda\cdot\vec{\lambda}}e^{-i\vec{q}_\rho\cdot\vec{\rho}}\left\langle\Sigma_c(1/2^+)\left|\vec{\nabla}_\lambda\cdot\vec{\sigma}\right|\Lambda_c(1/2^-)\right\rangle,\\
&= -iG\frac{\omega_\pi}{m}\int d^3\lambda\int d^3\rho\; e^{-i\vec{q}_\lambda\cdot\vec{\lambda}}e^{-i\vec{q}_\rho\cdot\vec{\rho}}\left(-\frac{a_\lambda}{\sqrt{2}}\right)\psi_0(\lambda)\psi_0^*(\rho)\psi_{1m}(\rho)\\
&\quad\times\Big(\psi_{1-1}^*(\lambda)\left\langle\sigma_-\right\rangle-\psi_{11}^*(\lambda)\left\langle\sigma_+\right\rangle+\psi_{10}^*(\lambda)\left\langle\sigma_z\right\rangle\Big),\\
&= iG\frac{\omega_\pi}{m}\left(\frac{a_\lambda}{\sqrt{2}}\right)\int d^3\lambda e^{-i\vec{q}_\lambda\cdot\vec{\lambda}}\int d^3\rho\; e^{-i\vec{q}_\rho\cdot\vec{\rho}}\psi_0(\lambda)\psi_0^*(\rho)\\
&\quad\times\left[\left(-\frac{\sqrt{2}}{6}\right)\psi_{1-1}(\rho)\psi_{1-1}^*(\lambda)-\left(\frac{\sqrt{2}}{2}\right)\psi_{11}(\rho)\psi_{11}^*(\lambda)+\left(-\frac{\sqrt{2}}{3}\right)\psi_{10}(\rho)\psi_{10}^*(\lambda)\right],\\
&= iG\frac{\omega_\pi}{m}\left(\frac{a_\lambda}{\sqrt{2}}\right)\left(-\frac{\sqrt{2}}{3}\right)\left\{\int d^3\lambda e^{-i\vec{q}_\lambda\cdot\vec{\lambda}}\psi_0^*(\lambda)\psi_{10}(\lambda)\right\}\left\{\int d^3\rho\; e^{-i\vec{q}_\rho\cdot\vec{\rho}}\psi_{10}(\rho)\psi_0^*(\rho)\right\},\\
&= iG\frac{\omega_\pi}{m}\left(-\frac{a_\lambda}{3}\right)\left(-i\frac{q_\lambda}{\sqrt{2}a_\lambda}e^{-\frac{q_\rho^2}{4a_\rho^2}}\right)\left(-i\frac{q_\rho}{\sqrt{2}a_\rho}e^{-\frac{q_\rho^2}{4a_\rho^2}}\right),\\
&= iG\frac{\omega_\pi}{m}\frac{1}{6a_\rho}(q_\lambda q_\rho)F(q).
\end{aligned}
\tag{A.76}
$$

and the ρ piece is calculated as follow

$$
\begin{aligned}
A_h^{\nabla_\rho\cdot\sigma} &= -iG\frac{\omega_\pi}{m}\int d^3\lambda\int d^3\rho\; e^{-i\vec{q}_\lambda\cdot\vec{\lambda}}e^{-i\vec{q}_\rho\cdot\vec{\rho}}\left\langle\Sigma_c(1/2^+)\left|2\vec{\nabla}_\rho\cdot\vec{\sigma}\right|\Lambda_c(1/2^-)\right\rangle,\\
&= -2iG\frac{\omega_\pi}{m}\int d^3\lambda\int d^3\rho\; e^{-i\vec{q}_\lambda\cdot\vec{\lambda}}e^{-i\vec{q}_\rho\cdot\vec{\rho}}\left(-\frac{a_\rho}{\sqrt{2}}\right)\psi_0(\lambda)\psi_0^*(\lambda)\psi_{1m}(\rho)\\
&\quad\times\Big(\psi_{1-1}^*(\rho)\left\langle\sigma_-\right\rangle-\psi_{11}^*(\rho)\left\langle\sigma_+\right\rangle+\psi_{10}^*(\rho)\left\langle\sigma_z\right\rangle\Big),\\
&= -2iG\frac{\omega_\pi}{m}\left\{\left(\frac{a_\rho}{\sqrt{2}}\right)\int d^3\rho e^{-i\vec{q}_\rho\cdot\vec{\rho}}\left[\left(-\frac{\sqrt{2}}{6}\right)\psi_{11}^*(\rho)-\left(\frac{\sqrt{2}}{2}\right)\psi_{11}^*(\rho)\right.\right.\\
&\quad\left.\left.+\left(-\frac{\sqrt{2}}{3}\right)\psi_{10}^*(\rho)\right]\psi_{1m}(\rho)\right\}\left\{\int d^3\lambda\; e^{-i\vec{q}_\lambda\cdot\vec{\lambda}}\psi_0^*(\lambda)\psi_0(\lambda)\right\},\\
&= 2iG\frac{\omega_\pi}{m}\left(e^{-\frac{q_\lambda^2}{4a_\lambda^2}}\right)\left(\left(-a_\rho+\frac{q_\rho^2}{6a_\rho}\right)e^{-\frac{q_\rho^2}{4a_\rho^2}}\right),\\
&= 2iG\frac{\omega_\pi}{m}\left(-a_\rho+\frac{q_\rho^2}{6a_\rho}\right)F(q).
\end{aligned}
\tag{A.77}
$$

Therefore, in total the decay amplitude of derivative part is given by

$$\begin{aligned} A_h^{\nabla\cdot\sigma} &= A_h^{\nabla_\lambda\cdot\sigma} + A_h^{\nabla_\rho\cdot\sigma}, \\ &= -iG\frac{\omega_\pi}{m}\left\{2a_\rho + \left(-\frac{\sqrt{2}}{3}\right) I_{\nabla\cdot\sigma}\frac{q_\rho}{\sqrt{2}a_\rho}\right\}F(q). \end{aligned} \tag{A.78}$$

The other amplitudes can be computed similarly by the procedures shown above.

A.5 Concrete form of decay amplitudes

In this section, we will provide decay amplitudes for the Λ_c and Σ_c baryons in the quark model. We will sandwich the amplitude in Eq. (4.63) by various heavy baryon wavefunctions. The resulting amplitudes are given in the helicity basis. Here, we calculate the amplitude for the charmed baryons. The amplitude for bottom baryons have the same amplitude structures, only the parameters are different.

To simplify the notations, we define the normalization factor as

$$G = \frac{g_A^q}{2f_\pi}\sqrt{2M_{\Lambda_c}}\sqrt{2M_{\Sigma_c}} \tag{A.79}$$

and the Gaussian form factor as

$$F(q) = \exp(-q_\lambda^2/4a_\lambda^2)\,\exp(-q_\rho^2/4a_\rho^2) \tag{A.80}$$

where $q = |\vec{q}|$ is the pion momentum. We also define some quantities as following

$$C_1 = G\left[2 + \frac{\omega_\pi}{2m}\left(1 - \frac{M}{2m+M}\right)\right]F(p), \tag{A.81}$$

$$C_0^\lambda = iG\frac{\omega_\pi}{m}a_\lambda F(p), \tag{A.82}$$

$$C_0^\rho = iG\frac{\omega_\pi}{m}a_\rho F(p), \tag{A.83}$$

$$C_2^\lambda = \frac{iGM}{a_\lambda(2m+M)}\left[2 + \frac{\omega_\pi}{2m}\left(1 - \frac{M}{2m+M}\right)\right]F(p), \tag{A.84}$$

$$C_2^\rho = \frac{iG}{2a_\rho}\left[2 + \frac{\omega_\pi}{2m}\left(1 - \frac{M}{2m+M}\right)\right]F(p), \tag{A.85}$$

$$C_1^{\lambda\lambda} = G\frac{\omega_\pi}{m}\left(\frac{M}{2m+M}\right)F(p), \tag{A.86}$$

$$C_1^{\rho\rho} = G\frac{\omega_\pi}{2m}F(p), \tag{A.87}$$

$$C_3^{\lambda\lambda} = \frac{GM^2}{a_\lambda^2(2m+M)^2}\left[2 + \frac{\omega_\pi}{2m}\left(1 - \frac{M}{2m+M}\right)\right]F(p), \tag{A.88}$$

$$C_3^{\rho\rho} = \frac{G}{4a_\rho^2}\left[2 + \frac{\omega_\pi}{2m}\left(1 - \frac{M}{2m+M}\right)\right]F(p), \tag{A.89}$$

$$C_1^{\lambda\rho} = \frac{\omega_\pi}{m}\left((-1)^l\frac{2a_\rho M}{a_\lambda(2m+M)} + \frac{a_\lambda}{2a_\rho}\right)F(p), \tag{A.90}$$

$$C_3^{\lambda\rho} = \frac{GM}{2a_\lambda a_\rho(2m+M)}\left[2 + \frac{\omega_\pi}{2m}\left(1 - \frac{M}{2m+M}\right)\right]F(p). \tag{A.91}$$

Here, we will only summarize the resulting form of the amplitudes. The derivation of how to obtain the amplitudes can be found in Appendix A.

A.5.1 $\Sigma_c^{(*)} \to \Lambda_c \pi$ amplitude

The amplitude can be expressed as

$$-iA_{1/2} = c\ q\ C_1 \tag{A.92}$$

where the coefficient c is given by

$$c = \begin{cases} -1/\sqrt{3} & \text{for } \Sigma_c, \\ \sqrt{2/3} & \text{for } \Sigma_c^*. \end{cases} \tag{A.93}$$

Since both Σ_c and Σ_c^* decay in p wave, the amplitude will be propotional to the pion momentum q. For convenience, we have defined that $\Sigma_c^{(*)}$ stands for Σ_c and Σ_c^*.

A.5.2 $\Lambda_c^* \to \Sigma_c^{(*)}\pi$ amplitude

Negative parity state

The amplitude for $\Lambda_c^*(J^-) \to \Sigma_c^{(*)}\pi$ is given by

$$-iA_h = c_0\ C_0^\zeta + c_2\ q^2\ C_2^\zeta \tag{A.94}$$

where ζ is either λ or ρ mode. The coefficients c_0 and c_2 are summarized in Table A.1. It is worth noting that $\Lambda_c(1/2^-)$ decay into $\Sigma_c^*\pi$ in d wave such that the coeficient c_0 become zero. Similarly, it also happens for $\Lambda_c(3/2^-)$ and $\Lambda_c(5/2^-)$ case. Note that there are two possible helicities, 1/2 and 3/2 for the case of $\Lambda_c(3/2^-)$ and $\Lambda_c(5/2^-)$ decaying into $\Sigma_c^*\pi$.

Another important observation is that $\Lambda_c(1P_\rho, 1/2(0)^-)$ has both coefficient c_0 and c_2 zero. It is occured because of the brown muck selection rule, namely the diquark transition $0^- \to 1^+ + 0^-$ is forbidden. Intuitively, such forbidden transition is described in Fig. **??**. Similarly, for s-wave decay of $\Lambda_c(1P_\rho, 3/2(2)^-) \to \Sigma_c^*\pi$ is not allowed because the diquark transition $2^- \to 1^+ + 0^-$ only occur in d wave.

Positive parity state

The amplitude for $\Lambda_c^*(J^+) \to \Sigma_c^{(*)}\pi$ is given by

$$-iA_h = c_1\ q\ C_1^\zeta + c_3\ q^3\ C_3^\zeta \tag{A.95}$$

where ζ either $\lambda\lambda, \rho\rho$ or $\lambda\rho$, which belong to $N = 2$ excitations. As we may notice, the coefficients c_1 and c_3 now correspond to p- and f-wave decays, respectively. These positve parity states are either radial (n=1) or D-wave ($l = 2$) excitations whose coefficients are summarized in Table A.2. And for those the mixed $\lambda\rho$ mode excitations, the coefficients are tabulated in Table A.3 and A.4.

Table A.1. Coefficients in the amplitude for the decay of negative parity states.

Excitation	$J_{\Lambda_c}(j)^P$	$J^P_{\Sigma_c}$	h	c_0	c_2
$1P_\lambda$	$1/2(1)^-$	$1/2^+$	$1/2$	$-\frac{1}{\sqrt{2}}$	$\frac{1}{3\sqrt{2}}$
		$3/2^+$	$1/2$	0	$-\frac{1}{3}$
	$3/2(1)^-$	$1/2^+$	$1/2$	0	$-\frac{1}{3}$
		$3/2^+$	$1/2$	$-\frac{1}{\sqrt{2}}$	$\frac{\sqrt{2}}{3}$
			$3/2$	$-\frac{1}{\sqrt{2}}$	0
$1P_\rho$	$1/2(0)^-$	$1/2^+$	$1/2$	0	0
		$3/2^+$	$1/2$	0	0
	$1/2(1)^-$	$1/2^+$	$1/2$	2	$-\frac{1}{3}$
		$3/2^+$	$1/2$	0	$-\frac{1}{3\sqrt{2}}$
	$3/2(1)^-$	$1/2^+$	$1/2$	0	$-\frac{1}{3\sqrt{2}}$
		$3/2^+$	$1/2$	2	$-\frac{1}{6}$
			$3/2$	2	$-\frac{1}{2}$
	$3/2(2)^-$	$1/2^+$	$1/2$	0	$\frac{1}{\sqrt{10}}$
		$3/2^+$	$1/2$	0	$\frac{1}{2\sqrt{5}}$
			$3/2$	0	$-\frac{1}{2\sqrt{5}}$
	$5/2(2)^-$	$1/2^+$	$1/2$	0	$\frac{1}{\sqrt{15}}$
		$3/2^+$	$1/2$	0	$\frac{1}{\sqrt{30}}$
			$3/2$	0	$\frac{1}{\sqrt{5}}$

Table A.2. Coefficients in the amplitude for the decay of negative parity states.

Excitation	$J_{\Lambda_c}(j)^P$	$J^P_{\Sigma_c}$	h	c_1	c_3
$2S_{\lambda\lambda}$	$1/2(0)^+$	$1/2^+$	$1/2$	$\frac{1}{3\sqrt{2}}$	$-\frac{1}{6\sqrt{2}}$
		$3/2^+$	$1/2$	$-\frac{1}{3}$	$\frac{1}{6}$
$1D_{\lambda\lambda}$	$3/2(2)^+$	$1/2^+$	$1/2$	$\frac{1}{3}\sqrt{\frac{5}{2}}$	$-\frac{1}{3\sqrt{10}}$
		$3/2^+$	$1/2$	$-\frac{1}{6\sqrt{5}}$	$\frac{1}{3\sqrt{5}}$
			$3/2$	$-\frac{1}{2\sqrt{5}}$	0
	$5/2(2)^+$	$1/2^+$	$1/2$	0	$\frac{1}{2\sqrt{15}}$
		$3/2^+$	$1/2$	$\sqrt{\frac{3}{10}}$	$-\frac{1}{\sqrt{30}}$
			$3/2$	$\frac{1}{\sqrt{5}}$	0
$2S_{\rho\rho}$	$1/2(0)^+$	$1/2^+$	$1/2$	$\frac{\sqrt{2}}{3}$	$-\frac{1}{6\sqrt{2}}$
		$3/2^+$	$1/2$	$-\frac{2}{3}$	$\frac{1}{6}$
$1D_{\rho\rho}$	$3/2(2)^+$	$1/2^+$	$1/2$	$\frac{\sqrt{10}}{3}$	$-\frac{1}{3\sqrt{10}}$
		$3/2^+$	$1/2$	$-\frac{1}{3\sqrt{5}}$	$\frac{1}{3\sqrt{5}}$
			$3/2$	$-\frac{1}{\sqrt{5}}$	0
	$5/2(2)^+$	$1/2^+$	$1/2$	0	$\frac{1}{2\sqrt{15}}$
		$3/2^+$	$1/2$	$\sqrt{\frac{6}{5}}$	$-\frac{1}{\sqrt{30}}$
			$3/2$	$\frac{2}{\sqrt{5}}$	0

Table A.3. Coefficients for the positive parity Λ_b^* (ρ mode) decays with $\lambda\rho$ mixed excitations. l denotes the total angular momentum defined by $l = l_\lambda + l_\rho$.

Excitation	l	$J_{\Lambda_c}(j)^P$	$J^P_{\Sigma_c}$	h	c_1	c_3
$1D_{\lambda\rho}$	0	$1/2(1)^+$	$1/2^+$	1/2	$-\frac{1}{3\sqrt{3}}$	$\frac{1}{3\sqrt{3}}$
			$3/2^+$	1/2	$-\frac{1}{3\sqrt{6}}$	$\frac{1}{3\sqrt{6}}$
		$3/2(1)^+$	$1/2^+$	1/2	$-\frac{1}{3\sqrt{6}}$	$\frac{1}{3\sqrt{6}}$
			$3/2^+$	1/2	$-\frac{1}{6\sqrt{3}}$	$\frac{1}{6\sqrt{3}}$
				3/2	$-\frac{1}{2\sqrt{3}}$	$\frac{1}{2\sqrt{3}}$
	1	$1/2(0)^+$	$1/2^+$	1/2	$\frac{1}{3\sqrt{2}}$	0
			$3/2^+$	1/2	$-\frac{1}{3}$	0
		$1/2(1)^+$	$1/2^+$	1/2	$-\frac{1}{6}$	0
			$3/2^+$	1/2	$-\frac{1}{6\sqrt{2}}$	0
		$3/2(1)^+$	$1/2^+$	1/2	$-\frac{1}{6\sqrt{2}}$	0
			$3/2^+$	1/2	$-\frac{1}{12}$	0
				3/2	$-\frac{1}{4}$	0
		$3/2(2)^+$	$1/2^+$	1/2	$-\frac{\sqrt{5}}{6\sqrt{2}}$	0
			$3/2^+$	1/2	$\frac{1}{12\sqrt{5}}$	0
				3/2	$\frac{1}{4\sqrt{5}}$	0
		$5/2(2)^+$	$1/2^+$	1/2	0	0
			$3/2^+$	1/2	$-\frac{1}{2}\sqrt{\frac{3}{10}}$	0
				3/2	$-\frac{1}{2}\sqrt{\frac{1}{5}}$	0

Table A.4. Coefficients for the positive parity Λ_b^* (ρ mode) decays with $\lambda\rho$ mixed excitations. l denotes the total angular momentum defined by $l = l_\lambda + l_\rho$.

Excitation	l	$J_{\Lambda_c}(j)^P$	$J^P_{\Sigma_c}$	h	c_1	c_3
$1D_{\lambda\rho}$	2	$1/2(1)^+$	$1/2^+$	$1/2$	$\frac{1}{6}\sqrt{\frac{5}{3}}$	$-\frac{1}{3\sqrt{15}}$
			$3/2^+$	$1/2$	$\frac{1}{6}\sqrt{\frac{5}{6}}$	$-\frac{1}{3\sqrt{30}}$
		$3/2(1)^+$	$1/2^+$	$1/2$	$\frac{1}{6}\sqrt{\frac{5}{6}}$	$-\frac{1}{3\sqrt{30}}$
			$3/2^+$	$1/2$	$\frac{1}{12}\sqrt{\frac{5}{3}}$	$-\frac{1}{6\sqrt{15}}$
				$3/2$	$\frac{1}{4}\sqrt{\frac{5}{3}}$	$-\frac{1}{2\sqrt{15}}$
		$3/2(2)^+$	$1/2^+$	$1/2$	$-\frac{1}{2}\sqrt{\frac{5}{6}}$	$\frac{1}{\sqrt{30}}$
			$3/2^+$	$1/2$	$\frac{1}{4\sqrt{15}}$	$\frac{1}{2\sqrt{15}}$
				$3/2$	$\frac{1}{4}\sqrt{\frac{3}{5}}$	$-\frac{1}{2\sqrt{15}}$
		$5/2(2)^+$	$1/2^+$	$1/2$	0	$\frac{1}{3}\sqrt{\frac{1}{5}}$
			$3/2^+$	$1/2$	$-\frac{3}{2}\sqrt{\frac{1}{10}}$	$\frac{1}{3}\sqrt{\frac{1}{10}}$
				$3/2$	$-\frac{3}{2}\sqrt{\frac{1}{15}}$	$\frac{1}{\sqrt{15}}$
		$5/2(3)^+$	$1/2^+$	$1/2$	0	$-\frac{2}{3}\sqrt{\frac{2}{35}}$
			$3/2^+$	$1/2$	0	$-\frac{2}{3}\sqrt{\frac{1}{35}}$
				$3/2$	0	$\sqrt{\frac{2}{105}}$
		$7/2(3)^+$	$1/2^+$	$1/2$	0	$-\sqrt{\frac{2}{105}}$
			$3/2^+$	$1/2$	0	$-\frac{1}{\sqrt{105}}$
				$3/2$	0	$-\frac{1}{\sqrt{21}}$

Appendix B
Angular momentum

B.1 Clebsh-Gordan coefficients

The Clebsh-Gordan coefficients are essential in the construction of the heavy baryon wave function. Here, we use the notation $\langle j_1 j_2 m_1 m_2 | j_3 m_3 \rangle$ for the Clebsh-Gordan coefficient. The coefficient is related to the unitary transformation of state as given by

$$|j_3 m_3\rangle = \sum_{m_1,m_2} \langle j_1 j_2 m_1 m_2 | j_3 m_3 \rangle \, |j_1 m_1\rangle \, |j_2 m_2\rangle \,, \tag{B.1}$$

where $\langle j_1 j_2 m_1 m_2 | j_3 m_3 \rangle = 0$ unless $j_1 + j_2 \geq j_3 \geq |j_1 - j_2|$ and $m_3 = m_1 + m_2$. Also, the coefficient has symmetry property as

$$\langle j_1 j_2 m_1 m_2 | j_3 m_3 \rangle = (-1)^{j_1+j_2-j_3} \langle j_2 j_1 m_2 m_1 | j_3 m_3 \rangle \,. \tag{B.2}$$

and orthogonality relation as

$$\begin{aligned} \sum_{m_1,m_2} \langle j_1 j_2 m_1 m_2 | j_3 m_3 \rangle \langle j_1 j_2 m_1 m_2 | j_3' m_3' \rangle &= \delta_{j_3,j_3'} \delta_{m_3,m_3'}, && \text{(B.3)} \\ \sum_{j_3,m_3} \langle j_1 j_2 m_1 m_2 | j_3 m_3 \rangle \langle j_1 j_2 m_1' m_2' | j_3 m_3 \rangle &= \delta_{m_1,m_1'} \delta_{m_2,m_2'}. && \text{(B.4)} \end{aligned}$$

The coefficients are also related to the other symbols, such as 3-j symbols

$$\langle j_1 j_2 m_1 m_2 | j_3 m_3 \rangle = (-1)^{j_2-j_1-m_3} \hat{j}_3 \begin{pmatrix} j_1 & j_2 & j_3 \\ m_1 & m_2 & -m_3 \end{pmatrix}, \tag{B.5}$$

which have more symmetry properties such as

$$\begin{aligned} \begin{pmatrix} j_1 & j_2 & j_3 \\ m_1 & m_2 & m_3 \end{pmatrix} &= \begin{pmatrix} j_2 & j_3 & j_1 \\ m_2 & m_3 & m_1 \end{pmatrix} = \begin{pmatrix} j_3 & j_1 & j_2 \\ m_3 & m_1 & m_2 \end{pmatrix} && \text{(B.6)} \\ &= (-1)^{j_1+j_2+j_3} \begin{pmatrix} j_2 & j_1 & j_3 \\ m_2 & m_1 & m_3 \end{pmatrix} && \text{(B.7)} \\ &= (-1)^{j_1+j_2+j_3} \begin{pmatrix} j_1 & j_2 & j_3 \\ -m_1 & -m_2 & -m_3 \end{pmatrix}. && \text{(B.8)} \end{aligned}$$

Here, we have defined $\hat{j}_3 = \sqrt{2j_3+1}$. Then, we can construct the 6-j symbols by using the 3-j symbols as

$$\begin{pmatrix} j_1 & j_2 & j_3 \\ m_1 & m_2 & m_3 \end{pmatrix} \begin{Bmatrix} j_1 & j_2 & j_3 \\ l_1 & l_2 & l_3 \end{Bmatrix} = \sum_{m_1',m_2',m_3'} (-1)^{l_1+l_2+l_3+m_1'+m_2'+m_3'} \begin{pmatrix} j_1 & l_2 & l_3 \\ m_1 & m_2' & -m_3' \end{pmatrix} \times \begin{pmatrix} l_1 & j_2 & l_3 \\ -m_1' & m_2 & m_3' \end{pmatrix} \begin{pmatrix} l_1 & l_2 & j_3 \\ m_1' & -m_2' & m_3 \end{pmatrix} \tag{B.9}$$

The 6-j symbol have the symmetry properties as given by

$$\begin{Bmatrix} j_1 & j_2 & j_3 \\ l_1 & l_2 & l_3 \end{Bmatrix} = \begin{Bmatrix} j_2 & j_3 & j_1 \\ l_2 & l_3 & l_1 \end{Bmatrix} = \begin{Bmatrix} j_3 & j_1 & j_2 \\ l_3 & l_1 & l_2 \end{Bmatrix} = \begin{Bmatrix} j_2 & j_1 & j_3 \\ l_2 & l_1 & l_3 \end{Bmatrix} = \begin{Bmatrix} l_1 & l_2 & j_3 \\ j_1 & j_2 & l_3 \end{Bmatrix} \tag{B.10}$$

Here are some special cases for Clebsh-Gordan coefficients, 3-j and 6-j symbols which are essential in the calculations as

$$\langle jj'00|00\rangle = (-1)^{j'-j} \begin{pmatrix} j & j' & 0 \\ m & -m' & 0 \end{pmatrix} = \frac{(-1)^{j-m}}{\sqrt{2j+1}} \delta_{mm'}\delta_{jj'}, \tag{B.11}$$

$$\begin{pmatrix} j & j & 1 \\ m & -m & 0 \end{pmatrix} = (-1)^{j-m} \frac{m}{\sqrt{j(2j+1)(j+1)}}, \tag{B.12}$$

$$\begin{Bmatrix} j_1 & j_2' & j_3 \\ j_2 & j_1' & 0 \end{Bmatrix} = (-1)^{j_1+j_2+j_3} \frac{1}{\sqrt{(2j_1+1)(2j_2+1)}} \delta_{j_1 j_1'} \delta_{j_2 j_2'}, \tag{B.13}$$

$$\begin{Bmatrix} j_1 & j_2 & j_3 \\ j_2 & j_1 & 1 \end{Bmatrix} = (-1)^{j_1+j_2+j_3+1} \frac{\frac{1}{2}\left[j_1(j_1+1)+j_2(j_2+1)-j_3(j_3+1)\right]}{\sqrt{j_1(j_1+1)(2j_1+1)j_2(j_2+1)(2j_2+1)}}, \tag{B.14}$$

In some cases, we need to couple three different angular momenta, j_1, j_2, and j_3. In this case, we have two choices of coupling:

1. coupling j_1 with j_2 to form J_{12}, and then coupling J_{12} with j_3,
2. coupling j_1 with j_3 to form J_{13}, and then coupling J_{13} with j_2.

Two choices of coupling can be related as

$$\left|\{(j_1,j_3)^{J_{13}}, j_2\}_M^J\right\rangle = \sum_{J_{12}} (-1)^{j_2+j_3+J_{12}+J_{13}} \hat{J_{12}}\hat{J_{13}} \begin{Bmatrix} j_1 & j_2 & J_{12} \\ J & j_3 & J_{13} \end{Bmatrix} \left|\{(j_1,j_2)^{J_{12}}, j_3\}_M^J\right\rangle, \tag{B.15}$$

which follow the 6-j symbols. For the case of the coupling of four angular momenta, we can also write the similar relation with 9-j symbols as

$$\left|\{(j_1,j_3)^{J_{13}}, (j_2,j_4)^{J_{24}}\}_M^J\right\rangle = \hat{J_{12}}\hat{J_{13}}\hat{J_{24}}\hat{J_{34}} \begin{Bmatrix} j_1 & j_2 & J_{12} \\ j_3 & j_4 & J_{34} \\ J_{13} & J_{24} & J \end{Bmatrix} \left|\{(j_1,j_2)^{J_{12}}, (j_3,j_4)^{J_{34}}\}_M^J\right\rangle, \tag{B.16}$$

We can get the tensor product between two irredicule tensors with the Clebsh-Gordan coefficients as

$$[\mathbf{T}^{(k_2)} \otimes \mathbf{T}^{(k_2)}]^{(k_3)}_{\kappa_3} = \sum_{\kappa_1\kappa_2} \langle k_1 k_2 \kappa_1 \kappa_2 | k_3 \kappa_3 \rangle \, T^{(k_1)}_{\kappa_1} T^{(k_2)}_{\kappa_2}, \tag{B.17}$$

and reverely we can also express the tensor product as

$$T^{(k_1)}_{\kappa_1} T^{(k_2)}_{\kappa_2} = \sum_{k_3\kappa_3} \langle k_1 k_2 \kappa_1 \kappa_2 | k_3 \kappa_3 \rangle \, [\mathbf{T}^{(k_2)} \otimes \mathbf{T}^{(k_2)}]^{(k_3)}_{\kappa_3}. \tag{B.18}$$

Moreover, the scalar product of two irreducible tensor is given by

$$\left(\mathbf{T}^{(k)} \cdot \mathbf{U}^{(k)}\right) = (-1)^k \hat{k} \left[\mathbf{T}^{(k)} \otimes \mathbf{U}^{(k)}\right]^{(0)}_0 = \sum_{\kappa} (-1)^{\kappa} T^{(k)}_{\kappa} U^{(k)}_{-\kappa}. \tag{B.19}$$

These sort of product of two irredicule tensors is crucial in the calculation of wavefunction and amplitudes.

In doing the calculation of the transition amplitude, we can use the Wigner-Eckart theorem given by

$$\left\langle JM \left| T^{(k)}_{\kappa} \right| J'M' \right\rangle = (-1)^{J-M} \begin{pmatrix} J & k & J' \\ -M & \kappa & M' \end{pmatrix} \left\langle J \left|\left| \mathbf{T}^{(k)} \right|\right| J' \right\rangle \tag{B.20}$$

to factor out the 3-j symbol or Clebsh-Gordan coefficients. $\left\langle J \left|\left| \mathbf{T}^{(k)} \right|\right| J' \right\rangle$ is called the reduced matrix element. For the special case, the spherical harmonics, the reduced matrix elements are given by

$$\langle l_1 \, || Y_L || \, l_2 \rangle = (-1)^{l_1} \frac{\hat{l}_1 \hat{l}_2 \hat{L}}{\sqrt{4\pi}} \begin{pmatrix} l_1 & L & l_2 \\ 0 & 0 & 0 \end{pmatrix}, \tag{B.21}$$

and for the angular momentum operator, we obtain

$$\langle j \, || \mathbf{j} || \, j \rangle = \hat{j} \sqrt{j(j+1)}, \qquad \langle j \, || 1 || \, j \rangle = \hat{j}. \tag{B.22}$$

and for the spin 1/2 operator, the reduced matrix element is computed as

$$\left\langle \tfrac{1}{2} \, || \boldsymbol{\sigma} || \, \tfrac{1}{2} \right\rangle = \sqrt{6}, \qquad \left\langle \tfrac{1}{2} \, || 1 || \, \tfrac{1}{2} \right\rangle = \sqrt{2}. \tag{B.23}$$

B.2 Spherical harmonics

The spherical harmonis are given in Table B.1, which are useful for the quark model calculation.

Table B.1. The spherical harmonics $Y_{lm}(\theta, \phi)$ for $l \leq 3$.

(l, m)	Angular representation	Spherical representation
$(0,0)$	$+\frac{1}{\sqrt{4\pi}}$	$+\frac{1}{\sqrt{4\pi}}$
$(1,0)$	$+\sqrt{\frac{3}{4\pi}}\frac{z}{r}$	$+\sqrt{\frac{3}{4\pi}}\cos\theta$
$(1,\pm1)$	$\mp\sqrt{\frac{3}{8\pi}}\frac{1}{r}(x \pm iy)$	$\mp\sqrt{\frac{3}{8\pi}}\sin\theta e^{\pm i\phi}$
$(2,0)$	$+\sqrt{\frac{5}{16\pi}}\frac{1}{r^2}(2z^2 - x^2 - y^2)$	$+\sqrt{\frac{5}{16\pi}}(3\cos^2\theta - 1)$
$(2,\pm1)$	$\mp\sqrt{\frac{15}{8\pi}}\frac{z}{r^2}(x \pm iy)$	$\mp\sqrt{\frac{15}{8\pi}}\cos\theta\sin\theta e^{\pm i\phi}$
$(2,\pm2)$	$+\sqrt{\frac{15}{32\pi}}\frac{1}{r^2}(x \pm iy)^2$	$+\sqrt{\frac{15}{32\pi}}\sin^2\theta e^{\pm 2i\phi}$
$(3,0)$	$+\sqrt{\frac{7}{16\pi}}\frac{z}{r}\left(\frac{5z^2}{r^2} - 3\right)$	$+\sqrt{\frac{7}{16\pi}}(5\cos^3\theta - 3\cos\theta)$
$(3,\pm1)$	$\mp\sqrt{\frac{21}{64\pi}}\frac{1}{r^3}\left(4z^2 - x^2 - y^2\right)(x \pm iy)$	$\mp\sqrt{\frac{21}{64\pi}}(4\cos^2\theta\sin\theta - sin^3\theta)e^{\pm i\phi}$
$(3,\pm2)$	$+\sqrt{\frac{105}{32\pi}}\frac{z}{r^3}\left(x^2 - y^2 \pm i2xy\right)$	$+\sqrt{\frac{105}{32\pi}}\cos\theta\sin^2\theta e^{\pm 2i\phi}$
$(3,\pm3)$	$\mp\sqrt{\frac{35}{64\pi}}\frac{1}{r^3}\left[(x^3 - 3xy^2) \pm i(3x^2y - y^3)\right]$	$\mp\sqrt{\frac{15}{32\pi}}\sin^3\theta e^{\pm 3i\phi}$

Finally, a plane wave can be expanded in terms of spherical harmonics as

$$\exp(i\boldsymbol{k}\cdot\boldsymbol{r}) = 4\pi\sum_{l,m} i^l j_l(kr) Y_{lm}(\hat{\boldsymbol{k}}) Y^*_{lm}(\hat{\boldsymbol{r}}) \tag{B.24}$$

$$\exp(-i\boldsymbol{k}\cdot\boldsymbol{r}) = 4\pi\sum_{l,m} (-i)^l j_l(kr) Y^*_{lm}(\hat{\boldsymbol{k}}) Y_{lm}(\hat{\boldsymbol{r}}) \tag{B.25}$$

where $j_l(k, r)$ represents a spherical Basel function. This plane wave expansion is crucial for calculations of matrix elements in the quark model.

Appendix C
Three-body decay amplitude

C.1 Spin transition: $l = 1$ (p-wave)

C.1.1 Spin 1/2 to 1/2

The Pauli matrices are completely determined by the Clebsh-Gordan coefficients as described by using Wigner-Eckart theorem as follows

$$\begin{aligned}
\left\langle 1/2\ m'\right|\sigma_\lambda\left|1/2\ m\right\rangle &= \left(1/2\ m\ 1\ \lambda\ |1/2\ m'\right)\frac{\langle 1/2\ ||\ \boldsymbol{\sigma}\ ||1/2\ \rangle}{\sqrt{2(1/2)+1}} \\
&= \left(1/2\ m\ 1\ \lambda\ |1/2\ m'\right)\frac{\sqrt{6}}{\sqrt{2}} \\
\left\langle 1/2\ m'\right|\sigma_\lambda\left|1/2\ m\right\rangle &= \sqrt{3}\times\left(1/2\ m\ 1\ \lambda\ |1/2\ m'\right) \qquad \text{(C.1)}
\end{aligned}$$

where we have use the reduced matrix elements

$$\langle j\ ||\ \mathbf{j}\ ||j\ \rangle = \sqrt{j(2j+1)(j+1)}. \qquad \text{(C.2)}$$

For $j = 1/2$, and $\mathbf{j} = \frac{1}{2}\boldsymbol{\sigma}$, we will obtain

$$\langle 1/2\ ||\ \boldsymbol{\sigma}\ ||1/2\ \rangle = 2\,\langle 1/2\ ||\ \mathbf{j}\ ||1/2\ \rangle = \sqrt{6} \qquad \text{(C.3)}$$

If we evaluate Eq. (C.1), we will reproduce the Pauli matrices in spherical coordinate as

$$\sigma_+ = \begin{pmatrix} 0 & -\sqrt{2} \\ 0 & 0 \end{pmatrix}, \qquad \sigma_0 = \begin{pmatrix} 1 & 0 \\ 0 & -1 \end{pmatrix}, \qquad \sigma_- = \begin{pmatrix} 0 & 0 \\ \sqrt{2} & 0 \end{pmatrix}, \qquad \text{(C.4)}$$

The cartesian and spherical components of Pauli matrices are related by

$$\begin{aligned}
\sigma_x &= -\frac{1}{\sqrt{2}}\left(\sigma_+ - \sigma_-\right), \qquad &\text{(C.5)} \\
\sigma_y &= \frac{i}{\sqrt{2}}\left(\sigma_+ + \sigma_-\right), \qquad &\text{(C.6)} \\
\sigma_z &= \sigma_0. \qquad &\text{(C.7)}
\end{aligned}$$

The Cartesian components of Pauli matrices are written as

$$\sigma_x = \begin{pmatrix} 0 & 1 \\ 1 & 0 \end{pmatrix}, \qquad \sigma_y = \begin{pmatrix} 0 & -i \\ i & 0 \end{pmatrix}, \qquad \sigma_z = \begin{pmatrix} 1 & 0 \\ 0 & -1 \end{pmatrix}, \qquad \text{(C.8)}$$

C.1.2 Spin 3/2 to 3/2

The $\mathbf{\Sigma}$ matrices are completely determined by the Clebsh-Gordan coefficients as described by using Wigner-Eckart theorem as follows

$$\begin{aligned}
\left\langle 3/2\ m' | \Sigma_\lambda | 3/2\ m \right\rangle &= \left(3/2\ m\ 1\ \lambda\ | 3/2\ m'\right) \frac{\langle 3/2 \ ||\ \mathbf{\Sigma}\ || 3/2\ \rangle}{\sqrt{2(3/2)+1}} \\
&= \left(3/2\ m\ 1\ \lambda\ | 3/2\ m'\right) \frac{\sqrt{60}}{\sqrt{4}} \\
\left\langle 3/2\ m' | \Sigma_\lambda | 3/2\ m \right\rangle &= \sqrt{15} \times \left(3/2\ m\ 1\ \lambda\ | 3/2\ m'\right) \qquad \text{(C.9)}
\end{aligned}$$

where we have use the reduced matrix elements

$$\langle j \ ||\ \mathbf{j}\ || j\ \rangle = \sqrt{j(2j+1)(j+1)}. \qquad \text{(C.10)}$$

For $j = 1/2$, and $\mathbf{j} = \frac{1}{2}\mathbf{\Sigma}$, we will obtain

$$\langle 3/2 \ ||\ \mathbf{\Sigma}\ || 3/2\ \rangle = 2\,\langle 3/2 \ ||\ \mathbf{S}\ || 3/2\ \rangle = \sqrt{60} \qquad \text{(C.11)}$$

If we evaluate Eq. (C.1), we will reproduce the $\mathbf{\Sigma}$ matrices in spherical coordinate as

$$\Sigma_+ = -\frac{1}{\sqrt{2}} \begin{pmatrix} 0 & \sqrt{3} & 0 & 0 \\ 0 & 0 & 2 & 0 \\ 0 & 0 & 0 & \sqrt{3} \\ 0 & 0 & 0 & 0 \end{pmatrix}, \quad \Sigma_- = \frac{1}{\sqrt{2}} \begin{pmatrix} 0 & 0 & 0 & 0 \\ \sqrt{3} & 0 & 0 & 0 \\ 0 & 2 & 0 & 0 \\ 0 & 0 & \sqrt{3} & 0 \end{pmatrix}, \quad \Sigma_0 = \begin{pmatrix} 3 & 0 & 0 & 0 \\ 0 & 1 & 0 & 0 \\ 0 & 0 & -1 & 0 \\ 0 & 0 & 0 & -3 \end{pmatrix}, \qquad \text{(C.12)}$$

C.1.3 Spin 3/2 to 1/2 and vice versa

The matrix element between spin 1/2 and spin 3/2 is given by

$$\left\langle 3/2\ m' \middle| S^\dagger_\lambda \middle| 1/2\ m \right\rangle = (1/2\ m\ 1\ \lambda\ |\ 3/2\ m'). \qquad \text{(C.13)}$$

We have used the convention that the reduced matrix element equals 1 meaning that

$$\frac{\langle 3/2 \ ||\ \mathbf{S}^\dagger\ || 1/2\ \rangle}{\sqrt{2(3/2)+1}} = 1. \qquad \text{(C.14)}$$

Then, we have

$$\left\langle 3/2 \ ||\ \mathbf{S}^\dagger\ || 1/2\ \right\rangle = \sqrt{4} \qquad \text{(C.15)}$$

The spin transition matrices can be expressed by

$$S_+^\dagger = \frac{1}{\sqrt{3}}\begin{pmatrix} \sqrt{3} & 0 \\ 0 & 1 \\ 0 & 0 \\ 0 & 0 \end{pmatrix}, \qquad S_0^\dagger = \frac{1}{\sqrt{3}}\begin{pmatrix} 0 & 0 \\ \sqrt{2} & 0 \\ 0 & \sqrt{2} \\ 0 & 0 \end{pmatrix}, \qquad S_-^\dagger = \frac{1}{\sqrt{3}}\begin{pmatrix} 0 & 0 \\ 0 & 0 \\ 1 & 0 \\ 0 & \sqrt{3} \end{pmatrix}. \tag{C.16}$$

The matrix element between spin 3/2 and spin 1/2 is given by

$$\begin{aligned} \left\langle 1/2\ m' \,|\, S_\lambda \,|\, 3/2\ m \right\rangle &= (3/2\ m\ 1\ \lambda \mid 1/2\ m')\, \frac{\langle 1/2 \mid\mid \mathbf{S} \mid\mid 3/2 \rangle}{\sqrt{2(1/2)+1}} \\ &= (3/2\ m\ 1\ \lambda \mid 1/2\ m')\, \frac{\sqrt{4}}{\sqrt{2}} \\ \left\langle 1/2\ m' \,|\, S_\lambda \,|\, 3/2\ m \right\rangle &= \sqrt{2} \times (3/2\ m\ 1\ \lambda \mid 1/2\ m') \end{aligned} \tag{C.17}$$

Then, the spin transition matrices read

$$S_- = \frac{1}{\sqrt{3}}\begin{pmatrix} \sqrt{3} & 0 & 0 & 0 \\ 0 & 1 & 0 & 0 \end{pmatrix}, S_0 = \frac{1}{\sqrt{3}}\begin{pmatrix} 0 & \sqrt{2} & 0 & 0 \\ 0 & 0 & \sqrt{2} & 0 \end{pmatrix}, S_+ = \frac{1}{\sqrt{3}}\begin{pmatrix} 0 & 0 & 1 & 0 \\ 0 & 0 & 0 & \sqrt{3} \end{pmatrix}. \tag{C.18}$$

If we simply use Clebsh-Gordan coefficient without the reduced matrix element, we will get a slightly different result by factor $\sqrt{2}$ compared to the one calculated by taking hermitian conjugate directly $S_\lambda = (S_{-\lambda}^\dagger)^\dagger$ from Eq. (16). The conventional factor $\sqrt{2j'+1}$ in denominator is convenient because the reduced matrix element will not change by interchanging bra and ket, namely,

$$\langle 1/2 \mid\mid \mathbf{S} \mid\mid 3/2 \rangle = \left\langle 3/2 \mid\mid \mathbf{S}^\dagger \mid\mid 1/2 \right\rangle. \tag{C.19}$$

This is important especially when spin j in bra and ket are different. Please note that we will also use the reduced matrix element equal to 1 for later calculation.

C.1.4 Spin 5/2 to 3/2 and vice versa

The matrix element between spin 3/2 and spin 5/2 is given by

$$\left\langle 5/2\ m' \middle| T_\lambda^\dagger \middle| 3/2\ m \right\rangle = (3/2\ m\ 1\ \lambda \mid 5/2\ m'). \tag{C.20}$$

The spin transition matrices are explicitly written by

$$T_{+}^{\dagger} = \frac{1}{\sqrt{10}}\begin{pmatrix} \sqrt{10} & 0 & 0 & 0 \\ 0 & \sqrt{6} & 0 & 0 \\ 0 & 0 & \sqrt{3} & 0 \\ 0 & 0 & 0 & 1 \\ 0 & 0 & 0 & 0 \\ 0 & 0 & 0 & 0 \end{pmatrix}, \tag{C.21}$$

$$T_{0}^{\dagger} = \frac{1}{\sqrt{10}}\begin{pmatrix} 0 & 0 & 0 & 0 \\ 2 & 0 & 0 & 0 \\ 0 & \sqrt{6} & 0 & 0 \\ 0 & 0 & \sqrt{6} & 0 \\ 0 & 0 & 0 & 2 \\ 0 & 0 & 0 & 0 \end{pmatrix}, \tag{C.22}$$

$$T_{-}^{\dagger} = \frac{1}{\sqrt{10}}\begin{pmatrix} 0 & 0 & 0 & 0 \\ 0 & 0 & 0 & 0 \\ 1 & 0 & 0 & 0 \\ 0 & \sqrt{3} & 0 & 0 \\ 0 & 0 & \sqrt{6} & 0 \\ 0 & 0 & 0 & \sqrt{10} \end{pmatrix}. \tag{C.23}$$

If we take a hermitian conjugate, we will obtain

$$T_{-} = \frac{1}{\sqrt{10}}\begin{pmatrix} \sqrt{10} & 0 & 0 & 0 & 0 & 0 \\ 0 & \sqrt{6} & 0 & 0 & 0 & 0 \\ 0 & 0 & \sqrt{3} & 0 & 0 & 0 \\ 0 & 0 & 0 & 1 & 0 & 0 \end{pmatrix}, \tag{C.24}$$

$$T_{0} = \frac{1}{\sqrt{10}}\begin{pmatrix} 0 & 2 & 0 & 0 & 0 & 0 \\ 0 & 0 & \sqrt{6} & 0 & 0 & 0 \\ 0 & 0 & 0 & \sqrt{6} & 0 & 0 \\ 0 & 0 & 0 & 0 & 2 & 0 \end{pmatrix}, \tag{C.25}$$

$$T_{+} = \frac{1}{\sqrt{10}}\begin{pmatrix} 0 & 0 & 1 & 0 & 0 & 0 \\ 0 & 0 & 0 & \sqrt{3} & 0 & 0 \\ 0 & 0 & 0 & 0 & \sqrt{6} & 0 \\ 0 & 0 & 0 & 0 & 0 & \sqrt{10} \end{pmatrix}. \tag{C.26}$$

C.1.5 Spin 7/2 to 5/2 and vice versa

For the case of the spin transition from 5/2 to 7/2, the matrices are constructed by

$$\left\langle 7/2\ m' \left| U^\dagger_\lambda \right| 5/2\ m \right\rangle \quad = \quad \left(7/2\ m\ 1\ \lambda\ \middle| 5/2\ m'\right). \tag{C.27}$$

which are explicitly given by

$$U^\dagger_+ \quad = \quad \frac{1}{\sqrt{21}} \begin{pmatrix} \sqrt{21} & 0 & 0 & 0 & 0 & 0 \\ 0 & \sqrt{15} & 0 & 0 & 0 & 0 \\ 0 & 0 & \sqrt{10} & 0 & 0 & 0 \\ 0 & 0 & 0 & \sqrt{6} & 0 & 0 \\ 0 & 0 & 0 & 0 & \sqrt{3} & 0 \\ 0 & 0 & 0 & 0 & 0 & 1 \\ 0 & 0 & 0 & 0 & 0 & 0 \\ 0 & 0 & 0 & 0 & 0 & 0 \end{pmatrix}, \tag{C.28}$$

$$U^\dagger_0 \quad = \quad \frac{1}{\sqrt{21}} \begin{pmatrix} 0 & 0 & 0 & 0 & 0 & 0 \\ \sqrt{6} & 0 & 0 & 0 & 0 & 0 \\ 0 & \sqrt{10} & 0 & 0 & 0 & 0 \\ 0 & 0 & \sqrt{12} & 0 & 0 & 0 \\ 0 & 0 & 0 & \sqrt{12} & 0 & 0 \\ 0 & 0 & 0 & 0 & \sqrt{10} & 0 \\ 0 & 0 & 0 & 0 & 0 & \sqrt{6} \\ 0 & 0 & 0 & 0 & 0 & 0 \end{pmatrix}, \tag{C.29}$$

$$U^\dagger_- \quad = \quad \frac{1}{\sqrt{21}} \begin{pmatrix} 0 & 0 & 0 & 0 & 0 & 0 \\ 0 & 0 & 0 & 0 & 0 & 0 \\ 1 & 0 & 0 & 0 & 0 & 0 \\ 0 & \sqrt{3} & 0 & 0 & 0 & 0 \\ 0 & 0 & \sqrt{6} & 0 & 0 & 0 \\ 0 & 0 & 0 & \sqrt{10} & 0 & 0 \\ 0 & 0 & 0 & 0 & \sqrt{15} & 0 \\ 0 & 0 & 0 & 0 & 0 & \sqrt{21} \end{pmatrix}. \tag{C.30}$$

Its hermitian conjugate is given by

$$U_- = \frac{1}{\sqrt{21}} \begin{pmatrix} \sqrt{21} & 0 & 0 & 0 & 0 & 0 & 0 & 0 \\ 0 & \sqrt{15} & 0 & 0 & 0 & 0 & 0 & 0 \\ 0 & 0 & \sqrt{10} & 0 & 0 & 0 & 0 & 0 \\ 0 & 0 & 0 & \sqrt{6} & 0 & 0 & 0 & 0 \\ 0 & 0 & 0 & 0 & \sqrt{3} & 0 & 0 & 0 \\ 0 & 0 & 0 & 0 & 0 & 1 & 0 & 0 \end{pmatrix}, \tag{C.31}$$

$$U_0 = \frac{1}{\sqrt{21}} \begin{pmatrix} 0 & \sqrt{6} & 0 & 0 & 0 & 0 & 0 & 0 \\ 0 & 0 & \sqrt{10} & 0 & 0 & 0 & 0 & 0 \\ 0 & 0 & 0 & \sqrt{12} & 0 & 0 & 0 & 0 \\ 0 & 0 & 0 & 0 & \sqrt{12} & 0 & 0 & 0 \\ 0 & 0 & 0 & 0 & 0 & \sqrt{10} & 0 & 0 \\ 0 & 0 & 0 & 0 & 0 & 0 & \sqrt{6} & 0 \end{pmatrix}, \tag{C.32}$$

$$U_+ = \frac{1}{\sqrt{21}} \begin{pmatrix} 0 & 0 & 1 & 0 & 0 & 0 & 0 & 0 \\ 0 & 0 & 0 & \sqrt{3} & 0 & 0 & 0 & 0 \\ 0 & 0 & 0 & 0 & \sqrt{6} & 0 & 0 & 0 \\ 0 & 0 & 0 & 0 & 0 & \sqrt{10} & 0 & 0 \\ 0 & 0 & 0 & 0 & 0 & 0 & \sqrt{15} & 0 \\ 0 & 0 & 0 & 0 & 0 & 0 & 0 & \sqrt{21} \end{pmatrix}. \tag{C.33}$$

C.2 Spin transition: $l = 2$ (d-wave)

C.2.1 Spin 3/2 to 3/2

The d-wave transition matrix from spin 3/2 to spin 3/2 is defined by

$$\left\langle 3/2\ m' \left| V_\lambda \right| 3/2\ m \right\rangle = \left(3/2\ m\ 2\ \lambda \middle| 3/2\ m' \right). \tag{C.34}$$

Explicitly, the matrices can be expressed as

$$V_{+2} = \frac{1}{\sqrt{5}} \begin{pmatrix} 0 & 0 & \sqrt{2} & 0 \\ 0 & 0 & 0 & \sqrt{2} \\ 0 & 0 & 0 & 0 \\ 0 & 0 & 0 & 0 \end{pmatrix}, \tag{C.35}$$

$$V_{+1} = \frac{1}{\sqrt{5}} \begin{pmatrix} 0 & -\sqrt{2} & 0 & 0 \\ 0 & 0 & 0 & 0 \\ 0 & 0 & 0 & \sqrt{2} \\ 0 & 0 & 0 & 0 \end{pmatrix}, \tag{C.36}$$

$$V_{0} = \frac{1}{\sqrt{5}} \begin{pmatrix} 1 & 0 & 0 & 0 \\ 0 & -1 & 0 & 0 \\ 0 & 0 & -1 & 0 \\ 0 & 0 & 0 & 1 \end{pmatrix}, \tag{C.37}$$

$$V_{-1} = \frac{1}{\sqrt{5}} \begin{pmatrix} 0 & 0 & 0 & 0 \\ \sqrt{2} & 0 & 0 & 0 \\ 0 & 0 & 0 & 0 \\ 0 & 0 & -\sqrt{2} & 0 \end{pmatrix}, \tag{C.38}$$

$$V_{-2} = \frac{1}{\sqrt{5}} \begin{pmatrix} 0 & 0 & 0 & 0 \\ 0 & 0 & 0 & 0 \\ \sqrt{2} & 0 & 0 & 0 \\ 0 & \sqrt{2} & 0 & 0 \end{pmatrix}, \tag{C.39}$$

C.3 Spin transition: $l = 3$ (f-wave)

C.3.1 Spin 3/2 to 3/2

The f-wave transition matrix from spin 3/2 to spin 3/2 is defined by

$$\left\langle 3/2\ m' \left| W_\lambda \right| 3/2\ m \right\rangle \quad = \quad \left(3/2\ m\ 3\ \lambda \middle| 3/2\ m' \right). \tag{C.40}$$

Explicitly, the matrices can be expressed as

$$W_{+3} \quad = \quad \frac{1}{\sqrt{7}} \begin{pmatrix} 0 & 0 & 0 & -2 \\ 0 & 0 & 0 & 0 \\ 0 & 0 & 0 & 0 \\ 0 & 0 & 0 & 0 \end{pmatrix}, \tag{C.41}$$

$$W_{+2} \quad = \quad \frac{1}{\sqrt{7}} \begin{pmatrix} 0 & 0 & \sqrt{2} & 0 \\ 0 & 0 & 0 & -\sqrt{2} \\ 0 & 0 & 0 & 0 \\ 0 & 0 & 0 & 0 \end{pmatrix}, \tag{C.42}$$

$$W_{+1} \quad = \quad \frac{1}{\sqrt{35}} \begin{pmatrix} 0 & -2 & 0 & 0 \\ 0 & 0 & 2\sqrt{3} & 0 \\ 0 & 0 & 0 & -2 \\ 0 & 0 & 0 & 0 \end{pmatrix}, \tag{C.43}$$

$$W_{0} \quad = \quad \frac{1}{\sqrt{35}} \begin{pmatrix} 1 & 0 & 0 & 0 \\ 0 & -3 & 0 & 0 \\ 0 & 0 & 3 & 0 \\ 0 & 0 & 0 & -1 \end{pmatrix}, \tag{C.44}$$

$$W_{-1} \quad = \quad \frac{1}{\sqrt{35}} \begin{pmatrix} 0 & 0 & 0 & 0 \\ 2 & 0 & 0 & 0 \\ 0 & -2\sqrt{3} & & 0 \\ 0 & 0 & 2 & 0 \end{pmatrix}, \tag{C.45}$$

$$W_{-2} \quad = \quad \frac{1}{\sqrt{7}} \begin{pmatrix} 0 & 0 & 0 & 0 \\ 0 & 0 & 0 & 0 \\ \sqrt{2} & 0 & 0 & 0 \\ 0 & -\sqrt{2} & 0 & 0 \end{pmatrix}, \tag{C.46}$$

$$W_{-3} \quad = \quad \frac{1}{\sqrt{7}} \begin{pmatrix} 0 & 0 & 0 & 0 \\ 0 & 0 & 0 & 0 \\ 0 & 0 & 0 & 0 \\ 2 & 0 & 0 & 0 \end{pmatrix}, \tag{C.47}$$

C.3.2 Spin 5/2 to 3/2 and vice versa

The f-wave transition matrix from spin 3/2 to spin 5/2 is defined by

$$\left\langle 5/2\ m' \middle| X^\dagger_\lambda \middle| 3/2\ m \right\rangle \;=\; \big(3/2\ m\ 3\ \lambda \big| 5/2\ m'\big)\,. \tag{C.48}$$

Explicitly, the matrices can be expressed as

$$X^\dagger_{+3} \;=\; \frac{1}{\sqrt{28}} \begin{pmatrix} 0 & 0 & \sqrt{15} & 0 \\ 0 & 0 & 0 & 3 \\ 0 & 0 & 0 & 0 \\ 0 & 0 & 0 & 0 \\ 0 & 0 & 0 & 0 \\ 0 & 0 & 0 & 0 \end{pmatrix}, \tag{C.49}$$

$$X^\dagger_{+2} \;=\; \frac{1}{\sqrt{14}} \begin{pmatrix} 0 & -\sqrt{5} & 0 & 0 \\ 0 & 0 & 1 & 0 \\ 0 & 0 & 0 & \sqrt{6} \\ 0 & 0 & 0 & 0 \\ 0 & 0 & 0 & 0 \\ 0 & 0 & 0 & 0 \end{pmatrix}, \tag{C.50}$$

$$X^\dagger_{+1} \;=\; \frac{1}{\sqrt{140}} \begin{pmatrix} \sqrt{15} & 0 & 0 & 0 \\ 0 & -7 & 0 & 0 \\ 0 & 0 & -\sqrt{2} & 0 \\ 0 & 0 & 0 & 3\sqrt{6} \\ 0 & 0 & 0 & 0 \\ 0 & 0 & 0 & 0 \end{pmatrix}, \tag{C.51}$$

$$X^\dagger_{0} \;=\; \frac{1}{\sqrt{35}} \begin{pmatrix} 0 & 0 & 0 & 0 \\ 3 & 0 & 0 & 0 \\ 0 & -\sqrt{6} & 0 & 0 \\ 0 & 0 & -\sqrt{6} & 0 \\ 0 & 0 & 0 & 3 \\ 0 & 0 & 0 & 0 \end{pmatrix}, \tag{C.52}$$

$$X^\dagger_{-1} \;=\; \frac{1}{\sqrt{140}} \begin{pmatrix} 0 & 0 & 0 & 0 \\ 0 & 0 & 0 & 0 \\ 3\sqrt{6} & 0 & 0 & 0 \\ 0 & -\sqrt{2} & 0 & 0 \\ 0 & 0 & -7 & 0 \\ 0 & 0 & 0 & \sqrt{15} \end{pmatrix}, \tag{C.53}$$

$$X^\dagger_{-2} = \frac{1}{\sqrt{14}} \begin{pmatrix} 0 & 0 & 0 & 0 \\ 0 & 0 & 0 & 0 \\ 0 & 0 & 0 & 0 \\ \sqrt{6} & 0 & 0 & 0 \\ 0 & 1 & 0 & 0 \\ 0 & 0 & -\sqrt{5} & 0 \end{pmatrix}, \tag{C.54}$$

$$X^\dagger_{-3} = \frac{1}{\sqrt{28}} \begin{pmatrix} 0 & 0 & 0 & 0 \\ 0 & 0 & 0 & 0 \\ 0 & 0 & 0 & 0 \\ 0 & 0 & 0 & 0 \\ 3 & 0 & 0 & 0 \\ 0 & \sqrt{15} & 0 & 0 \end{pmatrix}, \tag{C.55}$$

C.4 Amplitudes for various spin and parity assignment

Here we, will show the explicit form of the amplitude for $\Lambda_c^* \to \Lambda_c \pi\pi$ decay.
For $\Lambda_c^*(1/2^-)$, the amplitude is given by

$$\begin{aligned}
-i\mathcal{T}(\Sigma_c^0) &= F_1\, \chi^\dagger_{\Lambda_c} (\boldsymbol{\sigma}\cdot\mathbf{p_2})\, \chi_{\Lambda_c^*} && \text{(C.56)}\\
-i\mathcal{T}(\Sigma_c^{*0}) &= F_2\, \chi^\dagger_{\Lambda_c} (\mathbf{S}\cdot\mathbf{p_2})\, (\mathbf{S}^\dagger\cdot\mathbf{p_1})(\boldsymbol{\sigma}\cdot\mathbf{p_1})\chi_{\Lambda_c^*} && \text{(C.57)}\\
-i\mathcal{T}(\Sigma_c^{++}) &= F_3\, \chi^\dagger_{\Lambda_c} (\boldsymbol{\sigma}\cdot\mathbf{p_1})\, \chi_{\Lambda_c^*} && \text{(C.58)}\\
-i\mathcal{T}(\Sigma_c^{*++}) &= F_4\, \chi^\dagger_{\Lambda_c} (\mathbf{S}\cdot\mathbf{p_1})\, (\mathbf{S}^\dagger\cdot\mathbf{p_2})(\boldsymbol{\sigma}\cdot\mathbf{p_2})\chi_{\Lambda_c^*} && \text{(C.59)}\\
-i\mathcal{T}(\text{Direct}) &= F_5\, \chi^\dagger_{\Lambda_c} (\boldsymbol{\sigma}\cdot(\mathbf{p_1}+\mathbf{p_2}))\, \chi_{\Lambda_c^*} && \text{(C.60)}
\end{aligned}$$

For $\Lambda_b^*(3/2^-)$, the amplitude is given by

$$\begin{aligned}
-i\mathcal{T}(\Sigma_c^0) &= F_1\, \chi^\dagger_{\Lambda_c} (\boldsymbol{\sigma}\cdot\mathbf{p_2})\, (\mathbf{S}^\dagger\cdot\mathbf{p_1})(\boldsymbol{\sigma}\cdot\mathbf{p_1})\chi_{\Lambda_c^*} && \text{(C.61)}\\
-i\mathcal{T}(\Sigma_c^{*0}) &= F_2\, \chi^\dagger_{\Lambda_c} (\mathbf{S}\cdot\mathbf{p_2})\, \chi_{\Lambda_c^*} && \text{(C.62)}\\
-i\mathcal{T}(\Sigma_c^{++}) &= F_3\, \chi^\dagger_{\Lambda_c} (\boldsymbol{\sigma}\cdot\mathbf{p_1})\, (\mathbf{S}^\dagger\cdot\mathbf{p_2})(\boldsymbol{\sigma}\cdot\mathbf{p_2})\chi_{\Lambda_c^*} && \text{(C.63)}\\
-i\mathcal{T}(\Sigma_c^{*++}) &= F_4\, \chi^\dagger_{\Lambda_c} (\mathbf{S}\cdot\mathbf{p_1})\, \chi_{\Lambda_c^*} && \text{(C.64)}\\
-i\mathcal{T}(\text{Direct}) &= F_5\, \chi^\dagger_{\Lambda_c} (\mathbf{S}\cdot(\mathbf{p_1}+\mathbf{p_2}))\, \chi_{\Lambda_c^*} && \text{(C.65)}
\end{aligned}$$

For $\Lambda_b^*(1/2^+)$, the amplitude is given by

$$
\begin{aligned}
-i\mathcal{T}(\Sigma_c^0) &= F_1\ \chi^\dagger_{\Lambda_c}\,(\boldsymbol{\sigma}\cdot\mathbf{p_2})\,(\boldsymbol{\sigma}\cdot\mathbf{p_1})\,\chi_{\Lambda_c^*} & \text{(C.66)}\\
-i\mathcal{T}(\Sigma_c^{*0}) &= F_2\ \chi^\dagger_{\Lambda_c}\,(\mathbf{S}\cdot\mathbf{p_2})\left(\mathbf{S}^\dagger\cdot\mathbf{p_1}\right)\chi_{\Lambda_c^*} & \text{(C.67)}\\
-i\mathcal{T}(\Sigma_c^{++}) &= F_3\ \chi^\dagger_{\Lambda_c}\,(\boldsymbol{\sigma}\cdot\mathbf{p_1})\,(\boldsymbol{\sigma}\cdot\mathbf{p_2})\,\chi_{\Lambda_c^*} & \text{(C.68)}\\
-i\mathcal{T}(\Sigma_c^{*++}) &= F_4\ \chi^\dagger_{\Lambda_c}\,(\mathbf{S}\cdot\mathbf{p_1})\left(\mathbf{S}^\dagger\cdot\mathbf{p_2}\right)\chi_{\Lambda_c^*} & \text{(C.69)}\\
-i\mathcal{T}(\text{Direct}) &= F_5\ \chi^\dagger_{\Lambda_c}\chi_{\Lambda_b^*} & \text{(C.70)}
\end{aligned}
$$

For $\Lambda_b^*(3/2^+)$, the amplitude is given by

$$
\begin{aligned}
-i\mathcal{T}(\Sigma_c^0) &= F_1\ \chi^\dagger_{\Lambda_c}\,(\boldsymbol{\sigma}\cdot\mathbf{p_2})\,(\mathbf{S}\cdot\mathbf{p_1})\,\chi_{\Lambda_c^*} & \text{(C.71)}\\
-i\mathcal{T}(\Sigma_c^{*0}) &= F_2\ \chi^\dagger_{\Lambda_c}\,(\mathbf{S}\cdot\mathbf{p_2})\,(\boldsymbol{\Sigma}\cdot\mathbf{p_1})\,\chi_{\Lambda_c^*} & \text{(C.72)}\\
-i\mathcal{T}(\Sigma_c^{++}) &= F_3\ \chi^\dagger_{\Lambda_c}\,(\boldsymbol{\sigma}\cdot\mathbf{p_1})\,(\mathbf{S}\cdot\mathbf{p_2})\,\chi_{\Lambda_c^*} & \text{(C.73)}\\
-i\mathcal{T}(\Sigma_c^{*++}) &= F_4\ \chi^\dagger_{\Lambda_c}\,(\mathbf{S}\cdot\mathbf{p_1})\,(\boldsymbol{\Sigma}\cdot\mathbf{p_2})\,\chi_{\Lambda_c^*} & \text{(C.74)}\\
-i\mathcal{T}(\text{Direct}) &= F_5\ \chi^\dagger_{\Lambda_c}(\mathbf{S}^\dagger\cdot(\mathbf{p_1}+\mathbf{p_2}))(\boldsymbol{\sigma}\cdot(\mathbf{p_1}+\mathbf{p_2}))\chi_{\Lambda_c^*} & \text{(C.75)}
\end{aligned}
$$

For $\Lambda_c^*(5/2^-)$, the amplitude is given by

$$
\begin{aligned}
-i\mathcal{T}(\Sigma_c^0) &= F_1\ \chi^\dagger_{\Lambda_c}\,(\boldsymbol{\sigma}\cdot\mathbf{p_2})\,(\mathbf{S}\cdot\mathbf{p_1})(\mathbf{T}\cdot\mathbf{p_1})\chi_{\Lambda_c^*} & \text{(C.76)}\\
-i\mathcal{T}(\Sigma_c^{*0}) &= F_2\ \chi^\dagger_{\Lambda_c}\,(\mathbf{S}\cdot\mathbf{p_2})\,(\boldsymbol{\Sigma}\cdot\mathbf{p_1})(\mathbf{T}\cdot\mathbf{p_1})\chi_{\Lambda_c^*} & \text{(C.77)}\\
-i\mathcal{T}(\Sigma_c^{++}) &= F_3\ \chi^\dagger_{\Lambda_c}\,(\boldsymbol{\sigma}\cdot\mathbf{p_1})\,(\mathbf{S}\cdot\mathbf{p_2})(\mathbf{T}\cdot\mathbf{p_2})\chi_{\Lambda_b^*} & \text{(C.78)}\\
-i\mathcal{T}(\Sigma_c^{*++}) &= F_4\ \chi^\dagger_{\Lambda_c}\,(\mathbf{S}\cdot\mathbf{p_1})\,(\boldsymbol{\Sigma}\cdot\mathbf{p_2})(\mathbf{T}\cdot\mathbf{p_2})\chi_{\Lambda_c^*} & \text{(C.79)}\\
-i\mathcal{T}(\text{Direct}) &= F_5\ \chi^\dagger_{\Lambda_c}(\boldsymbol{\sigma}\cdot(\mathbf{p_1}+\mathbf{p_2}))(\mathbf{S}\cdot(\mathbf{p_1}+\mathbf{p_2}))(\mathbf{T}\cdot(\mathbf{p_1}+\mathbf{p_2}))\chi_{\Lambda_c^*} & \text{(C.80)}
\end{aligned}
$$

For $\Lambda_c^*(5/2^+)$, the amplitude is given by

$$
\begin{aligned}
-i\mathcal{T}(\Sigma_c^0) &= F_1\ \chi^\dagger_{\Lambda_c}\,(\boldsymbol{\sigma}\cdot\mathbf{p_2})\,(\boldsymbol{\sigma}\cdot\mathbf{p_1})\,(\mathbf{S}\cdot\mathbf{p_1})\,(\mathbf{T}\cdot\mathbf{p_1})\,\chi_{\Lambda_c^*} & \text{(C.81)}\\
-i\mathcal{T}(\Sigma_c^{*0}) &= F_2\ \chi^\dagger_{\Lambda_c}\,(\mathbf{S}\cdot\mathbf{p_2})\,(\mathbf{T}\cdot\mathbf{p_1})\,\chi_{\Lambda_c^*} & \text{(C.82)}\\
-i\mathcal{T}(\Sigma_c^{++}) &= F_3\ \chi^\dagger_{\Lambda_c}\,(\boldsymbol{\sigma}\cdot\mathbf{p_1})\,(\boldsymbol{\sigma}\cdot\mathbf{p_2})\,(\mathbf{S}\cdot\mathbf{p_2})\,(\mathbf{T}\cdot\mathbf{p_2})\,\chi_{\Lambda_c^*} & \text{(C.83)}\\
-i\mathcal{T}(\Sigma_c^{*++}) &= F_4\ \chi^\dagger_{\Lambda_c}\,(\mathbf{S}\cdot\mathbf{p_1})\,(\mathbf{T}\cdot\mathbf{p_2})\,\chi_{\Lambda_c^*} & \text{(C.84)}\\
-i\mathcal{T}(\text{Direct}) &= F_5\ \chi^\dagger_{\Lambda_c}(\mathbf{S}\cdot(\mathbf{p_1}+\mathbf{p_2}))(\mathbf{T}\cdot(\mathbf{p_1}+\mathbf{p_2}))\chi_{\Lambda_c^*} & \text{(C.85)}
\end{aligned}
$$

We have defined the coupling F_i for each amplitude which consists of the coupling strength and the Breit-Wigner function for sequential decay. For the cross diagrams, we can also obtain the amplitude by changing the $\mathbf{p_1}\to\mathbf{p_2}$, $\mathbf{p_2}\to\mathbf{p_1}$, and $m_{23}\to m_{13}$. The higher partial wave for certain process is neglected. For example $\Lambda_c^*(3/2^-)\to\Sigma_c^*\pi$ in D-wave is neglected. It is because the contribution is very small compared with that of S-wave.

C.5 Squared amplitudes

For $\Lambda_c^*(1/2^-)$, we only consider Σ_c sequential process and direct process. Then, we have the squared amplitude (spin averaged) as

$$\overline{|\mathcal{T}_1|^2} = |F_1|^2|\mathbf{p_2}|^2 \tag{C.86}$$
$$\overline{|\mathcal{T}_2|^2} = \frac{1}{9}|F_2|^2|\mathbf{p_1}|^2\Big(3(\mathbf{p}_1\cdot\mathbf{p}_2)^2+|\mathbf{p}_1|^2\ |\mathbf{p}_2|^2\Big) \tag{C.87}$$
$$\overline{|\mathcal{T}_3|^2} = |F_3|^2|\mathbf{p_1}|^2 \tag{C.88}$$
$$\overline{|\mathcal{T}_4|^2} = \frac{1}{9}|F_4|^2|\mathbf{p_2}|^2\Big(3(\mathbf{p}_1\cdot\mathbf{p}_2)^2+|\mathbf{p}_1|^2\ |\mathbf{p}_2|^2\Big) \tag{C.89}$$
$$\overline{|\mathcal{T}_5|^2} = |F_5|^2\left(|\mathbf{p_1}|^2+|\mathbf{p_2}|^2+2\mathbf{p_1}\cdot\mathbf{p_2}\right) \tag{C.90}$$
$$\overline{|\mathcal{T}_1\mathcal{T}_2^*|} = \frac{1}{3}F_1F_2^*\ \Big(3(\mathbf{p}_1\cdot\mathbf{p}_2)^2-|\mathbf{p}_1|^2\ |\mathbf{p}_2|^2\Big) \tag{C.91}$$
$$\overline{|\mathcal{T}_3\mathcal{T}_4^*|} = \frac{1}{3}F_3F_4^*\ \Big(3(\mathbf{p}_1\cdot\mathbf{p}_2)^2-|\mathbf{p}_1|^2\ |\mathbf{p}_2|^2\Big) \tag{C.92}$$
$$\overline{|\mathcal{T}_1\mathcal{T}_4^*|} = \frac{2}{3}F_1F_4^*\ (\mathbf{p}_1\cdot\mathbf{p}_2)|\mathbf{p}_2|^2 \tag{C.93}$$
$$\overline{|\mathcal{T}_2\mathcal{T}_3^*|} = \frac{2}{3}F_2F_3^*\ (\mathbf{p}_1\cdot\mathbf{p}_2)|\mathbf{p}_1|^2 \tag{C.94}$$
$$\overline{|\mathcal{T}_1\mathcal{T}_3^*|} = F_1F_3^*\ (\mathbf{p}_1\cdot\mathbf{p}_2) \tag{C.95}$$
$$\overline{|\mathcal{T}_2\mathcal{T}_4^*|} = \frac{1}{9}F_2F_4^*\ (\mathbf{p}_1\cdot\mathbf{p}_2)\Big(9(\mathbf{p}_1\cdot\mathbf{p}_2)^2-5|\mathbf{p}_1|^2\ |\mathbf{p}_2|^2\Big) \tag{C.96}$$
$$\overline{|\mathcal{T}_1\mathcal{T}_5^*|} = F_1F_5^*\ \left(|\mathbf{p}_2|^2+\mathbf{p}_1\cdot\mathbf{p}_2\right) \tag{C.97}$$
$$\overline{|\mathcal{T}_2\mathcal{T}_5^*|} = \frac{1}{3}F_2F_5^*\ \left(2|\mathbf{p}_1|^2(\mathbf{p}_1\cdot\mathbf{p}_2)+3(\mathbf{p}_1\cdot\mathbf{p}_2)^2-|\mathbf{p}_1|^2\ |\mathbf{p}_2|^2\right) \tag{C.98}$$
$$\overline{|\mathcal{T}_3\mathcal{T}_5^*|} = F_3F_5^*\ \left(|\mathbf{p}_1|^2+\mathbf{p}_1\cdot\mathbf{p}_2\right) \tag{C.99}$$
$$\overline{|\mathcal{T}_4\mathcal{T}_5^*|} = \frac{1}{3}F_4F_5^*\ \left(2|\mathbf{p}_2|^2(\mathbf{p}_1\cdot\mathbf{p}_2)+3(\mathbf{p}_1\cdot\mathbf{p}_2)^2-|\mathbf{p}_1|^2\ |\mathbf{p}_2|^2\right) \tag{C.100}$$

For $\Lambda_b^*(1/2^+)$, we only consider Σ_c and Σ_c^* sequential processes. We ignore direct process for the simplicity. Then, we have the squared amplitude (spin averaged) as

$$\overline{|\mathcal{T}_1|^2} = |F_1|^2|\mathbf{p_1}|^2|\mathbf{p_2}|^2 \tag{C.101}$$
$$\overline{|\mathcal{T}_2|^2} = \frac{1}{9}|F_2|^2 \left(3(\mathbf{p}_1 \cdot \mathbf{p}_2)^2 + |\mathbf{p}_1|^2 \ |\mathbf{p}_2|^2\right) \tag{C.102}$$
$$\overline{|\mathcal{T}_3|^2} = |F_3|^2|\mathbf{p_1}|^2|\mathbf{p_2}|^2 \tag{C.103}$$
$$\overline{|\mathcal{T}_4|^2} = \frac{1}{9}|F_4|^2 \left(3(\mathbf{p}_1 \cdot \mathbf{p}_2)^2 + |\mathbf{p}_1|^2 \ |\mathbf{p}_2|^2\right) \tag{C.104}$$
$$\overline{|\mathcal{T}_5|^2} = |F_5|^2 \tag{C.105}$$
$$\overline{|\mathcal{T}_1\mathcal{T}_2^*|} = \frac{1}{3}F_1F_2^* \left(3(\mathbf{p}_1 \cdot \mathbf{p}_2)^2 - |\mathbf{p}_1|^2 \ |\mathbf{p}_2|^2\right) \tag{C.106}$$
$$\overline{|\mathcal{T}_3\mathcal{T}_4^*|} = \frac{1}{3}F_3F_4^* \left(3(\mathbf{p}_1 \cdot \mathbf{p}_2)^2 - |\mathbf{p}_1|^2 \ |\mathbf{p}_2|^2\right) \tag{C.107}$$
$$\overline{|\mathcal{T}_1\mathcal{T}_4^*|} = \frac{1}{3}F_1F_4^* \left((\mathbf{p}_1 \cdot \mathbf{p}_2)^2 + |\mathbf{p}_1|^2 \ |\mathbf{p}_2|^2\right) \tag{C.108}$$
$$\overline{|\mathcal{T}_2\mathcal{T}_3^*|} = \frac{1}{3}F_2F_3^* \left((\mathbf{p}_1 \cdot \mathbf{p}_2)^2 + |\mathbf{p}_1|^2 \ |\mathbf{p}_2|^2\right) \tag{C.109}$$
$$\overline{|\mathcal{T}_1\mathcal{T}_3^*|} = F_1F_3^* \left(2(\mathbf{p}_1 \cdot \mathbf{p}_2)^2 - |\mathbf{p}_1|^2 \ |\mathbf{p}_2|^2\right) \tag{C.110}$$
$$\overline{|\mathcal{T}_2\mathcal{T}_4^*|} = \frac{1}{9}F_2F_4^* \left(5(\mathbf{p}_1 \cdot \mathbf{p}_2)^2 - |\mathbf{p}_1|^2 \ |\mathbf{p}_2|^2\right) \tag{C.111}$$
$$\overline{|\mathcal{T}_1\mathcal{T}_5^*|} = F_1F_5^* \ (\mathbf{p}_1 \cdot \mathbf{p}_2) \tag{C.112}$$
$$\overline{|\mathcal{T}_3\mathcal{T}_5^*|} = F_3F_5^* \ (\mathbf{p}_1 \cdot \mathbf{p}_2) \tag{C.113}$$
$$\overline{|\mathcal{T}_2\mathcal{T}_5^*|} = \frac{2}{3} \ F_2F_5^* \ (\mathbf{p}_1 \cdot \mathbf{p}_2) \tag{C.114}$$
$$\overline{|\mathcal{T}_4\mathcal{T}_5^*|} = \frac{2}{3} \ F_4F_5^* \ (\mathbf{p}_1 \cdot \mathbf{p}_2) \tag{C.115}$$

For $\Lambda_c^*(3/2^-)$, we consider Σ_c and Σ_c^* sequential processes and direct process. Thus, we have

$$
\begin{aligned}
\overline{|\mathcal{T}_1|^2} &= \frac{1}{3}\,|F_1|^2\ |\mathbf{p}_1|^4\ |\mathbf{p}_2|^2 && \text{(C.116)}\\
\overline{|\mathcal{T}_2|^2} &= \frac{1}{3}\,|F_2|^2\ |\mathbf{p}_2|^2 && \text{(C.117)}\\
\overline{|\mathcal{T}_3|^2} &= \frac{1}{3}\,|F_3|^2\ |\mathbf{p}_2|^4\ |\mathbf{p}_1|^2 && \text{(C.118)}\\
\overline{|\mathcal{T}_4|^2} &= \frac{1}{3}\,|F_4|^2\ |\mathbf{p}_1|^2 && \text{(C.119)}\\
\overline{|\mathcal{T}_5|^2} &= \frac{1}{3}\,|F_5|^2\ \left(|\mathbf{p}_1|^2+|\mathbf{p}_2|^2+2\mathbf{p}_1\cdot\mathbf{p}_2\right) && \text{(C.120)}\\
\overline{|\mathcal{T}_1\mathcal{T}_2^*|} &= \frac{1}{6}\,F_1F_2^*\ \Big(3(\mathbf{p}_1\cdot\mathbf{p}_2)^2-|\mathbf{p}_1|^2\ |\mathbf{p}_2|^2\Big) && \text{(C.121)}\\
\overline{|\mathcal{T}_3\mathcal{T}_4^*|} &= \frac{1}{6}\,F_3F_4^*\ \Big(3(\mathbf{p}_1\cdot\mathbf{p}_2)^2-|\mathbf{p}_1|^2\ |\mathbf{p}_2|^2\Big) && \text{(C.122)}\\
\overline{|\mathcal{T}_1\mathcal{T}_4^*|} &= \frac{1}{3}\,F_1F_4^*\ |\mathbf{p}_1|^2(\mathbf{p}_1\cdot\mathbf{p}_2) && \text{(C.123)}\\
\overline{|\mathcal{T}_2\mathcal{T}_3^*|} &= \frac{1}{3}\,F_2F_3^*\ |\mathbf{p}_2|^2(\mathbf{p}_1\cdot\mathbf{p}_2) && \text{(C.124)}\\
\overline{|\mathcal{T}_1\mathcal{T}_3^*|} &= \frac{1}{3}\,F_1F_3^*\ \left(3(\mathbf{p}_1\cdot\mathbf{p}_2)^2-2|\mathbf{p}_1|^2|\mathbf{p}_2|^2\right)(\mathbf{p}_1\cdot\mathbf{p}_2) && \text{(C.125)}\\
\overline{|\mathcal{T}_2\mathcal{T}_4^*|} &= \frac{1}{6}\,F_2F_4^*\ \mathbf{p}_1\cdot\mathbf{p}_2 && \text{(C.126)}\\
\overline{|\mathcal{T}_1\mathcal{T}_5^*|} &= \frac{1}{2}\,F_1F_5^*\ \Big(2|\mathbf{p}_1|^2\mathbf{p}_1\cdot\mathbf{p}_2+\Big(3(\mathbf{p}_1\cdot\mathbf{p}_2)^2-2|\mathbf{p}_1|^2|\mathbf{p}_2|^2\Big)\Big) && \text{(C.127)}\\
\overline{|\mathcal{T}_3\mathcal{T}_5^*|} &= \frac{1}{2}\,F_3F_5^*\ \Big(2|\mathbf{p}_2|^2\mathbf{p}_1\cdot\mathbf{p}_2+\Big(3(\mathbf{p}_1\cdot\mathbf{p}_2)^2-2|\mathbf{p}_1|^2|\mathbf{p}_2|^2\Big)\Big) && \text{(C.128)}\\
\overline{|\mathcal{T}_2\mathcal{T}_5^*|} &= \frac{1}{6}\,F_2F_5^*\ \left(|\mathbf{p}_2|^2+\mathbf{p}_1\cdot\mathbf{p}_2\right) && \text{(C.129)}\\
\overline{|\mathcal{T}_4\mathcal{T}_5^*|} &= \frac{1}{6}\,F_4F_5^*\ \left(|\mathbf{p}_1|^2+\mathbf{p}_1\cdot\mathbf{p}_2\right) && \text{(C.130)}
\end{aligned}
$$

For $\Lambda_c^*(3/2^+)$, we only consider Σ_c and Σ_c^*, but we ignore direct process.

$$\overline{|\mathcal{T}_1|^2} = \frac{1}{3}|F_1|^2|\mathbf{p_1}|^2|\mathbf{p_2}|^2 \tag{C.131}$$

$$\overline{|\mathcal{T}_2|^2} = \frac{1}{3}|F_2|^2 \left(7|\mathbf{p}_1|^2\ |\mathbf{p}_2|^2 - 6(\mathbf{p}_1\cdot\mathbf{p}_2)^2\right) \tag{C.132}$$

$$\overline{|\mathcal{T}_3|^2} = \frac{1}{3}|F_3|^2|\mathbf{p_1}|^2|\mathbf{p_2}|^2 \tag{C.133}$$

$$\overline{|\mathcal{T}_4|^2} = \frac{1}{3}|F_4|^2 \left(7|\mathbf{p}_1|^2\ |\mathbf{p}_2|^2 - 6(\mathbf{p}_1\cdot\mathbf{p}_2)^2\right) \tag{C.134}$$

$$\overline{|\mathcal{T}_5|^2} = \frac{1}{3}|F_5|^2\ \left(|\mathbf{p}_1|^2 + |\mathbf{p}_2|^2 + 2\mathbf{p}_1\cdot\mathbf{p}_2\right)^2 \tag{C.135}$$

$$\overline{|\mathcal{T}_1\mathcal{T}_2^*|} = \frac{1}{6}F_1F_2^* \left(3(\mathbf{p}_1\cdot\mathbf{p}_2)^2 - |\mathbf{p}_1|^2\ |\mathbf{p}_2|^2\right) \tag{C.136}$$

$$\overline{|\mathcal{T}_3\mathcal{T}_4^*|} = \frac{1}{6}F_3F_4^* \left(3(\mathbf{p}_1\cdot\mathbf{p}_2)^2 - |\mathbf{p}_1|^2\ |\mathbf{p}_2|^2\right) \tag{C.137}$$

$$\overline{|\mathcal{T}_1\mathcal{T}_4^*|} = \frac{1}{3}F_1F_4^* \left(2|\mathbf{p}_1|^2\ |\mathbf{p}_2|^2 - (\mathbf{p}_1\cdot\mathbf{p}_2)^2\right) \tag{C.138}$$

$$\overline{|\mathcal{T}_2\mathcal{T}_3^*|} = \frac{1}{3}F_2F_3^* \left(2|\mathbf{p}_1|^2\ |\mathbf{p}_2|^2 - (\mathbf{p}_1\cdot\mathbf{p}_2)^2\right) \tag{C.139}$$

$$\overline{|\mathcal{T}_1\mathcal{T}_3^*|} = \frac{1}{6}F_1F_3^* \left((\mathbf{p}_1\cdot\mathbf{p}_2)^2 + |\mathbf{p}_1|^2\ |\mathbf{p}_2|^2\right) \tag{C.140}$$

$$\overline{|\mathcal{T}_2\mathcal{T}_4^*|} = \frac{1}{9}F_2F_4^* \left(5(\mathbf{p}_1\cdot\mathbf{p}_2)^2 - |\mathbf{p}_1|^2\ |\mathbf{p}_2|^2\right) \tag{C.141}$$

$$\overline{|\mathcal{T}_1\mathcal{T}_5^*|} = \frac{1}{6}F_1F_5^* \left(2\left(|\mathbf{p}_1|^2 + |\mathbf{p}_2|^2\right)(\mathbf{p}_1\cdot\mathbf{p}_2) + (\mathbf{p}_1\cdot\mathbf{p}_2)^2 + 3|\mathbf{p}_1|^2\ |\mathbf{p}_2|^2\right) \tag{C.142}$$

$$\overline{|\mathcal{T}_2\mathcal{T}_5^*|} = \frac{1}{6}F_2F_5^* \left(2\left(|\mathbf{p}_1|^2 + |\mathbf{p}_2|^2\right)(\mathbf{p}_1\cdot\mathbf{p}_2) + (\mathbf{p}_1\cdot\mathbf{p}_2)^2 + 3|\mathbf{p}_1|^2\ |\mathbf{p}_2|^2\right) \tag{C.143}$$

$$\overline{|\mathcal{T}_3\mathcal{T}_5^*|} = \frac{1}{6}F_3F_5^* \left(2\left(|\mathbf{p}_1|^2 + |\mathbf{p}_2|^2\right)(\mathbf{p}_1\cdot\mathbf{p}_2) + (\mathbf{p}_1\cdot\mathbf{p}_2)^2 + 3|\mathbf{p}_1|^2\ |\mathbf{p}_2|^2\right) \tag{C.144}$$

$$\overline{|\mathcal{T}_4\mathcal{T}_5^*|} = \frac{1}{6}F_4F_5^* \left(2\left(|\mathbf{p}_1|^2 + |\mathbf{p}_2|^2\right)(\mathbf{p}_1\cdot\mathbf{p}_2) + (\mathbf{p}_1\cdot\mathbf{p}_2)^2 + 3|\mathbf{p}_1|^2\ |\mathbf{p}_2|^2\right) \tag{C.145}$$

For $\Lambda_c^*(5/2^-)$, we only consider Σ_c and Σ_c^* and direct process.

$$\overline{|\mathcal{T}_1|^2} = \frac{4}{30}|F_1|^2|\mathbf{p_1}|^4|\mathbf{p_2}|^2 \tag{C.146}$$

$$\overline{|\mathcal{T}_2|^2} = \frac{1}{30}|F_2|^2 \ |\mathbf{p_1}|^2\Big(19|\mathbf{p}_1|^2 \ |\mathbf{p}_2|^2 - 15(\mathbf{p}_1\cdot\mathbf{p}_2)^2\Big) \tag{C.147}$$

$$\overline{|\mathcal{T}_3|^2} = \frac{4}{30}|F_3|^2|\mathbf{p_1}|^2|\mathbf{p_2}|^4 \tag{C.148}$$

$$\overline{|\mathcal{T}_4|^2} = \frac{1}{30}|F_4|^2 \ |\mathbf{p_2}|^2\Big(19|\mathbf{p}_1|^2 \ |\mathbf{p}_2|^2 - 15(\mathbf{p}_1\cdot\mathbf{p}_2)^2\Big) \tag{C.149}$$

$$\overline{|\mathcal{T}_1\mathcal{T}_2^*|} = \frac{2}{30}F_1F_2^* \ |\mathbf{p_1}|^2\Big(3(\mathbf{p}_1\cdot\mathbf{p}_2)^2 - |\mathbf{p}_1|^2 \ |\mathbf{p}_2|^2\Big) \tag{C.150}$$

$$\overline{|\mathcal{T}_3\mathcal{T}_4^*|} = \frac{2}{30}F_3F_4^* \ |\mathbf{p_2}|^2\Big(3(\mathbf{p}_1\cdot\mathbf{p}_2)^2 - |\mathbf{p}_1|^2 \ |\mathbf{p}_2|^2\Big) \tag{C.151}$$

$$\overline{|\mathcal{T}_1\mathcal{T}_4^*|} = \frac{4}{30}F_1F_4^* \ (\mathbf{p}_1\cdot\mathbf{p}_2)\Big(2|\mathbf{p}_1|^2 \ |\mathbf{p}_2|^2 - (\mathbf{p}_1\cdot\mathbf{p}_2)^2\Big) \tag{C.152}$$

$$\overline{|\mathcal{T}_2\mathcal{T}_3^*|} = \frac{4}{30}F_2F_3^* \ (\mathbf{p}_1\cdot\mathbf{p}_2)\Big(2|\mathbf{p}_1|^2 \ |\mathbf{p}_2|^2 - (\mathbf{p}_1\cdot\mathbf{p}_2)^2\Big) \tag{C.153}$$

$$\overline{|\mathcal{T}_1\mathcal{T}_3^*|} = \frac{2}{30}F_1F_3^* \ (\mathbf{p}_1\cdot\mathbf{p}_2)\Big((\mathbf{p}_1\cdot\mathbf{p}_2)^2 + |\mathbf{p}_1|^2 \ |\mathbf{p}_2|^2\Big) \tag{C.154}$$

$$\overline{|\mathcal{T}_2\mathcal{T}_4^*|} = \frac{1}{30}F_2F_4^* \ (\mathbf{p}_1\cdot\mathbf{p}_2)\Big(17(\mathbf{p}_1\cdot\mathbf{p}_2)^2 - 13|\mathbf{p}_1|^2 \ |\mathbf{p}_2|^2\Big) \tag{C.155}$$

For $\Lambda_c^*(5/2^+)$, we only consider Σ_c and Σ_c^* and direct process.

$$\overline{|\mathcal{T}_1|^2} = \frac{4}{30}|F_1|^2|\mathbf{p_1}|^6|\mathbf{p_2}|^2 \tag{C.156}$$

$$\overline{|\mathcal{T}_2|^2} = \frac{1}{30}|F_2|^2 \ \Big(3|\mathbf{p}_1|^2 \ |\mathbf{p}_2|^2 + (\mathbf{p}_1\cdot\mathbf{p}_2)^2\Big) \tag{C.157}$$

$$\overline{|\mathcal{T}_3|^2} = \frac{4}{30}|F_3|^2|\mathbf{p_1}|^2|\mathbf{p_2}|^6 \tag{C.158}$$

$$\overline{|\mathcal{T}_4|^2} = \frac{1}{30}|F_4|^2 \ \Big(3|\mathbf{p}_1|^2 \ |\mathbf{p}_2|^2 + (\mathbf{p}_1\cdot\mathbf{p}_2)^2\Big) \tag{C.159}$$

$$\overline{|\mathcal{T}_1\mathcal{T}_2^*|} = \frac{2}{30}F_1F_2^* \ |\mathbf{p}_1|^2\Big(3(\mathbf{p}_1\cdot\mathbf{p}_2)^2 - |\mathbf{p}_1|^2 \ |\mathbf{p}_2|^2\Big) \tag{C.160}$$

$$\overline{|\mathcal{T}_3\mathcal{T}_4^*|} = \frac{2}{30}F_3F_4^* \ |\mathbf{p}_2|^2\Big(3(\mathbf{p}_1\cdot\mathbf{p}_2)^2 - |\mathbf{p}_1|^2 \ |\mathbf{p}_2|^2\Big) \tag{C.161}$$

$$\overline{|\mathcal{T}_1\mathcal{T}_4^*|} = \frac{2}{30}F_1F_4^* \ |\mathbf{p}_1|^2\Big(3(\mathbf{p}_1\cdot\mathbf{p}_2)^2 - |\mathbf{p}_1|^2 \ |\mathbf{p}_2|^2\Big) \tag{C.162}$$

$$\overline{|\mathcal{T}_2\mathcal{T}_3^*|} = \frac{2}{30}F_2F_3^* \ |\mathbf{p}_2|^2\Big(3(\mathbf{p}_1\cdot\mathbf{p}_2)^2 - |\mathbf{p}_1|^2 \ |\mathbf{p}_2|^2\Big) \tag{C.163}$$

$$\overline{|\mathcal{T}_1\mathcal{T}_3^*|} = \frac{2}{30}F_1F_3^* \ \Big(|\mathbf{p}_1|^4|\mathbf{p}_2|^4 + (\mathbf{p}_1\cdot\mathbf{p}_2)^2(10(\mathbf{p}_1\cdot\mathbf{p}_2)^2 - 9|\mathbf{p}_1|^2|\mathbf{p}_2|^2)\Big) \tag{C.164}$$

$$\overline{|\mathcal{T}_2\mathcal{T}_4^*|} = \frac{1}{30}F_2F_4^* \ \Big(3(\mathbf{p}_1\cdot\mathbf{p}_2)^2 + |\mathbf{p}_1|^2 \ |\mathbf{p}_2|^2\Big) \tag{C.165}$$

References

[1] M. Tanabashi *et al.* (Particle Data Group), *Review of particle physics*, Phys. Rev. D **98**, 030001 (2018).

[2] M. Gell-Mann, *A Schematic Model of Baryons and Mesons*, Phys. Lett. **8**, 214 (1964).

[3] H.-X. Chen, W. Chen, X. Liu, Y.-R. Liu, and S.-L. Zhu, *A review of the open charm and open bottom systems*, Rept. Prog. Phys. **80**, 076201 (2017), arXiv:1609.08928 [hep-ph] .

[4] M. Neubert, *Heavy quark symmetry*, Phys. Rept. **245**, 259 (1994), arXiv:hep-ph/9306320 .

[5] A. Hosaka, T. Iijima, K. Miyabayashi, Y. Sakai, and S. Yasui, *Exotic hadrons with heavy flavors: X, Y, Z, and related states*, PTEP **2016**, 062C01 (2016), arXiv:1603.09229 [hep-ph] .

[6] H.-X. Chen, W. Chen, X. Liu, and S.-L. Zhu, *The hidden-charm pentaquark and tetraquark states*, Phys. Rept. **639**, 1 (2016), arXiv:1601.02092 [hep-ph] .

[7] R. Aaij *et al.* (LHCb), *Observation of $J/\psi p$ resonances consistent with pentaquark states in $\Lambda_b^0 \to J/\psi K^- p$ decays*, Phys. Rev. Lett. **115**, 072001 (2015), arXiv:1507.03414 [hep-ex] .

[8] R. Aaij *et al.* (LHCb), *Observation of a narrow pentaquark state, $P_c(4312)^+$, and of two-peak structure of the $P_c(4450)^+$*, Phys. Rev. Lett. **122**, 222001 (2019), arXiv:1904.03947 [hep-ex] .

[9] J. Korner, M. Kramer, and D. Pirjol, *Heavy baryons*, Prog. Part. Nucl. Phys. **33**, 787 (1994), arXiv:hep-ph/9406359 .

[10] E. Klempt and J.-M. Richard, *Baryon spectroscopy*, Rev. Mod. Phys. **82**, 1095 (2010), arXiv:0901.2055 [hep-ph] .

[11] V. Crede and W. Roberts, *Progress towards understanding baryon resonances*, Rept. Prog. Phys. **76**, 076301 (2013), arXiv:1302.7299 [nucl-ex] .

[12] A. Bevan *et al.* (BaBar, Belle), *The physics of the B factories*, Eur. Phys. J. C **74**, 3026 (2014), arXiv:1406.6311 [hep-ex] .

[13] H.-Y. Cheng, *Charmed baryons circa 2015*, Front. Phys. (Beijing) **10**, 101406 (2015).

[14] W. Altmannshofer *et al.* (Belle-II), *The Belle II physics book*, PTEP **2019**, 123C01 (2019), [Erratum: PTEP 2020, 029201 (2020)], arXiv:1808.10567 [hep-ex] .

[15] Y. Kato and T. Iijima, *Open charm hadron spectroscopy at B-factories*, Prog. Part. Nucl. Phys. **105**, 61 (2019), arXiv:1810.03748 [hep-ex] .

[16] D. Boutigny *et al.* (BaBar), *The BABAR physics book: Physics at an asymmetric B factory* (1998).

[17] B. Knapp *et al.*, *Observation of a narrow anti-baryon state at 2.26-GeV/c^2*, Phys. Rev. Lett. **37**, 882 (1976).

[18] B. Aubert *et al.* (BaBar), *A precision measurement of the Λ_c^+ baryon mass*, Phys. Rev. D **72**, 052006 (2005), arXiv:hep-ex/0507009 .

[19] H. Albrecht *et al.* (ARGUS), *Observation of a new charmed baryon*, Phys. Lett. B **317**, 227 (1993).

[20] H. Albrecht *et al.* (ARGUS), *Evidence for $\Lambda_c^+(2593)$ production*, Phys. Lett. B **402**, 207 (1997).

[21] P. Frabetti *et al.* (E687), *An observation of an excited state of the Λ_c^+ baryon*, Phys. Rev. Lett. **72**, 961 (1994).

[22] P. Frabetti *et al.* (E687), *Study of higher mass charm baryons decaying to Λ_c^+*, Phys. Lett. B **365**, 461 (1996).

[23] K. Edwards *et al.* (CLEO), *Observation of excited baryon states decaying to $\Lambda_c^+\pi^+\pi^-$*, Phys. Rev. Lett. **74**, 3331 (1995).

[24] T. Aaltonen *et al.* (CDF), *Measurements of the properties of $\Lambda_c(2595)$, $\Lambda_c(2625)$, $\Sigma_c(2455)$, and $\Sigma_c(2520)$ baryons*, Phys. Rev. D **84**, 012003 (2011), arXiv:1105.5995 [hep-ex] .

[25] M. Niiyama *et al.* (Belle), *Production cross sections of hyperons and charmed baryons from e^+e^- annihilation near $\sqrt{s} = 10.52$ ˜GeV*, Phys. Rev. D **97**, 072005 (2018), arXiv:1706.06791 [hep-ex] .

[26] M. Artuso *et al.* (CLEO), *Observation of new states decaying into $\Lambda_c^+\pi^-\pi^+$*, Phys. Rev. Lett. **86**, 4479 (2001), arXiv:hep-ex/0010080 .

[27] R. Aaij *et al.* (LHCb), *Study of the D^0p amplitude in $\Lambda_b^0 \to D^0p\pi^-$ decays*, JHEP. **05**, 030 (2017), arXiv:1701.07873 [hep-ex] .

[28] B. Aubert *et al.* (BaBar), *Observation of a charmed baryon decaying to D^0p at a mass near 2.94-GeV/c^2*, Phys. Rev. Lett. **98**, 012001 (2007), arXiv:hep-ex/0603052 .

[29] R. Mizuk *et al.* (Belle), *Experimental constraints on the possible J^P quantum numbers of the $\Lambda_c(2880)^+$*, Phys. Rev. Lett. **98**, 262001 (2007), arXiv:hep-ex/0608043 .

[30] A. Abdesselam *et al.* (Belle), in *18th International Conference on Hadron Spectroscopy and Structure* (2019) arXiv:1908.06235 [hep-ex] .

[31] C. Joo, Y. Kato, K. Tanida, and Y. Kato, *Study of spin-parity of the $\Lambda_c(2765)^+$*, PoS **Hadron2013**, 201 (2013).

[32] E. Cazzoli, A. Cnops, P. Connolly, R. Louttit, M. Murtagh, R. Palmer, N. Samios, T. Tso, and H. Williams, *Evidence for $\Delta S = -\Delta Q$ currents or charmed baryon production by neutrinos*, Phys. Rev. Lett. **34**, 1125 (1975).

[33] M. Calicchio *et al.* (BEBC TST Neutrino), *First observation of the production and decay of the Σ_c^+*, Phys. Lett. B **93**, 521 (1980).

[34] T. Bowcock *et al.* (CLEO), *Σ_c^{++} and Σ_c^0 production from e^+e^- annihilation in the Υ energy region*, Phys. Rev. Lett. **62**, 1240 (1989).

[35] M. Diesburg *et al.*, *Measurements of the $\Sigma_c^0 - \Lambda_c^+$ and $\Sigma_c^{++} - \Lambda_c^+$ mass differences*, Phys. Rev. Lett. **59**, 2711 (1987).

[36] H. Albrecht *et al.* (ARGUS), *Observation of the charmed baryon Σ_c in e^+e^- annihilations*, Phys. Lett. B **211**, 489 (1988).

[37] J. Anjos *et al.* (TPS), *Observation of $\Sigma_c^0 \to \Lambda_c^+\pi^-$ decays*, Phys. Rev. Lett. **62**, 1721 (1989).

[38] M. Artuso *et al.* (CLEO), *Measurement of the masses and widths of the Σ_c^{++} and Σ_c^0 charmed baryons*, Phys. Rev. D **65**, 071101 (2002), arXiv:hep-ex/0110071 .

[39] R. Ammar *et al.* (CLEO), *First observation of the Σ_c^{*+} baryon and a new measurement of the Σ_c^+ mass*, Phys. Rev. Lett. **86**, 1167 (2001), arXiv:hep-ex/0007041 .

[40] G. D. Crawford *et al.* (CLEO), *Observation of the charmed baryon Σ_c^+ and measurement of the isospin mass splittings of the Σ_c*, Phys. Rev. Lett. **71**, 3259 (1993).

[41] E. Aitala *et al.* (E791), *Mass splitting and production of Σ_c^0 and Σ_c^{++} measured in 500-GeV $\pi - n$ interactions*, Phys. Lett. B **379**, 292 (1996), arXiv:hep-ex/9604007 .

[42] J. Link *et al.* (FOCUS), *Measurements of the Σ_c^0 and Σ_c^{++} mass splittings*, Phys. Lett. B **488**, 218 (2000), arXiv:hep-ex/0005011 .

[43] J. Link *et al.* (FOCUS), *Measurement of natural widths of Σ_c^0 and Σ_c^{++} baryons*, Phys. Lett. B **525**, 205 (2002), arXiv:hep-ex/0111027 .

[44] S. Lee *et al.* (Belle), *Measurements of the masses and widths of the $\Sigma_c(2455)^{0/++}$ and $\Sigma_c(2520)^{0/++}$ baryons*, Phys. Rev. D **89**, 091102 (2014), arXiv:1404.5389 [hep-ex] .

[45] B. Aubert *et al.* (BaBar), *Measurements of $\mathcal{B}(\bar{B}^0 \to \Lambda_c^+\bar{p})$ and $\mathcal{B}(B^- \to \Lambda_c^+\bar{p}\pi^-)$ and studies of $\Lambda_c^+\pi^-$ resonances*, Phys. Rev. D **78**, 112003 (2008), arXiv:0807.4974 [hep-ex] .

[46] V. Ammosov *et al.*, *Observation of the production of charmed Σ_c^{*++} baryons in neutrino interactions at the SKAT bubble chamber*, JETP Lett. **58**, 247 (1993).

[47] G. Brandenburg *et al.* (CLEO), *Observation of two excited charmed baryons decaying into $\Lambda_c^+\pi^\pm$*, Phys. Rev. Lett. **78**, 2304 (1997).

[48] R. Mizuk *et al.* (Belle), *Observation of an isotriplet of excited charmed baryons decaying to* $\Lambda_c^+\pi$, Phys. Rev. Lett. **94**, 122002 (2005), arXiv:hep-ex/0412069 .

[49] S. Athar *et al.* (CLEO), *A new measurement of the masses and widths of the* Σ_c^{*++} *and* Σ_c^{*0} *charmed baryons*, Phys. Rev. D **71**, 051101 (2005), arXiv:hep-ex/0410088 .

[50] S. Biagi *et al.*, *Observation of a narrow state at 2.46-GeV/c^2: a candidate for the charmed strange baryon a^+*, Phys. Lett. B **122**, 455 (1983).

[51] P. Avery *et al.* (CLEO), *Observation of the charmed strange baryon* Ξ_c^0, Phys. Rev. Lett. **62**, 863 (1989).

[52] C. Jessop *et al.* (CLEO), *Observation of two narrow states decaying into* Ξ_c^+ *gamma and* Ξ_c^0 *gamma*, Phys. Rev. Lett. **82**, 492 (1999), arXiv:hep-ex/9810036 .

[53] P. Avery *et al.* (CLEO), *Observation of a narrow state decaying into* $\Xi_c^+\pi^-$, Phys. Rev. Lett. **75**, 4364 (1995), arXiv:hep-ex/9508010 .

[54] L. Gibbons *et al.* (CLEO), *Observation of an excited charmed baryon decaying into* $\Xi_c^0\pi^+$, Phys. Rev. Lett. **77**, 810 (1996).

[55] J. Alexander *et al.* (CLEO), *Evidence of new states decaying into* $\Xi_c^*\pi$, Phys. Rev. Lett. **83**, 3390 (1999), arXiv:hep-ex/9906013 .

[56] S. Csorna *et al.* (CLEO), *Evidence of new states decaying into* $\Xi_c'\pi$, Phys. Rev. Lett. **86**, 4243 (2001), arXiv:hep-ex/0012020 .

[57] R. Aaij *et al.* (LHCb), *Observation of new* Ξ_c^0 *baryons decaying to* $\Lambda_c^+K^-$, (2020), arXiv:2003.13649 [hep-ex] .

[58] R. Chistov *et al.* (Belle), *Observation of new states decaying into* $\Lambda_c^+K^-\pi^+$ *and* $\Lambda_c^+K_S^0\pi^-$, Phys. Rev. Lett. **97**, 162001 (2006), arXiv:hep-ex/0606051 .

[59] T. Lesiak *et al.* (Belle), *Measurement of masses of the* $\Xi_c(2645)$ *and* $\Xi_c(2815)$ *baryons and observation of* $\Xi_c(2980)\to\Xi_c(2645)\pi$, Phys. Lett. B **665**, 9 (2008), arXiv:0802.3968 [hep-ex] .

[60] B. Aubert *et al.* (BaBar), *A study of excited charm-strange baryons with evidence for new baryons* $\Xi_c(3055)^+$ *and* $\Xi_c(3123)^+$, Phys. Rev. D **77**, 012002 (2008), arXiv:0710.5763 [hep-ex] .

[61] Y. Kato *et al.* (Belle), *Studies of charmed strange baryons in the* ΛD *final state at Belle*, Phys. Rev. D **94**, 032002 (2016), arXiv:1605.09103 [hep-ex] .

[62] P. Frabetti *et al.* (E687), *Observation of a narrow state decaying into* $\Xi_c^0\pi^+$, Phys. Lett. B **426**, 403 (1998).

[63] Y. Kato *et al.* (Belle), *Search for doubly charmed baryons and study of charmed strange baryons at Belle*, Phys. Rev. D **89**, 052003 (2014), arXiv:1312.1026 [hep-ex] .

[64] J. Yelton *et al.* (Belle), *Study of excited Ξ_c states decaying into Ξ_c^0 and Ξ_c^+ baryons*, Phys. Rev. D **94**, 052011 (2016), arXiv:1607.07123 [hep-ex] .

[65] B. Aubert *et al.* (BaBar), *A study of $\bar{B} \to \Xi_c \bar{\Lambda}_c$ and $\bar{B} \to \bar{\Lambda}_c^+ \bar{\Lambda}_c \bar{K}$ decays at BABAR*, Phys. Rev. D **77**, 031101 (2008), arXiv:0710.5775 [hep-ex] .

[66] Y. Li *et al.* (Belle), *Observation of $\Xi_c(2930)^0$ and updated measurement of $B^- \to K^- \Lambda_c^+ \bar{\Lambda}_c^-$ at Belle*, Eur. Phys. J. C **78**, 252 (2018), arXiv:1712.03612 [hep-ex] .

[67] S. Biagi *et al.*, *Properties of the charmed strange baryon A^+ and evidence for the charmed doubly strange baryon T^0 at 2.74-GeV/c^2*, Z. Phys. C **28**, 175 (1985).

[68] B. Aubert *et al.* (BaBar), *Observation of an excited charm baryon Ω_c^* decaying to $\Omega_c^0\gamma$*, Phys. Rev. Lett. **97**, 232001 (2006), arXiv:hep-ex/0608055 .

[69] E. Solovieva *et al.* (Belle), *Study of Ω_c^0 and Ω_c^{*0} baryons at Belle*, Phys. Lett. B **672**, 1 (2009), arXiv:0808.3677 [hep-ex] .

[70] R. Aaij *et al.* (LHCb), *Observation of five new narrow Ω_c^0 states decaying to $\Xi_c^+ K^-$*, Phys. Rev. Lett. **118**, 182001 (2017), arXiv:1703.04639 [hep-ex] .

[71] J. Yelton *et al.* (Belle), *Observation of excited Ω_c charmed baryons in e^+e^- collisions*, Phys. Rev. D **97**, 051102 (2018), arXiv:1711.07927 [hep-ex] .

[72] M. Basile *et al.*, *Evidence for a new particle with naked 'beauty' and for Its associated production in high-energy (pp) interactions*, Lett. Nuovo Cim. **31**, 97 (1981).

[73] R. Aaij *et al.* (LHCb), *Observation of excited Λ_b^0 baryons*, Phys. Rev. Lett. **109**, 172003 (2012), arXiv:1205.3452 [hep-ex] .

[74] T. A. Aaltonen *et al.* (CDF), *Evidence for a bottom baryon resonance Λ_b^{*0} in CDF data*, Phys. Rev. D **88**, 071101 (2013), arXiv:1308.1760 [hep-ex] .

[75] A. M. Sirunyan *et al.* (CMS), *Study of excited Λ_b^0 states decaying to $\Lambda_\mathrm{b}^0\pi^+\pi^-$ in proton-proton collisions at $\sqrt{s} = 13$ TeV*, Phys. Lett. B **803**, 135345 (2020), arXiv:2001.06533 [hep-ex] .

[76] R. Aaij *et al.* (LHCb), *Observation of a new baryon state in the $\Lambda_b^0\pi^+\pi^-$ mass spectrum,* (2020), arXiv:2002.05112 [hep-ex] .

[77] R. Aaij *et al.* (LHCb), *Observation of new resonances in the $\Lambda_b^0\pi^+\pi^-$ system*, Phys. Rev. Lett. **123**, 152001 (2019), arXiv:1907.13598 [hep-ex] .

[78] T. Aaltonen *et al.* (CDF), *First observation of heavy baryons Σ_b and Σ_b^**, Phys. Rev. Lett. **99**, 202001 (2007), arXiv:0706.3868 [hep-ex] .

[79] T. Aaltonen *et al.* (CDF), *Measurement of the masses and widths of the bottom baryons Σ_b^{+-} and Σ_b^{*+-}*, Phys. Rev. D **85**, 092011 (2012), arXiv:1112.2808 [hep-ex] .

[80] R. Aaij *et al.* (LHCb), *Observation of two resonances in the $\Lambda_b^0\pi^\pm$ systems and precise measurement of $\Sigma_b^\pm$ and $\Sigma_b^{*\pm}$ properties*, Phys. Rev. Lett. **122**, 012001 (2019), arXiv:1809.07752 [hep-ex] .

[81] P. Abreu *et al.* (DELPHI), *Production of strange B baryons decaying into Ξ^- lepton pairs at LEP*, Z. Phys. C **68**, 541 (1995).

[82] R. Aaij *et al.* (LHCb), *Observation of two new Ξ_b^- baryon resonances*, Phys. Rev. Lett. **114**, 062004 (2015), arXiv:1411.4849 [hep-ex] .

[83] S. Chatrchyan *et al.* (CMS), *Observation of a new Ξ_b baryon*, Phys. Rev. Lett. **108**, 252002 (2012), arXiv:1204.5955 [hep-ex] .

[84] R. Aaij *et al.* (LHCb), *Observation of a new Ξ_b^- resonance*, Phys. Rev. Lett. **121**, 072002 (2018), arXiv:1805.09418 [hep-ex] .

[85] V. Abazov *et al.* (D0), *Observation of the doubly strange b baryon Ω_b^-*, Phys. Rev. Lett. **101**, 232002 (2008), arXiv:0808.4142 [hep-ex] .

[86] R. Aaij *et al.* (LHCb), *First observation of excited Ω_b^- states*, Phys. Rev. Lett. **124**, 082002 (2020), arXiv:2001.00851 [hep-ex] .

[87] N. Isgur and M. B. Wise, *Spectroscopy with heavy quark symmetry*, Phys. Rev. Lett. **66**, 1130 (1991).

[88] X.-H. Zhong and Q. Zhao, *Charmed baryon strong decays in a chiral quark model*, Phys. Rev. D **77**, 074008 (2008), arXiv:0711.4645 [hep-ph] .

[89] H. Nagahiro, S. Yasui, A. Hosaka, M. Oka, and H. Noumi, *Structure of charmed baryons studied by pionic decays*, Phys. Rev. D **95**, 014023 (2017), arXiv:1609.01085 [hep-ph] .

[90] L.-H. Liu, L.-Y. Xiao, and X.-H. Zhong, *Charm-strange baryon strong decays in a chiral quark model*, Phys. Rev. D **86**, 034024 (2012), arXiv:1205.2943 [hep-ph] .

[91] K.-L. Wang, L.-Y. Xiao, and X.-H. Zhong, *Understanding the newly observed Ξ_c^0 states through their decays*, (2020), arXiv:2004.03221 [hep-ph] .

[92] K.-L. Wang, L.-Y. Xiao, X.-H. Zhong, and Q. Zhao, *Understanding the newly observed Ω_c states through their decays*, Phys. Rev. D **95**, 116010 (2017), arXiv:1703.09130 [hep-ph] .

[93] Y.-X. Yao, K.-L. Wang, and X.-H. Zhong, *Strong and radiative decays of the low-lying D-wave singly heavy baryons*, Phys. Rev. D **98**, 076015 (2018), arXiv:1803.00364 [hep-ph] .

[94] K.-L. Wang, Y.-X. Yao, X.-H. Zhong, and Q. Zhao, *Strong and radiative decays of the low-lying S- and P-wave singly heavy baryons*, Phys. Rev. D **96**, 116016 (2017), arXiv:1709.04268 [hep-ph] .

[95] K.-L. Wang, Q.-F. L, and X.-H. Zhong, *Interpretation of the newly observed* $\Lambda_b(6146)^0$ *and* $\Lambda_b(6152)^0$ *states in a chiral quark model*, Phys. Rev. D **100**, 114035 (2019), arXiv:1908.04622 [hep-ph] .

[96] L.-Y. Xiao and X.-H. Zhong, *Toward establishing the low-lying* P*-wave* Σ_b *states*, (2020), arXiv:2004.11106 [hep-ph] .

[97] K.-L. Wang, Q.-F. L, and X.-H. Zhong, *Interpretation of the newly observed* $\Sigma_b(6097)^\pm$ *and* $\Xi_b(6227)^-$ *states as the* P*-wave bottom baryons*, Phys. Rev. D **99**, 014011 (2019), arXiv:1810.02205 [hep-ph] .

[98] E. Hernandez and J. Nieves, *Study of the strong* $\Sigma_b \to \Lambda_b\,\pi$ *and* $\Sigma_b^* \to \Lambda_b\,\pi$ *in a non-relativistic quark model*, Phys. Rev. D **84**, 057902 (2011), arXiv:1108.0259 [hep-ph] .

[99] L.-Y. Xiao, K.-L. Wang, M.-S. Liu, and X.-H. Zhong, *Possible interpretation of the newly observed* Ω_b *states*, Eur. Phys. J. C **80**, 279 (2020), arXiv:2001.05110 [hep-ph] .

[100] C. Chen, X.-L. Chen, X. Liu, W.-Z. Deng, and S.-L. Zhu, *Strong decays of charmed baryons*, Phys. Rev. D **75**, 094017 (2007), arXiv:0704.0075 [hep-ph] .

[101] Q.-F. L, L.-Y. Xiao, Z.-Y. Wang, and X.-H. Zhong, *Strong decay of* $\Lambda_c(2940)$ *as a* $2P$ *state in the* Λ_c *family*, Eur. Phys. J. C **78**, 599 (2018), arXiv:1806.01076 [hep-ph] .

[102] Q.-F. L, *Canonical interpretations of the newly observed* $\Xi_c(2923)^0$, $\Xi_c(2939)^0$ *and* $\Xi_c(2965)^0$ *resonances*, (2020), arXiv:2004.02374 [hep-ph] .

[103] W. Liang, Q.-F. L, and X.-H. Zhong, *Canonical interpretation of the newly observed* $\Lambda_b(6146)^0$ *and* $\Lambda_b(6152)^0$ *via strong decay behaviors*, Phys. Rev. D **100**, 054013 (2019), arXiv:1908.00223 [hep-ph] .

[104] W. Liang and Q.-F. L, *The newly observed* $\Lambda_b(6072)^0$ *structure and its* $\rho-$*mode nonstrange partners*, (2020), arXiv:2004.13568 [hep-ph] .

[105] A. Limphirat, C. Kobdaj, P. Suebka, and Y. Yan, *Decay widths of ground-state and excited* Ξ_b *baryons in a nonrelativistic quark model*, Phys. Rev. C **82**, 055201 (2010).

[106] W. Liang and Q.-F. L, *Strong decays of the newly observed narrow* Ω_b *structures*, Eur. Phys. J. C **80**, 198 (2020), arXiv:2001.02221 [hep-ph] .

[107] B. Chen, K.-W. Wei, X. Liu, and T. Matsuki, *Low-lying charmed and charmed-strange baryon states*, Eur. Phys. J. C **77**, 154 (2017), arXiv:1609.07967 [hep-ph] .

[108] B. Chen, X. Liu, and A. Zhang, *Newly observed* $\Lambda_c(2860)^+$ *at LHCb and its* D*-wave partners* $\Lambda_c(2880)^+$, $\Xi_c(3055)^+$ *and* $\Xi_c(3080)^+$, Phys. Rev. D **95**, 074022 (2017), arXiv:1702.04106 [hep-ph] .

[109] B. Chen and X. Liu, *New Ω_c^0 baryons discovered by LHCb as the members of $1P$ and $2S$ states*, Phys. Rev. D **96**, 094015 (2017), arXiv:1704.02583 [hep-ph] .

[110] B. Chen, S.-Q. Luo, X. Liu, and T. Matsuki, *Interpretation of the observed $\Lambda_b(6146)^0$ and $\Lambda_b(6152)^0$ states as 1D bottom baryons*, Phys. Rev. D **100**, 094032 (2019), arXiv:1910.03318 [hep-ph] .

[111] B. Chen and X. Liu, *Assigning the newly reported $\Sigma_b(6097)$ as a P-wave excited state and predicting its partners*, Phys. Rev. D **98**, 074032 (2018), arXiv:1810.00389 [hep-ph] .

[112] B. Chen, K.-W. Wei, X. Liu, and A. Zhang, *Role of newly discovered $\Xi_b(6227)^-$ for constructing excited bottom baryon family*, Phys. Rev. D **98**, 031502 (2018), arXiv:1805.10826 [hep-ph] .

[113] H.-Y. Cheng and C.-K. Chua, *Strong decays of charmed baryons in heavy hadron chiral perturbation theory*, Phys. Rev. D **75**, 014006 (2007), arXiv:hep-ph/0610283 .

[114] H.-Y. Cheng and C.-K. Chua, *Strong decays of charmed baryons in heavy hadron chiral perturbation theory: an update*, Phys. Rev. D **92**, 074014 (2015), arXiv:1508.05653 [hep-ph] .

[115] K. Gandhi, Z. Shah, and A. K. Rai, *Decay properties of singly charmed baryons*, Eur. Phys. J. Plus **133**, 512 (2018), arXiv:1811.00251 [hep-ph] .

[116] K. Gandhi, Z. Shah, and A. K. Rai, *Spectrum of nonstrange singly charmed baryons in the constituent quark model*, Int. J. Theor. Phys. **59**, 1129 (2020), arXiv:1912.05859 [hep-ph] .

[117] H.-Y. Cheng and C.-W. Chiang, *Quantum numbers of Ω_c states and other charmed baryons*, Phys. Rev. D **95**, 094018 (2017), arXiv:1704.00396 [hep-ph] .

[118] H.-X. Chen, Q. Mao, W. Chen, A. Hosaka, X. Liu, and S.-L. Zhu, *Decay properties of P-wave charmed baryons from light-cone QCD sum rules*, Phys. Rev. D **95**, 094008 (2017), arXiv:1703.07703 [hep-ph] .

[119] H.-M. Yang, H.-X. Chen, and Q. Mao, *Identifying the Ξ_c^0 baryons observed by LHCb as P-wave Ξ_c' baryons*, (2020), arXiv:2004.00531 [hep-ph] .

[120] H.-M. Yang, H.-X. Chen, E.-L. Cui, A. Hosaka, and Q. Mao, *Decay properties of P-wave bottom baryons within light-cone sum rules*, Eur. Phys. J. C **80**, 80 (2020), arXiv:1909.13575 [hep-ph] .

[121] E.-L. Cui, H.-M. Yang, H.-X. Chen, and A. Hosaka, *Identifying the $\Xi_b(6227)$ and $\Sigma_b(6097)$ as P-wave bottom baryons of $J^P = 3/2^-$*, Phys. Rev. D **99**, 094021 (2019), arXiv:1903.10369 [hep-ph] .

[122] A. Arifi, H. Nagahiro, and A. Hosaka, *Three-body decay of $\Lambda_c^*(2595)$ and $\Lambda_c^*(2625)$ with consideration of $\Sigma_c(2455)\pi$ and $\Sigma_c^*(2520)\pi$ in intermediate states*, Phys. Rev. D **95**, 114018 (2017), arXiv:1704.00464 [hep-ph] .

[123] Y. Kawakami and M. Harada, *Analysis of* $\Lambda_c(2595)$*,* $\Lambda_c(2625)$*,* $\Lambda_b(5912)$*,* $\Lambda_b(5920)$ *based on a chiral partner structure*, Phys. Rev. D **97**, 114024 (2018), arXiv:1804.04872 [hep-ph] .

[124] Y. Kawakami and M. Harada, *Singly heavy baryons with chiral partner structure in a three-flavor chiral model*, Phys. Rev. D **99**, 094016 (2019), arXiv:1902.06774 [hep-ph] .

[125] A. Arifi, H. Nagahiro, and A. Hosaka, *Three-body decay of* $\Lambda_c^*(2595)$ *and* $\Lambda_c^*(2625)$ *with the inclusion of a direct two-pion coupling*, Phys. Rev. D **98**, 114007 (2018), arXiv:1809.10290 [hep-ph] .

[126] A. Arifi, H. Nagahiro, A. Hosaka, and K. Tanida, *Three-body decay of* $\Lambda_c^*(2765)$ *and determination of its spin-parity*, Phys. Rev. D **101**, 094023 (2020), arXiv:2003.08202 [hep-ph] .

[127] A. J. Arifi, H. Nagahiro, A. Hosaka, and K. Tanida, *Roper-like resonances with various flavor contents and their two-pion emission decays*, Phys. Rev. **D101**, 111502 (R) (2020), arXiv:2004.07423 [hep-ph] .

[128] S. Sakai, F.-K. Guo, and B. Kubis, *Extraction of* ND *scattering lengths from the* $\Lambda_b \to \pi^- p D^0$ *decay and properties of the* $\Sigma_c(2800)^+$, (2020), arXiv:2004.09824 [hep-ph] .

[129] S. Sakai, *Role of the triangle mechanism in the* $\Lambda_b \to \Lambda_c \pi^- f_0(980)$ *reaction*, Phys. Rev. D **101**, 074041 (2020), arXiv:2002.08594 [hep-ph] .

[130] J.-J. Xie and L.-S. Geng, *The* $a_0(980)$ *and* $\Lambda(1670)$ *in the* $\Lambda_c^+ \to \pi^+\eta\Lambda$ *decay*, Eur. Phys. J. C **76**, 496 (2016), arXiv:1604.02756 [nucl-th] .

[131] K. Miyahara, T. Hyodo, and E. Oset, *Weak decay of* Λ_c^+ *for the study of* Λ*(1405) and* Λ*(1670)*, Phys. Rev. C **92**, 055204 (2015), arXiv:1508.04882 [nucl-th] .

[132] L. Copley, N. Isgur, and G. Karl, *Charmed baryons in a quark model with hyperfine interactions*, Phys. Rev. D **20**, 768 (1979), [Erratum: Phys.Rev.D 23, 817 (1981)].

[133] W. Roberts and M. Pervin, *Heavy baryons in a quark model*, Int. J. Mod. Phys. A **23**, 2817 (2008), arXiv:0711.2492 [nucl-th] .

[134] T. Yoshida, E. Hiyama, A. Hosaka, M. Oka, and K. Sadato, *Spectrum of heavy baryons in the quark model*, Phys. Rev. D **92**, 114029 (2015), arXiv:1510.01067 [hep-ph] .

[135] T. Hyodo, *Structure of near-threshold s-wave resonances*, Phys. Rev. Lett. **111**, 132002 (2013), arXiv:1305.1999 [hep-ph] .

[136] Z.-H. Guo and J. Oller, *Resonance on top of thresholds: the* $\Lambda_c(2595)^+$ *as an extremely fine-tuned state*, Phys. Rev. D **93**, 054014 (2016), arXiv:1601.00862 [hep-ph] .

[137] J.-X. Lu, H.-X. Chen, Z.-H. Guo, J. Nieves, J.-J. Xie, and L.-S. Geng, $\Lambda_c(2595)$ *resonance as a dynamically generated state: The compositeness condition and the large* N_c *evolution*, Phys. Rev. D **93**, 114028 (2016), arXiv:1603.05388 [hep-ph] .

[138] J. Haidenbauer, G. Krein, U.-G. Meissner, and L. Tolos, *DN interaction from meson exchange*, Eur. Phys. J. A **47**, 18 (2011), arXiv:1008.3794 [nucl-th] .

[139] P. Gubler, T. T. Takahashi, and M. Oka, *Flavor structure of Λ baryons from lattice QCD: From strange to charm quarks*, Phys. Rev. D **94**, 114518 (2016), arXiv:1609.01889 [hep-lat] .

[140] J. Nieves and R. Pavao, *Nature of the lowest-lying odd parity charmed baryon $\Lambda_c(2595)$ and $\Lambda_c(2625)$ resonances*, Phys. Rev. D **101**, 014018 (2020), arXiv:1907.05747 [hep-ph] .

[141] S. Gerasyuta and E. Matskevich, *Charmed (70,1-) baryon multiplet*, Int. J. Mod. Phys. E **17**, 585 (2008), arXiv:0709.0397 [hep-ph] .

[142] H.-X. Chen, W. Chen, Q. Mao, A. Hosaka, X. Liu, and S.-L. Zhu, *P-wave charmed baryons from QCD sum rules*, Phys. Rev. D **91**, 054034 (2015), arXiv:1502.01103 [hep-ph] .

[143] B. Wang, L. Meng, and S.-L. Zhu, *$D^{(*)}N$ interaction and the structure of $\Sigma_c(2800)$ and $\Lambda_c(2940)$ in chiral effective field theory*, Phys. Rev. D **101**, 094035 (2020), arXiv:2003.05688 [hep-ph] .

[144] J.-R. Zhang, *S-wave $D^{(*)}N$ molecular states: $\Sigma_c(2800)$ and $\Lambda_c(2940)^+$?*, Phys. Rev. D **89**, 096006 (2014), arXiv:1212.5325 [hep-ph] .

[145] L. Zhao, H. Huang, and J. Ping, *ND and NB systems in quark delocalization color screening model*, Eur. Phys. J. A **53**, 28 (2017), arXiv:1612.00350 [hep-ph] .

[146] Y. Dong, A. Faessler, T. Gutsche, and V. E. Lyubovitskij, *Charmed baryon $\Sigma_c(2800)$ as a ND hadronic molecule*, Phys. Rev. D **81**, 074011 (2010), arXiv:1002.0218 [hep-ph] .

[147] H. Zhu, N. Ma, and Y. Huang, *Description of the newly observed Ξ_c^0 states as molecular states*, (2020), arXiv:2005.02642 [hep-ph] .

[148] M. Karliner and J. L. Rosner, *Very narrow excited Ω_c baryons*, Phys. Rev. D **95**, 114012 (2017), arXiv:1703.07774 [hep-ph] .

[149] W. Wang and R.-L. Zhu, *Interpretation of the newly observed Ω_c^0 resonances*, Phys. Rev. D **96**, 014024 (2017), arXiv:1704.00179 [hep-ph] .

[150] Z.-G. Wang, *Analysis of $\Omega_c(3000)$, $\Omega_c(3050)$, $\Omega_c(3066)$, $\Omega_c(3090)$ and $\Omega_c(3119)$ with QCD sum rules*, Eur. Phys. J. C **77**, 325 (2017), arXiv:1704.01854 [hep-ph] .

[151] H. Huang, J. Ping, and F. Wang, *Investigating the excited Ω_c^0 states through $\Xi_c K$ and $\Xi_c^{'} K$ decay channels*, Phys. Rev. D **97**, 034027 (2018), arXiv:1704.01421 [hep-ph] .

[152] M. Padmanath and N. Mathur, *Quantum numbers of recently discovered Ω_c^0 baryons from Lattice QCD*, Phys. Rev. Lett. **119**, 042001 (2017), arXiv:1704.00259 [hep-ph] .

[153] H.-C. Kim, M. V. Polyakov, and M. Praszał owicz, *Possibility of the existence of charmed exotica*, Phys. Rev. D **96**, 014009 (2017), [Addendum: Phys.Rev.D 96, 039902 (2017)], arXiv:1704.04082 [hep-ph] .

[154] H.-C. Kim, M. V. Polyakov, M. Praszalowicz, and G.-S. Yang, *Strong decays of exotic and nonexotic heavy baryons in the chiral quark-soliton model*, Phys. Rev. D **96**, 094021 (2017), [Erratum: Phys.Rev.D 97, 039901 (2018)], arXiv:1709.04927 [hep-ph] .

[155] C. An and H. Chen, *Observed Ω_c^0 resonances as pentaquark states*, Phys. Rev. D **96**, 034012 (2017), arXiv:1705.08571 [hep-ph] .

[156] G. Yang and J. Ping, *Dynamical study of Ω_c^0 in the chiral quark model*, Phys. Rev. D **97**, 034023 (2018), arXiv:1703.08845 [hep-ph] .

[157] V. Debastiani, J. Dias, W. Liang, and E. Oset, *Molecular Ω_c states generated from coupled meson-baryon channels*, Phys. Rev. D **97**, 094035 (2018), arXiv:1710.04231 [hep-ph] .

[158] G. Montaa, A. Feijoo, and . Ramos, *A meson-baryon molecular interpretation for some Ω_c excited states*, Eur. Phys. J. A **54**, 64 (2018), arXiv:1709.08737 [hep-ph] .

[159] R. Chen, A. Hosaka, and X. Liu, *Searching for possible Ω_c-like molecular states from meson-baryon interaction*, Phys. Rev. D **97**, 036016 (2018), arXiv:1711.07650 [hep-ph] .

[160] Y.-s. Oh and B.-Y. Park, *Excited states of heavy baryons in the Skyrme model*, Phys. Rev. D **53**, 1605 (1996), arXiv:hep-ph/9510268 .

[161] D. Ebert, R. Faustov, and V. Galkin, *Masses of excited heavy baryons in the relativistic quark model*, Phys. Lett. B **659**, 612 (2008), arXiv:0705.2957 [hep-ph] .

[162] A. Valcarce, H. Garcilazo, and J. Vijande, *Towards an understanding of heavy baryon spectroscopy*, Eur. Phys. J. A **37**, 217 (2008), arXiv:0807.2973 [hep-ph] .

[163] B. Chen, D.-X. Wang, and A. Zhang, *J^P assignments of Λ_c^+ baryons*, Chin. Phys. C **33**, 1327 (2009), arXiv:0906.3934 [hep-ph] .

[164] B. Chen, K.-W. Wei, and A. Zhang, *Assignments of Λ_Q and Ξ_Q baryons in the heavy quark-light diquark picture*, Eur. Phys. J. A **51**, 82 (2015), arXiv:1406.6561 [hep-ph] .

[165] Z. Shah, K. Thakkar, A. K. Rai, and P. Vinodkumar, *Mass spectra and Regge trajectories of Λ_c^+, Σ_c^0, Ξ_c^0 and Ω_c^0 baryons*, Chin. Phys. C **40**, 123102 (2016), arXiv:1609.08464 [nucl-th] .

[166] Q.-F. L, Y. Dong, X. Liu, and T. Matsuki, *Puzzle of the Λ_c spectrum*, Nucl. Phys. Rev. **35**, 1 (2018), arXiv:1610.09605 [hep-ph] .

[167] K. Kumakawa and D. Jido, *Excitation energy spectra of the Λ_c and Λ_b baryons in a finite-size diquark model*, PTEP **2017**, 123D01 (2017), arXiv:1708.02012 [nucl-th] .

[168] J.-J. Guo, P. Yang, and A. Zhang, *Strong decays of observed Λ_c baryons in the $^3P_0$ model*, Phys. Rev. D **100**, 014001 (2019), arXiv:1902.07488 [hep-ph] .

[169] N. Suzuki, B. Julia-Diaz, H. Kamano, T.-S. Lee, A. Matsuyama, and T. Sato, *Disentangling the dynamical origin of P-11 nucleon resonances*, Phys. Rev. Lett. **104**, 042302 (2010), arXiv:0909.1356 [nucl-th] .

[170] J.-j. Wu, D. B. Leinweber, Z.-w. Liu, and A. W. Thomas, *Structure of the Roper resonance from Lattice QCD constraints*, Phys. Rev. D **97**, 094509 (2018), arXiv:1703.10715 [nucl-th] .

[171] C. Lang, L. Leskovec, M. Padmanath, and S. Prelovsek, *Pion-nucleon scattering in the Roper channel from lattice QCD*, Phys. Rev. D **95**, 014510 (2017), arXiv:1610.01422 [hep-lat] .

[172] G. Brown, J. Durso, and M. Johnson, *Zero point motion in the bag description of the nucleon*, Nucl. Phys. A **397**, 447 (1983).

[173] M. Takayama, H. Toki, and A. Hosaka, *Systematics of the SU(3) baryon spectra and deformed oscillator quark model*, Prog. Theor. Phys. **101**, 1271 (1999).

[174] L. Glozman and D. Riska, *The spectrum of the nucleons and the strange hyperons and chiral dynamics*, Phys. Rept. **268**, 263 (1996), arXiv:hep-ph/9505422 .

[175] D.-D. Ye, Z. Zhao, and A. Zhang, *Study of P-wave excitations of observed charmed strange baryons*, Phys. Rev. D **96**, 114009 (2017), arXiv:1709.00689 [hep-ph] .

[176] Z.-G. Wang, *The $\Lambda_c(2860)$, $\Lambda_c(2880)$, $\Xi_c(3055)$ and $\Xi_c(3080)$ as D-wave baryon states in QCD*, Nucl. Phys. B **926**, 467 (2018), arXiv:1705.07745 [hep-ph] .

[177] D. Ebert, R. Faustov, and V. Galkin, *Spectroscopy and Regge trajectories of heavy baryons in the relativistic quark-diquark picture*, Phys. Rev. D **84**, 014025 (2011), arXiv:1105.0583 [hep-ph] .

[178] S. Capstick and N. Isgur, *Baryons in a relativized quark model with chromodynamics*, AIP Conf. Proc. **132**, 267 (1985).

[179] H. Garcilazo, J. Vijande, and A. Valcarce, *Faddeev study of heavy baryon spectroscopy*, J. Phys. G **34**, 961 (2007), arXiv:hep-ph/0703257 .

[180] X.-G. He, X.-Q. Li, X. Liu, and X.-Q. Zeng, *$\Lambda_c^+(2940)$: A possible molecular state?*, Eur. Phys. J. C **51**, 883 (2007), arXiv:hep-ph/0606015 .

[181] J. He, Y.-T. Ye, Z.-F. Sun, and X. Liu, *The observed charmed hadron $\Lambda_c(2940)^+$ and the D^*N interaction*, Phys. Rev. D **82**, 114029 (2010), arXiv:1008.1500 [hep-ph] .

[182] P. Ortega, D. Entem, and F. Fernandez, *Quark model description of the $\Lambda_c(2940)^+$ as a molecular D^*N state and the possible existence of the $\Lambda_b(6248)$*, Phys. Lett. B **718**, 1381 (2013), arXiv:1210.2633 [hep-ph] .

[183] D.-D. Ye, Z. Zhao, and A. Zhang, *Study of $2S$- and $1D$- excitations of observed charmed strange baryons*, Phys. Rev. D **96**, 114003 (2017), arXiv:1710.10165 [hep-ph] .

[184] C. Mu, X. Wang, X.-L. Chen, X. Liu, and S.-L. Zhu, *Dipion decays of heavy baryons*, Chin. Phys. C **38**, 113101 (2014), arXiv:1405.3128 [hep-ph] .

[185] C. Garcia-Recio, J. Nieves, O. Romanets, L. Salcedo, and L. Tolos, *Odd parity bottom-flavored baryon resonances*, Phys. Rev. D **87**, 034032 (2013), arXiv:1210.4755 [hep-ph] .

[186] J.-X. Lu, Y. Zhou, H.-X. Chen, J.-J. Xie, and L.-S. Geng, *Dynamically generated $J^P = 1/2^-(3/2^-)$ singly charmed and bottom heavy baryons*, Phys. Rev. **D92**, 014036 (2015), arXiv:1409.3133 [hep-ph] .

[187] C. Garcia-Recio, C. Hidalgo-Duque, J. Nieves, L. Salcedo, and L. Tolos, *Compositeness of the strange, charm, and beauty odd parity Λ states*, Phys. Rev. D **92**, 034011 (2015), arXiv:1506.04235 [hep-ph] .

[188] W. H. Liang, C. W. Xiao, and E. Oset, *Baryon states with open beauty in the extended local hidden gauge approach*, Phys. Rev. **D89**, 054023 (2014), arXiv:1401.1441 [hep-ph] .

[189] J. M. Torres-Rincon, L. Tolos, and O. Romanets, *Open bottom states and the $\bar{B}$-meson propagation in hadronic matter*, Phys. Rev. D **89**, 074042 (2014), arXiv:1403.1371 [hep-ph] .

[190] M. Karliner and J. L. Rosner, *Scaling of P-wave excitation energies in heavy-quark systems*, Phys. Rev. **D98**, 074026 (2018), arXiv:1808.07869 [hep-ph] .

[191] M. Karliner and J. L. Rosner, *Prospects for observing the lowest-lying odd-parity Σ_c and Σ_b baryons*, Phys. Rev. **D92**, 074026 (2015), arXiv:1506.01702 [hep-ph] .

[192] K. Thakkar, Z. Shah, A. K. Rai, and P. C. Vinodkumar, *Excited state mass spectra and Regge trajectories of bottom baryons*, Nucl. Phys. **A965**, 57 (2017), arXiv:1610.00411 [nucl-th] .

[193] P. Yang, J.-J. Guo, and A. Zhang, *Identification of the newly observed $\Sigma_b(6097)^\pm$ baryons from their strong decays*, Phys. Rev. **D99**, 034018 (2019), arXiv:1810.06947 [hep-ph] .

[194] T. M. Aliev, K. Azizi, Y. Sarac, and H. Sundu, *Determination of the quantum numbers of $\Sigma_b(6097)^\pm$ via their strong decays*, Phys. Rev. **D99**, 094003 (2019), arXiv:1811.05686 [hep-ph] .

[195] Q. Mao, H.-X. Chen, W. Chen, A. Hosaka, X. Liu, and S.-L. Zhu, *QCD sum rule calculation for P-wave bottom baryons*, Phys. Rev. D **92**, 114007 (2015), arXiv:1510.05267 [hep-ph] .

[196] T. M. Aliev, K. Azizi, Y. Sarac, and H. Sundu, *Structure of the $\Xi_b(6227)^-$ resonance*, Phys. Rev. **D98**, 094014 (2018), arXiv:1808.08032 [hep-ph] .

[197] Q. X. Yu, R. Pavao, V. R. Debastiani, and E. Oset, *Description of the Ξ_c and Ξ_b states as molecular states*, Eur. Phys. J. **C79**, 167 (2019), arXiv:1811.11738 [hep-ph] .

[198] Y. Huang, C.-j. Xiao, L.-S. Geng, and J. He, *Strong decays of the $\Xi_b(6227)$ as a $\Sigma_b\bar{K}$ molecule*, Phys. Rev. **D99**, 014008 (2019), arXiv:1811.10769 [hep-ph] .

[199] J. Nieves, R. Pavao, and L. Tolos, *Ξ_c and Ξ_b excited states within a $\mathrm{SU}(6)_{\mathrm{lsf}}\times$HQSS model*, Eur. Phys. J. **C80**, 22 (2020), arXiv:1911.06089 [hep-ph] .

[200] H.-X. Chen, E.-L. Cui, A. Hosaka, Q. Mao, and H.-M. Yang, *Excited Ω_b baryons and fine structure of strong interaction*, Eur. Phys. J. **C80**, 256 (2020), arXiv:2001.02147 [hep-ph] .

[201] Z.-G. Wang, *Analysis of the $\Omega_b(6316)$, $\Omega_b(6330)$, $\Omega_b(6340)$ and $\Omega_b(6350)$ with QCD sum rules*, Int. J. Mod. Phys. **A35**, 2050043 (2020), arXiv:2001.02961 [hep-ph] .

[202] H. Mutuk, *A study of excited Ω_b^- states in hypercentral constituent quark model via artificial neural network*, Eur. Phys. J. **A56**, 146 (2020), arXiv:2002.03695 [hep-ph] .

[203] M. Karliner and J. L. Rosner, *Interpretation of excited Ω_b signals*, (2020), arXiv:2005.12424 [hep-ph] .

[204] S. S. Agaev, K. Azizi, and H. Sundu, *Decay widths of the excited Ω_b baryons*, Phys. Rev. **D96**, 094011 (2017), arXiv:1708.07348 [hep-ph] .

[205] W.-H. Liang, J. M. Dias, V. R. Debastiani, and E. Oset, *Molecular Ω_b states*, Nucl. Phys. **B930**, 524 (2018), arXiv:1711.10623 [hep-ph] .

[206] W.-H. Liang and E. Oset, *Observed Ω_b spectrum and meson-baryon molecular states*, Phys. Rev. **D101**, 054033 (2020), arXiv:2001.02929 [hep-ph] .

[207] K. Azizi, Y. Sarac, and H. Sundu, *New $\Lambda_b(6072)^0$ state as a $2S$ bottom baryon*, (2020), arXiv:2005.06772 [hep-ph] .

[208] G.-S. Yang and H.-C. Kim, *Isospin mass differences of singly heavy baryons*, (2020), arXiv:2004.08524 [hep-ph] .

[209] C.-W. Hwang and C.-H. Chung, *Isospin mass splittings of heavy baryons in HQS*, Phys. Rev. D **78**, 073013 (2008), arXiv:0804.4044 [hep-ph] .

[210] R. N. Faustov and V. O. Galkin, *Heavy baryon spectroscopy in the relativistic quark model*, Particles **3**, 234 (2020).

[211] D. Jia, W.-N. Liu, and A. Hosaka, *Regge behaviors in orbitally excited spectroscopy of charmed and bottom baryons*, Phys. Rev. **D101**, 034016 (2020), arXiv:1907.04958 [hep-ph] .

[212] Q. Mao, H.-M. Yang, and H.-X. Chen, *Identifying the $\Lambda_b(6146)^0$ and $\Lambda_b(6152)^0$ as D-wave bottom baryons*, (2020), arXiv:2002.11435 [hep-ph] .

[213] S. X. Nakamura, *Coupled-channel analysis of $D^+ \to K^-\pi^+\pi^+$ decay*, Phys. Rev. D **93**, 014005 (2016), arXiv:1504.02557 [hep-ph] .

[214] J. K. Ahn, S. Yang, and S.-I. Nam, *Hyperon production in $\Lambda_c^+ \to K^- p\pi^+$ and $\Lambda_c^+ \to K_S^0 p\pi^0$*, Phys. Rev. D **100**, 034027 (2019), arXiv:1907.04475 [hep-ph] .

[215] R. Dalitz, *On the analysis of τ-meson data and the nature of the τ-meson*, Phil. Mag. Ser. 7 **44**, 1068 (1953).

[216] P. L. Cho, *Strong and electromagnetic decays of two new Λ_c^* baryons*, Phys. Rev. D **50**, 3295 (1994), arXiv:hep-ph/9401276 .

[217] L. Roper, *Evidence for a P-11 pion-nucleon resonance at 556 MeV*, Phys. Rev. Lett. **12**, 340 (1964).

[218] V. D. Burkert and C. D. Roberts, *Roper resonance: Toward a solution to the fifty year puzzle*, Rev. Mod. Phys. **91**, 011003 (2019), arXiv:1710.02549 [nucl-ex] .